THE INTERACTIONS OF SMALL HEAT SHOCK PROTEINS WITH INTERMEDIATE FILAMENTS

BY

ANDREW LANDSBURY

A thesis submitted at the University of Durham

for the degree of Doctor of Philosophy

School of Biological and Biomedical Sciences

University of Durham, May 2012

ABSTRACT

The interaction of small heat shock proteins (sHsps) and intermediate filaments (IFs) is essential to the cell. Mutations both in sHsps and IFs cause disease in humans, characterised by aggregates containing both sHsps and IFs, demonstrating the importance of this interaction. However, the molecular details of this interaction and the mechanisms which lead to disease are unknown. Investigations into the sHsp-IF interaction may allow future development of new therapeutic approaches to maintain the sHsp-IF interaction and therefore inhibit the formation of the pathological aggregates which cause disease. This thesis analyses the sHsp-IF interaction *in vitro* using the sHsp 'aB crystallin' and the IF 'desmin'. I investigate the domains in both aB crystallin and desmin which are important for their interaction. I also analyse the effect of IF assembly conditions on filament properties and interaction with aB crystallin. In addition, I investigate the 'beaded filament' to gain insight into the factors affecting filament assembly, filament properties and filament interactions with aB crystallin. Furthermore, I investigate the effects of a disease causing aB crystallin mutation on activity *in vitro*. I also attempt to model the potential structural changes in aB crystallin resulting from mutation, using the sHsp, Hsp16.5. These studies provide important insight into the interaction between sHsps and IFs.

DECLARATION

I declare that, unless otherwise stated, the experiments described in this thesis were carried out by myself in the School of Biological and Biomedical Sciences, University of Durham, under the supervision of Prof. Roy A. Quinlan.

This thesis has been composed by myself and is a record of work that has not been submitted previously for a higher degree.

Andrew Landsbury

ACKNOWLEDGEMENTS

My excellent supervisor, Prof. Roy Quinlan, has provided constant help, guidance and encouragement throughout my PhD. Thank you Roy, for the great kindness you've shown me and for always listening and understanding.

Thanks also to past and current members of the RAQ Lab Jayne Elliot, Terry Gibbons, Antal Tapodi, Fred Tholozan and Weiju Wu for countless help with experiments and for many helpful discussions.

Andrew Landsbury

PUBLICATION OF WORK IN THIS THESIS

JOURNAL ARTICLES

Houck SA*, Landsbury A*, Clark JI, Quinlan RA. (2011). Multiple sites in αB-crystallin modulate interactions with desmin filaments assembled *in vitro*. PLoS ONE *6(11)*. (*Joint first author) (See thesis chapter 7)

Qu B*, Landsbury A*, Schönthaler HB, Dahm R, Liu Y, Clark JI, Prescott AR, Quinlan RA. (2012). Evolution of the vertebrate beaded filament protein, Bfsp2; comparing the in vitro assembly properties of a "tailed" zebrafish Bfsp2 to its "tailless" human orthologue. Experimental Eye Research *94*, 192-202. (*Joint first author) (See thesis chapter 5)

PUBLISHED REVIEWS

Landsbury, A., Der Perng, M., Pohl, E. and Quinlan, R.A. (2010). Functional symbiosis between the intermediate filament cytoskeleton and small heat shock proteins. Nova Biomedical. Small stress proteins and human diseases. *ISBN* 978-1-61668-198-2.

Song, S., Landsbury, A., Dahm, R., Liu, Y., Zhang, Q., and Quinlan, R.A. (2009). Functions of the intermediate filament cytoskeleton in the eye lens. J Clin Invest *119*, 1837-1848.

CONTENTS

TABLES & FIGURES

ABBREVIATIONS

Chemicals

ATP	adenosine triphosphate
BCA	bicinchoninic acid
bis-ANS	4,4-dianilino-1,1-binaphthyl-5,5-disulfonic acid
BSA	bovine serum albumin
DEAE	diethylaminoethyl
DTT	dithiothreitol
EDTA	ethylenediaminetetraacetic acid
EGTA	ethyleneglycoltetraacetic acid
HA	hydroxyapatite
Hepes	2-(4-(2-Hydroxyethyl)-1-piperazinyl)-ethane sulfonic acid
IPTG	isopropyl-beta-D-thiogalactopyranoside
LB	Luria-Bertani
PBS	phosphate buffered saline
PEI	polyethylimine
PES	polyethersulphone
PMSF	phenylmethlysulphonylfluride
TMAE	trimethylaminoethyl
Tris	tris(hydroxymethyl)aminomethane

Techniques

BLAST	basic local alignment searth tool
CD	circular dichroism
DSF	differential scanning fluorimetry
EM	electron microscopy
HPLC	high performance liquid chromatography
HRM	high resolution melting
HX	hydrogen-deuterium exchange
IEC	ion exchange chromatography
LPLC	low pressure liquid chromatography
NMR	nuclear magnetic resonance

SAXS	small angle X-ray scattering
SDS-PAGE	sodium dodecyl sulfate - polyacrylamide gel electrophoresis
SEC	size exclusion chromatography
SPR	surface plasmon resonance
TEM	transmission electron microscopy

Diseases

ADCC	autosomal dominant congenital cataract
CMT	Charcot-Marie-Tooth
DCM	dilated cardiomyopathy
DRM	desmin related myopathy

Quantities

Ave	average
bp	base pair
cv	column volume
Da	dalton
g	g-force at max radius (r_{max})
g/l	grams per litre
M	molar
MW	molecular weight
MWCO	molecular weight cut off
OD	optical density
pI	isoelectric point
rpm	revolutions per minute
SD	standard deviation
ul	microlitre
UV	ultra-violet
v/v	volume per volume
w/v	weight per volume

Protein Related

a-crystallin	α-crystallin
aB	αB-crystallin
aB crystallin	αB-crystallin
ACD	α-crystallin domain
BF	beaded filament
Bfsp	beaded filament structural protein (zebrafish)
BFSP	beaded filament structural protein (human or bovine)
Bo	bovine (*Bos taurus*)
CS	citrate synthase
CT	C-terminus truncated
del	deletion
des	desmin
Hu	human (*Homo sapiens*)
Hsp	heat shock protein
IF	intermediate filament
MT	microtubule
PT	post-translational
PTM	post-translational modification
sHsp	small heat shock protein
SPF	soluble protein fraction
WT	wild-type
Zf	zebrafish (*Danio rerio*)
53k	53kDa breakdown product of BSFP1

CHAPTER 1: INTRODUCTION

SMALL HEAT SHOCK PROTEINS

Heat shock proteins (Hsps), found in both prokaryotes and eukaryotes, are upregulated in response to heat shock (Schlesinger, 1990). The principal Hsps belong to five conserved classes: Hsp100, Hsp90, Hsp70, Hsp60 and the small heat shock proteins (sHsps). Hsp90, Hsp70 and Hsp60 proteins are involved in protein folding (Young et al., 2004), while the Hsp100 proteins act as protein disaggregases, dissociating large insoluble aggregates for subsequent refolding in cooperation with Hsp70 (Mogk et al., 2008).

The human genome encodes ten sHsps: HspB1-10 (Franck et al., 2004). These include HspB1 (Hsp27), HspB4 (aA crystallin), HspB5 (aB crystallin) and HspB6 (Hsp20) (Kappe et al., 2003). sHsps are 12-43 kDa but can assemble into large, dynamic oligomeric complexes of 50-800 kDa (Fig 1.0). In contrast to Hsp100 and Hsp70 chaperones, sHsp activity is independent of ATP hydrolysis. All sHsps share an evolutionarily conserved sequence of 80-100 residues called the a-crystallin domain (ACD) (Augusteyn, 2004a).

Protein aggregation resulting from stress or disease is a serious threat to cells. Stress or disease can cause proteins to expose hydrophobic surfaces, and in the crowded cellular environment, these surfaces can interact and cause protein aggregation. Even in the absence of stress or disease, proteins are susceptible to aggregation during conformational transitions, which may expose hydrophobic surfaces (Englander et al., 2007). A protein quality control network of chaperones and proteases regulates protein aggregation (Liberek et al., 2008). The sHsp chaperones can bind to a wide range of cellular proteins to prevent their irreversible aggregation (Basha et al., 2004a; Basha et al., 2004b). In contrast to the ATP dependent chaperones, the ATP independent sHsps function as holdases during cell stress, by binding and holding partially denatured proteins in a folding competent state (Haslbeck et al., 2005a; Van Montfort et al., 2001a). Stress destabilises client proteins, resulting in aggregation prone folding intermediates which associate with sHsps through exposed hydrophobic regions. sHsps therefore act as a reservoir for misfolded proteins, allowing subsequent disaggregation and refolding by ATP dependent chaperones when stress is mitigated (Ehrnsperger et al., 1997; Lee and Vierling, 2000; Mogk et al., 2003). The absence of energy consumption make sHsp proteins an efficient defence mechanism compared to the ATP dependent chaperones, which require cell energy resources (McHaourab et al., 2002). *In vivo*, sHsps protect cells

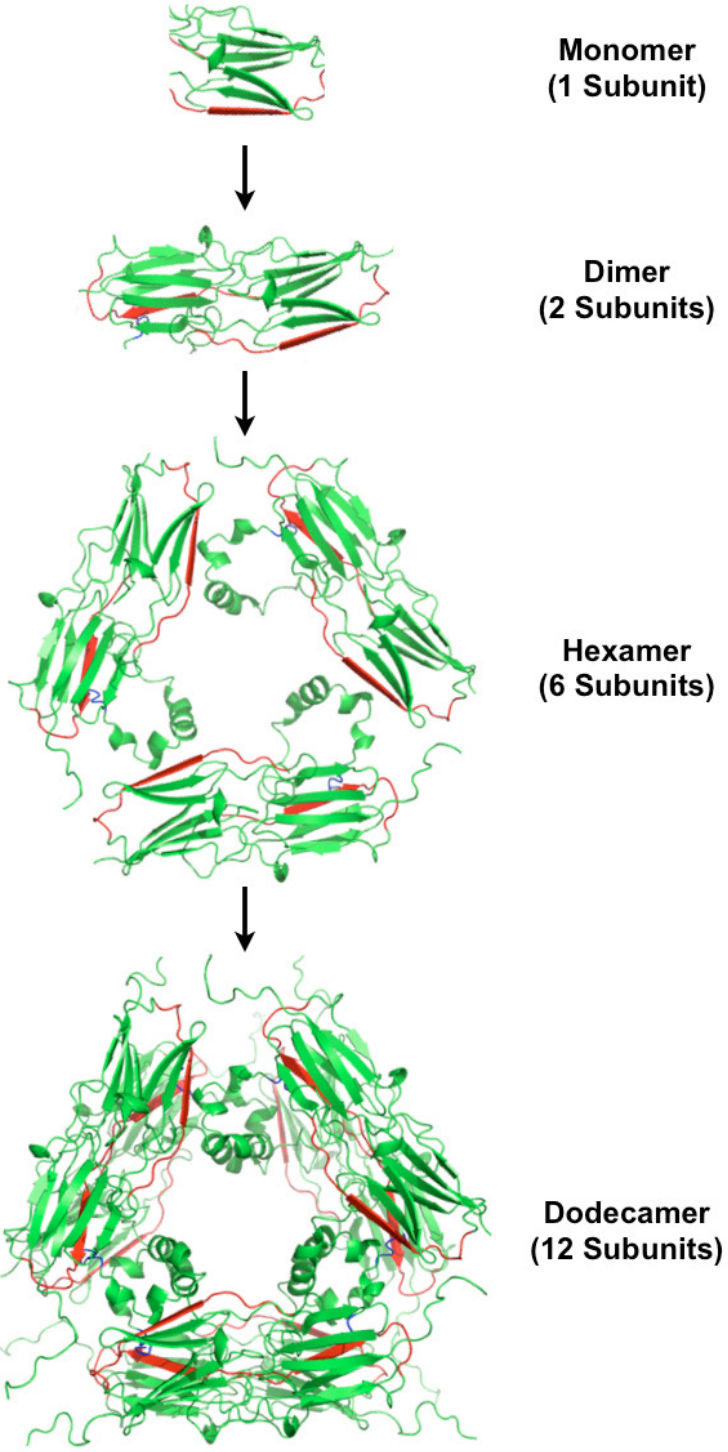

Fig 1.0. sHsp Oligomerisation.

Small heat shock proteins (sHsps) can assemble into large oligomeric complexes. Two sHsp monomers assemble into a dimer, which can then assemble into large oligomeric complexes. This figure shows a model of the small heat shock protein aB crystallin assembling into a dodecamer. The red regions are believed to be involved in substrate binding.

from heat stress (Basha et al., 2004a; Basha et al., 2004b) and apoptosis (Kamradt et al., 2005), but are also involved in the dynamics of the cytoskeleton, cellular growth, transcription and differentiation (Head and Goldman, 2000; Laskowska et al., 2010; Sun and MacRae, 2005). sHsps show differential expression dependent upon tissue type, which suggests specialised as well as general functions.

Four sHsps are associated with disease in humans; aA crystallin, aB crystallin, HSP27 and HSP22 (Raju et al., 2011; Selcen and Engel, 2003; Tang et al., 2005a; Tang et al., 2005b; Vicart et al., 1998). aA crystallin is abundantly expressed in the eye lens and its targeted disruption leads to cataract development in mice (Brady et al., 1997). Mutations in Hsp22 have been associated with neuropathies like distal hereditary motor neuropathy and Charcot Marie Tooth disease (Sun and MacRae, 2005). Upregulation of Hsp27 is associated with poor prognosis in gastric, liver, breast, lung and prostate cancer (Ciocca and Calderwood, 2005). Mutations in aB crystallin have been shown to cause cataract and cardiomyopathy (these mutations will be detailed in a later section). sHsps are also upregulated in a wide range of diseases, so defining the functions and mechanisms of sHsps has wide ranging implications for understanding cellular stress and disease.

sHsp chaperone mechanism

Structural, biochemical and biophysical studies have suggested different mechanisms of sHsp chaperone activity. However, all the proposed mechanisms involve structural rearrangement of the sHsp to expose hydrophobic regions, which act as substrate binding surfaces (Haslbeck et al., 2005a; Van Montfort et al., 2001a). sHsp-substrate complexes have a range of sizes depending on the sHsp and substrate, but also on the sHsp:substrate ratio and concentrations, and environmental conditions (Basha et al., 2006; Cheng et al., 2008; Ehrnsperger et al., 1997; Kelly et al., 2005; Lee et al., 1997; Rao et al., 1993; Stromer et al., 2003). The sHsp-substrate complex is also highly variable in structure. For example, a study of Hsp18.1 oligomer-substrate complexes showed over 300 stoichiometries of interaction (Stengel et al., 2010).

There are essentially two opposing sHsp chaperone activity theories; oligomer theory and dissociation theory. Oligomer theory (Augusteyn, 2004b; Avilov et al., 2004; Kim et al., 2003) suggests that the assembled oligomer is the active unit of chaperone activity and that substrates bind directly to the oligomer surface, without subunit dissociation (Kim et al., 2003). The model proposes that structural rearrangement of the oligomer exposes hydrophobic substrate binding regions on the oligomer surface (Ehrnsperger et al., 1999; Franzmann et al., 2005; Kim et al., 2003). Hsp26 has been proposed to protect substrates via heat induced rearrangement of a domain in the extended N-terminus, without subunit dissociation from the oligomer (Franzmann et al., 2008). Cross-linking studies with a-crystallin to prevent dissociation also showed chaperone activity for the assembled oligomer (Augusteyn, 2004b). In addition, an surface plasmon resonance (SPR) study suggested that a-crystallin subunits could only bind the substrate when assembled into an oligomer (Avilov et al., 2004). Furthermore, for sHsp Tsp36, association of dimers into tetramers increased chaperone activity (Kappe et al., 2004). However, experimental evidence in support of oligomer theory is limited.

Dissociation theory suggests that oligomer dissociation into smaller subunits exposes hydrophobic surfaces, which allows binding of client proteins. In fact, studies have shown substrate binding to sub-oligomeric species as small as monomers (Liu et al., 2006c). Once substrate binding has occurred, the subunits may re-associate into large soluble sHsp-substrate complexes, which may then interact with ATP dependent refolding machinery (Lee and Vierling, 2000; Mogk et al., 2003). It has also been suggested that, in cases where the sHsp cannot fully prevent substrate aggregation, sHsps may co-precipitate with the denaturing substrate (Basha et al., 2004a; Haslbeck et al., 2005b), forming insoluble sHsp-substrate complexes. These can then be more easily disaggregated by ATP dependent chaperones Hsp100/ClpB, and subsequently refolded by the Hsp70 system (Mogk et al., 2003). It has been suggested that sHsps are in dynamic equilibrium between an oligomeric state with low substrate affinity and a sub-oligomeric state with high substrate affinity (Sobott et al., 2002; Wintrode et al., 2003). Dissociation of subunits from the oligomer is thought to be required for chaperone activity, and sequences thought to mediate both oligomer assembly and chaperone activity have been proposed (Fu et al., 2005; Ghosh and Clark, 2005; Ghosh et al., 2005; Haslbeck et al., 2004; Lentze and Narberhaus, 2004; Pasta et al., 2004; Thampi and Abraham, 2003; Theriault et al., 2004). The oligomer may therefore act as a reservoir of sHsp

Fig 1.1. Theories of chaperone activity

Stress causes protein unfolding which can lead to aggregation, but sHsp chaperones can bind to unfolding substrate proteins to prevent their aggregation. There are two theories of sHsp chaperone activity; oligomer theory and dissociation theory. Oligomer theory suggests that stress causes a structural rearrangement of the sHsp oligomer, exposing hydrophobic regions which allows the unfolding substrate to bind directly to the oligomer surface. Dissociation theory suggests that stress causes oligomer dissociation into smaller subunits, exposing hydrophobic surfaces, which allows binding of the unfolding substrate proteins. Once substrate binding has occurred, the subunits may then re-associate into large soluble sHsp-substrate complexes.

(Figure on next page)

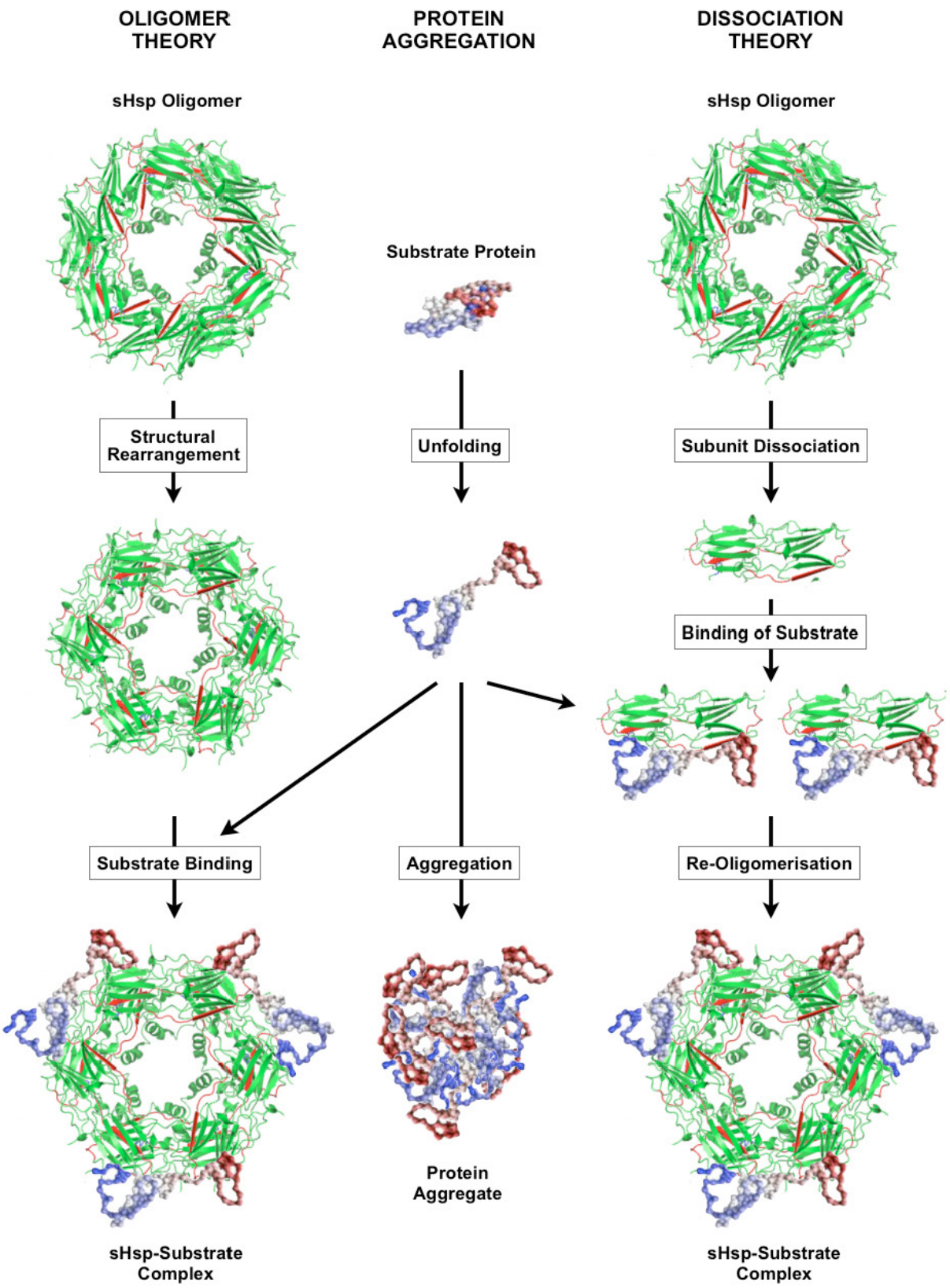

Fig 1.1. (Legend on previous page)

subunits, which are in continuous dynamic exchange with a pool of free subunits (Horwitz et al., 2004; Liu et al., 2006c; Narberhaus, 2002; Van Montfort et al., 2001a).

Many factors have been shown to influence subunit dynamics which subsequently affect oligomerisation and chaperone activity. These include temperature (Datta and Rao, 1999; Koretz et al., 1998; Liu et al., 2006c; Raman and Rao, 1994, 1997; Shashidharamurthy et al., 2005; Spinozzi et al., 2006), pH (Koretz et al., 1998; Liu et al., 2006c; Yun et al., 2002), divalent cations (del Valle et al., 2002; Duncan and Jacob, 1984; Ganadu et al., 2004; Marini et al., 1995; Marini et al., 2005), ATP (Biswas and Das, 2004; Ghosh et al., 2006c; Liu et al., 2006c; Muchowski et al., 1999a; Palmisano et al., 1995; Reddy et al., 1992) and phosphorylation (Aquilina et al., 2004; Ito et al., 2001; Kamei et al., 2001; Kantorow and Piatigorsky, 1998; Moroni and Garland, 2001). Interestingly, it has been reported that the sHsp oligomer:subunit equilibrium (Aquilina et al., 2003; Aquilina et al., 2005; Bova et al., 2000) is shifted to favour smaller subunits at elevated temperature (Giese and Vierling, 2002; Stromer et al., 2004; Van Montfort et al., 2001a; Van Montfort et al., 2001b; Wintrode et al., 2003), and that the rate of subunit exchange increases with temperature (Friedrich et al., 2004).

sHsp crystal structures

The dynamic nature of sHsps means that crystallographic data are difficult to obtain and are therefore limited. However, crystallographic studies have provided valuable insights into sHsp structure. The sequence of the conserved a-crystallin domain varies between sHsps, but the domain structure is highly conserved and thought to be responsible for dimer formation (Haslbeck et al., 2005a). sHsps Mj Hsp16.5 from the archaeon *Methanococcus jannaschii* and Ta Hsp16.9 from *Triticum aestivum* (wheat) share only 23% sequence identity, but the structures of the a-crystallin domains are very similar with an identical dimer interface (Van Montfort et al., 2001b). Indeed, studies have shown that dimer formation for both these proteins requires a-crystallin domain b2 and b6 strand exchange between monomers, and that both oligomeric structures assemble from dimeric units (Kim et al., 1998; Van Montfort et al., 2001b).

Mj Hsp16.5 assembles into a 24-subunit hollow sphere with eight triangular and six square pores arranged in octahedral symmetry (Kim et al., 1998). Cryo-EM and site-directed spin labelling showed that the 24 N-terminal arms of Mj Hsp16.5 occupy the centre of the hollow sphere of the oligomer (Haley et al., 2000; Koteiche et al., 2005). Ta Hsp16.9 assembles into a dodecamer (12 subunits) composed of two discs, each comprising three dimers and connected by a network of intersubunit contacts (Van Montfort et al., 2001b). Xa HspA from the plant pathogen *Xanthomonas* forms hexamers comprised of closed or open trimers of dimers, but size exclusion chromatography suggests the protein assembles into a 36 subunit oligomer in solution (Hilario et al., 2011).

The N-terminus of both Mj Hsp16.5 and Ta Hsp16.9 is thought to be highly flexible and was not resolved in the Mj Hsp16.5 crystal structure, with only 6 of the 12 N-termini resolved in the Ta Hsp16.9 crystal structure. Indeed, the crystal structures of Xa HspA and St Hsp14.0 (from *Sulfolobus tokodaii, a* thermoacidophilic crenarchaeon) also show disordered N-termini (Hilario et al., 2011; Takeda et al., 2011). However, the 6 N-termini that were resolved in Ta Hsp16.9 were involved in stabilising the oligomer by interaction of the a2 helix of one disc with the a2 helix of the other disc (Van Montfort et al., 2001b). In contrast, truncation of Mj Hsp 16.5 showed that the N-terminal arm is not required for Hsp16.5 oligomer formation (Koteiche and McHaourab, 2002).

Limited structural data is also available for the sHsp, aB crystallin. This will be discussed in a later section following an introduction to the functions of the protein.

aB crystallin

a-crystallin is a molecular chaperone (Borkman and McLaughlin, 1995; Carver et al., 1994; Horwitz, 1992; Rao et al., 1993). It comprises of two sHsps, aA crystallin (19.9kDa) and aB crystallin (20.2kDa), which assemble in a 3:1 ratio to form polydisperse heterogeneous oligomers of between 15-50 subunits, with an average molecular mass of 800kDa (Horwitz, 2008). a-crystallin accounts for ~35% of total mammalian lens protein and is vital to lens transparency, viscosity and refractive index (Augusteyn, 2004a; Horwitz, 2003). While aA crystallin is almost entirely lens specific, aB crystallin is widely expressed in other tissues

including cardiac and skeletal muscle (Salinthone et al., 2008) where it functions independently of aA crystallin.

aB crystallin can assemble into homologous oligomers as diverse as 10-40 subunits, but the dominant species is composed of 28 subunits (564 kDa) (Aquilina et al., 2003). aB crystallin provides essential protection against stress induced protein aggregation (Datta and Rao, 1999), responding to stress (Arrigo et al., 2007) in the kidney, brain, skin, heart, lens and muscle (Atomi et al., 1991; Bhat et al., 1991; Iwaki et al., 1991; Iwaki et al., 1990; Iwaki et al., 1989; Kato et al., 1992). Indeed, studies have shown that aB crystallin knock-out causes skeletal muscle dystrophy and shorter life spans in mice (Boyle et al., 2003).

Studies have also suggested that aB crystallin interacts with kidney specific cadherin (Ksp-cadherin). Indeed, Ksp-cadherin and aB crystallin have been shown to co-sediment with actin from kidney lysates (Thedieck et al., 2008). Although no function of Ksp-cadherin has been directly demonstrated, it is believed to act as a cell-cell adhesion molecule to maintain kidney tissue integrity (Wendeler et al., 2004) and may also play a role in cell signaling, as described for other cadherins (McLachlan and Yap, 2007). aB crystallin may act as a linker between Ksp-cadherin and the cytoskeleton. Studies have also suggested aB crystallin interactions with myosin, the molecular motor that drives actomyosin-based motility by ATP dependent conformational changes (Geeves et al., 2005). Indeed, although heat shock causes loss of myosin enzymatic activity followed by formation of aggregates (Nozais et al., 1992), aB crystallin is able to maintain the enzymatic activity of the motor and prevent its aggregation (Melkani et al., 2006). Indeed, aB crystallin may be critical for maintaining myosin integrity *in vivo* and sustaining muscle function during heat shock conditions. Interestingly, it has been found that aB crystallin is more highly expressed in the skeletal muscles of athletes compared to non-athletes where vigorous exercise results in heat shock conditions (Yoshioka et al., 2003).

In addition to chaperoning individual client proteins, studies have shown that aB crystallin also interacts with a range of multi-protein complexes, including filaments (Ghosh et al., 2007b), tubules (Ghosh et al., 2007a) and fibrils (Ghosh et al., 2008). Indeed, aB crystallin has been shown to stabilise actin filaments and regulate actin assembly dynamics, both *in vitro* (Ghosh et al., 2007b; Wieske et al., 2001) and in cultured cells (Singh et al., 2007). In addition, reduced aB crystallin expression leads to disruption of the actin microfilament

network (Iwaki et al., 1994). aB crystallin has also been shown to interact with microtubules (MTs) and can stabilise tubulin and modulate MT assembly and disassembly, both *in vitro* and in unstressed cells, thus maintaining MT integrity (Arai and Atomi, 1997; Bluhm et al., 1998; Fujita et al., 2004; Ghosh et al., 2007a; Kato et al., 1996). aB crystallin also interacts with intermediate filament (IF) networks *in vivo* (Kasakov et al., 2007; Perng et al., 1999a) to maintain the individuality of IFs (Perng et al., 1999a) and modulate filament-filament interactions within networks (Perng et al., 2004). This will be discussed in detail in a later section.

Studies have also suggested that aB crystallin may interact with cardiac muscle titan (Bullard et al., 2004; Golenhofen et al., 2002). Antibody labelling in sectioned fibers has shown that aB crystallin binds to cardiac titan via the N2B region, and also perhaps via the titan Ig domains (Bullard et al., 2004; Zhu et al., 2009). Titin is a large filamentous protein in vertebrate striated muscle which regulates sarcomere assembly and force transmission at the Z-line, maintains resting tension in the I-band region (Granzier and Labeit, 2004; Tskhovrebova and Trinick, 2003) and also acts as an anchoring protein for the other sarcomere/Z-disc proteins (Tskhovrebova and Trinick, 2003). Interestingly, under stress conditions aB crystallin moves from the cytosol to the I-band of skeletal muscle (Bullard et al., 2004; Golenhofen et al., 2004) and binds to myofibrils via the titin N2B region. This is thought to help prevent Ig domain unfolding and maintain elasticity in the titan N2B spring region (Kumarapeli and Wang, 2004; Zhu et al., 2009), which is essential for function.

There are 11 known human disease causing aB crystallin mutants (see Table 1.1). Of these 11 mutants, 9 have pathology restricted to either the lens or muscle, even though aB crystallin is highly expressed in both tissues (Kato et al., 1991). R120G and D109H are the only known aB crystallin mutations that cause both lens and muscle pathologies (Sacconi et al., 2011; Vicart et al., 1998). These data suggests that tissue specific interactions of aB crystallin may underlie the disease phenotypes. However, sub-clinical pathology may exist for other aB crystallin mutations, for example Q151X, as tissue biopsies from apparently unaffected tissues were not analysed in detail (Selcen and Engel, 2003).

The most widely studied aB crystallin mutant is the R120G, which causes both cataract and myopathy in humans. The R120G aB crystallin mutation alters the charge within the conserved a-crystallin domain causing decreased β-sheet secondary structure, partial unfolding and increased hydrophobicity which affects oligomerisation, chaperone activity and interaction with IFs (Bova et al., 1999; Kumar et al., 1999; Perng et al., 2004). Indeed, R120G aB crystallin oligomers are larger and more polydisperse than those formed by WT aB crystallin (Bova et al., 1999). In fact, R120G aB crystallin itself forms protein amyloid (Meehan et al., 2007), which inhibits the proteasome (Chen et al., 2005) and induces autophagy (Tannous et al., 2008). In addition, proteasome inhibition causes accumulation of aB crystallin into aggresomes (Ito et al., 2002) which can cause IF aggregation (Bardag-Gorce et al., 2004). The mutation also causes mitochondrial toxicity (Maloyan et al., 2005) and a state of reductive stress (Bova et al., 1999; Gupta and Srivastava, 2004; Rajasekaran et al., 2007; Treweek et al., 2005). The R120G mutation will be discussed further in a later section.

Mutation	Location	Disease	Reference
R11H	N-terminal head	cataract (AD)	(Chen et al., 2009)
P20S	N-terminal head	cataract (AD)	(Liu et al., 2006d)
R56W	N-terminal head	cataract (AR)	(Safieh et al., 2009)
D140N	a-crystallin domain	cataract (AD)	(Liu et al., 2006e)
A171T	C-terminal tail	cataract (AD)	(Devi et al., 2008)
del450A	-	cataract (AD)	(Berry et al., 2001)
Q151X	C-terminal tail	myofibrillar myopathy (AD)	(Selcen and Engel, 2003)
del464CT	-	myofibrillar myopathy (AD)	(Selcen and Engel, 2003)
R157H	C-terminal tail	cardiomyopathy (AD)	(Inagaki et al., 2006)
D109H	a-crystallin domain	cataract & myofibrillar myopathy (AD)	(Sacconi et al., 2011)
R120G	a-crystallin domain	cataract & cardiomyopathy (AD)	(Vicart et al., 1998)

Table 1.1. Naturally occurring, human disease causing mutations in aB crystallin.

The table shows the 11 known human disease causing aB crystallin mutants, 9 of which have pathology restricted to either the lens or muscle. The form of inheritance is also shown as autosomal dominant (AD) or autosomal recessive (AR). R120G and D109H are the only known aB crystallin mutations that cause both lens and muscle pathologies. The myopathy causing 464delCT aB crystallin mutation incorporates an 8 codon missense mutation and a premature stop codon resulting in a 162 residue mutant. The cataract causing 450delA frameshift mutation introduces a novel 35 amino acid sequence producing a 184 residue protein. The myopathy causing Q151X aB crystallin (Selcen and Engel, 2003) removes the entire C-terminal tail.

aB crystallin structure

Studies have shown that aB crystallin oligomers are polydisperse and in dynamic equilibrium with sub-assembly species, making crystallisation unobtainable to date (Aquilina et al., 2003; Bloemendal et al., 2004; Haley et al., 2000; Haley et al., 1998; Horwitz, 2008; McHaourab et al., 2009). It has even been suggested that the aB crystallin dimer itself may exhibit conformational flexibility (Clark et al., 2011). Cryo-EM studies into the oligomeric structure show spherical assemblies that are 8-18 nm in diameter with a central cavity (Haley et al., 2000). The full length aB crystallin protein has not yet been crystallised but removal of the hydrophobic N-terminal domain and hydrophilic C-terminal domain has allowed crystallisation of the core a-crystallin domain (ACD). Recently, the available structural data from crystallisation, solid state NMR, SAXS, and EM was used to produce an atomic-level model of full-length aB crystallin (Jehle et al., 2011). The model predicts that dimer formation occurs when monomers exchange the b6+7 strand within the a-crystallin domain (ACD) (Fig 1.2). The C-terminal IXI motif of one dimer is then predicted to interact with a hydrophobic groove created by the b4 and b8 strand edges of another dimer, and previous studies have suggested that this interaction may be essential for correct oligomer assembly (Bagneris et al., 2009; Jehle et al., 2010; Jehle et al., 2011; Laganowsky et al., 2010; Laganowsky and Eisenberg, 2010; Pasta et al., 2004). In addition, the C-terminal 163-REEK-166 motif is also predicted to be important for correct oligomer assembly (Hayes et al., 2008; Rajan et al., 2006) (Fig 1.2). aB crystallin dimers are thought to arrange in a triangular array that defines a threefold axis and assemble into a symmetric 24-subunit oligomer (Jehle et al., 2011). The model then predicts formation of larger oligomers via incorporation of dimers into 6 existing openings in the shell of the 24-mer. Thus, a 26-mer would contain one additional dimer in any one of 6 openings; a 28-mer would contain two dimers, distributed randomly, and so on, up to a 36-mer (Jehle et al., 2011).

It it has been suggested that dissociation of the C-terminal IXI motif from the b4-b8 hydrophobic groove both exposes a substrate binding site and partially destabilises the aB crystallin oligomer. In the full-length aB crystallin 24-mer model (Jehle et al., 2011), the b4-b8 hydrophobic groove faces outwards in half the subunits and inwards in the other half. Changes in environmental conditions which activate aB crystallin may cause dissociation of the C-terminal IXI motif (Jehle et al., 2010) from the outward-facing grooves, thus exposing

substrate binding sites, while the internal grooves maintain interactions with C-terminal IXI motifs, thus maintaining the hexameric unit (Jehle et al., 2011). Interestingly, Friedrich et al. 2004 reported that only a certain population of sHsp subunits within a sHsp-substrate complex can be exchanged (Friedrich et al., 2004). Limited proteolysis data also supports the theory of two populations of sHsps within a sHsp-substrate complex (Jaya et al., 2009).

Thus far, crystallographic studies of aB crystallin have only been made possible by truncating the N-terminus, so the structural details of the N-terminus are limited. The N-terminal 59-SWF-61 motif (Fig 1.2) is predicted to be involved in oligomer formation by interacting with the b3 strand from an adjacent dimer (Jehle et al., 2010). In addition, the N-terminal SXXFD (Fig 1.2) motif is also predicted to be involved in oligomer formation by interacting with a hydrophobic groove in the ACD of an adjacent dimer (Pasta et al., 2003). However, the specific nature and role of the N-terminus in aB crystallin structure remains to be determined.

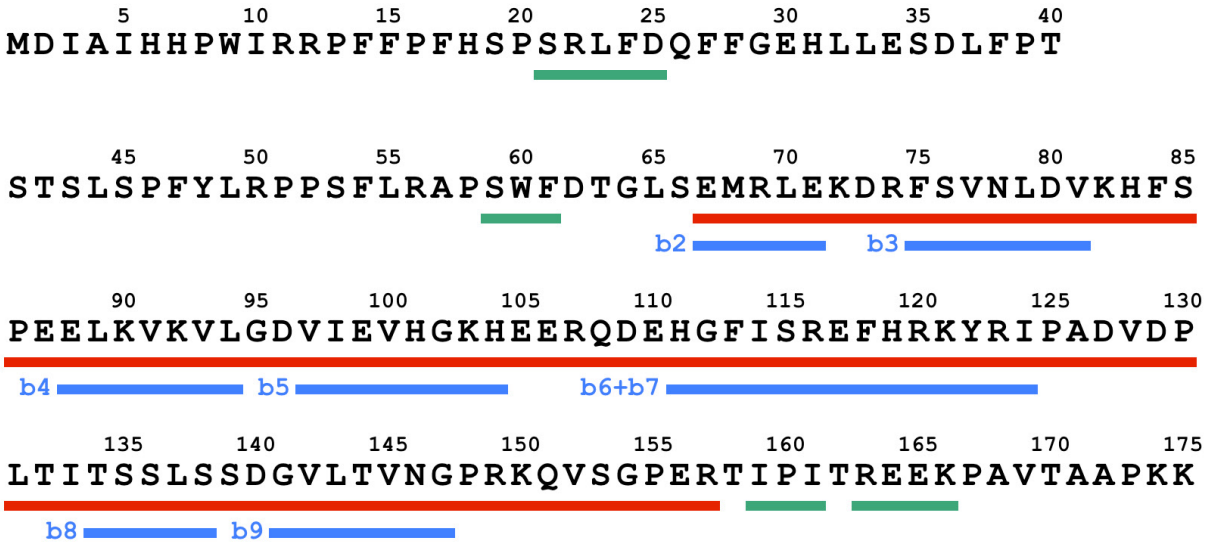

Fig 1.2. Domains in human aB crystallin.

The sequence for human aB crystallin is shown. The a-crystallin domain (ACD) (red line) and b-strands (blue lines) are shown. The 21-SRLFD-25, 59-SWF-61, 159-IXI-161 and 163-REEK-166 motifs are thought to be involved in oligomer formation (Jehle et al., 2010; Jehle et al., 2011; Pasta et al., 2003; Rajan et al., 2006).

INTERMEDIATE FILAMENTS

The cytoskeleton is a dynamic network of intermediate filaments (IFs), microfilaments (MFs) and microtubules (MTs), and is essential to cell mechanical properties, cell signaling, the stress response and cell integration into tissues (Herrmann et al., 2009; Janmey et al., 2009; Kim and Coulombe, 2007; Quinlan, 2002; Vogel and Sheetz, 2009). MTs are involved in intracellular trafficking, actin MFs are involved in contraction and cell polarity and motility, while IFs are involved in cell structural support, organisation and signaling (Fuchs and Yang, 1999; Kim and Coulombe, 2007).

The IF family is the largest of the three filament groups encoded by ~70 genes (Szeverenyi et al., 2008) and on basis of sequence, IFs are classified into six types (Fuchs and Weber, 1994). Types I–IV and Type VI are localised to the cytoplasm while type V are localised to the nuclear envelope and karyoplasm. Type I and Type II are keratins. Type III comprises vimentin, desmin, glial fibrillary acidic protein (GFAP) and peripherin which share >70% sequence identity. Type IV comprises the neurofilament proteins, α-internexin and syncoilin. Type V are lamins and Type VI comprises the beaded filament structural proteins, BFSP1 and BFSP2.

IFs provide mechanical resistance to physical and biochemical stresses (Herrmann et al., 2009; Kim and Coulombe, 2007). IFs also provide a scaffold for protein chaperones, (Perng et al., 1999a) the proteasome (Arcangeletti et al., 1997) and other cytoskeletal elements and are involved in stress signaling pathways and interact with stress activated kinases (D'Alessandro et al., 2002; Kim and Coulombe, 2007; Quinlan, 2002). While IFs can be membrane associated (Franke et al., 1987a; Sandilands et al., 1995a; Song et al., 2009), they can also traverse the cell cytoplasm (Janmey et al., 2009; Kim and Coulombe, 2007) and therefore require mechanisms to prevent unwanted filament-filament interactions which may lead to aggregation (Perng et al., 1999a; Quinlan, 2002).

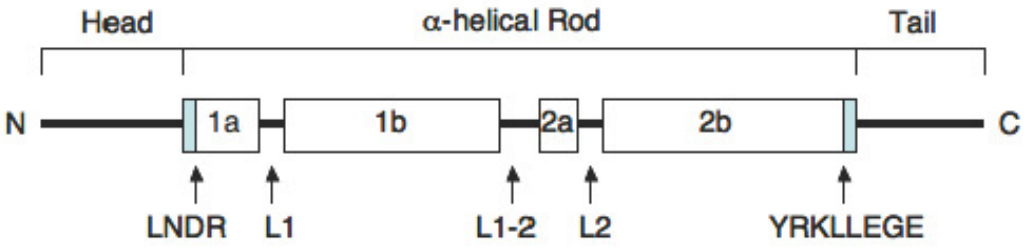

Fig 1.3. Predicted secondary structure for a typical IF protein.

IF proteins are composed of an α-helical coiled-coil domain flanked by two non-helical N- and C-termini. The boxes represent α-helical domains which are separated by the non-helical linkers, L1, L1-2 and L2. The blue boxes at the ends of helix 1a and 2b represent the highly conserved LNDR and YRKLLEGE motifs which are important for the assembly of IF proteins into filaments.

All IF proteins share a highly conserved central α-helical coiled-coil rod domain (Fig 1.3) of between 310-350 residues (~45 nm) which allows formation of parallel dimers. The α-helical domain comprises the four coiled coil sub-domains 1A, 1B, 2A and 2B which are connected by the three non-α-helical linkers L1, L1-2 and L2. The α-helical domain has a heptad repeat pattern with every 1st and 4th residue as an apolar Leu, Ile, Met or Val, which allows the formation of a coiled coil dimer (Parry, 2005). The highly conserved LNDR and TYRKLLEGEE motifs lie at the N- and C-terminal ends of the α-helical domain, respectively (Magin et al., 1987). The YRKLLEGEE motif has been shown to be crucial to tetramer formation and filament width control (Herrmann et al., 2000).

The α-helical domain is flanked by non-α-helical amino 'head' and carboxy 'tail' domains (Geisler et al., 1982; Herrmann and Aebi, 2004), which become ordered upon formation of higher order oligomers (Herrmann and Aebi, 2004). Between IF Types, the head and tail domains show most sequence diversity, but are usually well conserved within Types (Nielsen and Jorgensen, 2003; Parry, 2005). The tail domain length varies greatly between classes with, for example, 15 residues in keratin K19 and 1300 residues in nestin. The head domain contains the nonapeptide motif SSYRRXFGG which is conserved within IF proteins able to form copolymers (Herrmann et al., 1992, -1957). Unassembled IF proteins are insoluble in physiological conditions which prevents crystallisation, and as such and there is no atomic level data on IF structure (Strelkov et al., 2001).

Desmin

The IF protein desmin is expressed in cardiac, skeletal and smooth muscle (Lazarides, 1980) and has properties not observed for other Type III IFs, including developmentally regulated expression, polymorphic assembly and unusual mechanical properties (Herrmann et al., 1999; Kreplak et al., 2008a). Desmin filaments help to form a continuous cytoskeletal network that maintains a spatial relationship between the contractile apparatus and other structural elements of the cell, thus providing maintenance of cellular integrity, force transmission, and mechanochemical signaling (McLendon and Robbins, 2011; Selcen, 2011; Van Spaendonck-Zwarts et al., 2010). Indeed, mice lacking desmin have muscles which are mechanically fragile and degenerate upon repeated contractions (Li et al., 1996; Li et al., 1997; Milner et al., 1996). This leads to cardiomyopathy and skeletal myopathy, smooth muscle dysfunction, reduced life span and low tolerance to exercise induced muscle injury (Capetanaki and Milner, 1998). In mature skeletal muscle, desmin filaments interlink myofibrils and connect the myofibrillar apparatus to nuclei, subsarcolemmal cytoskeleton and cytoplasmic organelles via the plectin linker protein (Favre et al., 2011; Fuchs and Weber, 1994; Goldfarb et al., 2004; Herrmann and Aebi, 2000; Hijikata et al., 1999; Schroder et al., 2000).

There are many disease causing desmin mutations spread throughout the protein sequence which cause a range of phenotypes (Table 1.4), however all cause IF aggregation (Goldfarb and Dalakas, 2009). Desmin related myopathies (Levin et al., 2010) lead to intracellular accumulation of misfolded protein and production of soluble pre-amyloid oligomers, which leads to weakened skeletal and cardiac muscle (McLendon and Robbins, 2011). Mutations in desmin can also impair the proteasome system (Liu et al., 2006a; Liu et al., 2006b), as can other IF mutants (Cho and Messing, 2009; Yoneda et al., 2004) because IF proteins are normally turned over by the proteasome (Ku and Omary, 2000). Desmin is also an important binding partner of aB crystallin, which will be discussed in detail in a later section.

Table 1.4. Human disease causing desmin mutations.

The table shows all the known, naturally occurring, human disease causing desmin mutations. All mutations are autosomal dominant inheritance. The desmin region in which the mutation occurs is also shown. Adapted from: (Simon and Arrigo, 2011).

(Table on next page)

REGION	MUTATION	DISEASE	REFERENCES
head	S2I	cardioskeletal myopathy	(Selcen et al., 2004)
head	S13F	cardioskeletal myopathy	(Bergman et al., 2007; Pica et al., 2008)
head	R16C	restrictive cardiomyopathy	(Arbustini et al., 2006)
head	S46F	cardioskeletal myopathy	(Selcen et al., 2004)
head	S46Y	cardioskeletal myopathy	(Selcen et al., 2004)
head	E108K	cardiomyopathy	(Kostareva et al., 2006; Taylor et al., 2007)
1B	del173-179	cardioskeletal myopathy	(Munoz-Marmol et al., 1998)
1B	A213V	cardioskeletal myopathy	(Kostareva et al., 2006)
1B	del214-245	cardioskeletal myopathy	(Arbustini et al., 2006; Kostareva et al., 2006; Park et al., 2000a)
1B	K240del	skeletal myopathy	(Schroder et al., 2007)
1B	E245D	skeletal myopathy	(Vrabie et al., 2005)
2B	S298L	cardiomyopathy	(Taylor et al., 2007)
2B	D312N	cardiomyopathy	(Taylor et al., 2007)
2B	A337P	cardiomyopathy	(Dalakas et al., 2000; Goldfarb et al., 1998; Goudeau et al., 2006)
2B	L338R	cardiomyopathy	(Goudeau et al., 2006)
2B	N342D	cardiomyopathy	(Dalakas et al., 2000; Schroder et al., 2003)
2B	L345P	cardioskeletal myopathy	(Carlsson et al., 2002; Sjoberg et al., 1999)
2B	R350P	scapuloperoneal syndrome and myopathies	(Bar et al., 2005; Walter et al., 2007)
2B	R350W	cardiomyopathy	(Taylor et al., 2007)
2B	R355P	cardioskeletal myopathy	(Fidzianska et al., 2005)
2B	A357P	cardiomyopathy	(Dagvadorj et al., 2003)
2B	del359-361	skeletal myopathy	(Kaminska et al., 2004)
2B	A360P	cardiomyopathy	(Dalakas et al., 2000; Goldfarb et al., 1998)
2B	delN366	cardioskeletal myopathy	(Kaminska et al., 2004)
2B	I367F	cardioskeletal myopathy	(Olive et al., 2007)
2B	L370P	cardiomyopathy	(Sugawara et al., 2000)
2B	L385P	cardioskeletal myopathy	(Dagvadorj et al., 2003)
2B	Q389P	cardioskeletal myopathy	(Goudeau et al., 2001)
2B	L392P	cardioskeletal myopathy	(Olive et al., 2007)
2B	N393I	cardioskeletal myopathy	(Dalakas et al., 2000; Goldfarb et al., 1998; Goudeau et al., 2006)
2B	R406W	cardioskeletal myopathy	(Arbustini et al., 2006; Dalakas et al., 2000; Fidzianska et al., 2005; Olive et al., 2004; Park et al., 2000b)
tail	E413K	restrictive cardiomyopathy	(Pruszczyk et al., 2007)
tail	P419S	cardioskeletal myopathy	(Olive et al., 2007; Taylor et al., 2007)
tail	K449T	cardioskeletal myopathy	(Selcen et al., 2004)
tail	I451M	cardioskeletal myopathy	(Bluhm et al., 1998; Dalakas et al., 2000; Li et al., 1999)
tail	T453I	restrictive cardiomyopathy	(Arbustini et al., 2006)
tail	R454W	cardiomyopathy	(Bar et al., 2007)
tail	V459I	restrictive cardiomyopathy	(Taylor et al., 2007)
tail	V469M	EmeryDreyfuss muscular dystrophy	(Muntoni et al., 2006)

Table 1.4. (Legend on previous page)

Desmin assembly

Under suitable conditions, desmin self-assembles into ~10nm filaments (Herrmann et al., 2009) and assembly is thought to proceed via the same mechanism as vimentin assembly (Herrmann and Aebi, 2000). Unassembled desmin or vimentin proteins are insoluble in physiological buffer conditions, so Urea is used to solublise the monomeric subunits when assembling *in vitro*. Dialysis into buffers of low ionic strength and high pH (e.g. 20mM Tris-HCl pH 8.0) causes tetramer formation by lateral association of two anti-parallel, half staggered coiled coil dimers (Herrmann et al., 2009; Parry and Steinert, 1999). Further dialysis into buffers of physiological pH and ionic strength (e.g. 20mM Tris-HCl pH 7.6, 50mM NaCl) causes the lateral association of eight tetramers (Fig 1.5) to form non-compacted unit length filaments (ULFs), ~17 nm wide and ~60 nm long (Herrmann and Aebi, 2004; Herrmann et al., 1996; Herrmann et al., 2009; Kirmse et al., 2007). ULFs then associate longitudinally with possible molecular rearrangements (Herrmann et al., 2009; Kirmse et al., 2007). Finally, filaments compact radially (final width is 10-12nm) by intrafilamentous subunit reorganisation without a change in mass per length (MPL) (Herrmann et al., 2009). Time lapse TEM has been used to confirm the different filament assembly stages including ULF formation, longitudinal association, radial compaction and subsequent filament network formation (Kreplak et al., 2008b). Interestingly, studies have shown that IF proteins have different numbers of subunits per filament cross section and thus different MPLs (Herrmann et al., 1999). For example, desmin MPL is 48±8 kDa/nm which corresponds to ~37 subunits per filament cross section (Wickert et al., 2005). In contrast, vimentin MPL is 33±4 kDa/nm corresponding to only ~30 molecules per cross section (Wickert et al., 2005).

The N-terminal head domain of desmin and vimentin is thought to be essential for filament formation since removal or truncation prevents higher order filament assembly (Geisler et al., 1982; Traub and Vorgias, 1983, -1988). When the head domain of vimentin is removed, the protein cannot assemble beyond tetramers, which may indicate altered tetramer structure (Herrmann et al., 1996; Mucke et al., 2004). Indeed, it has been suggested that interaction of the basic N-terminal head domain with the acidic C-terminal tail, may help position dimers during tetramer formation (Parry et al., 2007). Interestingly, post-translational (PT) modifications are mostly found in the head and the tail domains (Fuchs and Weber, 1994) and phosphorylation (which introduces negative charge) of serine residues in the head domain of

vimentin or desmin can cause filament disassembly (Inada et al., 1999). The head domain of human desmin has 21 serine residues and many are potential phosphorylation sites (Sharma et al., 2009). Furthermore, 4 disease causing mutations in the desmin head domain involve serine substitution by hydrophobic residues (S2I, S13F, S46F and S46Y, see Table 1.4). In addition, the head domain also contains a highly conserved nonapeptide motif SSYRRXFGG (Herrmann et al., 1992) and deletion or mutation of this domain in vimentin can disturb filament assembly *in vitro* and filament networking *in vivo* (Sharma et al., 2009).

Unlike the N-terminal head domain, the C-terminal tail domain of IFs is not required for filament assembly, but is thought to play an important role in filament-filament interactions (Bousquet et al., 2001; Lin et al., 2010) and regulation of filament width (Herrmann and Aebi, 2004; Herrmann et al., 1996). Indeed, deletion of the GFAP tail domain alters its assembly and changes filament morphology in cells (Chen and Liem, 1994). In addition, the R416W point mutation in the C-terminal tail domain of GFAP causes IF aggregates and the neurodegenerative disease, Alexander disease (Der Perng et al., 2006; Quinlan et al., 2007). The C-terminal domain of IF proteins is therefore thought to be crucial to IF function in cells.

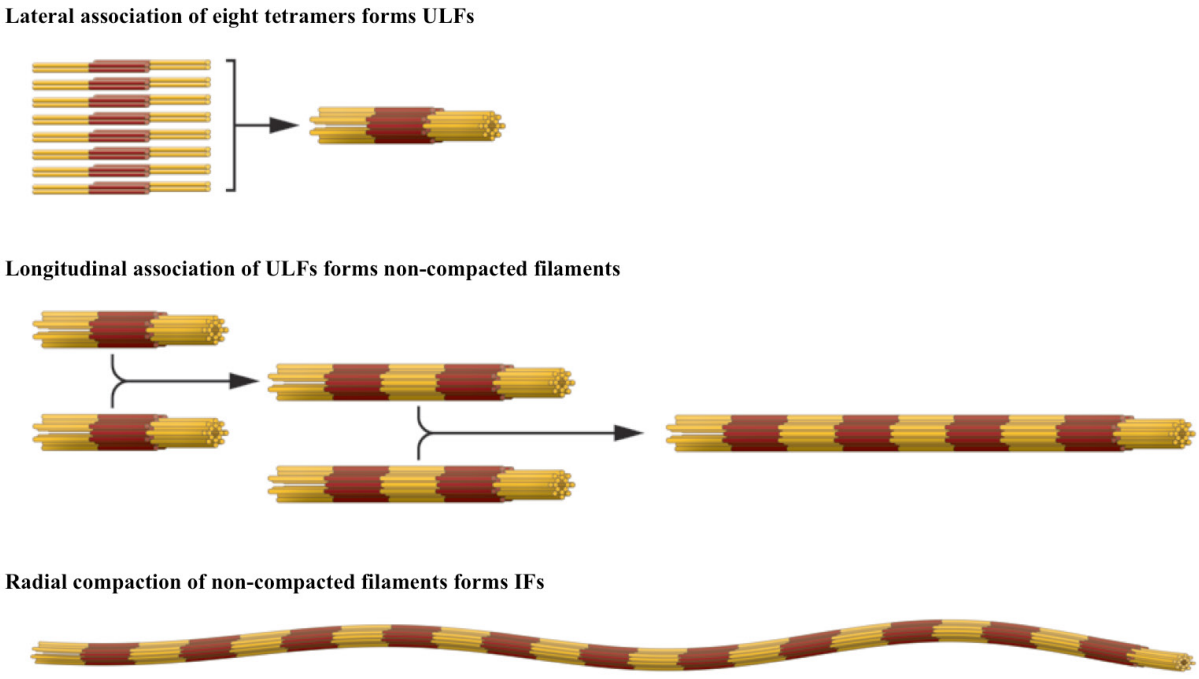

Fig 1.5. Diagram of IF assembly.

Lateral association of eight tetramers form unit length filaments (ULFs). UFLs associate longitudinally to form filaments, which then compact radially to form 10-12nm IFs. Figure adapted from: (Herrmann et al., 2009).

Beaded filaments

There are many IF proteins expressed in the lens including beaded filament structural protein 1 (BFSP1), BFSP2 (Ireland et al., 2000), vimentin (Ramaekers et al., 1980; Sandilands et al., 1995a), glial fibrillary acidic protein (GFAP) (Bozanic et al., 2006), simple epithelial keratins (Bozanic et al., 2006; Kasper and Viebahn, 1992), nestin (Mokry and Nemecek, 1998; Yang et al., 2000), and synemin (Tawk et al., 2003) (see Table 1.6). The lens specific beaded filaments (BFs) are composed of BFSP1 and BFSP2, members of the IF family (Masaki and Watanabe, 1992; Sawada et al., 1995), which co-assemble into 5-6nm filaments (Goulielmos et al., 1996; Merdes et al., 1993). These filaments have a unique relationship with the sHsp, a-crystallin, and are found *in vivo* with 12-15nm a-crystallin 'beads' bound along their length (FitzGerald and Casselman, 1991; Maisel and Perry, 1972). This will be discussed further in a later section.

BFs are essential to mammalian lens optical properties (Song et al., 2009). Indeed, BF mutations can cause cataracts in humans (Conley et al., 2000; Jakobs et al., 2000; Ma et al., 2008; Perng et al., 2007; Ramachandran et al., 2007) and BF proteins are targeted by proteolysis during cataract formation (Marcantonio, 1992; Oka et al., 2008). BFs are thought to contribute to the highly specialised cellular organisation of lens fibre cells (Augusteyn, 2007) and the precise alignment of fibre cell membranes which minimises intercellular spaces and maintains the high refractive index of the lens (Michael et al., 2003). Cytoplasmic protein concentrations in the lens are extremely high (>300 g/l) (Bloemendal et al., 2004) and protein crowding must be regulated by chaperones to preventing aggregation (Ellis and Minton, 2006). It has been suggested that BFs may help to stabilise these high protein concentrations through interactions with protein chaperones (Song et al., 2009), since beaded filaments are naturally complexed with a-crystallins in the lens (Carter et al., 1995; Quinlan et al., 1996). A review of proposed BF functions is shown in Fig 1.7 (Song et al., 2009).

IF PROTEIN	DEVELOPING LENS		ADULT LENS	
	Epithelium	Fibers	Epithelium	Fibers
BFSP1 (Filensin)	x	✓	x	✓
BFSP2 (CP49)	x	✓	x	✓
Vimentin	✓	✓	✓	✓
GFAP	✓	x	✓	x
K8 / 18 / 19	✓	x	✓	x
Nestin	✓	✓	x	x
Synemin	✓	✓	✓	✓

Table 1.6. IF expression in the lens.

The table shows the IF proteins expressed in the developing and adult lens. BFSP1 and BFSP2 are expressed in both the developing and adult lens but are fiber cell specific and are not present in epithelial cells. Ticks indicate the presence of a protein while crosses indicate the absence.

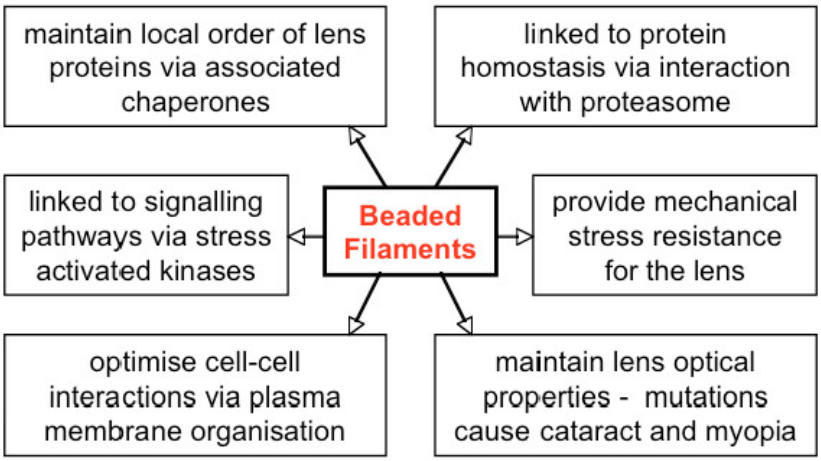

Fig 1.7. Predicted functions of the beaded filaments.

The diagram shows functions predicted for BFs (Song et al., 2009).

BF proteins are not expressed in the epithelial cells of the adult lens (Table 1.6), but are found in lens fibre cells (Sandilands et al., 1995b) at all stages of differentiation (Blankenship et al., 2001; Sandilands et al., 1995a) and during lens fibre cell elongation (Blankenship et al., 2001; Ireland et al., 2000). BFs can associate with the plasma membranes of lens fiber cells (Brunkener and Georgatos, 1992; FitzGerald, 1990) and association is thought to involve IF-binding proteins from the spectraplakin family (Franke et al., 1987b; Sandilands et al., 1995a; Song et al., 2009; Straub et al., 2003; Yoon and FitzGerald, 2009). It is though that BF association with the plasma membrane is dependent upon cell differentiation stage (Sandilands et al., 1995a) and influenced by proteolytic fragmentation (Sandilands et al., 1995b) and phosphorylation (Ireland et al., 1993). BFSP1 and BFSP2 have also been shown to bind periplakin, a vimentin binding protein (Yoon and FitzGerald, 2009) and AQP0, an integral plasma membrane protein (Lindsey Rose et al., 2006). In addition, BFSP1 has also been shown to interact with Tropomodulin, an actin binding protein (Fischer et al., 2003).

Mouse BF knockout studies have demonstrated the importance of BFSPs to lens optical properties (Alizadeh et al., 2003, 2004; Alizadeh et al., 2002; Sandilands et al., 2003; Sandilands et al., 2004). Indeed, removal of BFSP2 results in the loss of lenticular optical properties and changes in morphology of the lens fibre cell IF cytoskeleton (Alizadeh et al., 2002; Sandilands et al., 2003; Sandilands et al., 2004). Interestingly, removal of BFSP2 also causes a decrease in the levels of BFSP1, which suggests that BFSP1 is degraded by the proteosome in the absence of an assembly partner (Alizadeh et al., 2002; Sandilands et al., 2003).

The R287W and R339H BFSP2 mutations both cause cataract in humans (Conley et al., 2000; Ma et al., 2008) and the E233del BFSP2 mutant causes cataract and myopia in humans (Cui et al., 2007; Jakobs et al., 2000; Zhang et al., 2004). Only one mutation in BFSP1 has been reported, and it arises from a consanguineous marriage and causes autosomal recessive cataract (Ramachandran et al., 2007). The mutation is predicted to truncate BFSP1, introducing a premature stop codon and a frameshift from residue 246 which would remove most of helix 2 and the entire C-terminal tail domain. It is not known whether the mutated BFSP1 RNA is transcribed or removed by the nonsense-mediated decay RNA surveillance pathway, however, if removed this would effectively create a human BFSP1 knockout.

sHsp interaction has been demonstrated for all IF proteins *in vitro* and *in vivo*, but the interaction with BFs is unusual because a-crystallin association is so extensive that the 5-6nm BFSP1 and BFSP2 filament backbone (Goulielmos et al., 1996; Merdes et al., 1993) is almost completely obscured (Carter et al., 1995; Quinlan et al., 1996). The reasons for this unusual interaction of BFs and a-crystallin and the subsequent functional significance are unknown, but understanding this interaction may provide important insight into the sHsp-IF interaction.

INTERACTIONS OF aB CRYSTALLIN WITH IFs

IFs traverse the cell cytoplasm (Janmey et al., 2009; Kim and Coulombe, 2007) and thus require mechanisms to prevent filament-filament interactions which could lead to filament aggregation (Perng et al., 1999a; Quinlan, 2002). aB crystallin interacts with IF networks to modulate filament-filament interactions (Fig 1.8) (Perng et al., 1999a), stabilise IF assembly intermediates (Perng et al., 1999b) and assist in the formation of IF networks in cells (Perng et al., 2004). Studies have shown aB crystallin interaction with the IFs BFSP1, BFSP2, desmin, GFAP and vimentin, where aB crystallin is believed to function in the organisation and stabilisation of these filament networks (Bennardini et al., 1992; Djabali et al., 1999; Muchowski et al., 1999b). Indeed, studies show that in response to stress or disease, aB crystallin moves to the cytoskeletal fraction and remains associated with cytoplasmic IFs (Chiesi et al., 1990; Djabali et al., 1997; Golenhofen et al., 1999; Iwaki et al., 1993; Iwaki et al., 1989; Kato et al., 1993; Lowe et al., 1992; Muchowski et al., 1999b). However, aB crystallin also associates with IFs in unstressed cells (Perng et al., 1999a; Wisniewski and Goldman, 1998) and studies suggest it participates in the dynamic assembly, disassembly, reorganisation and stabilisation of the cytoskeleton during cell development and differentiation (Bennardini et al., 1992; Ghosh et al., 2007a; Nicholl and Quinlan, 1994).

The interaction of aB crystallin with GFAP filaments is thought to be important for normal astrocyte function (Quinlan et al., 2007). Indeed, Alexander disease (OMIM #203450) results from the accumulation of mutant GFAP into aggregates which sequester aB crystallin (and HSP27) (Der Perng et al., 2006; Iwaki et al., 1993; Iwaki et al., 1989) and may reduce the ability of astrocytes to resist stress (Head et al., 1994; Iwaki et al., 1994; Perng et al., 1999a) and prevent apoptosis (Mehlen et al., 1995). In fact, studies have shown that overexpression of aB crystallin is able to inhibit GFAP aggregation in tissue culture models (Koyama and Goldman, 1999) and prevent GFAP induced morbidity in a mouse model of Alexander disease (Hagemann et al., 2009), illustrating the importance of this interaction.

Desmin is also an important binding partner of aB crystallin (Perng et al., 1999b; Perng et al., 2004) and mutations in both desmin (Munoz-Marmol et al., 1998) and aB crystallin (Vicart et al., 1998) can cause myopathy. Indeed, the R120G aB crystallin mutation, which alters the interaction with desmin filaments, causes desmin related myopathy (DRM) characterised by

aggregates of desmin and R120G aB crystallin (Vicart et al., 1998). Furthermore, muscle cell lines transfected with R120G aB crystallin cDNA form intracellular aggregates containing both desmin and aB crystallin (Perng et al., 2004). Indeed, the R120G aB crystallin mutation has been shown to cause increased desmin filament binding, increased filament-filament interactions and subsequently, filament aggregation (Fig 1.8) (Perng et al., 1999b; Perng et al., 2004; Song et al., 2008; Vicart et al., 1998). Despite the inherent instability of R120G aB crystallin (Meehan et al., 2007; Treweek et al., 2005), the pathology is aB crystallin and desmin aggregates, rather than aB crystallin-only aggregates, demonstrating the importance of the sHsp-IF interaction (Vicart et al., 1998). Indeed, overexpression of WT aB crystallin in a tissue culture model has been shown to inhibit desmin aggregation (Wang et al., 2003). Furthermore, mutations in desmin can cause desmin related myopathies (Levin et al., 2010) leading to intracellular aggregates (Goldfarb and Dalakas, 2009) which weaken skeletal and cardiac muscle (McLendon and Robbins, 2011). The characteristic histopathological feature of the disease is protein aggregates containing both aB crystallin and desmin (Goldfarb and Dalakas, 2009; Goldfarb et al., 2008; Taylor et al., 2007), further demonstrating the importance of the sHsp-IF interaction.

Studies suggest that aB crystallin also binds to filament surfaces (Nicholl and Quinlan, 1994; Perng et al., 1999a). Indeed, sequences in aB crystallin predicted to bind both filament proteins and client proteins have shown preferential interaction with filament proteins at 23°C and preferential interactions with unfolding clients at 45°C (Ghosh et al., 2005). This may suggest that under normal physiological conditions, aB crystallin interacts with and stabilises filaments, while under conditions of stress aB crystallin dissociates from the filaments to interact with and stabilise unfolding clients.

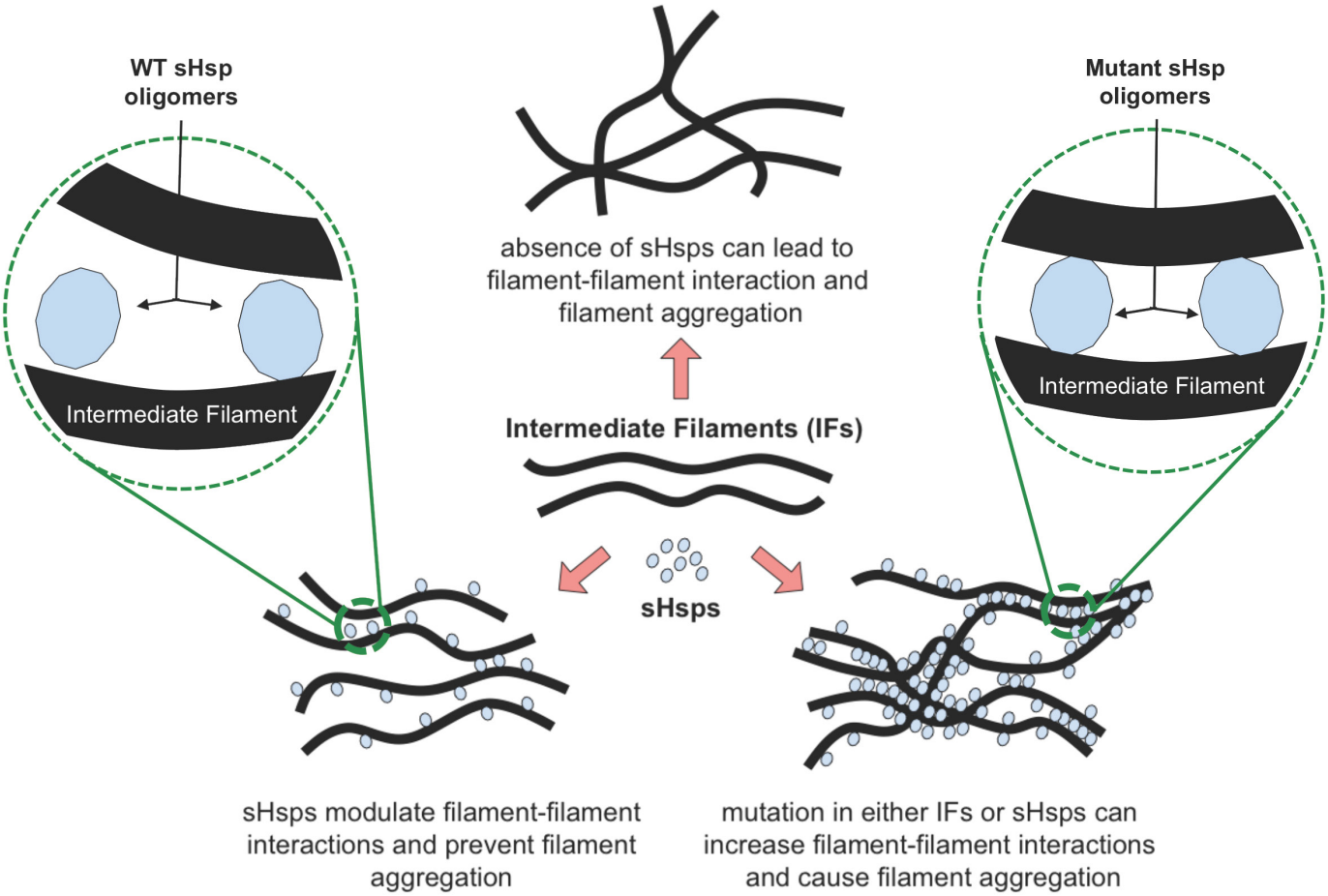

Fig 1.8. sHsps modulate filament-filament interactions and prevent aggregation.

In the absence of sHsps, exposed hydrophobic residues on filament surfaces can cause filament-filament interactions and filament aggregation. sHsps interact with IFs to prevent unwanted filament-filament interactions and prevent aggregation. However, mutations in sHsp or IF can alter the interaction and lead to promotion of filament-filament interactions and subsequent filament aggregation.

aB crystallin substrate binding domains

Studies have attempted to identify domains in sHsps involved in substrate binding, and have predicted binding sites spread throughout the sHsp sequence. Previous studies have suggested substrate binding sites in the a-crystallin domain, particularly in regions thought to be involved in oligomer assembly (Lee et al., 1997; Van Montfort et al., 2001a; Van Montfort et al., 2001b). Studies using hydrophobic probes and chemical cross-linkers have also implicated the b3 and b5 strands along with loop regions between b3-b4, b5-b6 and b8-b9 (Ahrman et al., 2007; Sharma et al., 1998) (see Fig 1.2). Previous studies using point and deletion mutations, chimeras and chemical cross linkers have also implicated the sHsp N-terminal arm in substrate interaction (Basha et al., 2006; Ghosh et al., 2006d; Giese et al., 2005; Giese and Vierling, 2004; Haslbeck et al., 2004; Jaya et al., 2009). However, is should be noted that mutations or incorporation of probes and cross-linkers can potentially affect sHsp subunit dynamics and thus indirectly affect substrate interaction. These studies do not distinguish between affecting the potential sHsp substrate binding domains, versus affecting sHsp subunit dynamics, which could indirectly affect substrate interaction.

For aB crystallin, binding sites for client proteins (Ghosh et al., 2005, 2006a; Ghosh et al., 2006b; Ghosh et al., 2006d, 2007c), desmin (Ghosh et al., 2007b), GFAP (Ghosh et al., 2007b), microtubules (Ghosh et al., 2007a; Ohto-Fujita et al., 2007) and growth factors (Ghosh et al., 2007c) have been predicted throughout the protein sequence (See Fig 1.9). Cross-linking studies have also suggested N-terminal residues 57-69 and a-crystallin domain residues 93-107 as potential substrate binding regions (Sharma et al., 1997; Sharma et al., 2000). Binding studies using hydrophobic probes have implicated b3, b4 and b5 strands of the a-crystallin domain, since binding of hydrophobic probes to these regions prevents substrate binding (Sharma et al., 1998). It has also been suggested that surface-exposed residues of the b8 motif combined with the surface-exposed residues of the b3 motif and the b9 motif form a substrate binding interface (Ghosh et al., 2006b; Muchowski et al., 1999c).

Fig 1.9. Proposed substrate binding domains in aB crystallin.

Proposed aB crystallin binding regions for oligomerisation (black), client proteins (dark green), desmin (red), GFAP (grey), actin (lime), microtubules (orange) and growth factors (blue). The sequence for aB crystallin is shown and red residues identify predicted substrate binding areas which are not predicted for oligomer assembly. The R120G mutation in human aB crystallin, which lies within a predicted desmin interaction region, causes abnormal interactions with desmin filaments leading to cataracts and desmin-related myopathy (Perng et al., 2004). Ser-59 which lies within a predicted actin interaction region has been shown to modulate interactions with actin filaments where phosphorylation causes increased interaction (Launay et al., 2006). Predicted oligomerisation sites (Bova et al., 2000; Ghosh and Clark, 2005; Ghosh et al., 2006d, 2007c; Sreelakshmi et al., 2004; Sreelakshmi and Sharma, 2005, 2006), client sites (Ghosh et al., 2005, 2006a; Ghosh et al., 2006b; Ghosh et al., 2006d, 2007c), desmin sites (Ghosh et al., 2007b), GFAP & actin sites (Ghosh et al., 2007b), microtuble sites (Ghosh et al., 2007a; Ohto-Fujita et al., 2007) and growth factors sites (Ghosh et al., 2007c) are shown.

(Figure on next page)

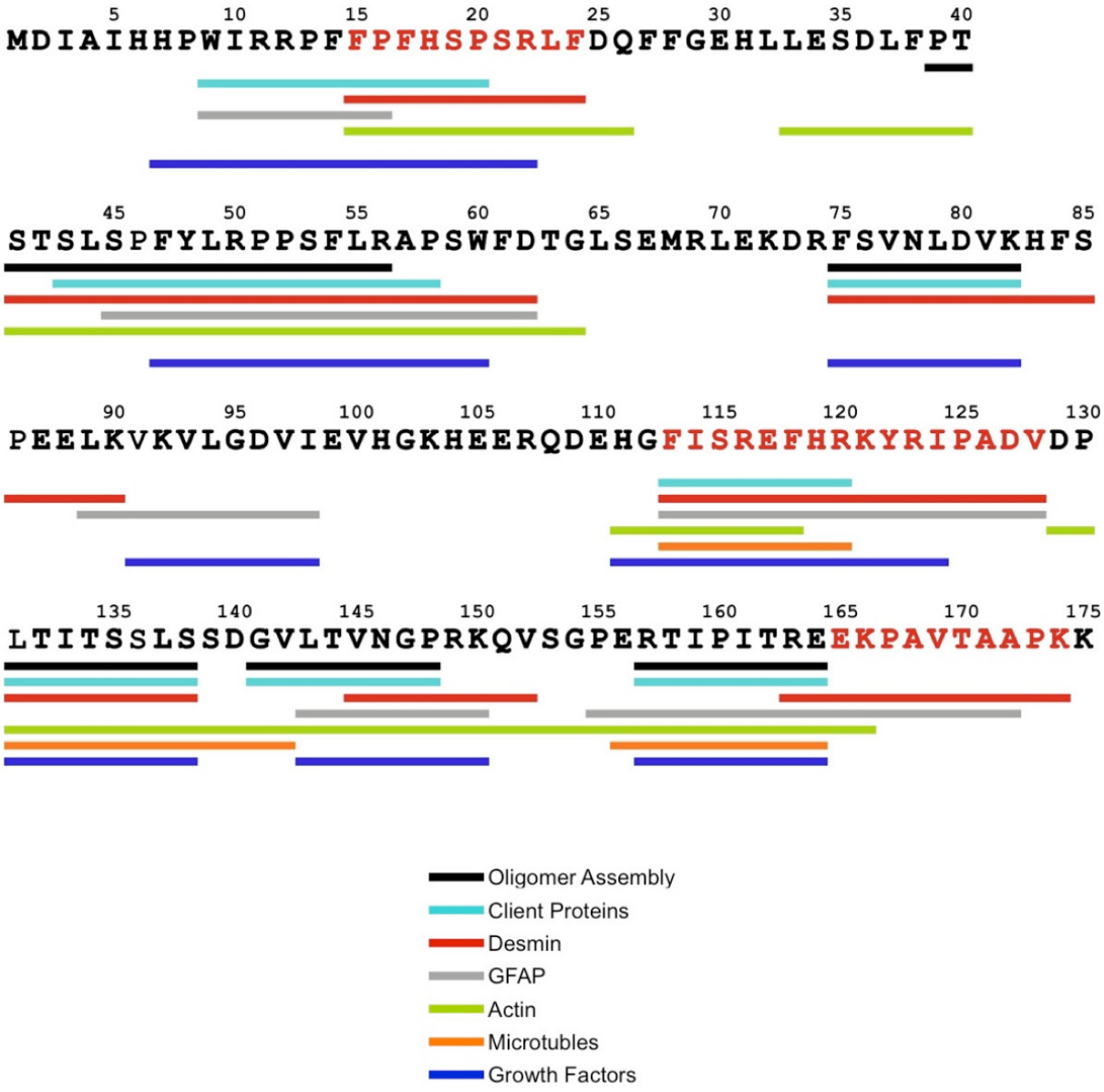

Fig 1.9. (Legend on previous page)

There is significant overlap between aB crystallin regions predicted for oligomerisation and those predicted for substrate binding (Fig 1.9). This may indicate that subunit dissociation from the oligomer is required for substrate binding. Indeed, sHsp dissociation theory suggests that oligomer dissociation into smaller subunits exposes hydrophobic surfaces, which allows binding of client proteins. Interestingly, some aB crystallin sites predicted to be involved in substrate binding, including IF binding, have not been implicated in oligomerisation (residues 15-24, 113-128 and 165-176, see Fig 1.9). These sites may potentially be accessible to substrates on the surface of the assembled aB crystallin oligomer. Indeed, sHsp oligomer theory (Augusteyn, 2004b; Avilov et al., 2004; Kim et al., 2003) suggests that the assembled oligomer is the active unit of chaperone activity and that substrates bind directly to the oligomer surface, without subunit dissociation (Kim et al., 2003). To investigate this further, I worked with Dr Ehmke Pohl (Durham University, UK) to model the structure of aB crystallin (Fig 1.10), based upon the crystal structure of the Hsp16.9 from wheat (Van Montfort et al., 2001b). Fig 1.10 shows the predicted hexamer and dodecamer for aB crystallin.

Whilst a homology model of aB crystallin oligomers based on the Hsp16.9 oligomer presents obvious drawbacks (Hsp16.9 shares 27% sequence identity with aB crystallin), the main message is that the regions predicted to be involved in substrate binding and not in oligomerisation (Fig 1.10, red and blue regions) are buried within the oligomer and are therefore not available to bind substrates, including IFs. However, electron micrographs and biochemical data show that assembled aB crystallin oligomers most certainly interact with IFs (Nicholl and Quinlan, 1994; Perng et al., 1999a; Perng et al., 2004).

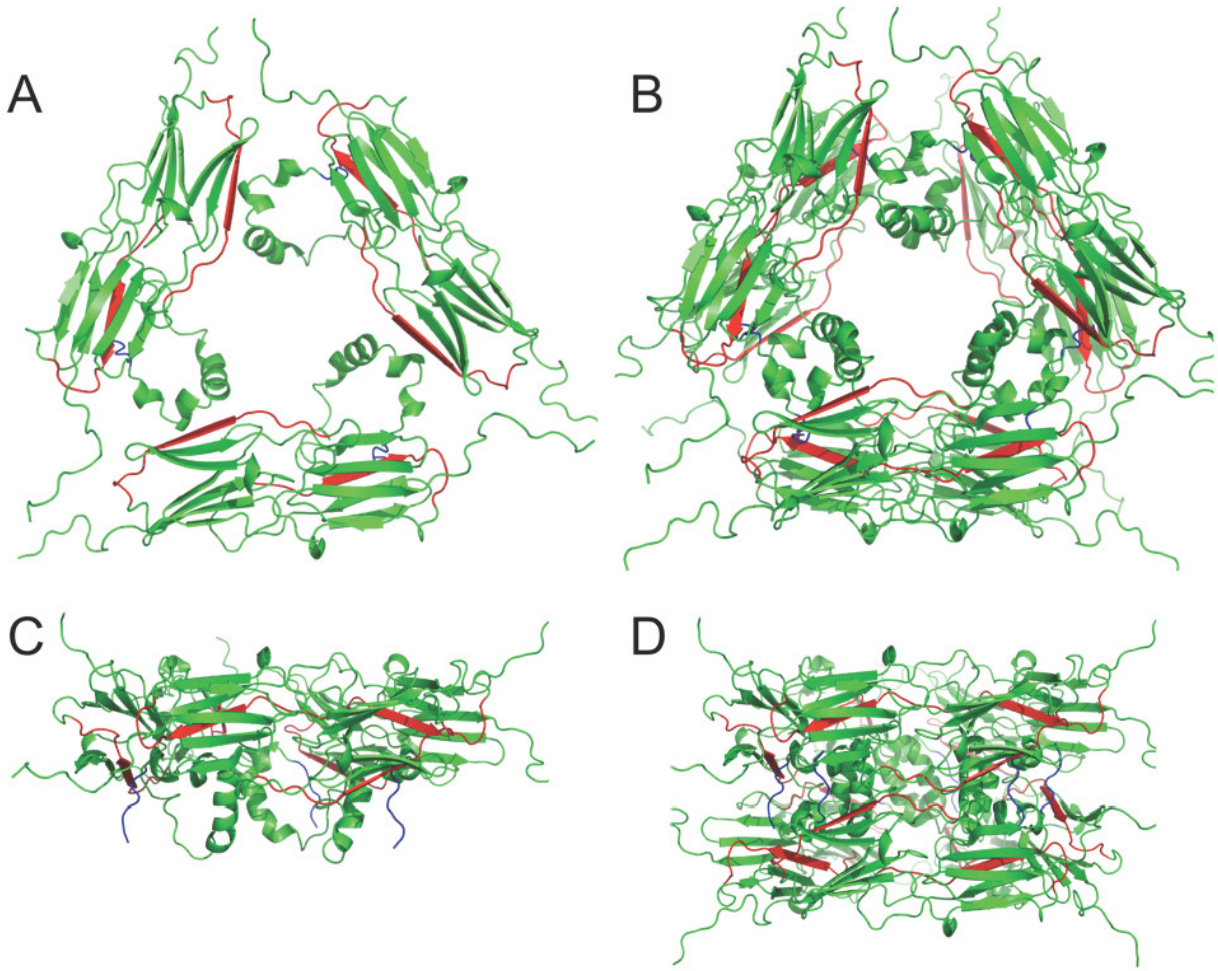

Fig 1.10. Homology model of aB crystallin hexameric and dodecameric structure.

Ribbon representation of a hexameric (A,C) and dodecameric (B,D) arrangement of an aB crystallin homology model, viewed from the top (A,B) and side (C,D). The homology model was built using the program MODELLER (Eswar et al., 2008) and based on the crystal structure of the Hsp16.9 from wheat (Van Montfort et al., 2001b). Hsp16.9 shares 27% sequence identity with aB crystallin and forms a dodecameric structure with four independent chains in the asymmetric unit. This was used to model the monomer of aB crystallin, which was then superimposed by least squares methods using COOT (Emsley and Cowtan, 2004; Krissinel and Henrick, 2004) onto each monomer from the Hsp16.9 dodecamer to create dodecameric and hexameric models for aB crystallin. Regions predicted to be involved in substrate binding, but not in oligomerisation, are shown in red (residues 113-128) and blue (residues 15-24). Note that each dimer contains only one N-terminal domain since the N-terminal domain of the neighboring subunit would clash. This figure was created by Dr Ehmke Pohl.

Proteolysis and binding studies have implicated the aB crystallin N-terminal arm (Aquilina and Watt, 2007; Thedieck et al., 2008) in substrate binding and N-terminal residues 73-92 have been shown capable of preventing aggregation of denatured substrates, similar to the action of full length aB crystallin (Bhattacharyya et al., 2006). Interestingly, the N-terminal arm of sHsps is intrinsically unstructured (Aquilina and Watt, 2007; Jiao et al., 2005; Kundu et al., 2007; Van Montfort et al., 2001a). Thus far, crystallographic studies of aB crystallin have only been made possible by truncating the N-terminus, so structural details of the N-terminus are limited. Proteolysis and hydrogen exchange (HX) studies suggest that the sHsp N-terminal arm is solvent exposed (Cheng et al., 2008; Jaya et al., 2009) and the inability to resolve any of the 24 N-terminal arms in Mj Hsp16.5 and six of the 12 N-terminal arms in Ta Hsp16.9 crystal structures suggest that the region is structurally disordered (Van Montfort et al., 2001b, -85). Intrinsically disordered or flexible regions of proteins are thought to be important protein-protein interaction surfaces (Dyson and Wright, 2005; Tompa and Csermely, 2004). Structural disorder potentially allows the sHsp N-terminal arm to present a variable and flexible ensemble of clusters of hydrophobic residues that can interact with diverse geometries of hydrophobic patches on substrate proteins. In addition, HX studies of the sHsp-substrate complex suggest that the N-terminal arm remains unstructured even when bound to a substrate (Cheng et al., 2008). Proteins with intrinsically disordered domains have previously been shown to bind protein partners without a disorder-to-order transition (Sigalov et al., 2008). These data may indicate that sHsps have transitory interaction with substrates at multiple sites which are locally dynamic. It may be the case that plasticity in binding site conformation allows sHsps to interact effectively with such a wide range of substrates. In contrast to the ATP-dependent chaperones GroEL, Hsp70 and Hsp90, which have distinct substrate binding regions (Horwich et al., 2007; Mayer and Bukau, 2005), sHsps may rely on multiple, variable contact sites distributed throughout the sHsp. There may be a complete lack of a specific sHsp substrate binding surface. Indeed, the fact that substrate binding domains have been predicted throughout the aB crystallin sequence supports this theory (See Fig 1.9). Very recently, solid state NMR, SAXS, and EM data was used to produce an atomic-level model of full-length aB crystallin (Jehle et al., 2011). In the full-length aB crystallin 24-mer model (Jehle et al., 2011), almost all residues are solvent exposed somewhere on the oligomer, which may explain the huge diversity in predicted binding sites spread throughout the aB crystallin sequence. The exceptions to this are helices a1 (P16-P21) and a2 (F27-L32) in the N-terminus, which are densely packed in the aB crystallin 24-mer model and are not accessible. Interestingly, the a2 region is one of the few regions in aB crystallin which has

never been implicated in substrate binding. In addition, when isolated, the N-terminal domain itself forms disordered aggregates (Augusteyn, 1998), so sequestration of this region within the oligomer may be important to prevent unwanted associations which could lead to aggregation (Jehle et al., 2011). Overall, these data suggest that sHsps may rely on multiple, variable contact sites distributed throughout the sHsp and there may in fact be a complete lack of a specific sHsp substrate binding surface. However, the validity of this theory remains to be determined.

THESIS AIMS

This thesis aims to gain further insight into sHsp-IF interactions, and investigates this theme from different in vitro experimental angles. Chapters 3 and 4 look exclusively at sHsps to further understanding of their structure and activity in vitro. Chapter 5 looks exclusively at an IF to further understanding of filament assembly and filament properties. Chapters 6, 7, 8 and 9 analyse the interaction between sHsps and IFs.

The sHsp 'aB crystallin' and the IF 'desmin' have been shown to cause disease in humans. Mutation in either protein can lead to aggregates containing both proteins, demonstrating the importance of their interaction. Therefore, aB crystallin and desmin will be used throughout this thesis to investigate the sHsp-IF interaction. In addition, the sHsp 'Hsp16.5' from Methanococcus jannaschii will be analysed, as this protein is one of only a few sHsps to have been crystallised, and therefore this protein can provide insight into sHsp structure, which will be critical to understanding the interaction with IFs. The IF 'beaded filament' will also be analysed as this IF has unique interactions with sHsps and may thus provide insight into the sHsp-IF interaction.

The results in this thesis are presented in Chapters 3 to 9. Separating the results into these 7 chapters has allowed each to have a tight focus and a clear message. Each results chapter begins with an introduction to the question being addressed, and when required, is followed by a brief explanation of the experimental techniques used and how to interpret the data they produce. Each results chapter ends with a summary of the chapter findings, but these findings are not discussed. All experimental findings from results Chapters 3 to 9 are discussed in Chapter 10. This allows the discussion to be arranged into themes which can draw data from multiple results chapters. This is important as multiple results chapters make contributions to understanding certain aspects of the sHsp-IF interaction.

In Chapter 3, I use the previously crystallised sHsp 'Hsp16.5' to model the potential structural changes resulting from disease causing mutations in aB crystallin. In Chapter 4, I investigate the in vitro effects of a cataract causing aB crystallin mutation. These chapters provide further insight into the structure and the activity of sHsps, which will be critical to understanding the sHsp-IF interaction.

In Chapter 5, I investigate the 'beaded filament'. Among IFs, the beaded filament has unique interactions with sHsps. Chapter 5 analyses an unusual 'tailed' zebrafish beaded filament protein to provide insight into beaded filament assembly and the factors affecting filament properties. Understanding these aspects of beaded filaments will be critical to understanding the sHsp-IF interaction. In Chapter 6, I further investigate the beaded filament using human disease causing beaded filament protein mutants. I also analyse the interaction of the beaded filament with aB crystallin.

In Chapter 7, I analyse the effects of mutations in aB crystallin on the interaction with desmin filaments, to determine domains in aB crystallin which are important for interaction with desmin. Conversely, in Chapter 8, I analyse the effects of mutations in desmin on the interaction with aB crystallin, to determine domains in desmin which are important for interaction with aB crystallin. In Chapter 9, I analyse the effect of filament assembly conditions on filaments properties and the interaction of filaments with aB crystallin.

CHAPTER 2: MATERIALS & METHODS

EXPRESSION CONSTRUCT PURIFICATION & TRANSFORMATION

Chemicals

All chemicals and reagents used in all procedures were purchased from Merck Ltd (UK) or Sigma Aldrich (UK) and were of analytical grade unless otherwise stated.

Protein expression constructs

All protein expression constructs were prepared by Terry Gibbons (Hu WT aB crystallin, D140N aB crystallin, Hu WT Desmin, Hu WT BFSP2, Hu R287W BFSP2, Hu E233del BFSP2, Zf WT Bfsp2, Zf CT Bfsp2, Mj WT Hsp16.5, Mj I140X Hsp16.5, Mj G143X Hsp16.5 and Mj R107G Hsp16.5), Antal Tapodi (Hu WT BFSP1 and Hu WT 53k), Scott Houck (aAb3, CEb3, aAb8, CEb8 and d155 aB crystallins), or Sarika Sharma (d431, d441, RDG and dTail desmins) using subcloning strategies. cDNAs were obtained from Geneservice in cloning vectors. Genes were amplified via PCR and the fragments cloned into pGEMTeasy (Promega, UK), sequenced and then subcloned into pET23b expression vector. Mutant proteins were generated by PCR mutagenesis. All WT and mutant sequences were confirmed by bi-directional DNA sequencing. All protein expression constructs used in this thesis are shown in Table 2.2.

Cultivation and purification of expression constructs

DH5α cells containing the expression plasmid were grown in 5ml of Luria-Bertani (LB) media with 50g/l carbenicillin and incubated for 16h at 37°C at 225rpm. The plasmid DNA was then purified using a plasmid mini prep kit (Sigma, UK) and following the recommended protocol. 5ml cultures were centrifuged for at 3,300g for 15min at 4°C in a bench-top microcentrifuge (5417R; Eppendorf, Germany), and the supernatant discarded. The pellet was resuspended in 400µl of 'resuspension buffer' and separated into two 200µl volumes for further purification in 1.5ml eppendorf tubes. The cells were lysed by the addition of 200µl 'lysis buffer' and gently inverted 6-8 times ensuring the 'neutralisation buffer' was added (350µl) within 5min of the 'lysis buffer'. The tubes were inverted 4-6 times and centrifuged for 10min at 16,000g. The supernatant was added to a spin column, which was prepared by the addition of 500µl of 'column preparation buffer' and centrifuged at 16,000g for 1min and

the flow through was discarded. With the plasmid DNA applied the spin column was centrifuged at 16,000g for 1min and the flow through discarded. The 750µl of 'wash solution' was added to the spin column and centrifuged at 16,000g for 1min and flow through discarded. The column was spun for a further 2min without any additional buffer, to ensure maximum removal of ethanol from the column membrane. The purified plasmid DNA was eluted with 50µl of sterile water, and the two aliquots per 5ml culture pooled and stored at -20°C.

Transformation of expression constructs into competent BL-21 (pLysS) cells

50µl competent BL-21 cells were thawed on ice and gently mixed with 2ul plasmid. The cells were incubated on ice for 30min, heat shocked at 42°C for 45 seconds, then incubated on ice for 2min. 200µl LB media was added and cells incubated for 90min at 37°C, shaking at 225rpm. 10µl transformation mixture was plated onto 90mm agar plates containing 50mg/l carbenicillin and 34mg/l chloramphenicol and incubated for 16h at 37°C. A colony was then placed into 20ml of LB media with the antibiotics (plus 0.05% (w/v) glucose) and incubated for 16h at 37°C at 225rpm.

PROTEIN EXPRESSION & PURIFICATION

Protein expression

All proteins, except the Hsp16.5 proteins, were expressed using isopropyl-beta-D-thiogalactopyranoside (IPTG) induction. 1L of LB media containing 34mg/l chloramphenicol, 50mg/l carbenicillin and 0.05% (w/v) glucose was inoculated with 10ml of a fresh overnight culture. The culture was mixed at 160rpm at 37°C and the optical density was monitored (Beckman DU640 Spectrophotometer) at OD_{600} until a value of 0.60 was observed, at which time protein expression was induced by adding 0.5mM IPTG. The cells were incubated for a further 3h at 37°C and then harvested.

The Hsp16.5 proteins were expressed using auto-induction media. 1L of 60g/l Overnight Express Instant TB Medium (Merck Chemicals, UK) containing 34mg/l chloramphenicol, 50mg/l carbenicillin and 0.05% (w/v) glucose was inoculated with 10ml of a fresh overnight culture. The culture was mixed at 200rpm at 37°C for 4h, then at 25°C for 20h. Cells were then harvested.

Cell harvesting and protein extraction

Cells were centrifuged at 16,000g for 30min at 4°C (JLA-8.1000 Beckman Coulter) and the supernatant discarded. The pellet was resuspended in 20ml of 50mM Tris-HCl pH 8, 1mM EDTA, 100mM NaCl, 10mM $MgCl_2$, 0.2mM PMSF and containing a Complete protease inhibitor cocktail tablet (Roche Diagnostics, UK). Cell lysis was initiated by 3 freeze thaw cycles at -20°C and followed by a 30min incubation at 22°C with 0.25g/l lysozyme (Sigma-Aldrich Ltd, USA). The resuspension was then homogenised using a Dounce glass homogeniser and then centrifuged at 48,000g for 30min at 4°C (JA-20 Beckman Coulter). The supernatant (soluble protein fraction) or pellet (insoluble protein fraction) was retained and processed further to purify either the soluble or insoluble proteins respectively.

Removal of DNA from the soluble protein fraction (SPF)

Benzonase nuclease (Novagen, UK) was added to a final concentration of 10 units/ml to the SPF and mixed gently at 22°C for 30min. DNA was then precipitated via addition of 0.1% (v/v) polyethylimine (PEI) and incubation on ice for 10min. Precipitated DNA was pelleted at 48,000g for 10min at 4°C (JA-20 Beckman Coulter). To remove the PEI, the supernatant was dialysed for 16h at 4°C into 20mM Tris-HCl pH 7.4, 1mM $MgCl_2$, 1mM EDTA, 1mM DTT, 0.2mM PMSF. Samples were then stored at 4°C for chromatography purification.

Insoluble protein extraction & solubilisation

The insoluble pellet was resuspended in 20ml of 20mM Tris-HCl pH 7.5, 1% (v/v) triton x100, 150mM NaCl, 5mM EDTA, 1mM EGTA, 0.5mM DTT, 0.2mM PMFS. Benzonase nuclease was added to a final concentration of 10 units/ml and the solution mixed gently at 22°C for 30min. The solution was centrifuged at 48,000g for 30min at 4°C (JA-20 Beckman Coulter) and the pellet resuspended in 20ml of 20mM Tris-HCl pH 7.5, 0.5% (v/v) Triton X100, 600mM NaCl, 5mM EDTA, 1mM EGTA, 0.5mM DTT, 0.2mM PMSF and was mixed gently at 22°C for 30min. The solution was centrifuged at 48,000g for 30min at 4°C and the pellet resuspended in 10mM Tris-HCl pH 7.5, 150mM NaCl, 5mM EDTA, 1mM EGTA, 0.5mM DTT, 0.2mM PMFS and was mixed gently at 22°C for 30min. The solution was centrifuged at 48,000g for 30min at 4°C and the pellet resuspended in 10 volumes of 6M Urea, 10mM Tris-HCl pH 8, 1mM EDTA, 1mM DTT, 0.2mM PMFS and incubated at 22°C for for 16h. The solution was then centrifuged at 48,000g for 10min at 4°C and the supernatant stored at 4°C for chromatography purification.

Extraction of native bovine BFSP1 and 53kDa

Native bovine BFSP1 and 53kDa were extracted essentially according to Quinlan et al. 1992. Bovine eyes were obtained from the abattoir and the lenses were immediately removed, decapsulated and placed in 10mM sodium phosphate pH 7.4, 150mM NaCl, 5mM EDTA using a volume of 4ml per lens. Up to 20 lenses were processed at one time. The lenses were stirred on ice for 15-30min to dissolve the outer membranes and the solid nuclear remnants were discard. The solution was Dounce homogenised on ice then centrifuged at 48,000g for 20min at 4°C (JA-20 Beckman Coulter). The pellet was resuspended in 10mM sodium

phosphate pH 7.4, 1.5M KCl, 5mM EDTA, 0.5% Triton X100 (4ml per lens), Dounce homogenised, and stirred at 4°C for 16h. The sample was centrifuged at 48,000rpm for 20min at 4°C and the pellet resuspended in 10mM sodium phosphate pH 7.4, 150mM NaCl, 5mM EDTA (4ml per lens). The sample was Dounce homogenised, stirred for 15min on ice and then centrifuged at 48,000g for 20min at 4°C. The pellet was stored at -20°C and the whole extraction process repeated until 10g of pellet was obtained from about 100 lenses. The 10g pellet was then resuspended in an equal volume of 8M Urea, 20mM Tris-HCl pH 8, 2mM EDTA, 50mM mercaptoethanol. The sample was Dounce homogenised, stirred on ice for 30min then centrifuged at 144,000g for 2h at 4°C in a Beckman Optima MAX Ultracentrifuge using a TLS-55 rotor (Beckman Instruments, USA). The lipid surface layer and pellet were removed and the supernatant was stored at 4°C for chromatography purification.

Liquid chromatography systems

All high performance liquid chromatography (HPLC) purifications were performed using a Merck Hitachi Biochromatography system (Merck Hitachi Ltd, Japan). All low pressure liquid chromatography purifications (LPLC) were performed using a LPLC system with a peristaltic pump and gradient maker (Merck, Germany). Cleaning in place was performed for all columns via a 2h sanitisation with 0.5M NaOH and a 10 column volumes (cv) wash with milliQ water. All column equilibrations were performed using 20cv of buffer. All column buffers were degassed and vacuum filtered through a 0.2um Whatman cellulose nitrate membrane disc filter (Whatman, UK). All protein samples were filtered through a 0.2um filter using a 32mm Acrodisc PES (polyethersulphone) syringe filter (Pall, UK) prior to column loading. UV absorbance at 280nm of the eluant was analysed using Chromeleon 6.3 software (Sunnyvale, USA). Eluant was collected as 1ml fractions using a Biorad Model 2110 fraction collector (Biorad Laboratories, UK) and analysed via SDS-PAGE using 12-16% (w/v) acrylamide gels. Fractions enriched with target protein were pooled and stored at -80°C. All columns were stored in 20mM Tris-HCl pH 7.4, 1M NaCl, 0.02% (v/v) sodium azide.

Chromatography columns

TYPE	COLUMN	RESIN	SYSTEM	FLOW RATE (ml/min)
Anion Exchange	10ml TMAE	Fractogel EMD TMAE (Merck, UK)	HPLC	1.0
	90ml TMAE	Fractogel EMD TMAE (Merck, UK)	HPLC	6.6
	60ml DEAE	DEAE Sepharose Fast Flow (GE Life Sciences, UK)	LPLC	1.0
Cation Exchange	10ml COO-	Fractogel EMD COO^- (Merck, UK)	HPLC	1.0
Mixed Mode Ion Exchange	45ml HA	Ultrogel Hydroxyapatite (Pall, UK)	LPLC	1.0
Size Exclusion	120ml SEC	Fractogel EMD BioSEC (Merck, UK)	HPLC	1.0
	24ml SEC	Superose 6 10/300 GL (GE Life Sciences, UK)	HPLC	0.2

Table 2.1. Chromatography columns used during protein purification.

Protein Expression Constructs

PROTEIN	WT / MUTATION	MUTATION TYPE
Hsp16.5 ***(M. jannaschii)***	WT	-
	R107G	Single Residue Substitution
	I140X	C-terminal Truncation
	G143X	C-terminal Truncation
aB crystallin ***(H. sapiens)***	WT	-
	D140N	Single Residue Substitution
	aAb3	Chimera
	CEb3	Chimera
	aAb8	Chimera
	CEb8	Chimera
	d155	11 Residue Deletion
BFSP2 ***(H. sapiens)***	WT	-
	E233del	Single Residue Deletion
	R287W	Single Residue Substitution
Bfsp2 ***(D. rerio)***	WT	-
	CT	C-terminal Truncation
BFSP1 ***(B. taurus)***	WT	-
BFSP1-53k (53k) ***(B. taurus)***	WT	-
Desmin ***(H. sapiens)***	WT	-
	d431	C-terminal Truncation
	d441	C-terminal Truncation
	RDG	3 Residue Deletion
	dTail	C-terminal Truncation

Table 2.2. Protein Expression Constructs

All the protein expression constructs used throughout this thesis are shown. The chimera mutants are domain substitutions. Detail for each protein is given in the results chapters.

Protein purification conditions

All BFSP2 proteins, human WT desmin, human WT BFSP1 and human WT BFSP1-53kDa were all purified by anion then cation exchange chromatography. Anion exchange was performed using a 10ml TMAE with 7M Urea, 20mM Tris-HCl pH 8, 1mM EDTA, 1mM DTT, 0.2mM PMSF and proteins were eluted using a 10cv linear gradient of 0-1M NaCl. Cation exchange was performed using a 10ml COO- column with 7M Urea, 20mM Sodium Formate pH 5, 5mM EDTA, 1mM DTT, 0.2mM PMSF and proteins were eluted using a 10cv linear gradient of 0-1M NaCl.

Native bovine BFSP1 and native bovine BFSP1-53kDa were purified by two anion exchange purifications then hydroxyapatite chromatography (Quinlan et al., 1992). The first anion exchange was performed using a 90ml TMAE with 8M Urea, 20mM Tris-HCl pH 8.0, 50mM Mercaptoethanol, 2mM EDTA and proteins were eluted using 0-1M Guanidine-HCl with the following non-linear gradient: 0.4cv 0.00-0.05M, 0.7cv 0.05-0.05M, 0.7cv 0.05-0.25M, 0.7cv 0.25-0.25M, 1.0cv 0.25-1.00M. The second anion exchange was performed using a 10ml TMAE with 8M Urea, 20mM Tris-HCl pH 8.0, 50mM Mercaptoethanol, 2mM EDTA. Hydroxyapatite chromatography was performed using a 45ml HA column with 7M Urea, 10mM Sodium Phosphate pH 7.4, 1mM DTT, 0.2mM PMSF and proteins were eluted using a 10cv linear gradient of 0-1M NaCl.

WT and D140N aB crystallin were both purified by anion exchange then size exclusion chromatography. Anion exchange was performed using a 10ml TMAE with 20mM Tris-HCl pH 7.4, 1mM $MgCl_2$, 1mM EDTA, 1mM DTT and 0.2mM PMSF and proteins were eluted using a 10cv linear gradient of 0-1M NaCl. Size exclusion chromatography was performed using a 120ml SEC column with 20mM Tris-HCl pH 7.4, 100mM NaCl.

I140X and G143X Hsp16.5 proteins were purified by heating and centrifugation, then two anion exchange purifications, then two size exclusion chromatography purifications. For the heat purification, the extracted soluble protein fraction was incubated in a water bath at 80°C for 30min in the presence of 1M NaCl. Samples were cooled on ice for 10min and then centrifuged at 48,000g for 30min at 4°C (JA-20 Beckman Coulter) and the pellets discarded. The first anion exchange was performed using a 60ml DEAE with 20mM Tris-HCl pH7.2, 1mM $MgCl_2$, 1mM EDTA, 2mM DTT and proteins were eluted using a 10cv linear gradient

of 0-1M NaCl. The second anion exchange was performed using a 10ml TMAE with 20mM Tris-HCl pH7.2, 1mM $MgCl_2$, 1mM EDTA, 2mM DTT and proteins were eluted using a 10cv linear gradient of 0-1M NaCl. The first size exclusion chromatography purification was performed using a 120ml Fractogel SEC column and the second using a 24ml Superose 6 SEC column with 10mM Hepes-HCl pH 7.4, 100mM NaCl, 2mM DTT. WT and R107G Hsp16.5 were purified by the same method as the I140X and G143X mutants, but did not require the second anion exchange or the second size exclusion steps, which were omitted.

All mutant desmin proteins were produced by Sarika Sharma at the German Cancer Research Center in Germany and were purified in using anion and cation exchange chromatography as described by Herrmann et al. 2004. The aB-crystallin mutant proteins aAb3, CEb3, aAb8, CEb8 and d155 were all produced by Scott Houck at the University of Washington in the USA and were purified using anion exchange and size exclusion chromatography as described by Muchowski et al 1999.

Analytical SEC

Analytical SEC was performed using a 24ml SEC column. Mwt determination used a calibration kit (Amersham Biosciences, UK) containing thyroglobulin (669kDa), ferritin (440kDa), aldolase (158kDa), conalbumin (75kDa) and ovalbumin (43kDa) to produce a calibration curve. Blue Dextran (2000kDa) was used to determine the void volume of the column.

Protein buffer exchange

All buffer exchanges were performed via dialysis using 12-14kDa molecular weight cut off (MWCO) dialysis tubing (Medicell International Ltd, UK). Tubing was prepared via boiling in 0.5M NaHCO3 for 1h then in 2mM EDTA for 1h and was rinsed and stored in 20% ethanol at 4°C.

Protein concentration

The Hsp16.5 proteins were concentrated using 3ml and 50ml Amicon Stirred Cells pressurised with nitrogen to 0.2 bar and using Amicon Ultracel regenerated cellulose membranes (Millipore, UK). All other proteins were concentrated by centrifugation at 3,300g at 4°C using an Amicon Ultra centrifugal filter device with a 10K MWCO (Millipore, UK).

Protein quantification

Protein samples were quantified using the BCA Protein Assay Kit (Thermo Scientific, UK). The assay reagent mix was used in a ratio 50:1 reagent A:B and 1ml was added to 50µl sample (diluted to 0.5-2.0g/l) and incubated at 37°C for 30min. Absorbance was measured at 562nm and BSA standards (0.5-2.0g/l) were used to create a standard curve. Protein samples were also quantified using absorbance at 280nm and the calculated extinction coefficient from the web resource at ExPASY (www.expasy.ch).

PROTEIN ANALYSIS

SDS-PAGE

One-dimensional SDS-PAGE analysis was performed essentially according to Laemmli (Laemmli, 1970), under reducing conditions. All gels were cast using the Mini-Protean Tetra Cell gel casting apparatus (Bio-Rad, UK) and using a pre-mixed 30% acrylamide solution (Biorad Laboratories, UK). Gels of 4% (w/v) were used to stack and concentrate while gels of 12-16% (w/v) were used to resolve using a 0.75mm gel thickness. A layer of water saturated 1-butanol was used temporarily during casting to ensure the concentrating and separating gel interface was flat. The gels were calibrated using a PageRuler Pre-stained Protein Ladder (Fermentas, UK).

Protein samples for analysis were diluted in Laemmli's sample buffer (50mM Tris-HCl pH 6.8, 100mM DTT, 2% (w/v) SDS, 0.1% (w/v) Bromophenol Blue, 10% (v/v) glycerol) to the target concentration required for specific gel loading. Samples were boiled at 95°C for 5min prior to loading. Gels were run for 45min at a constant 200V in running buffer (25mM Tris-HCl, 200mM glycine, 0.1% SDS). After electrophoresis, gels were fixed in 50% (v/v) methanol and 10% acetic acid for 20min then stained with 0.5% (w/v) Coomassie brilliant blue R-250 (Merck-BDH, UK) (solubilised in 50% (v/v) methanol and 10% (v/v) acetic acid) for 5min, and destained for 16h using 10% (v/v) methanol, 5% (v/v) acetic acid. Gels were then photographed using a light box and image analyser (LAS-1000plus, Fuji Film, UK) and protein band quantifications were preformed using the Image Gauge software (version 4.0; Fuji Film).

Chaperone & thermostability assays

For all chaperone and thermostability assays, absorbance at 360nm was measured at 15s intervals for the duration of the assay using a Beckman DU640 spectrophotometer and Beckman Tm cuvettes. For the citrate synthase assay, as described in Hayes et al 2008, 0.2g/l citrate synthase in 50mM Tris-HCl, 2mM EDTA, pH 8 was heat denatured for 30min at 44°C in the presence or absence of a protein chaperone. For the thermostability assays, samples at 0.1g/l were heat denatured at constant 70°C or 65°C for 80min, or using a gradient of 30–70°C with a 1°C/min ramp rate. For the insulin assay, adapted from Raman et al 1995, 0.3g/l

insulin in 100mM Na_2SO_4, 20mM NaH_2PO_4, pH 6.9 was reduced by the addition of 20mM DTT for 15min at 37°C. To prepare the insulin, a 20mg aliquot of 27 I.U./ml insulin from bovine pancreas was reconstituted in 5ml 100mM Na_2SO_4, 20mM NaH_2PO_4, pH 6.9 and solubilised by addition of 1ml acetic acid 30% (v/v) and gentle mixing for 30min at 22°C. The acid was then removed by dialysis for 16h and the sample centrifuged at 3,300g for 15min at 4°C in a bench-top microcentrifuge (5417R; Eppendorf, Germany). Insulin concentration was determined from its measured OD_{280} using the extinction coefficient.

Protein melting assay

Protein thermostability melting assays were performed using a Rotor-Gene cycler (Rotor-Gene Q, QIAGEN, Germany), chosen for protein stability measurement by differential scanning fluorimetry (DSF) due to extremely high temperature precision (±0.1°C, reported by Quigen UK). Measurements were preformed in 20mM Tris-HCl pH 7.2, 100mM NaCl using 200µl samples (36 well rotor) with a protein concentration of 0.2g/l. The hydrophobic probe, SYPRO Orange (Invitrogen, UK), was used at 10x concentration (1:200 dilution of 5000x stock). Excitation and emission used the high-resolution melting (HRM) channel (460nm excitation and 510nm emission) which was programmed to ramp the temperature from 25°C to 80°C, collecting the data every 0.6°C, with an equilibration (wait) time of 2 seconds. To calculate the melting point transition, the first derivative of the raw fluorescence (F) and temperature (T) data was calculated (dF/dT) with the peak inflection point indicating the melting point temperature. The first derivative was calculated using Microsoft Excel.

Circular dichroism (CD)

Far UV CD spectra were recorded at 22°C using a Jasco J-810 Spectropolarimeter. Samples were analysed at 0.2g/l in 10mM Tris-HCl, 150mM NaCl, 5mM EDTA, 1mM EGTA, pH 7.5. Four data sets were collected for each sample and averaged, by continuous scanning at 100nm/min, at 205-245nm. The UV CD spectra were baseline corrected, normalised and expressed as molar ellipticity.

Protein Crystallisation & Diffraction

High-throughput nanoliter crystallisation experiments were performed using the Innovadyne Screenmaker and standard crystallisation screens. Each tray consists of 96 crystallisation conditions and two 'sitting drops' per reservoir typically containing 100 and 200nl protein solutions, respectively. Trays were stored in low-vibration incubators at 18 and 4°C and crystal growth was monitored once per week. Crystals were observed in a number of MPD and low-molecular weight PEG containing drops. In parallel, 'hanging drop' trays were set up screening around published crystallisation conditions. Crystals grew to ~0.2-1.0mm and were subsequently used for diffraction experiments.

Initial screening experiments used an in-house Bruker MicroStar rotating anode, producing crystals diffractions up to 5Å resolution. All main data collections were performed at beam line I02 at the Diamond Light Source (DLS). Data was processed with XDS (Kabsch, 2010). The structure was solved and refined independently using the CCP4 program package (CCP4, 1994). Protein crystallisation and diffraction experiments and the subsequent data processing were performed by Ian Williamson or Dr Ehmke Pohl at Durham University.

Immunoblotting

Immunoblotting was performed using the semidry blotting method (Kyhse-Andersen, 1984) according to the manufacturer's specifications (Bio-Rad Laboratories, UK). Following one-dimensional SDS-PAGE, proteins were transferred onto NitroBind 0.45uM nitrocellulose membrane, (VWR, UK). After blotting, protein transfer was assessed by Ponceau S (Sigma Aldrich, UK) staining of the nitrocellulose membrane followed by destaining in Tris-buffered saline (TBS) (20mM Tris-HCl pH 7.4, 150mM NaCl). After incubation with blocking solution consisting of 5% (w/v) dried milk powder (Marvel, UK) in TBS containing 0.2% (v/v) Tween 20 (TBST) for 1h at 22°C with agitation the membranes were probed with a primary antibody in antibody buffer (1 part block solution: 2 parts TBS) for 2h at 22°C with agitation. The nitrocellulose membrane was washed 3 times with TBST and once with TBS over a 30min period then incubated with the appropriate secondary antibodies (Dako Cytomation, UK) diluted 1:1000 in antibody buffer for 1h at 22°C with agitation. Antibody labelling was detected by enhanced chemilluminescence using a luminescent image analyser (LAS-1000plus, Fuji Photo Film UK).

Assembly of filaments

Filament assembly was based on the method used by Quinlan et al 1989. Purified desmin at 0.2g/l in 6M Urea, 20mM Tris-HCl pH 8, 1mM DTT, 1mM EDTA, 0.2mM PMSF (in the presence or absence of aB crystallin at 0.08g/l) was dialysed to reduce the Urea concentration to 4M, then 2M, then 0M over a period of 24h at 22°C. Desmin filament assembly was finalised by dialysis into 20mM Tris-HCl pH 7.4 (or as otherwise stated), 50mM NaCl at either 22, 37 or 44°C for 16h. Assembly of 0.2g/l BFSP1 with 0.2g/l BFSP2 was carried out in the same way (in the presence or absence of aB crystallin at 0.08g/l), but with the addition of 1mM $MgCl_2$ to the final dialysis buffer.

Fast assembly of filaments using imidazole pH 6.8

Purified desmin at 0.2g/l in 6M Urea, 20mM Tris-HCl, pH 8, 1mM EDTA, 1mM EGTA, 1mM DTT, 0.2mM PMSF (in the presence or absence of aB crystallin at 0.08g/l) was dialysed by stepwise lowering of the Urea concentration into 10mM Tris-HCl pH 7, 1mM DTT, 0.2mM PMSF at 4°C. Assembly was finalised by rapid addition of a 20-fold concentrated assembly buffer to give a final concentration of 100mM imidazole-HCl pH 6.8, 1mM DTT, 0.2mM PMSF. Samples were then incubated for 1h at 22, 37 or 44°C.

Co-sedimentation assay

Co-sedimentation assays were based upon methods previously developed (Bennardini et al., 1992; Bousquet et al., 2001; Nicholl and Quinlan, 1994; Perng et al., 2004). Samples were centrifuged at 80,000g for 30min at 20°C in a Beckman Optima MAX Ultracentrifuge using a TLS-55 rotor (Beckman Instruments, USA) for the high speed assay and at 2,500g for 15min at 20°C in a bench top centrifuge (5417R; Eppendorf, Germany) for the low speed assay. The pellets and supernatants were separated and solubilised in equal final volumes of SDS-PAGE sample buffer and analysed via SDS-PAGE.

Transmission electron microscopy (TEM)

Samples were prepared essentially using the Valentine method (Valentine et al., 1968). A 0.5cm^2 carbon film, coated onto freshly cleaved mica, was floated on samples at 5mg/l for 5s and then on 1% (w/v) uranyl acetate (Agar Scientific, UK) for 5s. The carbon film was then retrieved using 400 mesh copper grids (Agar Scientific, UK) and gently blotted to remove excess stain from the surface of the grid. Grids were analysed using a Hitachi H-7600 scanning transmission electron microscope (Hitachi High-Technologies Corporation, Japan), using an accelerating voltage of 100kV. Images were acquired using a CCD camera (Advanced Microscopy Technology, USA) and assembled into figures using Adobe Photoshop CS (Adobe System, USA).

Quantification of TEM images

TEM quantifications were made using ImageJ 1.44 (http://rsb.info.nih.gov/ij). For measurement of filament width, 50 measurements were made using three different images to give a total of 150 width measurements for each sample. Measurements were made at 100nm intervals along the length of the filaments in randomly selected areas. Average and standard deviations of sample filament width were then calculated.

Data mining and analysis

Isoelectric points, molecular weights and extinction coefficients of proteins were calculated using the web resource at ExPASY (www.expasy.ch). Database mining used BLAST (http://blast.ncbi.nlm.nih.gov/Blast.cgi) and sequence alignments were made using the clustalW2 package (www.ebi.ac.uk).

CHAPTER 3: ROLE OF THE R107 RESIDUE AND THE C-TERMINAL IXI MOTIF OF Mj Hsp16.5

AIM

To determine the structural and functional effects of mutating the conserved R107 residue in Mj Hsp16.5 and of truncating the conserved C-terminal tail IXI domain.

INTRODUCTION

Studies have shown that aB crystallin oligomers are polydisperse and in dynamic equilibrium with sub-assembly species (Aquilina et al., 2003; Bloemendal et al., 2004; Haley et al., 2000; Haley et al., 1998; Horwitz, 2008; McHaourab et al., 2009), making crystallisation of the full length protein unattainable to date. The absence of atomic level structural data makes it difficult to predict the effects of disease causing aB crystallin mutations on protein structure, and subsequently on oligomerisation and chaperone activity. The R120G aB crystallin mutation causes cataract and myopathy and the Q151X aB crystallin mutation causes myopathy (Selcen and Engel, 2003; Vicart et al., 1998). Both these mutations are known to affect interactions with IFs (Hayes et al., 2008; Perng et al., 2004), but the effect of these mutations on aB crystallin structure is unknown. Investigating the potential structural changes these mutations cause, may therefore provide insight into the altered interaction with IFs.

At the time time of undertaking these studies, there was no crystal structure data available for aB crystallin. However, a crystal structure was available for the sHsp, Hsp16.5 from Methanococcus jannaschii (Van Montfort et al., 2001b). Therefore, this protein can be used to model the potential structural effects of disease causing aB crystallin mutations. This may provide insights into the altered interactions with IFs. Mutations equivalent to the R120G and Q151X aB crystallin mutations were created in Hsp16.5 to give R107G and I140X Hsp16.5, respectively (Fig 3.1). Hsp16.5 was also truncated at the IXI motif (G143X) (Fig 3.1), to determine the structural effects of removing this highly condserved motif, which is believed to be important for oligomer assembly (Jehle et al., 2010; Jehle et al., 2011; Laganowsky et al., 2010; Pasta et al., 2004). Both the arginine residue in the a-crystallin domain and the IXI motif in the C-terminal tail are highly conserved throughout sHsps, but at the time of undertaking these experiments, very little was known about their potential effects on sHsp structure.

In this chapter, I show that removal of the C-terminal IXI motif from Hsp16.5 causes loss of oligomerisation, increased chaperone activity and potentially altered protein structure. I also show that, in contrast, mutation of the conserved R107 residue does not affect Hsp16.5 structure or chaperone activity.

A.

```
1     MFGRDPFDSL FERMFKEFFA TPMTGTTMIQ
31    SSTGIQISGK GFMPISIIEG DQHIKVIAWL
61    PGVNKEDIIL NAVGDTLEIR AKRSPLMITE
91    SERIIYSEIP EEEEIYRTIK LPATVKEENA
121   SAKFENGVLS VILPKAESSI KKGINIE
```

B.

```
WT aB crystallin  1   MDIAIHHPWI RRPFFPFHSP SRLFDQFFGE HLLESDLFPT
WT Hsp16.5        1   -------MFG RDPFDSLF-- ERMFKEFFAT PMTGTTMIQS

WT aB crystallin  41  ST--SLSPFY LRPPSFLRAP SWFDTGLSEM RLEKDRFSVN
WT Hsp16.5        32  STGIQISGKG FMPISIIEGD QHIKVIAWLP GVNKEDIILN

WT aB crystallin  79  LDVKHFSPEE LKVKVLGDVI EVHGKHEERQ DEHGFISREF
WT Hsp16.5        72  AVGDTLEIRA KRSPLMITES ERIIYSEIPE EE------EI

WT aB crystallin  119 HRKYRIPADV DPLTITSSLS SDGVLTVNGP ---RKQVSGP
WT Hsp16.5        106 YRTIKLPATV KEENASAKFE N-GVLSVILP KAESSIKKG-

WT aB crystallin  156 ERTIPITREE KPAVTAAPKK
WT Hsp16.5        144 ---INIE
```

Fig 3.1. The WT Hsp16.5 protein sequence.

(A) WT Hsp16.5 protein sequence. The red residues were removed to create the G143X Hsp16.5 mutant and both the red and blue residues were removed to create the I140X Hsp16.5 mutant. Residue R107 (Green), which lies in the b7 strand, was changed to G107 to create the R107G Hsp16.5 mutant. (B) WT aB crystallin (Bold) and WT Hsp16.5 (Non-Bold) sequence allignment. The I140X and R107G Hsp16.5 mutations are equivalent to the disease causing Q151X and R120G aB crystallin mutations, respectively. The G143X Hsp16.5 removes the highly conserved IXI motif.

RESULTS

Purification of WT Hsp16.5

WT Hsp16.5 was expressed in *E. coli*, extracted from the water soluble fraction, then purified by anion exchange (Fig 3.2, A) and size exclusion chromatography (Fig 3.2, B). However, after these purifications, many contaminating proteins are still visible and the WT Hsp16.5 is only ~90% pure (Fig 3.2, B). However, these purification techniques do not appear to be sufficient to separate the WT Hsp16.5 from the contaminating *E. coli* proteins (Fig 3.2).

Methanococcus jannaschii (Mj) is a hyperthermophile and lives in hyperthermal oceanic vents, which experience temperatures of ~50-95°C and NaCl concentrations of ~0.2-1.0M (Bult et al., 1996). These organisms must therefore posses unique adaptations to allow survival in such high temperatures and salinity levels (Tsoka et al., 2004). It was thus hypothesised that if the *E. coli* soluble extract was subjected to these temperatures and salt levels, the contaminating native *E. coli* proteins would be denatured and aggregate out of solution, while the Mj WT Hsp16.5 protein would remain soluble, and hence purified.

To test this hypothesis, the extracted soluble protein fraction was incubated in a water bath at 80°C for 30 minutes in the presence of 1M, 0.5M or 0.0M NaCl. Samples were then cooled on ice for 10min and centrifuged at 48,000g for 30 minutes. The pellets and supernatants were separated and solubilised in equal final volumes of SDS-PAGE sample buffer to allow direct comparison of the proportions of material in the supernatant and pellet. Results were then visualised via SDS-PAGE and quantified by gel densitometry (Fig 3.3).

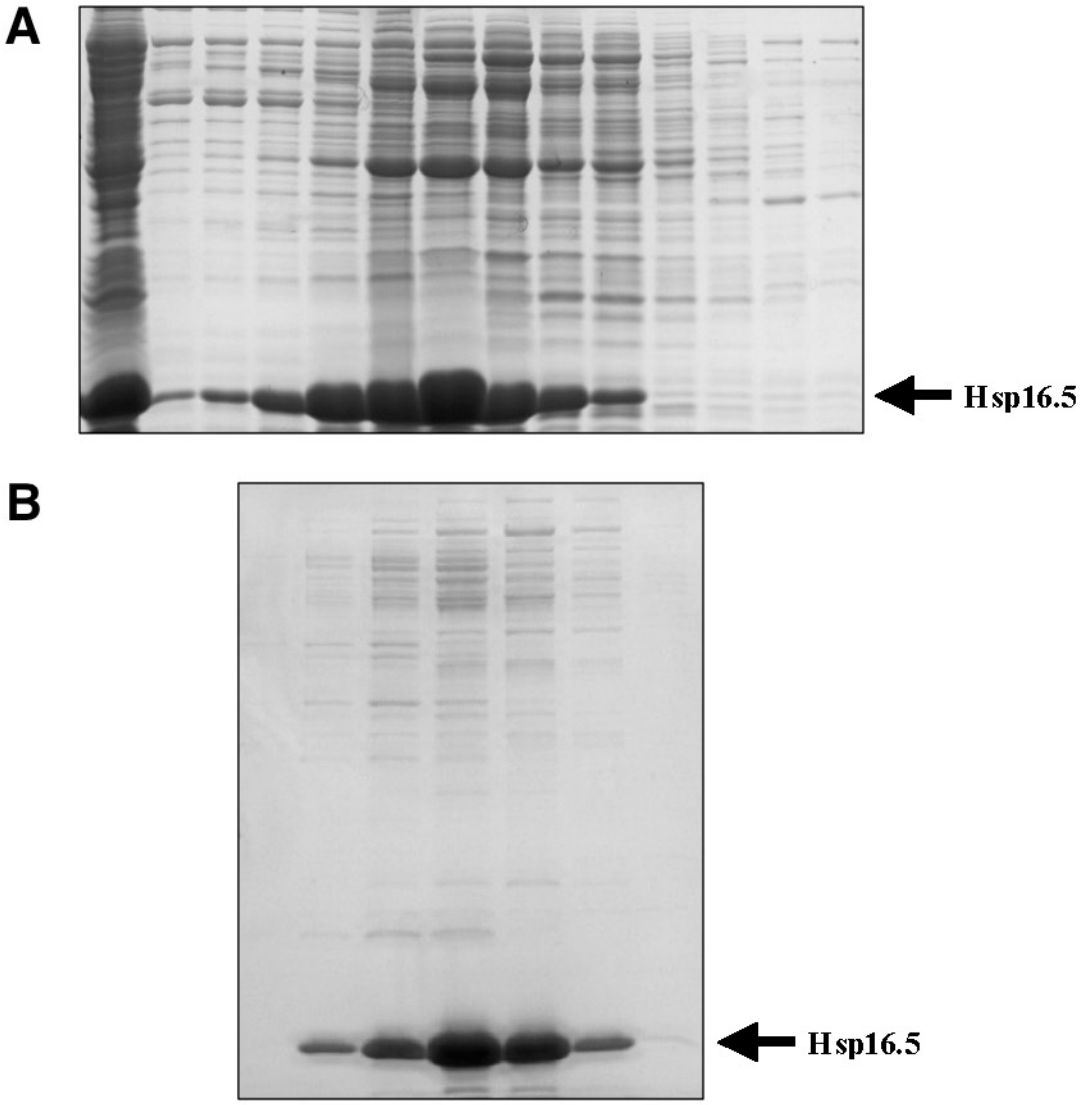

Fig 3.2. Anion exchange and size exclusion purification of WT Hsp16.5

Anion exchange (A) and size exclusion (B) chromatography elution profile for WT Hsp16.5. After soluble protein extraction, anion exchange and size exclusion purifications, many contaminating proteins are still visible and the WT Hsp16.5 is only ~90% pure. The original soluble protein fraction extracted from *E. coli,* which was loaded onto the anion exchange column, is shown in the far left lane of figure 'A'.

As expected, when the *E. coli* soluble protein extract is incubated at 80°C for 30 minutes, almost all contaminating proteins are denatured and precipitate out of solution, regardless of NaCl concentration (Fig 3.3). In contrast, the WT Hsp16.5 remains mostly soluble. Interestingly, as the NaCl concentration is increased from 0.0M to 0.5M to 1.0M, the proportion of WT Hsp16.5 which pellets, decreases from 45% to 25% to 20% respectively (Fig 3.3).

Therefore, to maximise WT Hsp16.5 yield, the protein was incubated for 30 minutes at 80°C in the presence of 1M NaCl, and the resulting soluble fraction was 90-95% pure. This procedure will be referred to as 'heating purification' in the remainder of this chapter. The heat purified sample was then purified further by the anion exchange and size exclusion chromatography, as detailed earlier, to >99% purity. The size exclusion elution profile is shown in Fig 3.4, A. The effect of the heating purification step on final achieved purity can be seen by comparing Fig 3.4, A with Fig 3.2, B.

The thermostability of the purified WT Hsp16.5 sample then was tested by incubating again at 80°C for 30 minutes in the absence of 1M salt. The sample was then centrifuged and the supernatant and pellet compared to show that >98% of the WT Hsp16.5 remains soluble (Fig 3.4, B). This demonstrates the extremely high thermostability of the WT Hsp16.5 protein.

Interestingly, when the WT Hsp16.5 is heated in the presence of contaminating *E. coli* proteins in the absence of NaCl, ~45% is pelleted (Fig 3.3) compared to the <2% pelleted when purified WT Hsp16.5 is heated. This may suggest that the WT Hsp16.5 is binding to the denaturing *E. coli* proteins and co-precipitating. In addition, increasing the NaCl concentration to 0.5M or 1.0M appears to reduce this effect (25% and 20% of WT Hsp16.5 pellets respectively) suggesting that the potential interaction of the WT Hsp16.5 with the *E. coli* proteins maybe heavily dependant upon salt concentration (Fig 3.3).

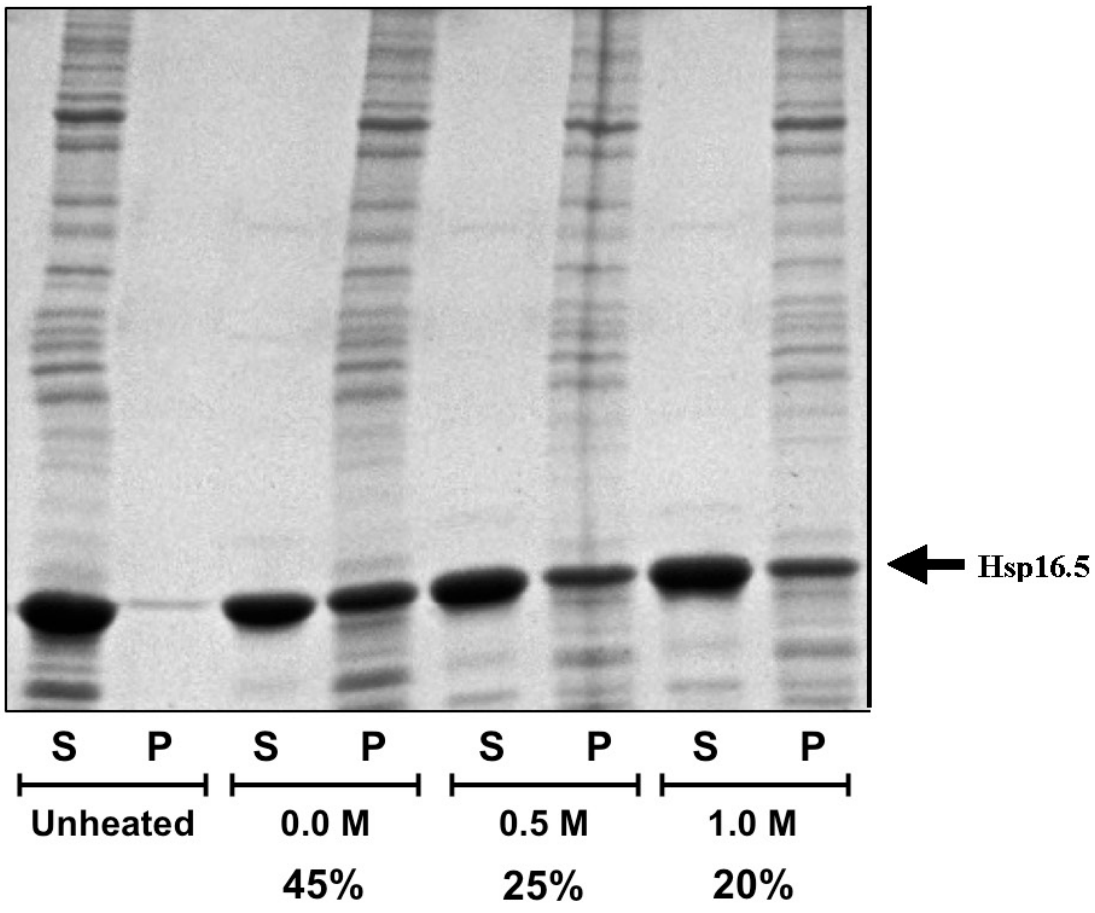

Fig 3.3. Heat purification of WT Hsp16.5.

The soluble protein fraction was extracted from *E. coli* and incubated in a water bath at 80°C for 30min in the presence of 1M, 0.5M or 0.0M NaCl. Samples were then cooled on ice for 10min and centrifuged at 48,000g for 30min. The pellets (P) and supernatants (S) were separated and solubilised in equal final volumes of SDS-PAGE sample buffer to allow direct comparison of the proportions of material in the supernatant and pellet. Gel densitometry was used to quantify the % of WT Hsp16.5 protein pelleted at the 3 different NaCl concentrations (shown as % values below each of the 3 salt concentrations). When incubated at 80°C with 1M NaCl, almost all contaminating proteins are denatured and pellet, whereas only 20% of WT Hsp16.5 is pelleted.

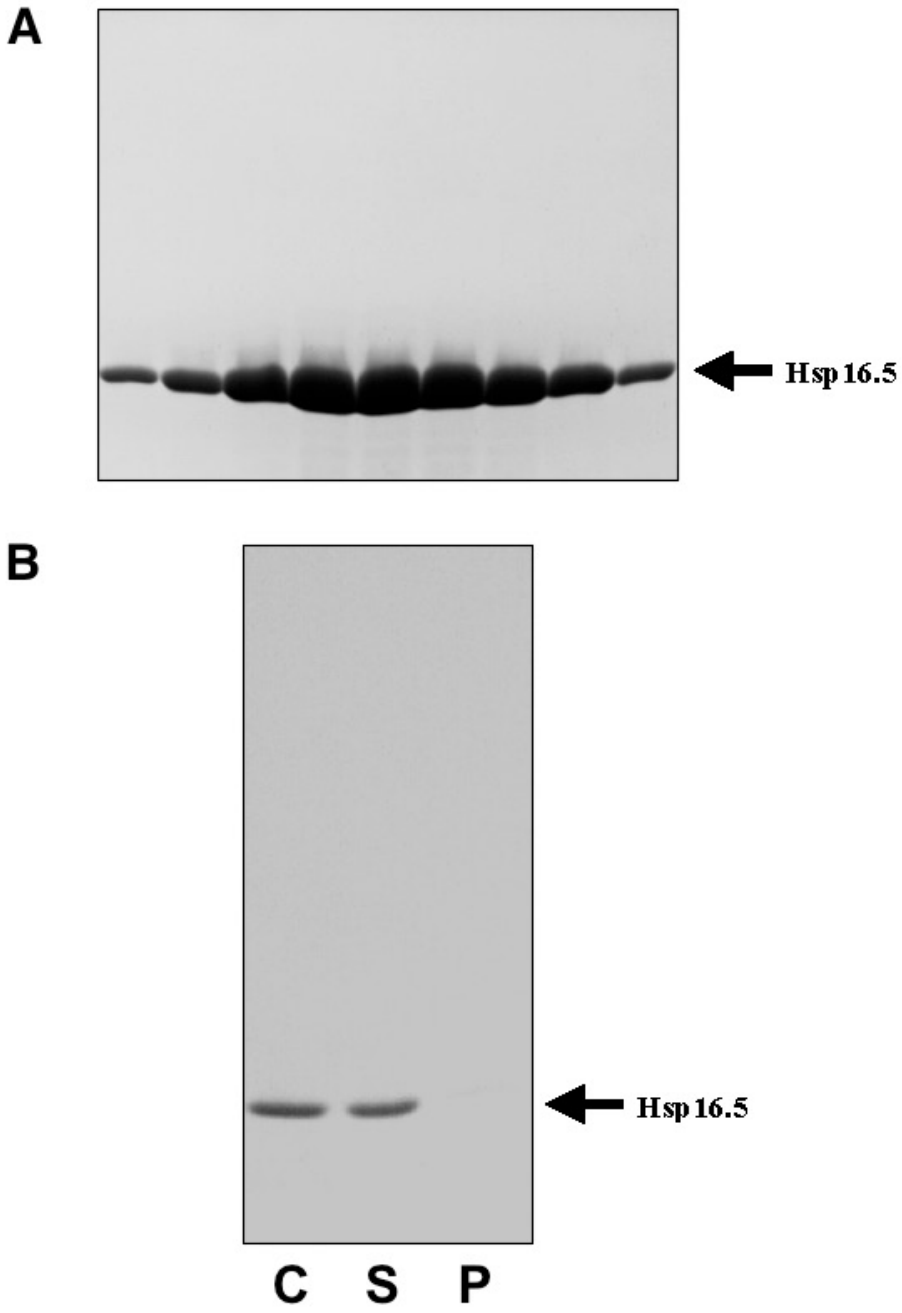

Fig 3.4. Size exclusion purification and thermostability of WT Hsp16.5

(A) Size exclusion chromatography (SEC) elution profile for WT Hsp16.5, after heating and anion exchange purifications. (B) The post-SEC purified WT Hsp16.5 was incubated at 80°C for 30 minutes (in the absence of NaCl) and then centrifuged at 48,000g. >98% of the protein remains soluble, demonstrating the extremely high thermostability of the WT Hsp16.5 protein. Unheated (C), supernatant (S) and pellet (P).

Purification of I140X, G143X and R107G Hsp16.5

The I140X, G143X and R107G Hsp16.5 mutant expression constructs were created by PCR mutagenesis and confirmed by bi-directional DNA sequencing. The proteins were expressed in *E. coli* and extracted from the water soluble fraction. Fig 3.5 shows the soluble protein extracts from *E. coli*. Notice that I140X and G143X Hsp16.5 appear to have higher concentrations of contaminating proteins than the WT or R107G Hsp16.5 extracts (Fig 3.5).

The R107G Hsp16.5 mutant was purified using the same purification methods as WT Hsp16.5, by heating and centrifugation, anion exchange and size exclusion chromatography (data not shown). This results in >98% purity (Fig 3.6, C).

Initially, the I140X and G143X Hsp16.5 mutants were also purified using the same methods as used for WT and R107G Hsp16.5. However, the heating purification was significantly less effective for I140X and G143X Hsp16.5 mutants compared to WT and R107G Hsp16.5. 'Fig 3.6, A' shows the result of the heating purification of G143X Hsp16.5. Similar to WT Hsp16.5, ~20% of the G143X Hsp16.5 protein precipitates and is pelleted. However, in contrast to WT, the G143X Hsp16.5 post heating soluble fraction contains ~10% contaminating proteins (Fig 3.6, A). This exact same result was also observed for the I140X Hsp16.5 (data not shown). This may suggest that, unlike the WT, the I140X and G143X Hsp16.5 proteins can protect the contaminating proteins from denaturation and aggregation.

The heat purified I140X and G143X Hsp16.5 proteins were then purified further using by anion exchange and size exclusion chromatography, as performed for WT and R107G Hsp16.5. However, these methods failed to purify the I140X and G143X mutants and samples remained only ~90% pure. 'Fig 3.6, B' shows the I140X and G143X Hsp16.5 samples after heat purification, anion exchange and size exclusion chromatography, and contaminating bands are easily visible (Fig 3.6, B).

In order to achieve >98% purity, the I140X and G143X proteins required heating purification, two separate anion exchange purifications using 60ml DEAE and 10ml TMAE columns, followed by two separate size exclusion chromatography purifications using 120ml Fractogel and 24ml Superose 6 columns. For details, see 'materials and methods'. The final purified I140X and G143X samples were >98% pure (Fig 3.6, C).

It is worth noting that the I140X and G143X Hsp16.5 mutations appeared to cause dramatically decreased protein solubility during purification. Throughout purification, the WT and R107G Hsp16.5 proteins remained soluble and did not precipitate, maintaining constant soluble protein concentrations over time (data not shown). In stark contrast, the I140X and G143X mutants were observed to continuously precipitate from solution with the effect of continually reducing the soluble protein concentration over time (data not shown). This observed insolubility and precipitation also appeared to be linked to protein purity, as the I140X and G143X precipitation appeared to reduce in line with increasing purity. This may suggest that binding of the I140X and G143X to contaminating proteins was causing the precipitation. In addition, the WT and R107G Hsp16.5 proteins remained soluble at concentrations >40g/l. In contrast, the I140X and G143X proteins appeared less soluble at high concentrations and were observed to precipitate at concentrations >10g/l (data not shown). However, these observation were not formally quantified.

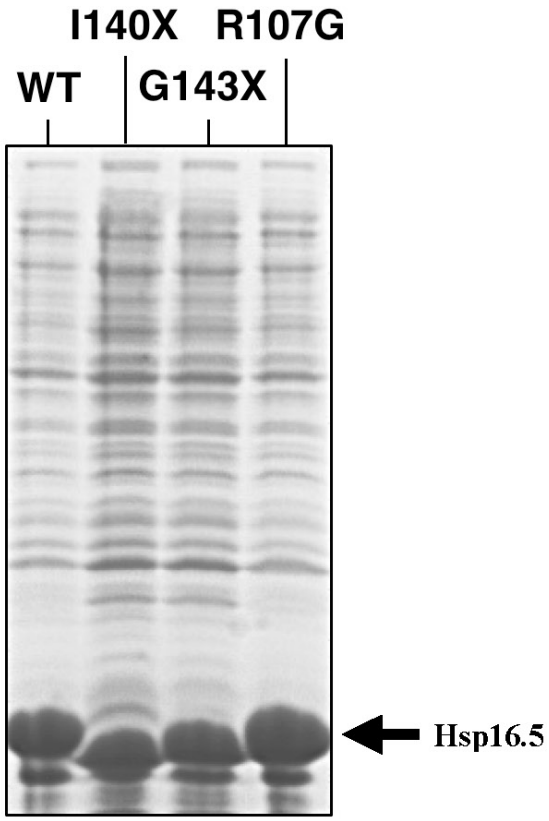

Fig 3.5. *E. coli* soluble protein extracts for WT, I140X, G143X, and R107G Hsp16.5.

The WT, I140X, G143X, and R107G Hsp16.5 proteins were expressed in *E. coli* and the soluble protein fractions were extracted. Notice that I140X and G143X Hsp16.5 samples appear to have higher concentrations of contaminating proteins than the WT or R107G Hsp16.5 samples.

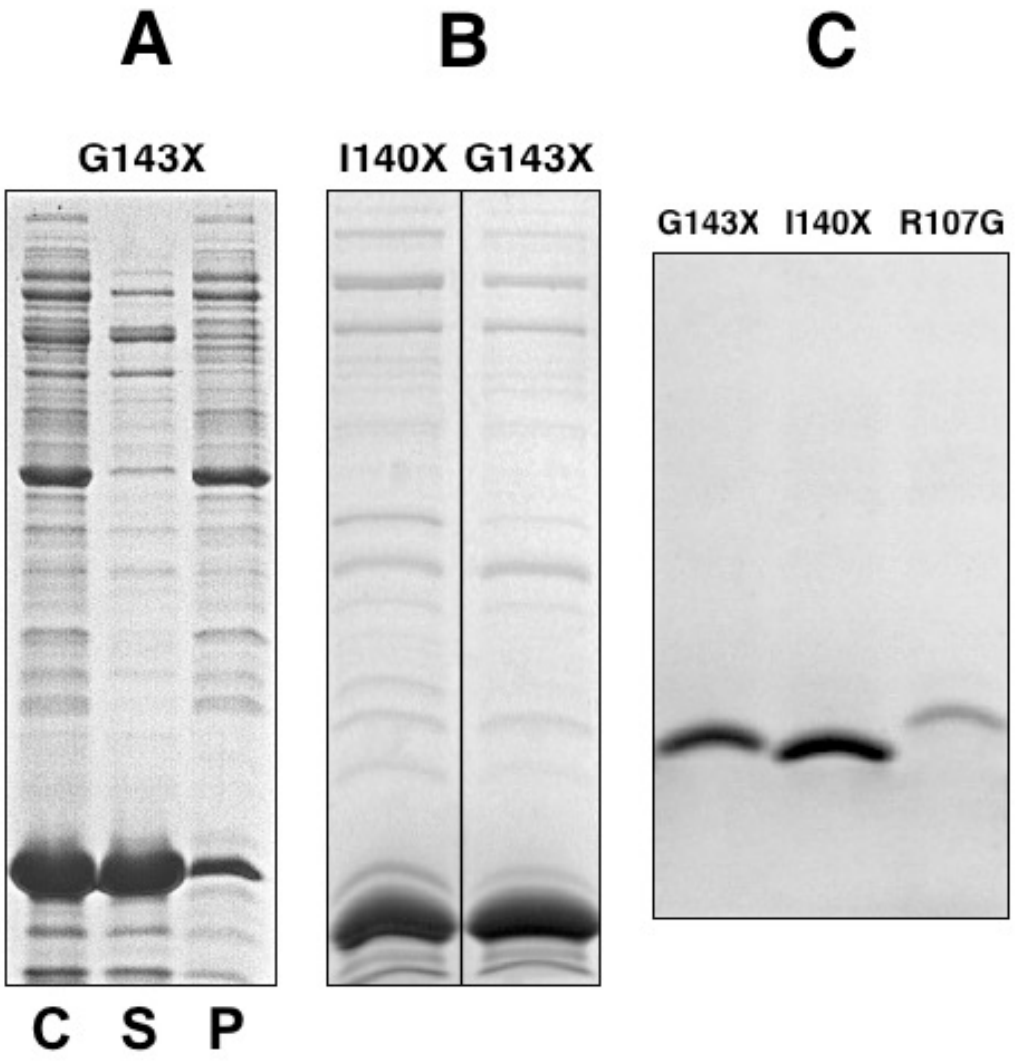

Fig 3.6. Purification of I140X and G143X Hsp16.5.

(A) Result of heating purification of G143X Hsp16.5. Unheated (C), supernatant (S) and pellet (P). (B) I140X and G143X Hsp16.5 samples after heat purification, anion exchange and size exclusion chromatography. Contaminating bands are easily visible. (C) Final purification achieved for G143X, I140X and R107G Hsp16.5 proteins. Samples are >98% pure.

Crystallisation of WT and mutant Hsp16.5 proteins

To determine the effect of the I140X, G143X and R107G Hsp16.5 mutations on protein structure, X-ray crystallography experiments were preformed. The highly pure Hsp16.5 protein samples (Fig 3.6, C) were grown into crystals (Fig 3.7) which were then tested by Dr Ehmke Pohl at beam line I02 at the Diamond Light Source.

As a control, I decided to crystallise the WT Hsp16.5 protein, and compare the results with the previously published data (Kim et al., 1998). X-ray diffraction data was collected for WT Hsp16.5 at 2.5Å, an improved resolution compared to the previously published data (2.9Å) (Kim et al., 1998). The crystallographic data collection and refinement statistics data are available in supplementary material (Sup Table 1). The data was then used to create a structural model (data not shown), which proved to be identical to the previously published structure (Kim et al., 1998).

Surprisingly, subsequent crystallisation of R107G revealed a structure identical to WT Hsp16.5 (Fig 3.8). The crystallographic data collection and refinement statistics data are available in supplementary material (Sup Table 1), but there was no detectable difference from WT Hsp16.5. The mutation was confirmed by mass spectroscopy (data not shown) and is also clearly visible in the R107G crystal structure model (Fig 3.9).

For the I140X and G143X Hsp16.5 mutants, crystals were smaller (~0.2mm) than those formed by WT or R107G Hsp16.5 (~0.5mm) and showed weaker diffraction properties. X-ray diffraction data was collected for I140X and G143X Hsp16.5 at ~4.0Å (Sup Table 1). Interestingly, data shows that the unit cell dimension and the potential space group have changed for both I140X and G143X Hsp16.5, compared to the WT Hsp16.5. This may indicate a possible change in overall structure, however the resolution of the data is not sufficient to verify this intriguing possibility. Despite purifying the I140X and G140X Hsp16.5 proteins for crystallisation on 10 separate occasions, I was unable improve the crystallographic resolution.

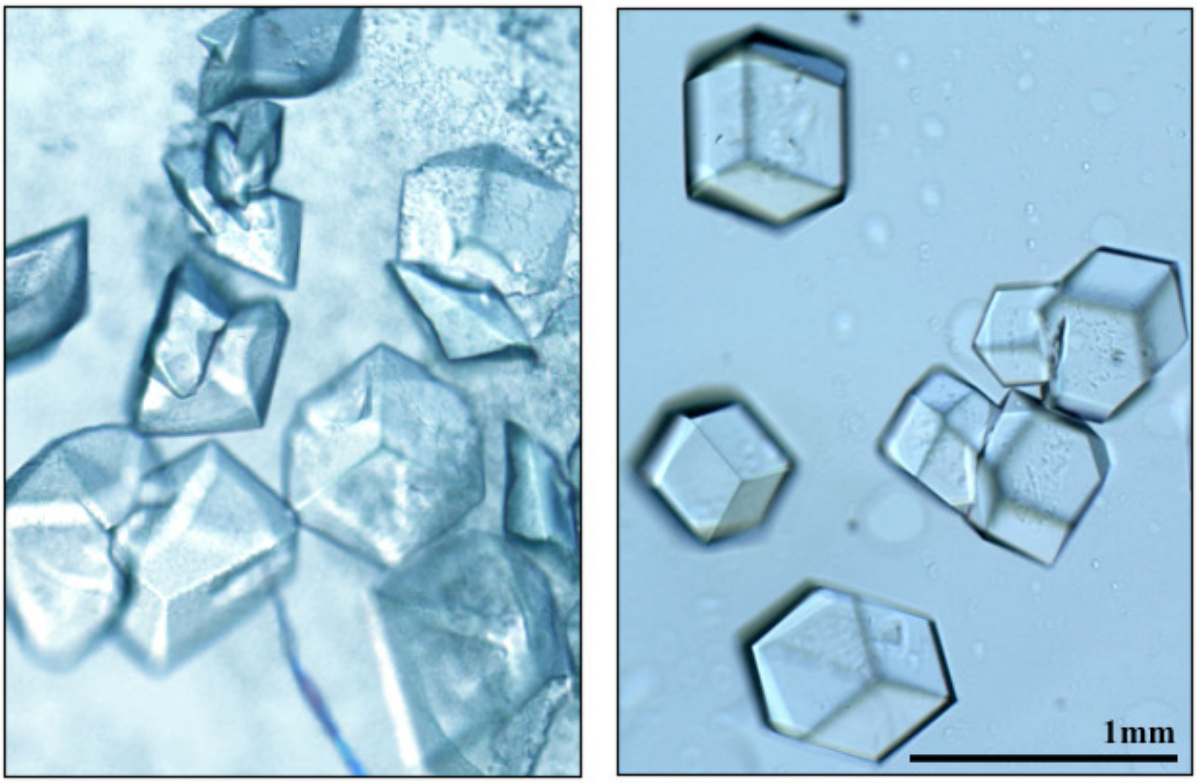

Fig 3.7. Photograph of crystals of WT and R107G Hsp16.5.

The photographs show crystals grown from WT and R107G Hsp16.5 which were subsequently used in X-ray crystallography experiments.

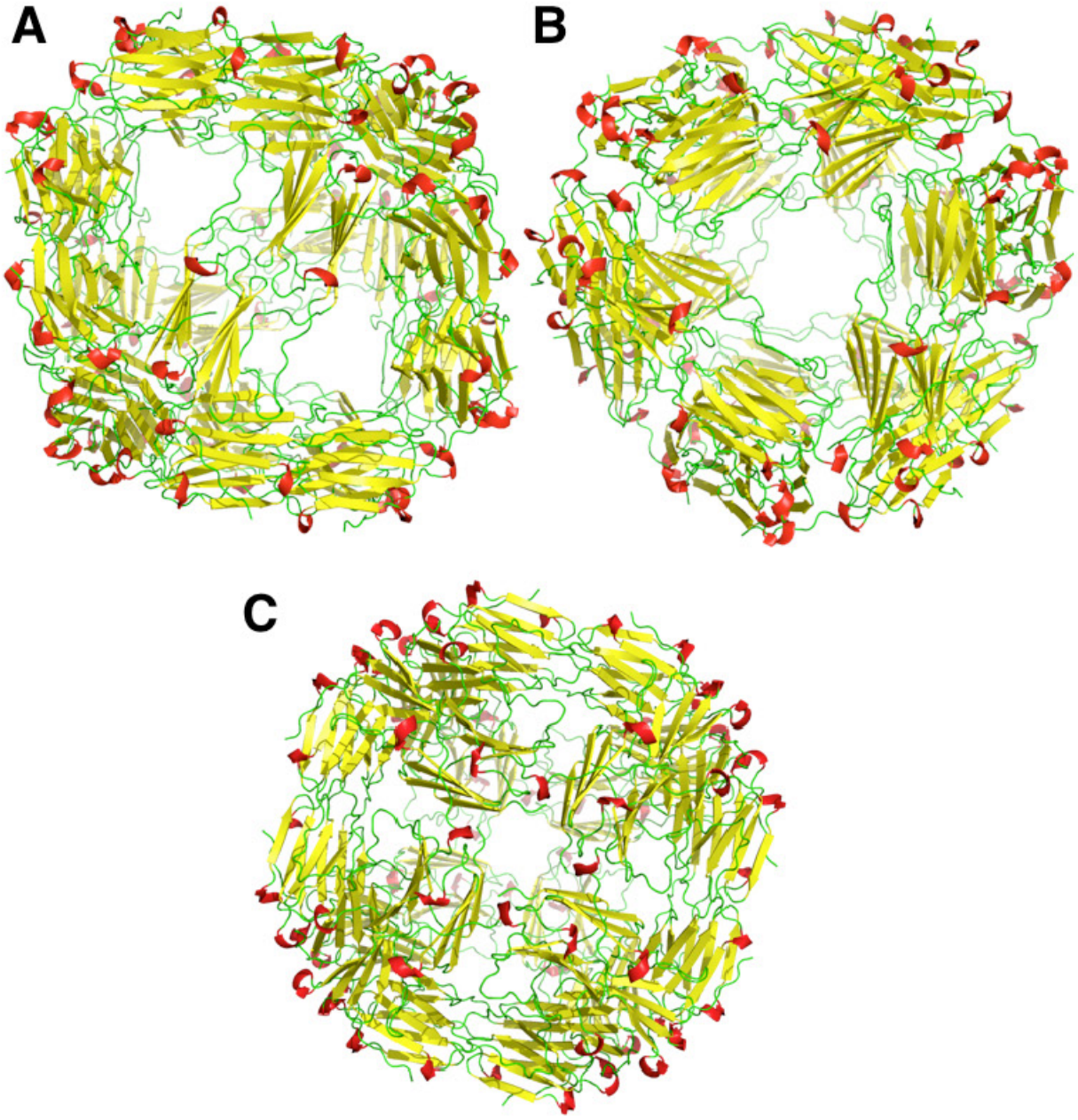

Fig 3.8. Crystal structure model of R107G Hsp16.5.

Crystal structure model of R107G Hsp16.5 showing 2-fold (A), 3-fold (B) and 4-fold (C)symmetry. The R107G Hsp16.5 is isostructural to WT Hsp16.5, which was previously reported by Kim et al., 1998. This figure was prepared by Dr Ehmke Pohl. α-helical regoins are shown in red, β-sheet regions are shown in yellow and other secondary structures are shown in green.

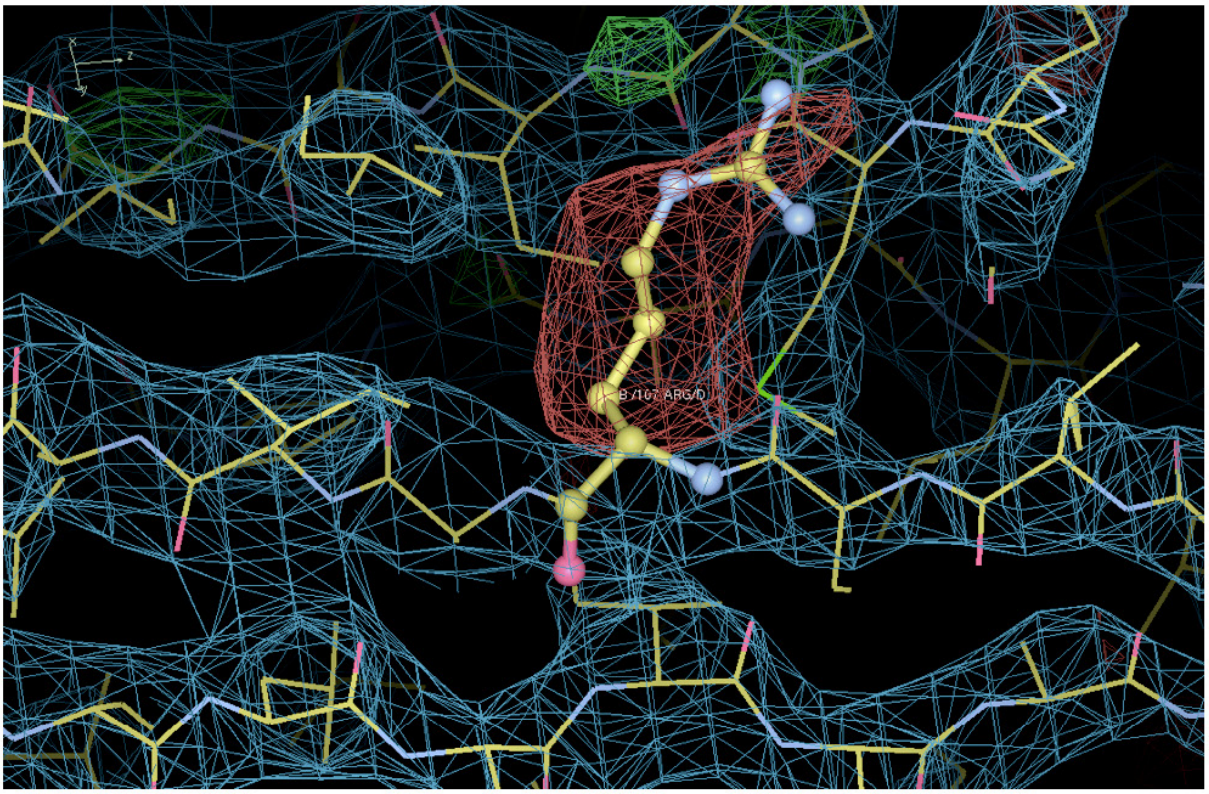

Fig 3.9. Confirmation of the Hsp16.5 R107G mutation.

The R107G crystal structure model confirms the R to G mutation. The red density map clearly shows that no side chain is present on residue 120, confirming the arginine to glycine mutation. The yellow chains represent the amino acid backbones while the amino acid densities are shown in blue. The R107G density is shown in red. This figure was prepared by Dr Ehmke Pohl.

Analysis of chaperone activity of WT, I140X, G143X and R107G Hsp16.5 proteins.

The X-ray diffraction studies suggested that the I140X and G143X Hsp16.5 mutations may cause altered structure (Sup Table 1), which could affect chaperone activity. In addition, the dramatically altered purification characteristics of the I140X and G143X Hsp16.5 mutants may indicate altered binding or chaperoning characteristics, such that the I140X and G143X mutants bind and chaperone contaminating proteins, thus preventing their separation. To investigate this further, the in vitro chaperone activity of the Hsp16.5 proteins was analysed.

WT, I140X, G143X and R107G Hsp16.5 proteins were analysed to compare the in vitro chaperone activity for heat denatured citrate synthase (Fig 3.10). Results show that both WT and R107G Hsp16.5 can protect against the heat induced aggregation of citrate synthase, providing comparable levels of protections of 26% and 30% respectively (Fig 3.10). Interestingly, the I140X and G143X Hsp16.5 mutants provide significantly increased (~2x) protection of 65% and 66% respectively (Fig 3.10), indicating increased chaperone activity.

Analysis of WT and G143X Hsp16.5 oligomer size

To further investigate the possible causes of the increased chaperone activity of G143X, the WT and G143X Hsp16.5 proteins were analysed by analytical size exclusion chromatography to investigate any changes in oligomerisation (Fig 3.11). Results show that the WT oligomer is composed of ~24 subunits. There is also an additional small species which elutes at ~17.9ml (corresponding to an estimated 27 kDa), which is likely the dimer. Interestingly, the G143X Hsp16.5 appears to have completely lost the ability to oligomerise and exists largely as a dimer (Fig 3.11). The G143X also produces an additional small peak at ~21.8ml, but this cannot be quantified as it lies outside of the separation range of the column. This species may be the monomer, but further analysis with a different SEC column would be required to confirm this hypothesis.

A

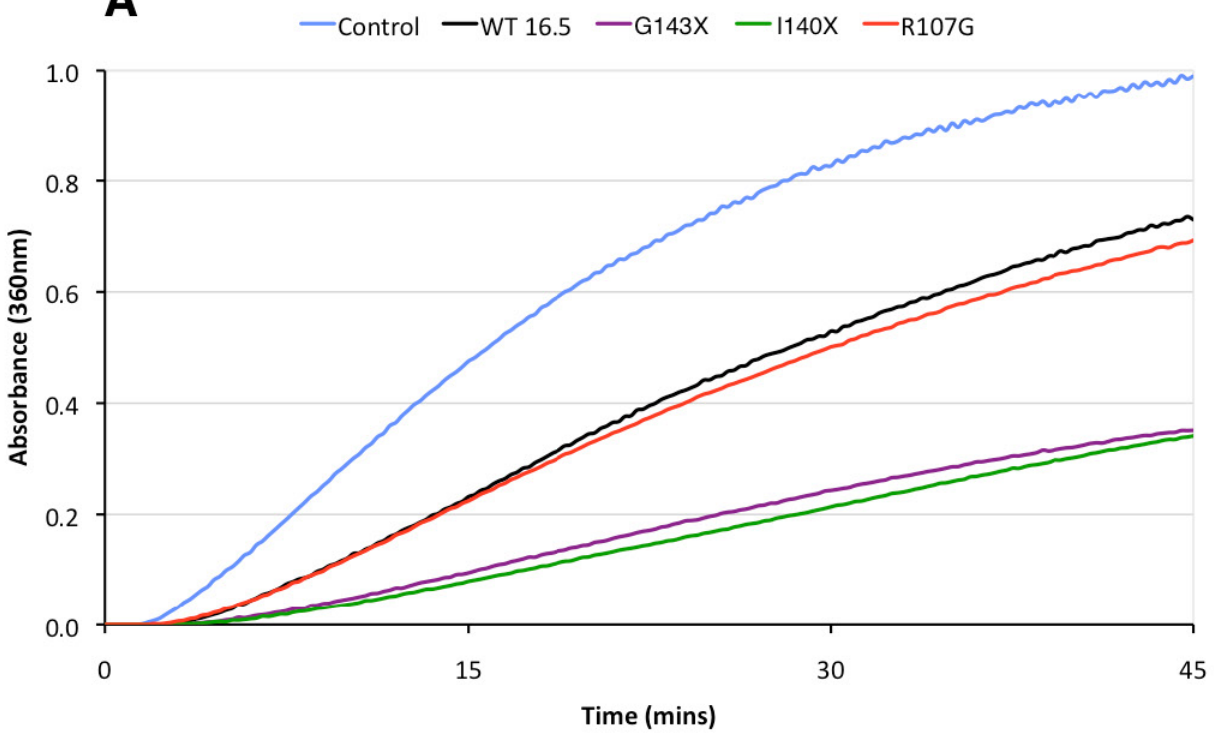

B

	% Protection	SD
WT 16.5	26	8
G143X	65	12
I140X	66	9
R107G	30	10

Fig 3.10. Chaperone activity of WT and mutant Hsp16.5 proteins for citrate synthase.

The graphs show the thermal aggregation of 0.2g/l citrate synthase at 44°C in the presence of 0.2g/l WT (black), G143X (purple), I140X (green) or R107G (red) Hsp16.5. The aggregation of citrate synthase alone is shown in blue (control). The table shows the final absorbance values as a percentage reduction, compared to the control (% Protection). Absorbance values are an average of 3 experimental repeats and standard deviations (SD) are also shown. G143X and I140X Hsp16.5 show significantly increased chaperone activity compared to WT and R107G Hsp16.5.

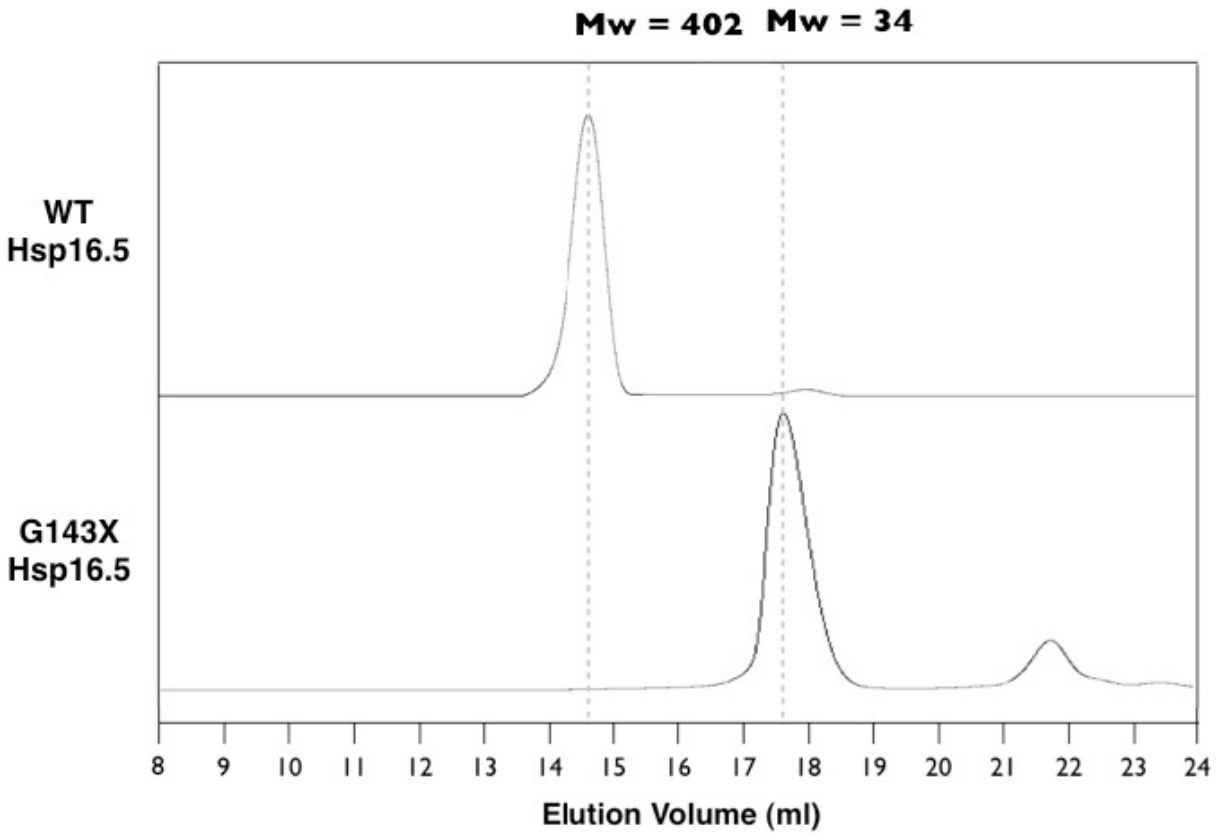

Fig 3.11. Analytical SEC alignment for WT and G143X Hsp16.5.

WT and G143X Hsp16.5 elution's from the analytical size exclusion column. The analytical SEC column calibration (see supplementary data Sup Fig 2) was used to calculate that the main peaks corresponds to ~402 kDa for WT and ~34 kDa for G143X. This indicates that the main oligomeric species for WT is composed of ~24 subunits, and the main oligomeric species for G143X is a dimer. The G143X Hsp16.5 appears to have completely lost the ability to oligomerise. In the G143X elution, the additional small peak at ~21.8ml cannot be quantified as it lies outside of the separation range of the column.

RESULTS SUMMARY

Overall, results in this chapter show that the I140X and G143X mutations dramatically affect the purification characteristics of the Hsp16.5 protein. In addition, these mutations significantly improve in vitro chaperone activity for citrate synthase and the G143X mutation causes a complete loss of oligomer formation, such that the dimer is the main species. Furthermore, crystallisation data suggests that these mutations may have caused significant structural changes.

In contrast, results show that the R107G mutation does not affect protein structure and has no effect on in vitro chaperone activity for citrate synthase.

In addition, results in this chapter show that the purification of WT Hsp16.5 proteins can be significantly improved using a heating and centrifugation step to denature contaminating *E. coli* proteins.

CHAPTER 4: THE IN VITRO EFFECTS OF THE CATARACT CAUSING D140N aB CRYSTALLIN MUTATION

AIM

To investigate the *in vitro* effects of the cataract causing D140N aB crystallin mutation.

INTRODUCTION

The D140N mutation of aB crystallin is associated with autosomal dominant congenital lamellar cataract (Liu et al., 2006e). The point mutation substitutes a negative charged aspartic acid with a neutral asparagine residue at codon 140 within the highly conserved a-crystallin domain. The a-crystallin domain has been shown to bind substrate proteins and is also thought to be involved in intersubunit interactions (Ghosh and Clark, 2005; Pasta et al., 2002).

A previous study reported that the D140N aB crystallin mutation results in altered tertiary structure and surface hydrophobicity with lower thermal stability and a significant loss of chaperone activity (Liu et al., 2006e). It was also reported that the D140N mutant behaves as a dominant negative which inhibits the chaperone activity of WT aB crystallin (Liu et al., 2006e).

Liu et al. 2006 suggested that the dominant negative effect of the D140N mutation was perhaps one of the major mechanisms of the cataract phenotype. It was also suggested that the mutant aB crystallin maybe rapidly degraded in muscles, which have active proteolytic systems, which could explain why the mutation causes cataract and not desmin related myopathy (DRM). It was suggested that due to the low expression levels observed in the muscle compared to the lens, the mutant aB crystallin may not reach the levels necessary for inhibiting chaperone activity of WT aB crystallin and other sHsps (Liu et al., 2006e).

The 450delA aB crystallin mutant also causes isolated congenital cataract and has no muscle phenotype. However, Hayes et al., 2008 suggested that aB crystallin self aggregation, rather than a loss of chaperone function, causes the 450delA aB crystallin mutant cataract phenotype (Hayes et al., 2008). In fact, 450delA was reported to have significantly increased chaperone activity for citrate synthase, compared to WT aB crystallin. In addition, Hayes et al., 2008

found that the myopathy causing Q151X and 464delCT aB crystallin mutations also showed significantly increased chaperone activity for citrate synthase *in vitro*. Hayes et al., 2008 suggested altered interaction with intermediate filaments, rather than loss of chaperone function, as a possible mechanism of the disease phenotype.

It is therefore important to further investigate the possible mechanisms which lead the D140N aB crystallin to cause cataract. In this chapter, I show that the D140N aB crystallin mutant forms oligomers comparable in size to WT aB crystallin, but has decreased thermostability and reduced secondary structure. In addition, I show that in contrast to previously published data (Liu et al., 2006e), the D140N mutation significantly increases chaperone activity *in vitro*. I use analytical size exclusion, absorbance spectroscopy, differential scanning fluorimetry and circular dichroism to analyse the mutant aB crystallin characteristics *in vitro*.

METHODS

WT aB crystallin was expressed in *E. coli*, extracted from the water soluble fraction, then purified by anion exchange (Fig 4.1) then size exclusion chromatography (Fig 4.2) to >98% purity. The D140N mutant aB crystallin was created by PCR mutagenesis and confirmed by bi-directional DNA sequencing. The D140N aB crystallin was then purified using the exact same method as WT aB crystallin with identical results (data not shown).

To investigate any effects of the D140N mutation on oligomer assembly, analytical size exclusion chromatography was performed on WT and D140N aB crystallin. The analytical SEC column calibration data is available in supplementary material (Sup Fig 2).

To investigate any effects of the D140N mutation on protein stability, the WT and D140N aB crystallin protein stability was measured directly using absorbance at 360nm and circular dichroism spectroscopy. Protein stability was also measured indirectly using the fluorescent dye, SYPRO Orange, which has weak fluorescence in hydrophilic environments and strong fluorescence in hydrophobic environments. The SYPRO Orange dye was chosen as it has excitation and emission spectra in the visible range and the signal is less affected by components of the buffer system compared to other commonly used dyes, for example, bis-ANS which is excited with near-UV light. The fluorescence of SYPRO Orange is dramatically increased when it binds to hydrophobic patches exposed by denaturing proteins. Protein stability was thus analysed using differential scanning fluorimetry (DSF) (Niesen et al., 2007) which quantified the temperature dependence of fluorescence intensity. To calculate the melting point transition, the first derivative of the raw fluorescence (F) and temperature (T) data was calculated (dF/dT) with the peak inflection point indicating the melting point temperature.

To investigate any effects of the D140N mutation on aB crystallin chaperone function, *in vitro* chaperone assays were performed. The ability of WT and D140N aB crystallin to prevent the heat induced aggregation of citrate synthase and the DTT induced aggregation of insulin was monitored via absorbance at 360nm.

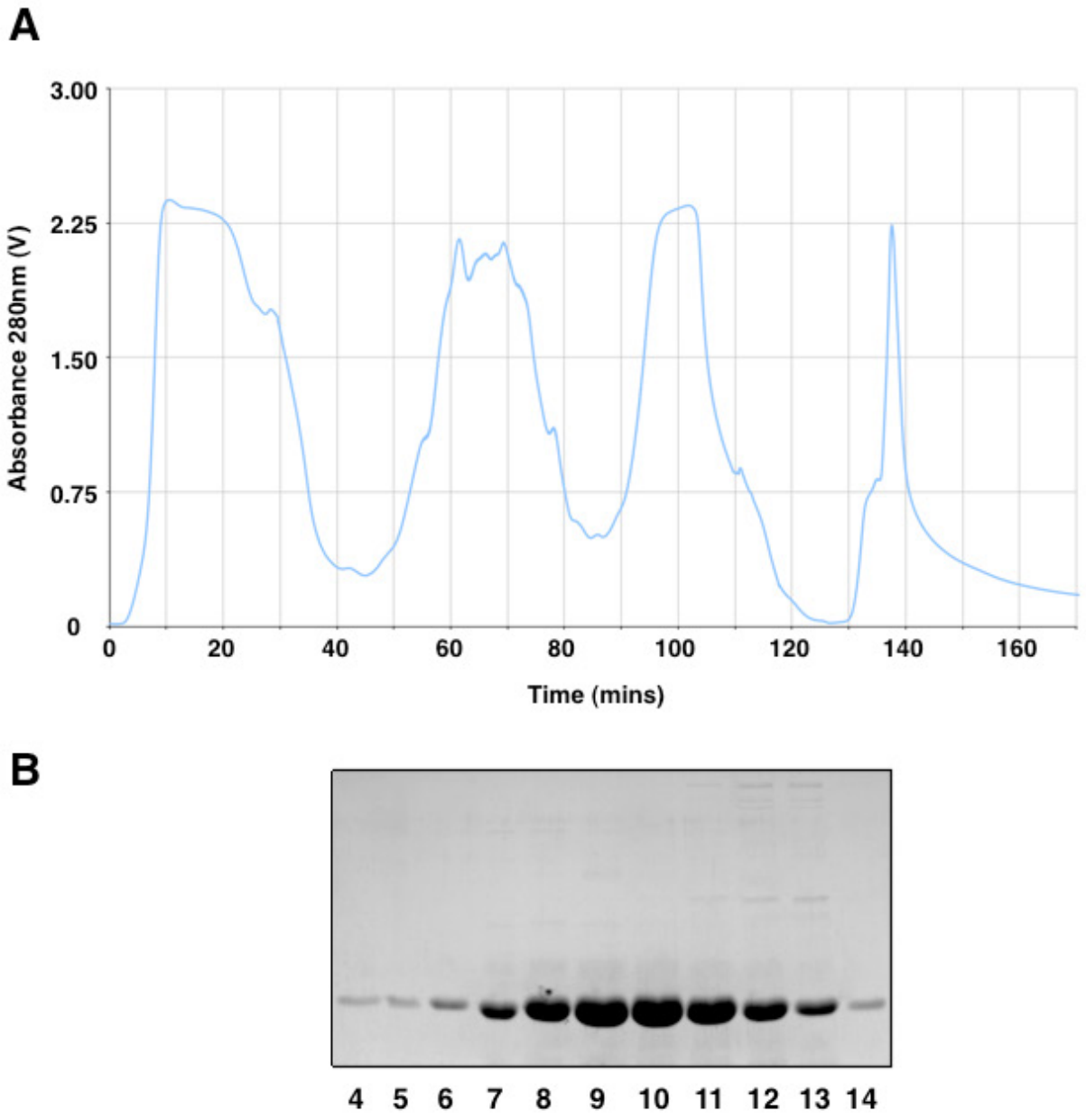

Fig 4.1. WT aB crystallin anion exchange purification.

(A) Anion exchange chromatography purification elution profile for WT aB crystallin. The protein was applied at 1ml/min in 20mM Tris HCl pH 7.4, 1mM MgCl2, 1mM EDTA, 1mM DTT and 0.2mM PMSF and eluted with a linear gradient of 0-1M NaCl. Eluted material was collected as 1ml fractions and analysed on a 12% SDS-PAGE gel. The first half of the first peak is aB crystallin, later peaks are contaminating proteins. (B) Each SDS-PAGE gel lane fraction is labelled with the corresponding chromatogram timescale. The aB crystallin enriched fractions show multiple contaminating proteins.

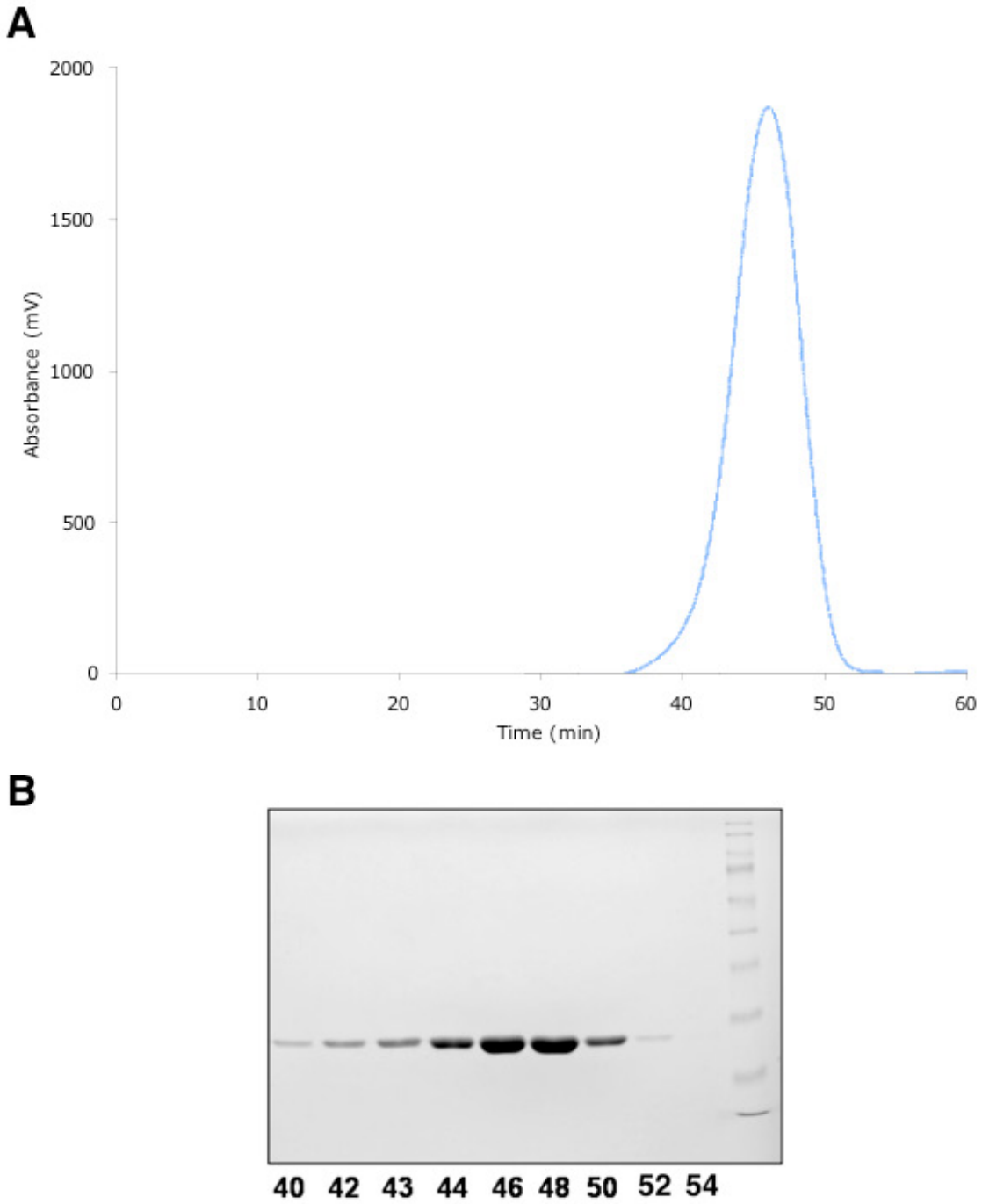

Fig 4.2. WT aB crystallin size exclusion purification.

(A) Size exclusion chromatography purification elution profile for WT aB crystallin. The protein was applied at 1ml/min in 20mM Tris HCl pH 7.4, 0.1M NaCl. Eluted material was collected as 1ml fractions, analysed on a 12% SDS-PAGE gel. (B) Each SDS-PAGE gel lane fraction is labelled with the corresponding chromatogram timescale. The sample is >98% pure.

RESULTS

Analysis of WT and D140N aB crystallin oligomer size

To investigate any effects of the D140N mutation on oligomer size, analytical size exclusion chromatography (SEC) was performed on WT and D140N aB crystallin (Fig 4.3). The analytical SEC column calibration data is available in the supplementary materials (Sup Fig 2).

Results show that both the WT and D140N aB crystallin elute from the SEC column as a single, symmetrical peak at 14.2ml (Fig 4.3). The analytical SEC column calibration (supplementary data, Sup Fig 2) was used to calculate that this peak corresponds to ~557kDa (±9kDa) (Fig 4.3). This indicates that the main oligomeric species, for both WT and D140N aB crystallin, is composed of ~28 subunits (aB crystallin Mw = 20.16kDa). These data indicate that the D140N mutation does not seem to affect average oligomer size.

Direct analysis of WT and D140N aB crystallin thermostability

To investigate any effects of the D140N mutation on protein stability, the thermal stability of WT and D140N aB crystallin was measured directly (Fig 4.4). When incubated at increasing temperature, D140N aB crystallin begins to aggregate ~2°C lower then WT aB crystallin at both 0.1 and 0.3g/l (Fig 4.4, A). In addition, when incubated at both 65 and 70°C, WT aB crystallin remains more soluble over time than D140N aB crystallin. These data suggest that the D140N mutation slightly reduces the thermostability of aB crystallin, such that the protein is slightly more susceptible to heat induced aggregation.

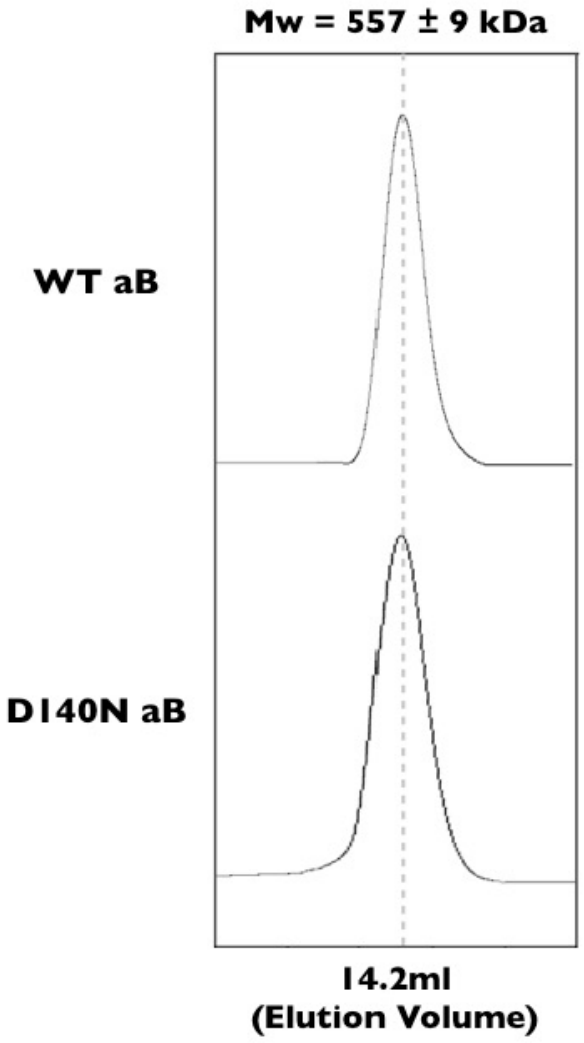

Fig 4.3. Analytical SEC alignment for WT and D140N aB crystallin.

WT and D140N aB crystallin both elute from the SEC column as a single, symmetrical peak at ~14.2ml. The analytical SEC column calibration (see supplementary data Sup Fig 2) was used to calculate that the peak corresponds to ~557kDa (±9kDa). This indicates that the main oligomeric species, for both WT and D140N aB crystallin, is composed of ~28 subunits (aB crystallin Mw = 20.16kDa).

Fig 4.4. Direct measurement of thermostability of WT and D140N aB crystallin.

The graphs show the thermostability of WT and D140N aB crystallin, measured directly via absorbance at 360nm. The graphs show average values from 3 independent experimental repeats. Final absorbance values are also shown with corresponding standard deviations. (A) WT and D140N aB crystallin were incubated at either 0.1 or 0.3g/l. The temperature was then increased by 1°C/min and absorbance at 360nm was monitored at 15 second intervals. (B) WT and D140N aB crystallin at 0.1g/l were incubated at either 65 or 75°C and the absorbance at 360nm was monitored at 15 second intervals. Thermal denaturation of proteins causes precipitation and increased absorbance at 360nm. D140N aB crystallin shows reduced thermostability compared with WT aB crystallin.

(Figure on next page)

A

	Final Abs	SD
D140N (0.3g/l)	0.217	0.011
WT aB (0.3g/l)	0.189	0.011
D140N (0.1g/l)	0.051	0.001
WT aB (0.1g/l)	0.041	0.002

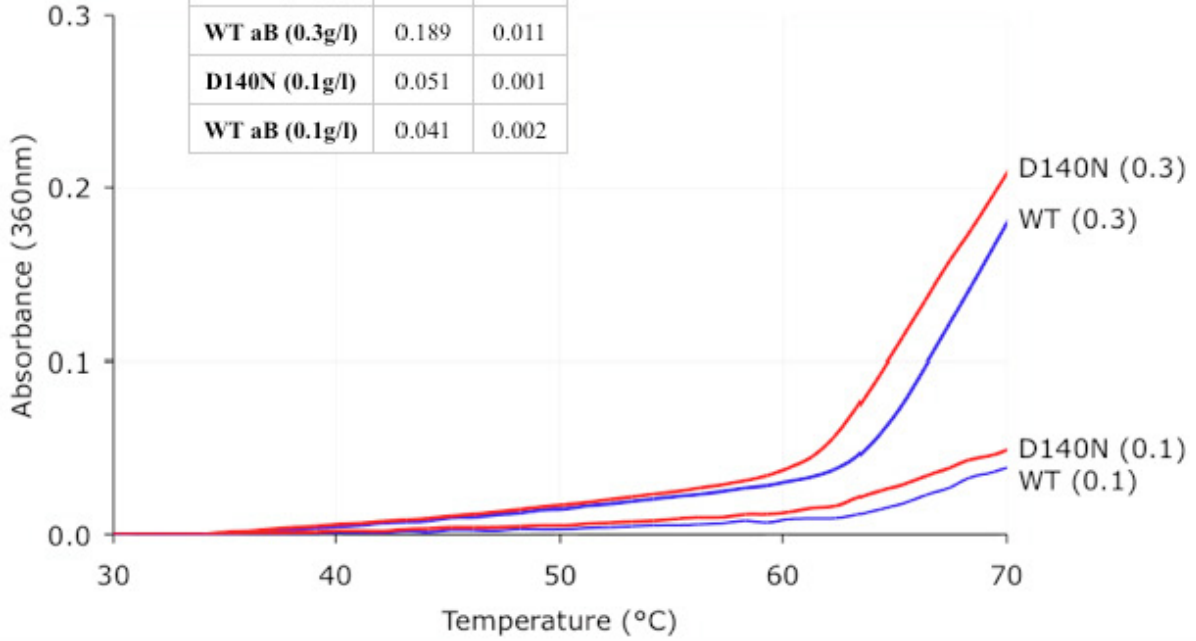

B

	Final Abs	SD
D140N (70°C)	0.249	0.007
WT aB (70°C)	0.200	0.009
D140N (65°C)	0.073	0.001
WT aB (65°C)	0.039	0.007

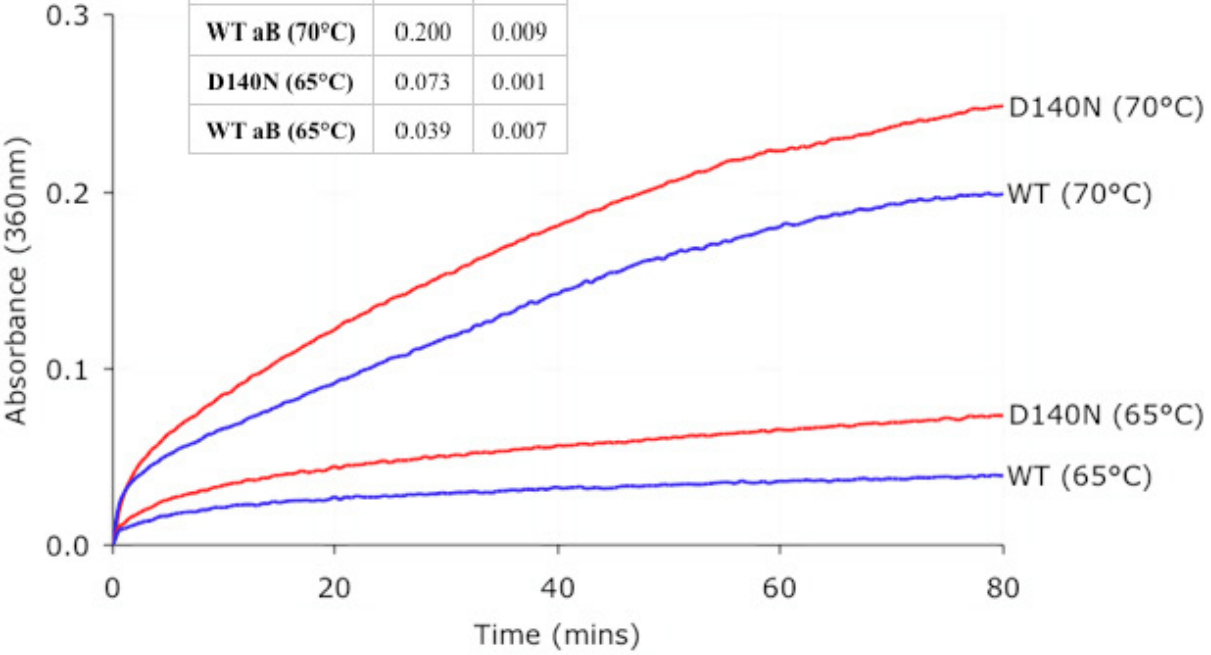

Fig 4.4 (Legend on previous page)

Indirect analysis of WT and D140N aB crystallin thermostability

Previous data in this chapter suggests that the D140N mutation reduces the thermostability of aB crystallin (Fig 4.4). Although these differences in thermostability are statistically significant, the difference is very small (<2°C) and the experimental technique used (measuring absorbance 360nm) is sensitive to differences in protein concentration. Therefore, in order to confirm the apparent small reduction in thermostability of D140N aB crystallin, the proteins were analysed using a Rotor-GeneQ with differential scanning fluorimetry and the SYPRO Orange dye, a technique less sensitive to differences in protein concentration and with a reported accuracy of ±0.1°C (Qiagen UK).

WT and D140N aB crystallin were incubated at increasing temperature and the fluorescence monitored (Fig 4.5, A). The protein melting points then were determined by calculating the first derivative of the raw fluorescence (F) and temperature (T) data (dF/dT) with the peak inflection point indicating the melting point temperature (Fig 4.5, B). The data shows that D140N aB crystallin has a melting point 0.8°C lower than that of WT aB crystallin (Fig 4.5, B), indicating reduced thermostability.

Circular dichroism analysis of WT and D140N aB crystallin

To investigate any effects of the D140N mutation on secondary structure, WT and D140N aB crystallin were analysed using circular dichroism spectroscopy (Fig 4.6) (Eftink, 1995; Ramsay and Eftink, 1994). WT aB crystallin showed a single, broad minima at 212nm (indicative of a protein rich in beta sheet) which is consistent with previously reported data (Hayes et al., 2008). D140N showed a decrease in negative ellipticity and a shift in wavelength minima to 216nm. This indicates a slight loss of secondary structure for D140N compared to WT aB crystallin (Fig 4.6).

Fig 4.5. Indirect measurement of thermostability of WT and D140N aB crystallin.

The graphs show the thermostability of WT and D140N aB crystallin, measured indirectly via differential scanning fluorimetry. (A) WT and D140N aB crystallin were incubated with SYPRO Orange dye at increasing temperature and the fluorescence monitored. The control shows SYPRO Orange dye alone, and is identical to the WT and D140N aB crystallin alone controls (not shown). (B) The first derivative of the raw fluorescence (F) and temperature (T) data (dF/dT). The peak inflection point indicates the protein melting point temperature. The graphs are the average of 3 independent repeats and the standard deviations of melting point values are shown. All fluorescence values were corrected using a buffer only control (not shown). D140N aB crystallin has a melting point 0.8°C lower than that of WT aB crystallin.

(Figure on next page)

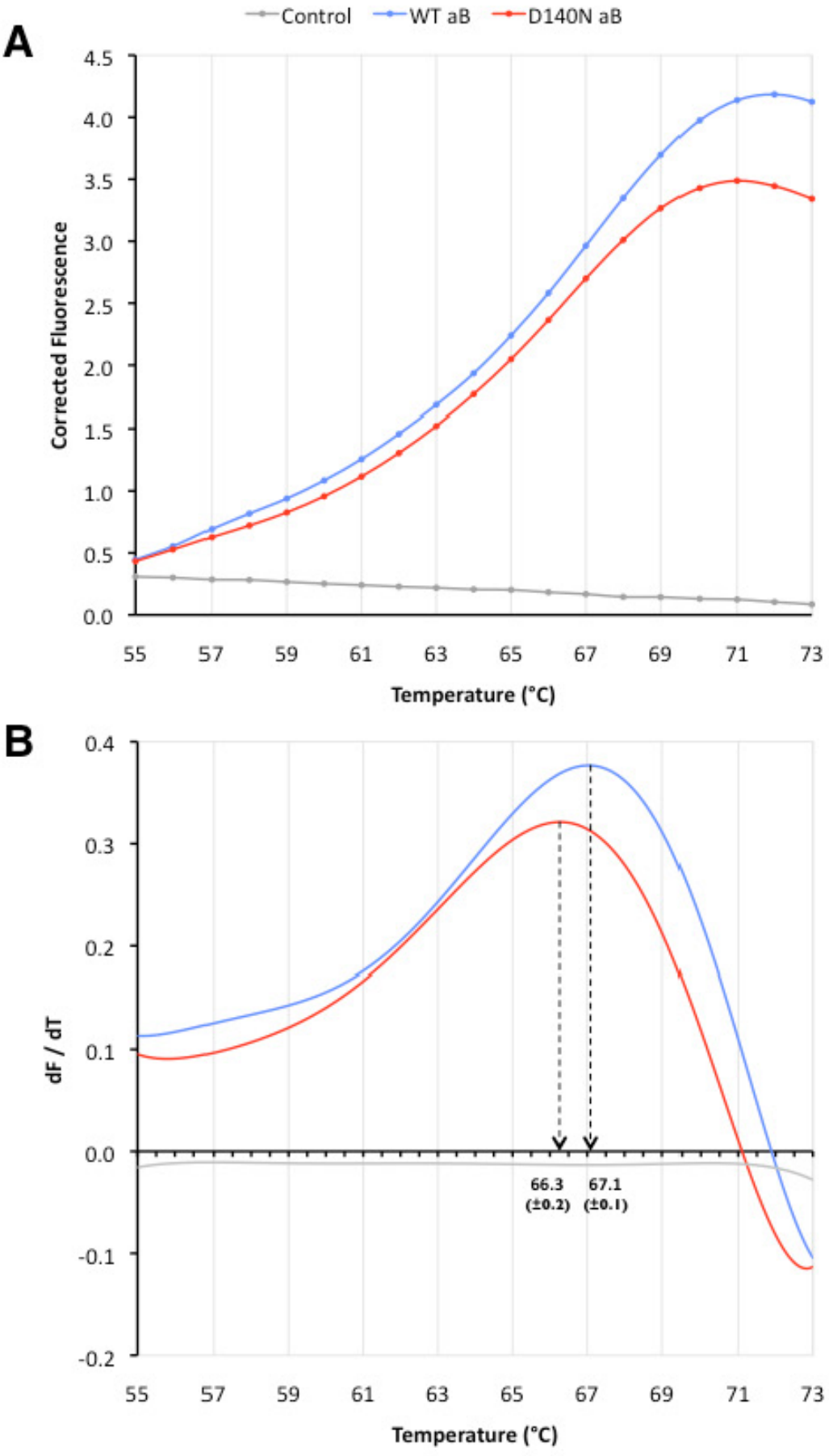

Fig 4.5 (Legend on previous page)

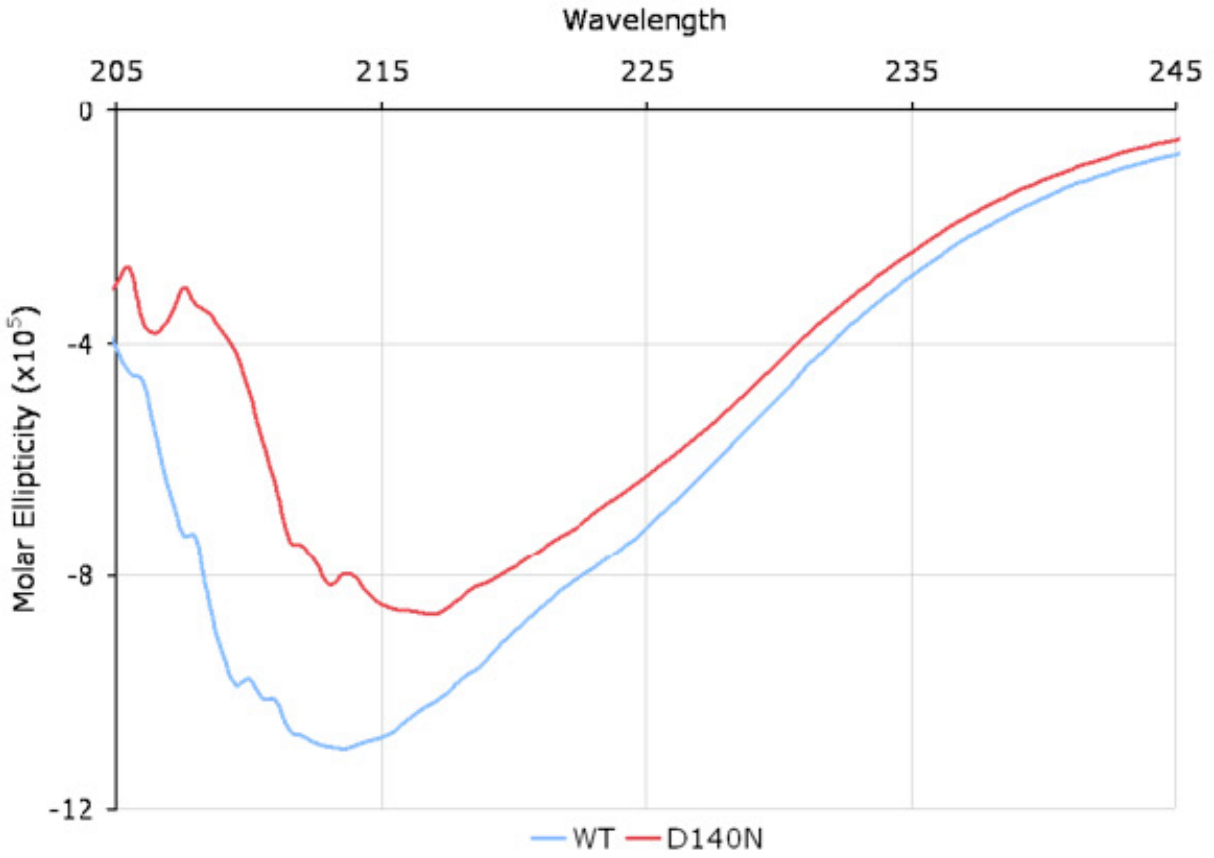

Fig 4.6. Circular dichroism of WT & D140N aB crystallin.

Far UV circular dichroism (CD) spectra (205-245 nm) for WT (blue) and D140N (red) aB crystallin. The graphs are the average of 4 spectra. The far UV CD signal was converted to molar ellipticity expressed as deg.cm^2.dmol^{-1}. The D140N mutant shows a slight loss of secondary structure reflected by a decrease in negative ellipticity and a shift in wavelength minima.

Analysis of WT and D140N aB crystallin chaperone activity

WT and D140N aB crystallin were analysed to compare *in vitro* chaperone activity for heat denatured citrate synthase (Fig 4.7) and DTT denatured insulin (Fig 4.8).

Results show that WT aB crystallin can protect against the heat induced aggregation of citrate synthase, providing 6%, 29% and 60% protection at 2:1, 1:1 and 1:2 substrate:chaperone ratios respectively (Fig 4.7). However, D140N aB crystallin provides significantly increased protection of 25%, 69% and 85% at 2:1, 1:1 and 1:2 substrate:chaperone ratios respectively. In fact, D140N aB crystallin provides more protection at a 1:1 substrate:chaperone ratio (69%) than WT aB crystallin at 1:2 substrate:chaperone ratio (60%) (Fig 4.7).

DTT (dithiothreitol) is a reducing agent, which breaks disulfide bonds in proteins causing unfolding which can lead to aggregation. WT aB crystallin can protect against the DTT induced aggregation of insulin, providing 20%, 65% and 91% protection at 4:1, 2:1 and 1:1 substrate:chaperone ratios respectively (Fig 4.8). However, D140N aB crystallin provides significantly increased protection of 49%, 80% and 97% at 4:1, 2:1 and 1:1 substrate:chaperone ratios respectively. At a 4:1 substrate:chaperone ratio, D140N aB crystallin provides ~2.5x more protection (49%) than WT aB crystallin (20%) (Fig 4.8).

Overall, these data show that, surprisingly, the D140N mutation has caused significantly increased aB crystallin chaperone activity *in vitro*, for citrate synthase and insulin.

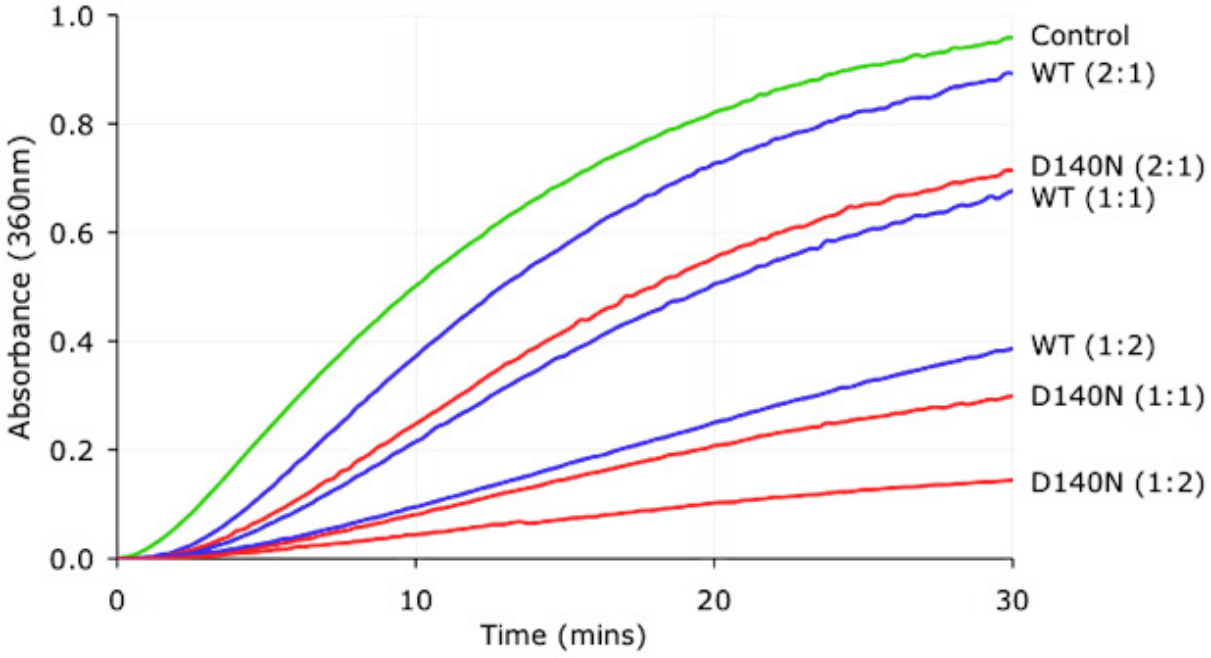

	% Protection	SD
WT (2:1)	7	2
D140N (2:1)	25	3
WT (1:1)	29	4
WT (1:2)	60	5
D140N (1:1)	69	5
D140N (1:2)	85	4

Fig 4.7. Chaperone activity of WT and D140N aB crystallin for citrate synthase.

The graphs show the thermal aggregation of 0.2g/l citrate synthase at 44°C in the presence of WT (blue) or D140N (red) aB crystallin at varying substrate:chaperone ratios (shown in brackets). The aggregation of citrate synthase alone is shown in green (Control). The table shows the final absorbance values as a percentage reduction, compared to the control (% Protection). Absorbance values are an average of 3 experimental repeats and standard deviations (SD) are also shown. D140N aB crystallin shows significantly increased chaperone activity compared to WT aB crystallin at all tested substrate:chaperone ratios.

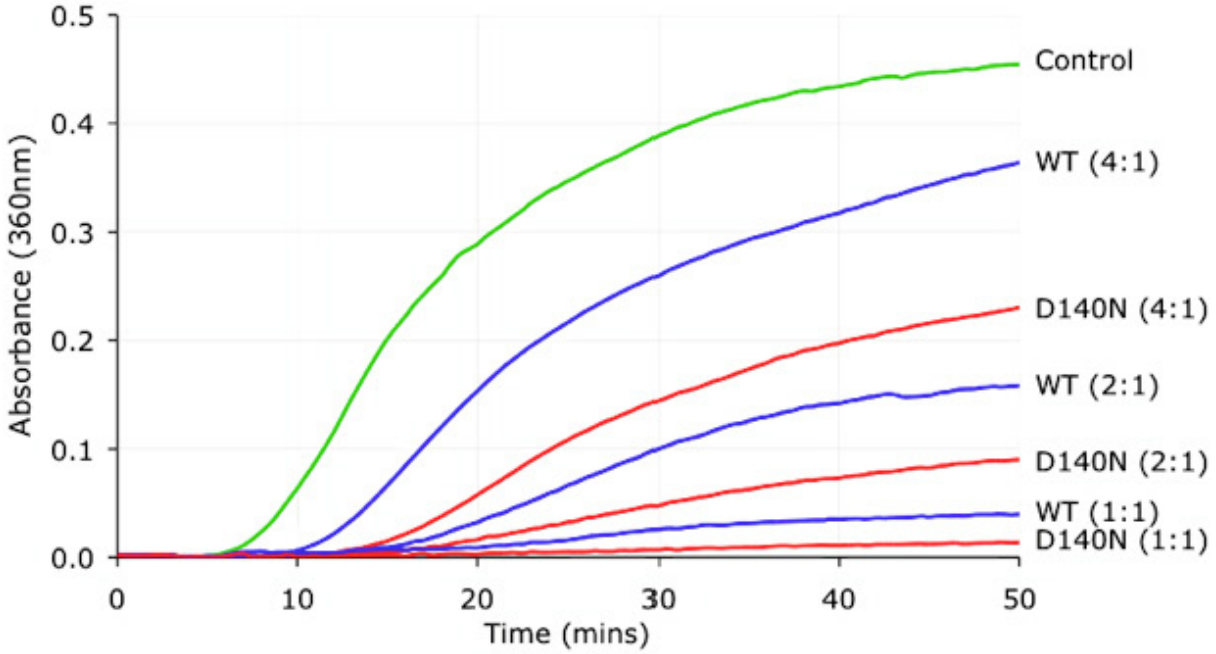

	% Protection	SD
WT (4:1)	20	3
D140N (4:1)	49	5
WT (2:1)	65	4
D140N (2:1)	80	5
WT (1:1)	91	4
D140N (1:1)	97	2

Fig 4.8. Chaperone activity of WT and D140N aB crystallin for insulin.

The graphs show the DTT induced aggregation of 0.2g/l insulin at 22°C in the presence of WT (blue) or D140N (red) aB crystallin at varying substrate:chaperone ratios (shown in brackets). The aggregation of insulin alone is shown in green (Control). The table shows the final absorbance values as a percentage reduction, compared to the control (% Protection). Absorbance values are an average of 3 experimental repeats and standard deviations (SD) are also shown. D140N aB crystallin shows significantly increased chaperone activity compared to WT aB crystallin at all tested substrate:chaperone ratios.

RESULTS SUMMARY

Overall, data in this chapter show that the cataract causing D140N aB crystallin mutation causes a slight loss of secondary structure and a small decrease in thermostability, with no apparent change in average oligomer size. Interestingly, data also shows that, for the substrates tested (insulin and citrate synthase), the D140N mutation causes significantly increased chaperone activity *in vitro*.

CHAPTER 5: FUNCTIONS OF THE C-TERMINAL TAIL OF ZEBRAFISH BEADED FILAMENT STRUCTURAL PROTEIN 2

AIM

To investigate the importance of the zebrafish Bfsp2 C-terminal tail domain in the assembly of beaded filaments and their subsequent interactions and morphology.

PUBLICATION NOTE

The data presented in this chapter has been published in the Experimental Eye Research:
Qu B*, Landsbury A*, Schönthaler HB, Dahm R, Liu Y, Clark JI, Prescott AR, Quinlan RA. (2012). Evolution of the vertebrate beaded filament protein, Bfsp2; comparing the in vitro assembly properties of a "tailed" zebrafish Bfsp2 to its "tailless" human orthologue. Experimental Eye Research *94*, 192-202. (*Joint first author).

INTRODUCTION

Beaded filaments (BFs) are essential to lens optical properties (Alizadeh et al., 2003, 2004; Alizadeh et al., 2002; Sandilands et al., 2003; Sandilands et al., 2004). In vivo, BFs are found with 12-15nm a-crystallin 'beads' extensively bound along their length (FitzGerald and Casselman, 1991; Maisel and Perry, 1972). sHsps interaction has been demonstrated for all IF proteins in vitro and in vivo, but the interaction with BFs is unusual because a-crystallin association is so extensive that the 5-6nm BFSP1 and BFSP2 filament backbone (Goulielmos et al., 1996; Merdes et al., 1993) is almost completely obscured (Carter et al., 1995; Quinlan et al., 1996). The reasons for this unusual interaction of BFs and a-crystallin and the subsequent functional significance are unknown, but understanding this interaction may provide important insight into the sHsp-IF interaction. However, before analysing the interaction with sHsps, it is important understand the interaction of BSFP1 and BFSP2, which co-assemble to form the filament backbone, potentially providing a scaffold for a-crystallin (Song et al., 2009). However, the assembly mechanism of BFSP1 and BFSP2 to form the 5-6nm BFs (Goulielmos et al., 1996; Merdes et al., 1993) is unknown. Furthermore, the impact of the different domains of the BFSP1 and BFSP2 proteins to filament properties has yet to be analysed in detail, and will likely be critical to a-crystallin association.

In all mammals and birds, BFSP2 and keratin 19 are the only IF proteins which lack a C-terminal tail domain (Sawada et al., 1995; Stasiak and Lane, 1987). In contrast, teleost fish Bfsp2 proteins are predicted to posess a C-terminal tail domain (Binkley et al., 2002). Database mining identified other fish species with a predicted Bfsp2 C-terminal tail (trout, puffer fish, stickleback and medaka), but there is no common motif (Fig 5.1). In zebrafish (Zf), this C-terminal tail domain extends the zebrafish Bfsp2 C-terminus by 44 residues, compared to its human orthologue (Fig 5.2). Data mining identified the full-length cDNA for zebrafish bfsp2 (Unigene; Dr.19486. Genbank: NM_001008633.1. MGC:103750. Clone ID: 7074672) which produces a protein of 49kDa compared to 46kDa for human (Hu) BFSP2. Over all, the zebrafish Bfsp2 is 23 residues longer than its human orthologue as the N-terminal non α-helical head domain is 17 residues shorter (Fig 5.2). bfsp2 expression has been confirmed in the zebrafish lens using a polyclonal antibody (Bo et al, 2012).

Analysis of the "tailed" zebrafish Bfsp2 may therefore provide further insight into beaded filament assembly and the protein domains which contribute to filament interactions and morphology. Therefore, I investigated the in vitro assembly properties of this protein, analysed by low and high speed sedimentation assays and TEM. Both BFSP1 and its 53kDa fragment (53k) (Masaki and Quinlan, 1997; Quinlan et al., 1992; Wang et al., 2009) have been shown to be competent assembly partners of BFSP2, forming 5-6nm filaments (Carter et al., 1995; Goulielmos et al., 1996; Song et al., 2009). However, since the cDNA was not available for zebrafish bfsp1 or bfsp1-53k, native bovine BFSP1 and its 53kDa fragment (53k) were selected as surrogate assembly partners for the recombinantly produced Zf Bfsp2 protein.

In order to assess the functional effects of the Zf Bfsp2 C-terminal tail, a C-terminally truncated (CT) Zf Bfsp2 construct was created for comparison (Zf CT Bfsp2). The Zf CT Bfsp2, created by PCR mutagenesis and confirmed by bi-directional DNA sequencing, truncates the Zf C-terminal tail at R394 and creates a zebrafish equivalent to the naturally tail-less human (Hu) WT BFSP2 (Fig 5.2). The Hu WT BFSP2 was also used as a comparison for the "tailed" Zf WT Bfsp2 and tail-less Zf CT Bfsp2 proteins.

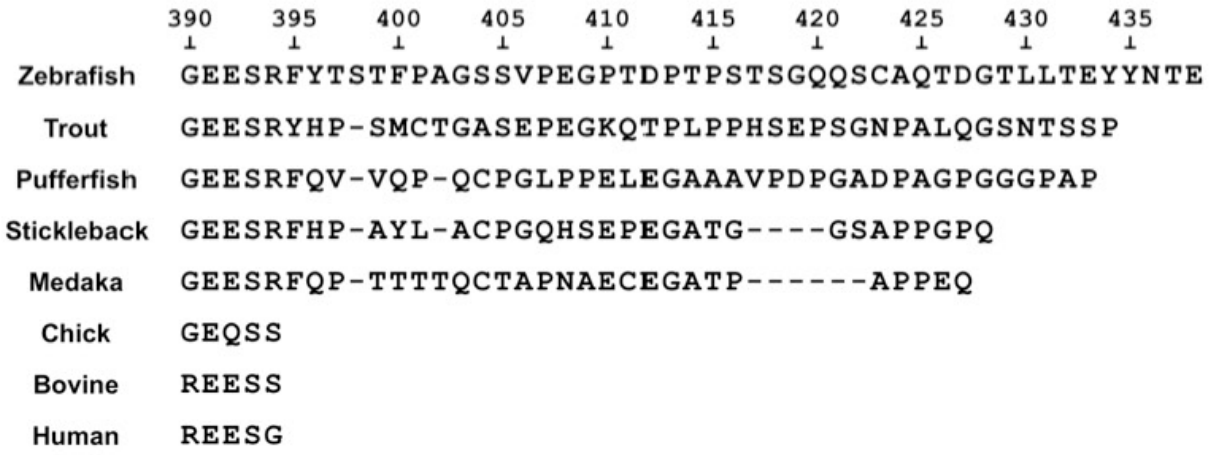

Fig 5.1. Bfsp2 sequence comparisons.

Results of BLAST searches of the ENSEMBL database to identify sequences for Bfsp2. Zebrafish, trout, pufferfish, stickleback and medaka Bfsp2 are predicted to have a C-terminal tail which is not present in chick, bovine or human BFSP2. Amino acid numbers for the zebrafish sequence are given for reference. Data was obtained from the following sources: zebrafish (ENSDART00000004712); trout (Binkley et al., 2002); pufferfish (ENSTNIT00000005791); stickleback (ENSGACT00000003202, DW600649, DW593699); medaka (ENSORLG00000007668, BJ739079); chick (ENSGALG00000011712); bovine (ENSBTAG00000017659); human (ENSG00000170819).

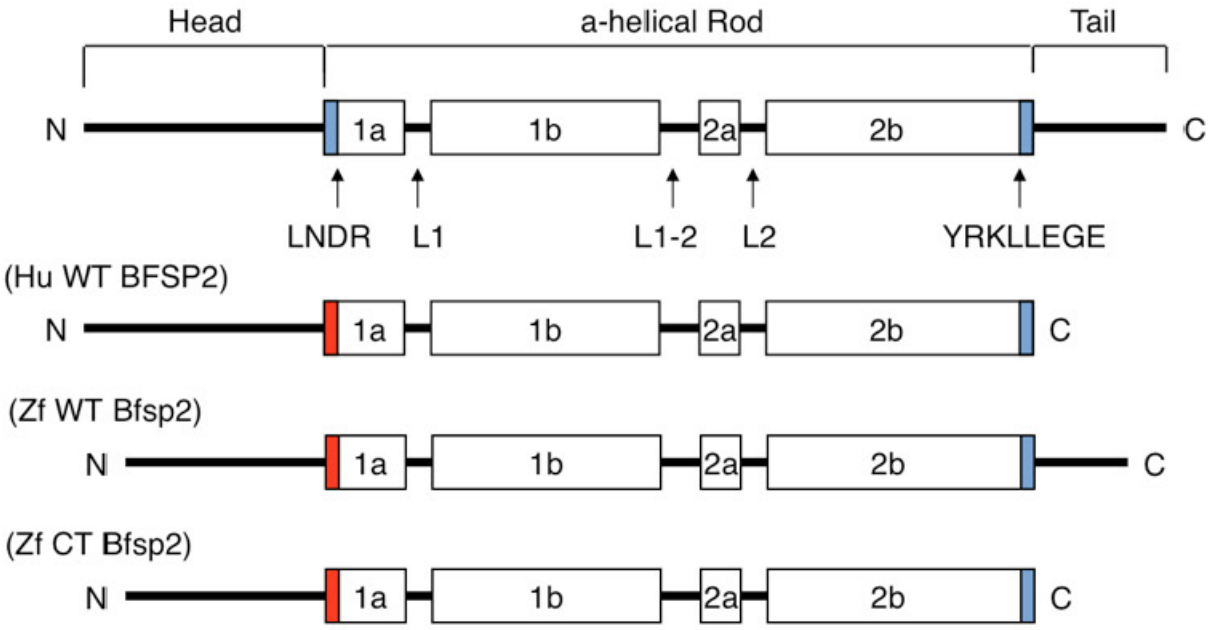

Fig 5.2. Characterisation of the C-terminal tail domain of zebrafish Bfsp2.

Predicted secondary structure of a typical IF protein (e.g. vimentin) compared with that predicted for Hu WT BFSP2 and Zf WT Bsfp2. Zf WT Bfsp2 has a predicted C-terminal tail, which extends the Zf C-terminus by 44 residues, compared to Hu WT BFSP2. Overall, the Zf WT Bfsp2 (49kDa) is 23 residues longer than Hu WT BFSP2 (46kDa) as the Zf N-terminal non α-helical head domain is 17 residues shorter. The Zf C-terminal tail was removed (R394X) to create the C-terminally truncated Zf CT Bfsp2. IF proteins are composed of an α-helical coiled coil domain flanked by two non-helical N- and C-termini. The boxes represent α-helical domains which are separated by the non-helical linkers, L1, L1-2 and L2. The blue boxes at the ends of helix 1a and 2b represent the highly conserved LNDR and YRKLLEGE motifs which are important for the assembly of IF proteins into filaments. These motifs are changed in Hu BFSP2 (LGGC and SYHALLDRE, respectively) and Zf Bfsp2 (LNTC and TYHGILDGE respectively). The R to C change in the LNDR motif of Bfsp2 would actually cause disease if found in, for example GFAP, so for this reason these motifs are colored red in the diagram.

In this chapter, I show that the zebrafish C-terminal tail actively influences the assembly of the Bfsp2 protein and the morphology and interactions of the filaments it forms. I also show that, in common with the lens IF vimentin, the zebrafish Bfsp2 C-terminal tail appears to regulate filament width.

METHODS

Hu WT, Zf WT and Zf CT Bsfp2 proteins were all expressed in *E. coli*, extracted from the water insoluble fraction and purified by anion then cation exchange chromatography, under denaturing conditions, to >98% purity (Fig 5.3). Native bovine BFSP1 and native bovine BFSP1-53kDa fragment (53k) were extracted from 100 bovine lenses and purified by two anion exchange purifications then hydroxyapatite purification (see Fig 5.8 later in the chapter).

For assembly, BF proteins at 0.2g/l were mixed and unfolded in 6M Urea buffer. Samples were then dialysed to reduce the Urea concentration to 4M, then 2M, then 0M over a period of 24h at 22°C. Samples were then dialysed into Tris-HCl pH 7.6, 50mM NaCl, 1mM $MgCl_2$ buffer at 22°C for 16h to finalise assembly.

To assess filament morphology, filaments were analysed by TEM. Samples were prepared essentially using the Valentine method (Valentine et al., 1968). TEM images were also analysed to measure filament width. 50 measurements were made using three different images to give a total of 150 width measurements for each sample. Measurements were made at 100nm intervals along the length of the filaments in randomly selected areas.

To monitor assembly and quantify filament-filament interactions, two separate centrifugation assays were used. Samples were centrifuged at either 80,000g for 30min (high speed assay) or 2,500g for 15min (low speed assay). The pellets and supernatants were separated and solubilised in equal final volumes of SDS-PAGE sample buffer to allow direct comparison of the proportions of material in the supernatant and pellet. Results were then visualised via SDS-PAGE and quantified by gel densitometry. For the high speed assay, the pellet (P) contains individual filaments and any aggregates formed as a result of filament-filament interactions. The supernatant (S) contains any unassembled BF proteins or assembly intermediates. Therefore this assay measures filament assembly. For the low speed assay, individual filaments are not pelleted, only those filaments which self associate into aggregates are pelleted. Therefore, this assay measures filament-filament interaction.

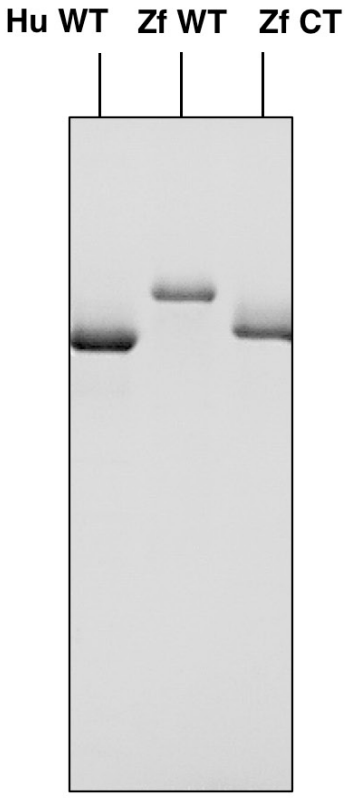

Fig 5.3. Purified Hu WT, Zf WT and Zf CT Bsfp2 proteins.

Hu WT, Zf WT and Zf CT Bsfp2 proteins were all expressed in *E. coli*, extracted from the water insoluble fraction and purified by anion then cation exchange chromatography, under denaturing conditions, to >98% purity. The above SDS-PAGE gel shows the final purified samples. Zf WT has a C-terminal tail domain (44 residues) which is removed in Zf CT is give a Zf equivalent to Hu WT BFSP2.

RESULTS

Effect of the Zf C-terminal tail on self assembly and solubility of Bfsp2

To assess the effect of the Zf tail on the self assembly and solubility of Bfsp2, the low (2500g) and high (80,000g) speed sedimentation properties of Hu WT, Zf WT and Zf CT Bfsp2 proteins were analysed by SDS-PAGE. Fig 5.4 represents 1 of 3 experimental repeats, which were quantified via gel densitometry, collated and averaged (Fig 5.5).

Results show that when assembled alone, Hu WT and Zf CT Bfsp2 are completely pelleted at high speed (>99%) whereas Zf WT Bfsp2 remains soluble (only 15% is pelleted) (Fig 5.4). Similarly, even at low speed, 98% of Hu WT and 78% of Zf CT Bfsp2 are pelleted, whereas only 9% of Zf WT is pelleted (Fig 5.4). This shows that Zf WT Bfsp2 has significantly enhanced solubility compared to Zf CT and Hu WT Bfsp2.

When co-assembled, Hu WT and Zf CT Bfsp2 are 93% and 100% pelleted at low and high speed, respectively (Fig 5.5). However, when either Hu WT or Zf CT is mixed with Zf WT Bfsp2, <65% is pelleted at high speed and <19% is pelleted at low speed (Fig 5.5). This shows that Zf WT Bfsp2 is capable of solubilising Zf CT and Hu WT Bfsp2.

Overall, these data suggest that the Zf C-terminal tail significantly enhances protein solubility and prevents aggregation of the self assembled Bfsp2 structures. In addition, this C-terminal tail is able to enhance the solubility of Zf CT and Hu WT Bfsp2 structures and thus decrease aggregation.

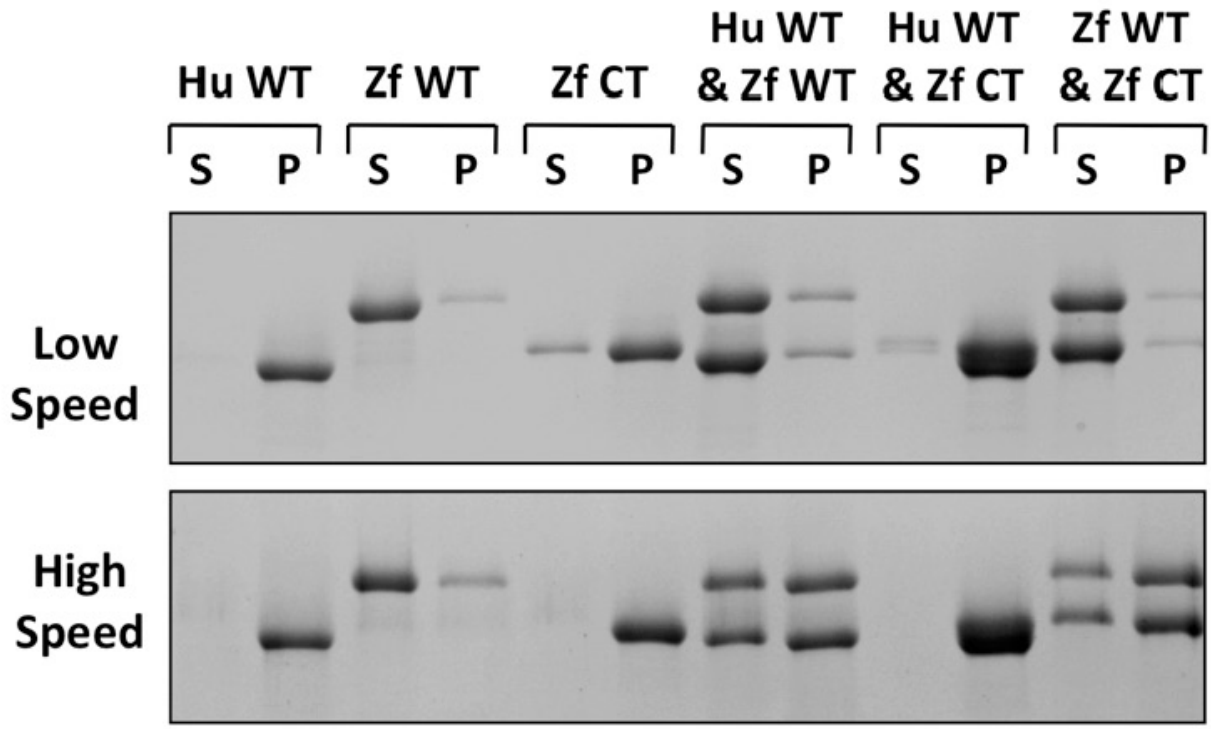

Fig 5.4. Sedimentation properties of self assembled Hu and Zf Bfsp2.

Low (2,500g) and high (80,000g) speed sedimentation of Hu and Zf Bfsp2 proteins assembled alone and co-assembled together, analysed by SDS-PAGE. When assembled alone, Zf WT Bfsp2 remains soluble, unlike Hu WT or Zf CT Bfsp2. Zf WT Bfsp2 can also solublise Hu WT or Zf CT Bfsp2 when assembled in a 1:1 molar ratio. When Hu WT BFSP2 is mixed with Zf CT Bfsp2 both proteins form aggregates and pellet. The above gels represent 1 of 3 repeats. Supernatant (S) and pellet (P).

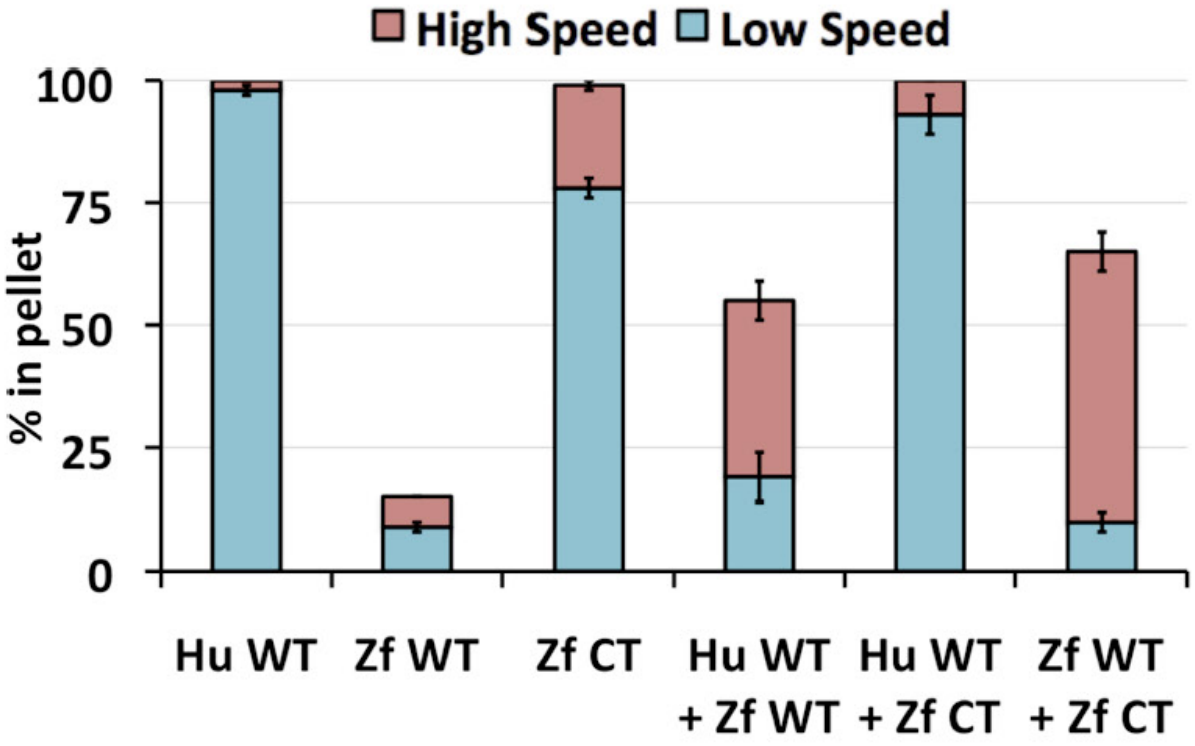

Fig 5.5. Quantification of sedimentation of self assembled Hu and Zf Bfsp2.

Bar chart of low (blue) and high (red) speed sedimentation of Hu and Zf Bfsp2 proteins assembled alone and co-assembled together. When assembled alone, Zf WT Bfsp2 remains soluble, unlike Hu WT or Zf CT Bfsp2 which pellet. Zf WT Bfsp2 can also solublise Hu WT or Zf CT Bfsp2 when co-assembled in a 1:1 molar ratio. When Hu WT BFSP2 is mixed with Zf CT Bfsp2 both proteins form aggregates and pellet. The amount of material pelleted is shown as a percentage of total material as quantified by gel densitometry. Average values and standard deviations were calculated from 3 or 4 experimental repeats.

Effect of the Zf C-terminal tail on the morphology of self assembled Bfsp2

To assess the effect of the Zf tail on the morphology of self assembled Bfsp2, samples were analysed by TEM (Fig 5.6). When assembled alone and when assembled together, Hu WT and Zf CT Bfsp2 assemble into large structures (Fig 5.6), which were previously shown to aggregate, even under low speed sedimentation (Fig 5.4).

Conversely, when assembled alone Zf WT Bfsp2 forms short, individual filament fragments (Fig 5.6) which do not assemble into large structures, and as previously shown, remain soluble even under high speed sedimentation (Fig 5.4). Similarly, when Zf WT Bfsp2 is co-assembled with either Hu WT or Zf CT Bfsp2, individual filament fragments are formed which do not assemble into large structures, as seen when Hu WT and Zf CT Bfsp2 are assembled alone (Fig 5.6).

Overall, these data suggest that the Zf C-terminal tail can prevent the self association of Zf WT Bfsp2 filament fragments, thus preventing aggregation, and can also help to solubilise Hu WT and Zf CT Bfsp2 filament fragments and prevent aggregation.

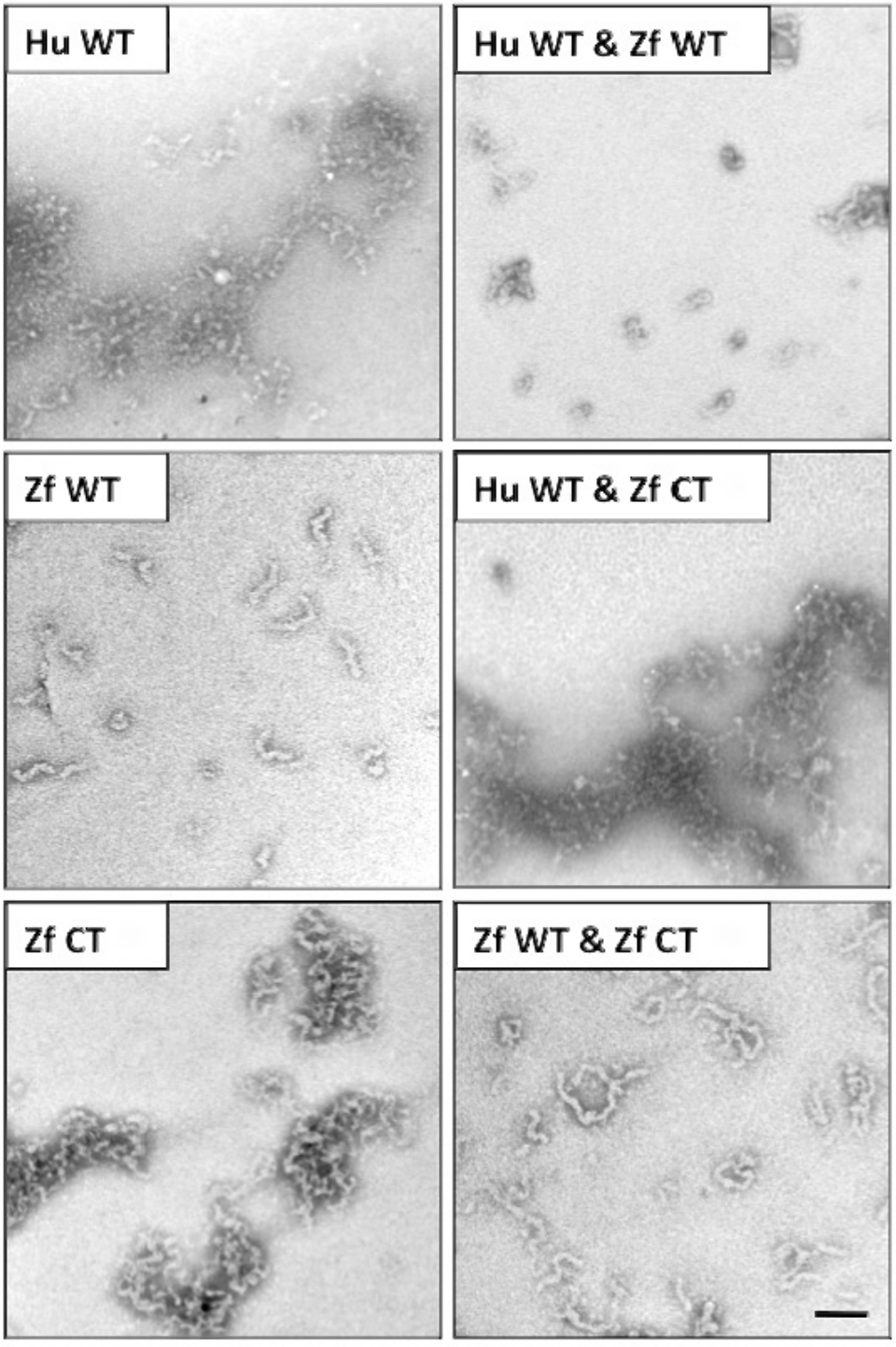

Fig 5.6. TEM analysis of self assembled Hu and Zf Bfsp2.

When assembled alone, Zf WT Bfsp2 remains soluble, unlike Hu WT or Zf CT Bfsp2 which form aggregates. Zf WT Bfsp2 can also solublise Hu WT or Zf CT Bfsp2 when co-assembled in a 1:1 molar ratio. When Hu WT BFSP2 is mixed with Zf CT Bfsp2 aggregates are formed. Scale bar represents 100nm.

Purification of bovine BFSP1 and BFSP1-53k

Bfsp2 has been shown to assemble into filaments with both BFSP1 and the naturally occuring 53kDa breakdown product of BFSP1, BFSP1-53k (53k). Therefore, in order to analyse the effects of the Zf WT Bfsp2 C-terminal tail on filament assembly, these Bfsp2 assembly partners were required. However, the cDNA for both Zf BFSP1 and Zf 53k were unavailable. Therefore, native bovine BFSP1 and its 53kDa fragment were selected as surrogate assembly partners for the recombinantly produced Bfsp2 proteins.

The rod domain of BFSP1 is predicted to be 2-3nm shorter than that of BFSP2 due to lack of the 2a helix and the L2 linker, but BFSP1 contains a long C-terminal tail not present in BFSP2 (Fig 5.7). The 53k protein is a 53kDa breakdown product of BFSP1 which truncates the C-terminal tail (Fig 5.7).

Native bovine BFSP1 and the native bovine 53k were extracted from >100 bovine lenses and purified to >98% purity by anion exchange and hydroxyapatite chromatography (Fig 5.8).

Self assembly and solubility of bovine BFSP1 and 53k

The low and high speed sedimentation properties of self assembled Bo BFSP1 and Bo 53k were analysed. At both low (2500g) and high (80,000g) speed sedimentation, >90% of both proteins remain soluble (Fig 5.9). TEM analysis shows that Bo BSFP1 assembles into short, individual filament fragments, while 53k assembles into larger structures, but both remain soluble and do not aggregate (Fig 5.9).

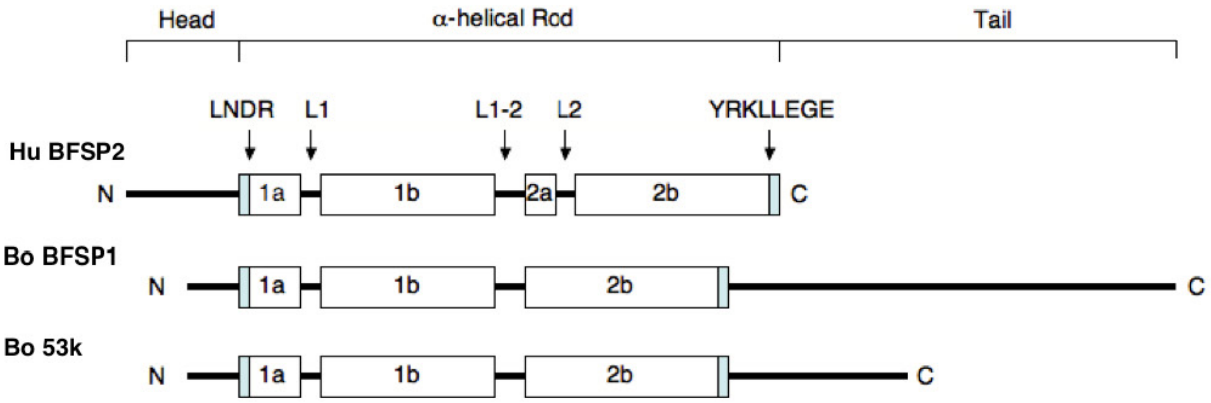

Fig 5.7. Predicted secondary structure of BFSP2, BFSP1 and 53k.

Predicted secondary structure of human BFSP2, bovine BFSP1 and bovine BFSP1-53k (53k). The boxes represent α-helical domains which are separated by the non-helical linkers, L1, L1-2 and L2. The blue boxes at the ends of helix 1a and 2b represent the highly conserved LNDR and YRKLLEGE motifs which are important for the assembly of IF proteins into filaments. BFSP2 lacks a C-terminal tail. The rod domain of BFSP1 is predicted to be 2-3nm shorter than that of BFSP2 due to lack of the 2a helix and the L2 linker. The 53k protein is a 53kDa breakdown product of BFSP1 which truncates the C-terminal tail.

Fig 5.8. Purification of native Bo BFSP1 and 53k.

Native bovine BFSP1 and the native bovine BFSP1-53kDa fragment (53k) were extracted from 100 bovine lenses and purified by two anion exchange purifications (A, B) then hydroxyapatite purification (C). The first ion exchange (A) removes the crystallins, the second ion exchange (B) removes the BFSP2 and the hydroxyapatite (C) removes the vimentin, and separates the BFSP1 from the 53k breakdown product. Identities were confirmed by mass spectrometry (data not shown) and BFSP1 was also confirmed by western blotting - see supplementary, Sup Fig 3. The final samples (D) are >98% pure.

(Figure on next page)

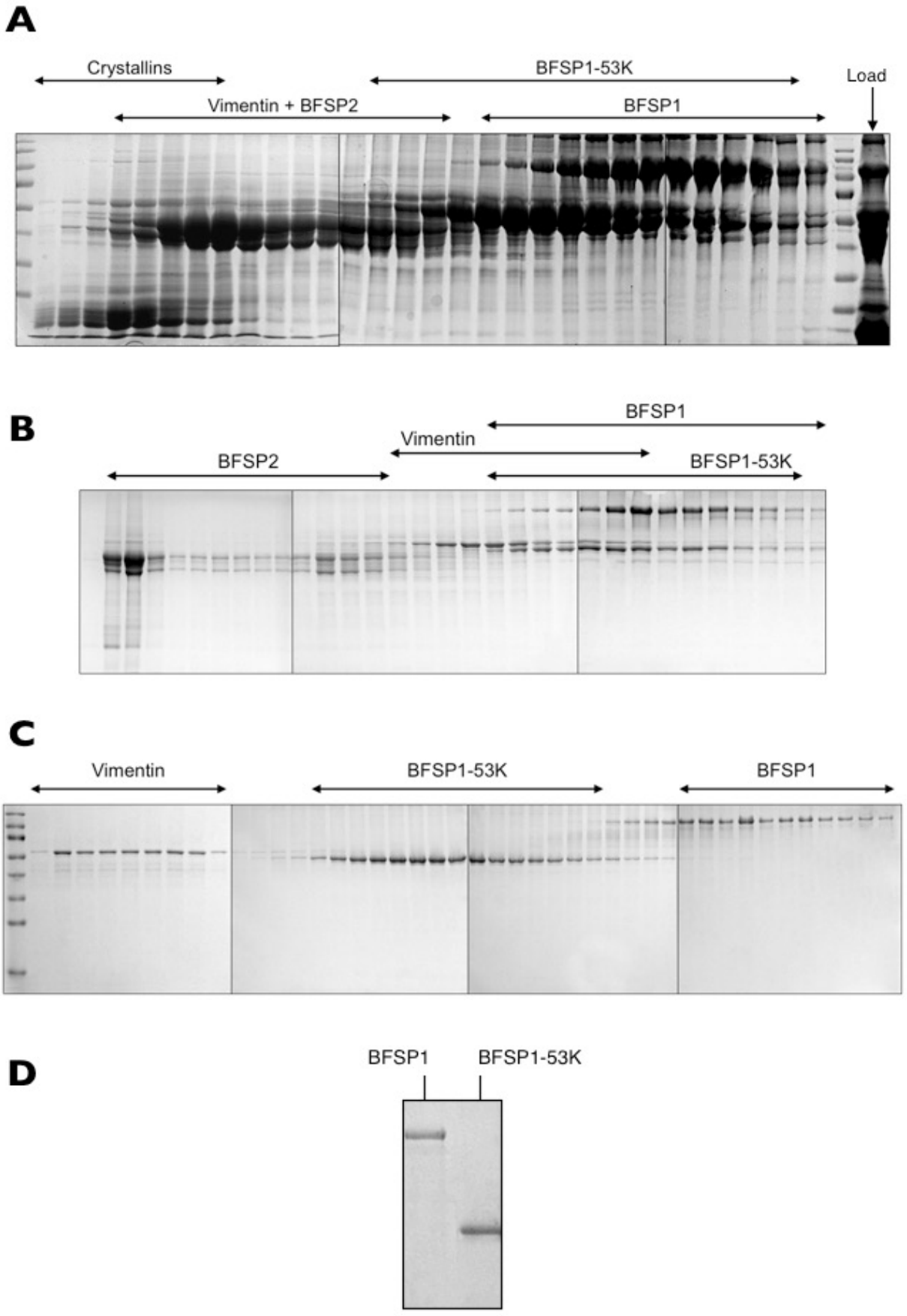

Fig 5.8 (Legend on previous page)

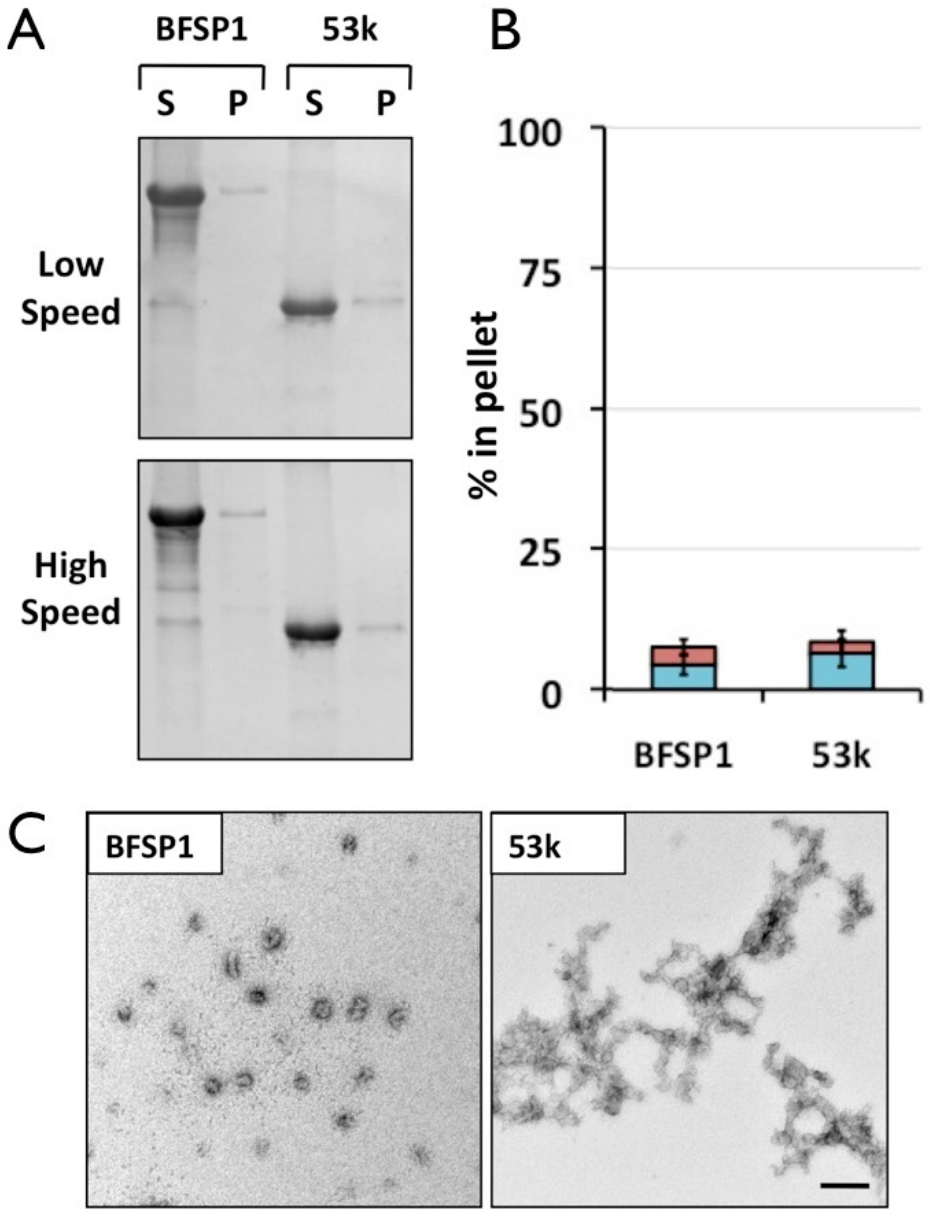

Fig 5.9. Sedimentation properties and TEM characterisation of assembled Bo BFSP1 and 53k.

(A) The low and high speed sedimentation properties of assembled Bo BFSP1 and 53k analysed by SDS-PAGE. At both low (2500g) and high (80,000g) speed, >90% of both proteins remain soluble. (B) Gel densitometry quantification of the low speed (blue) and high speed (red) sedimentation data for Bo BSFP1 and 53k. Average values and standard deviations were calculated from 3 or 4 experimental repeats. (C) Morphology of the assembled Bo BSFP1 and 53k analysed by TEM. Bo BSFP1 assembles into short fragments, while 53k assembles into larger structures, but both remain soluble and do not aggregate. Scale bar represents 100nm.

Analysis of BFSP1 and BFSP2 assembly ratio

In order to determine suitable BFSP1:BFSP2 and 53k:BFSP2 assembly ratios, filaments were assembled at 3 different ratios (1:2, 1:1 and 2:1) and then analysed by high speed sedimentation (Fig 5.10). At high speed, any BFSP1 or 53K material which assembles into filaments with BFSP2 will be pelleted, while any unassembled BFSP1 or 53K material will remain in the supernatant. If large amounts of BFSP1 or 53k remain in the pellet, this indicates an excess of BFSP1 or 53k, and the ratio of BFSP1:BFSP2 and 53k:BFSP2 can be adjusted. Hu WT was the only BFSP2 used in this experiment to maintain consistency and allow direct comparison of the different assembly ratios.

Gel quantification analysis shows that when Bo BFSP1 is assembled with Hu BFSP2 at either 1:2, 1:1 or 2:1, then 84%, 81% and 76% of the BFSP1 is pelleted respectively (Fig 5.10). When bovine 53k is assembled with Hu BFSP2 at either 1:2, 1:1 or 2:1, then 95%, 89% and 85% of the 53k is pelleted respectively (Fig 5.10). Although there is a slight decrease in BFSP1 or 53k pelleting with increasing assembly ratio (84% compared with 76%, and 95% compared with 85%), this difference is small compared with the large difference in assembly ratio (1:2 compared with 2:1).

Therefore, it appears that BFSP2 is capable of assembling with BFSP1 or 53k at all 3 ratios (1:2, 1:1 and 2:1). In order to analyse the effects of the Zf tail on assembly, a 1:1 mass ratio of BFSP1:BFSP2 or 53k:BFSP2 will be used in the rest of this chapter, as this ratio has been used previously (Carter et al., 1995), thus allowing direct comparison with the existing literature.

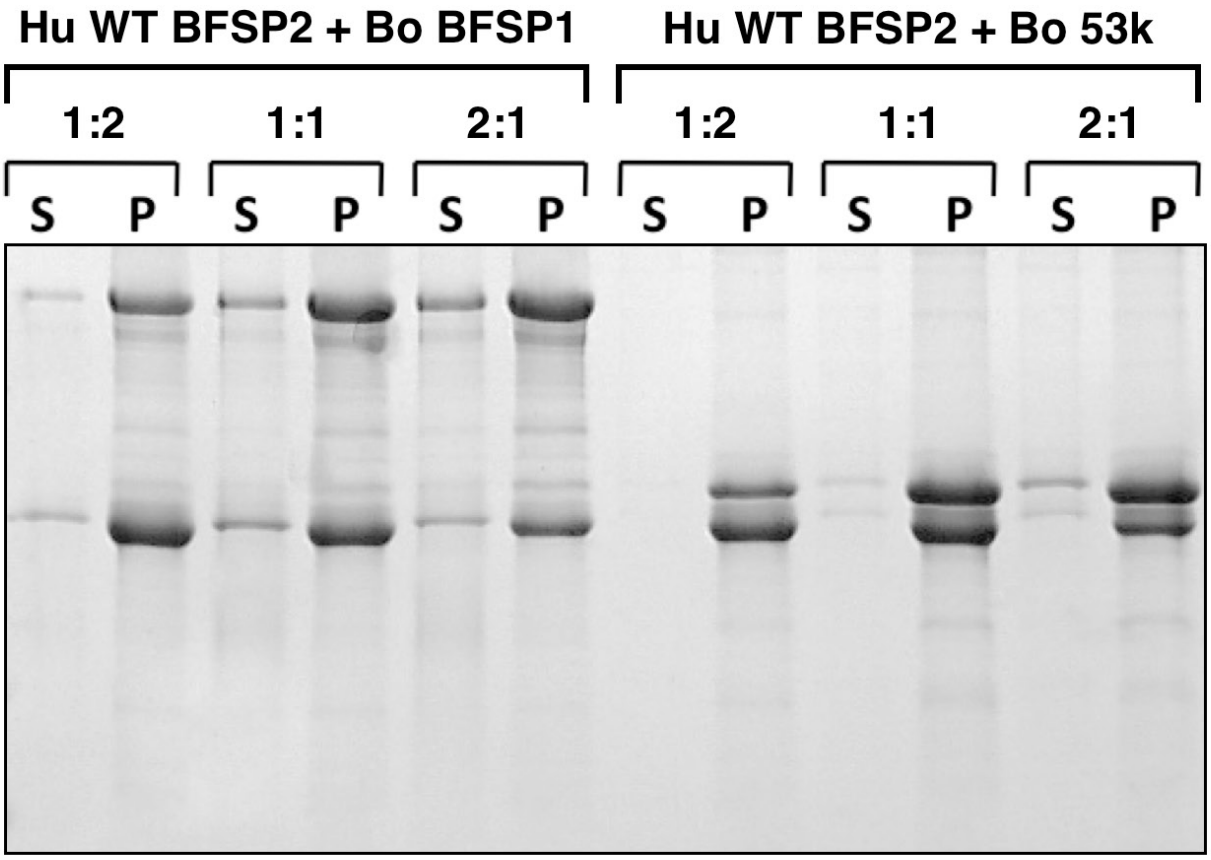

Fig 5.10. Analysis of BFSP1 and BFSP2 assembly ratio.

High speed (80,000g) sedimentation analysis of filaments assembled at different BFSP1:BFSP2 or 53k:BFSP2 mass ratios. At high speed, only BFSP1 or 53k which has assembled into filaments is pelleted. The above gel shows that BFSP2 is capable of assembling with BSFP1 or 53k at all 3 mass ratios (1:2, 1:1, 2:1). Supernatant (S) and pellet (P). The above gel represents 1 of 3 repeats.

Sedimentation properties of Hu WT, Zf WT or Zf CT Bfsp2 co-assembled with Bo BSFP1 or Bo 53k

In order to analyse the role of the Zf WT Bfsp2 tail in filament assembly and interactions, the Hu WT, Zf WT and Zf CT Bfsp2 proteins were assembled with Bo BFSP1 or Bo 53k, and the resulting filaments were analysed by high and low speed co-sedimentation (Fig 5.11). Fig 5.11 represents 1 of 3 experimental repeats, which were quantified via gel densitometry, collated and averaged (Fig 5.12).

When Hu WT, Zf WT or Zf CT Bfsp2 proteins are co-assembled with Bo BFSP1, ~70% of material pellets at high speed for all 3 assemblies, indicating comparable levels of assembly (Fig 5.12, red bars). At low speed, 7-10% of material pellets for all 3 assemblies, indicating comparable, low levels of filament-filament interactions (Fig 5.12, blue bars).

If Hu WT or Zf WT Bfsp2 proteins are co-assembled with Bo 53k, ~80% of material pellets at high speed for both assemblies, indicating comparable levels of assembly (Fig 5.12, red bars). However, when Zf CT Bfsp2 is co-assembled with Bo 53k, ~92% of material pellets, significantly higher than that for Hu WT or Zf WT Bfsp2 (Fig 5.12, red bars). This suggests that removing the Zf C-terminal tail has altered the assembly with 53k.

When Hu WT or Zf CT Bfsp2 proteins are co-assembled with Bo 53k, ~60% and ~78% of material pellets at low speed respectively, indicating comparable, high levels of filament-filament interactions (Fig 5.12, blue bars). However, when Zf WT Bfsp2 is co-assembled with Bo 53k, only 12% of material pellets, significantly lower than that for Hu WT or Zf CT Bfsp2 (Fig 5.12, blue bars).

It is also interesting to note that the filaments formed by Hu WT BFSP2 and Bo BFSP1 aggregate significantly less at low speed (10%) than filaments formed from Hu WT BFSP2 and Bo 53kDa (60%) (Fig 5.12, blue bars). This suggests that the BFSP1 C-terminal tail, which is truncated in 53k, may also prevent filament-filament interactions and subsequent aggregation.

Overall, these data indicate that the Zf Bfsp2 C-terminal tail significantly reduces filament-filament interactions and prevents aggregation when 53k is the assembly partner. In addition, the C-terminal tail of BFSP1 also significantly reduces filament-filament interactions and prevents aggregation when either Hu WT or Zf CT Bfps2 is the assembly partner.

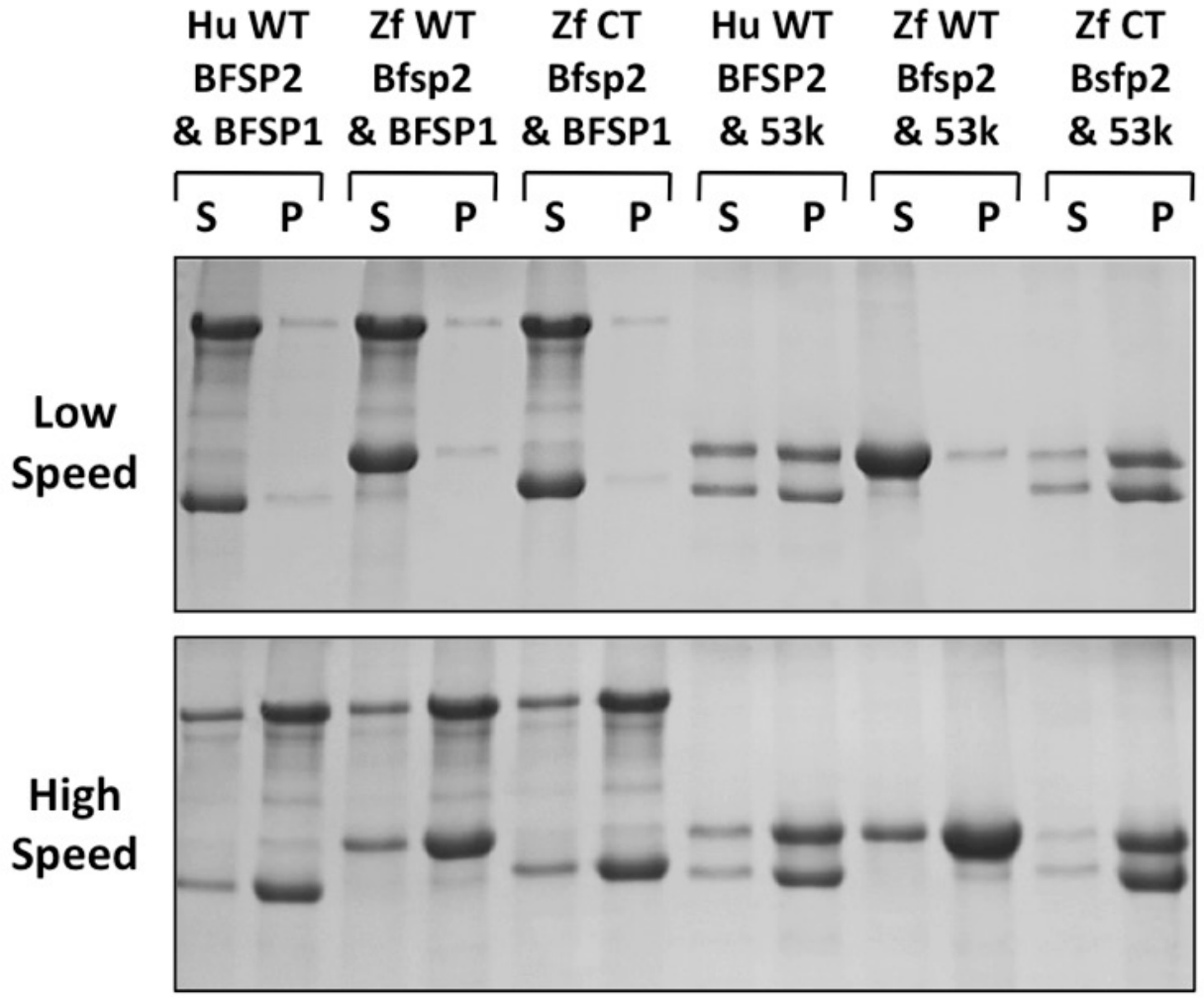

Fig 5.11. Co-sedimentation of Hu or Zf Bfsp2 co-assembled with Bo BSFP1 or Bo 53k.

Low (2,500g) and high (80,000g) speed co-sedimentation of Hu or Zf Bfsp2 co-assembled in a 1:1 mass ratio with Bo BSFP1 or Bo 53k, analysed by SDS-PAGE. At high speed, >70% of material pellets for all assemblies. At low speed, <12% of material pellets for all assemblies, except 'Hu WT & 53k' and 'Zf CT & 53k' which pellet 59% and 78% respectively. The above gels represent 1 of 3 repeats. Supernatant (S) and pellet (P).

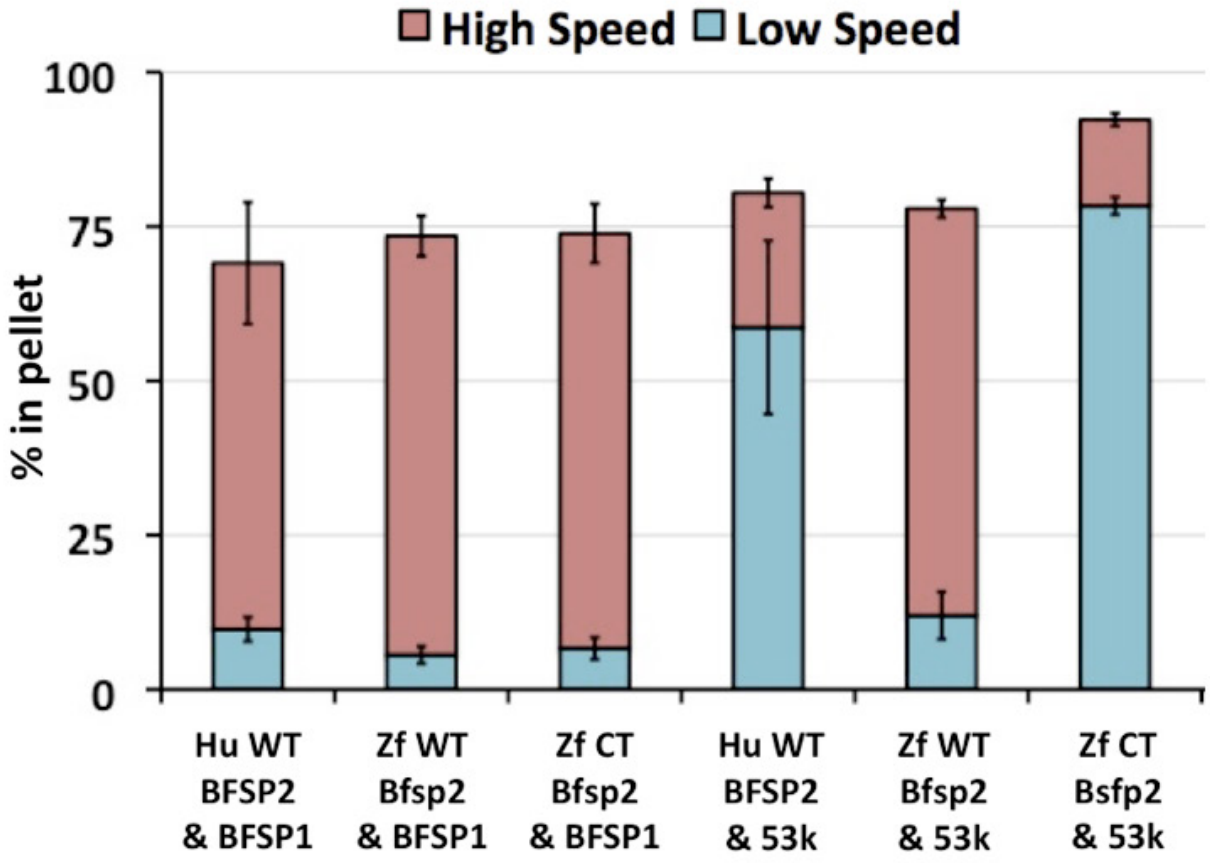

Fig 5.12. Quantification of co-sedimentation of Hu WT, Zf WT or Zf CT Bfsp2 co-assembled with Bo BSFP1 or Bo 53k.

Bar chart of low (blue) and high (red) speed sedimentation of Hu WT, Zf WT or Zf CT Bfsp2 co-assembled in a 1:1 mass ratio with Bo BSFP1 or Bo 53k. When assembled with Bo 53k, Zf WT Bfsp2 forms filaments which remain soluble, unlike those formed by Zf CT or Hu WT Bfsp2, as shown in the low speed assay. Filaments formed by Bfsp2 and BFSP1 aggregate less then those formed by Bsfp2 and 53k. The amount of material pelleted is shown as a percentage of total material as quantified by gel densitometry. Average values and standard deviations were calculated from 3 or 4 experimental repeats.

TEM analysis of Hu WT, Zf WT or Zf CT Bfsp2 co-assembled with Bo BSFP1 or Bo 53k

In order to analyse the role of the Zf WT Bfsp2 tail in filament morphology, the Hu WT, Zf WT and Zf CT Bfsp2 proteins were assembled with Bo BFSP1 or Bo 53k, and the resulting filaments were analysed by TEM (Fig 5.13).

When Hu WT BFSP2 is mixed with Bo BFSP1 or Bo 53k, the proteins co-assemble into long, smooth 5-6nm filaments (Fig 5.13, top row). These filaments appear morphologically identical, despite the Hu WT BFSP2 and Bo 53k filaments showing significantly increased tendency to aggregate (~60% at low speed, see Fig 5.12) compared to Hu WT BFSP2 and Bo BFSP1 filaments (~10% at low speed, see Fig 5.12).

If Zf WT Bfsp2 is mixed with Bo BFSP1 or Bo 53k, the proteins also co-assemble into long, smooth 5-6nm filaments (Fig 5.13, middle row) which resemble those formed by Hu WT BFSP2 and Bo BFSP1 or Bo 53k (Fig 5.13, top row). The filaments formed by Zf WT Bfsp2 and Bo 53k appear similar to those formed by Hu WT Bfsp2 and Bo 53k, despite significantly reduced tendency to aggregate (12% vs 59% sedimentation at low speed, see Fig 5.12, blue bars).

When Zf CT Bfsp2 is mixed with Bo BFSP1 or Bo 53k, the proteins also co-assemble into filaments (Fig 5.13, bottom row), however these filaments appear wider and less smooth and appear to have large variations in width along their length. To quantify this, filament width measurements were made using the TEM images to create filament width distribution profiles for all assemblies (Fig 5.14) (For the complete data set, see supplementary data, Sup Fig 4).

If Zf CT Bfsp2 is assembled with either BFSP1 or 53k, average filament width values are significantly higher (~1.5x) than values for Hu WT and Zf WT Bfsp2 assembled with either BFSP1 or 53k (Fig 5.14). P values of <0.01 in an unpaired two-tailed Students t-test confirmed the significance of this increase of average width. Filaments formed by Zf CT Bfsp2 also have larger (~1.8x) standard deviations of width than values for Hu WT and Zf WT Bfsp2. Overall these data suggest that, unlike Hu BFSP2, the Zf Bfsp2 C-terminal tail may play an important role in the formation of normal (5-6nm) filaments and may help to regulate filament width.

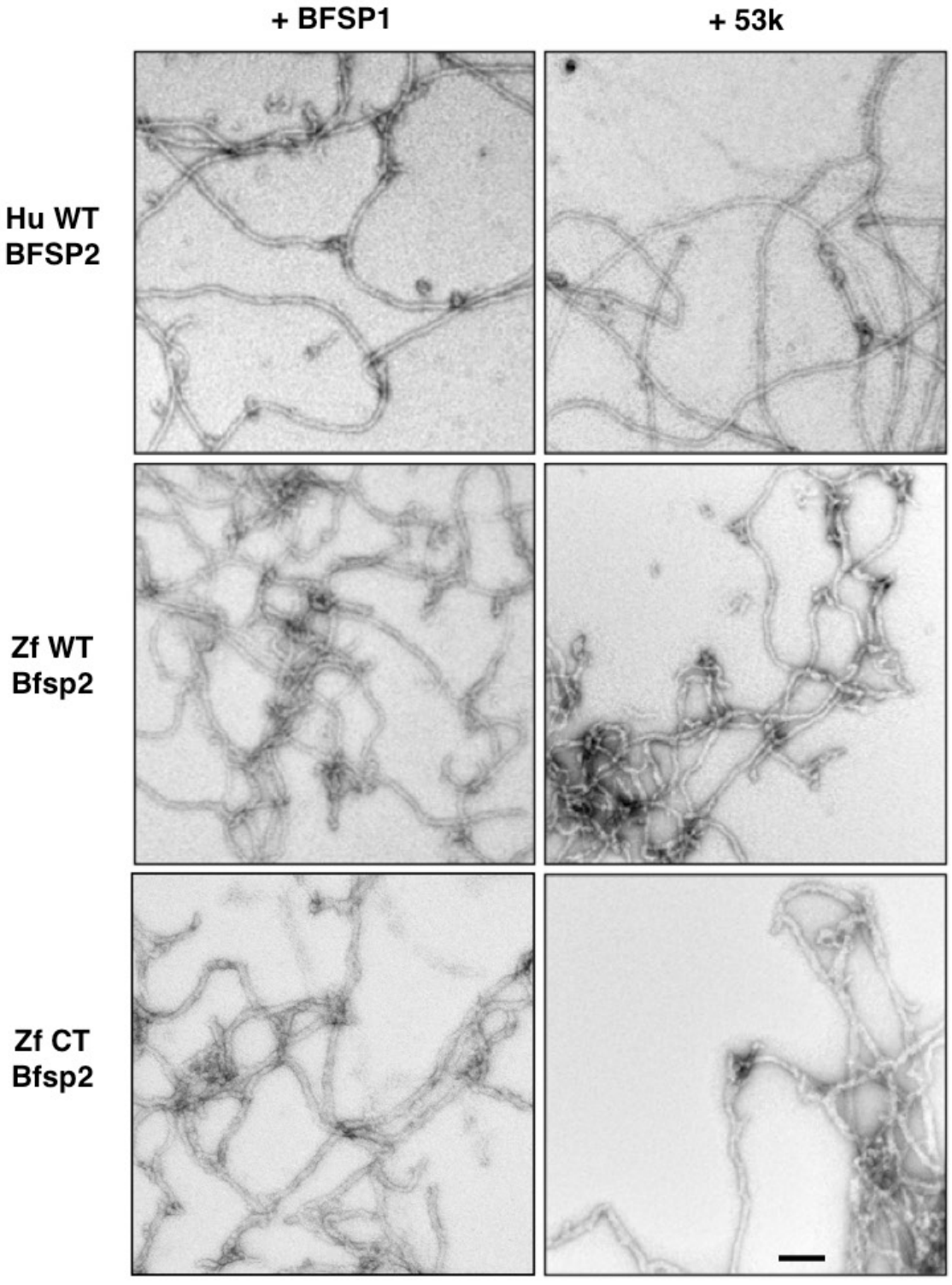

Fig 5.13. TEM analysis of Hu or Zf Bfsp2 co-assembled with Bo BSFP1 or Bo 53k.

The left column shows Hu WT, Zf WT and Zf CT Bfsp2 co-assembled with Bo BFSP1. The right column shows Hu WT, Zf WT and Zf CT Bfsp2 co-assembled with Bo 53k. Scale bar represents 100nm.

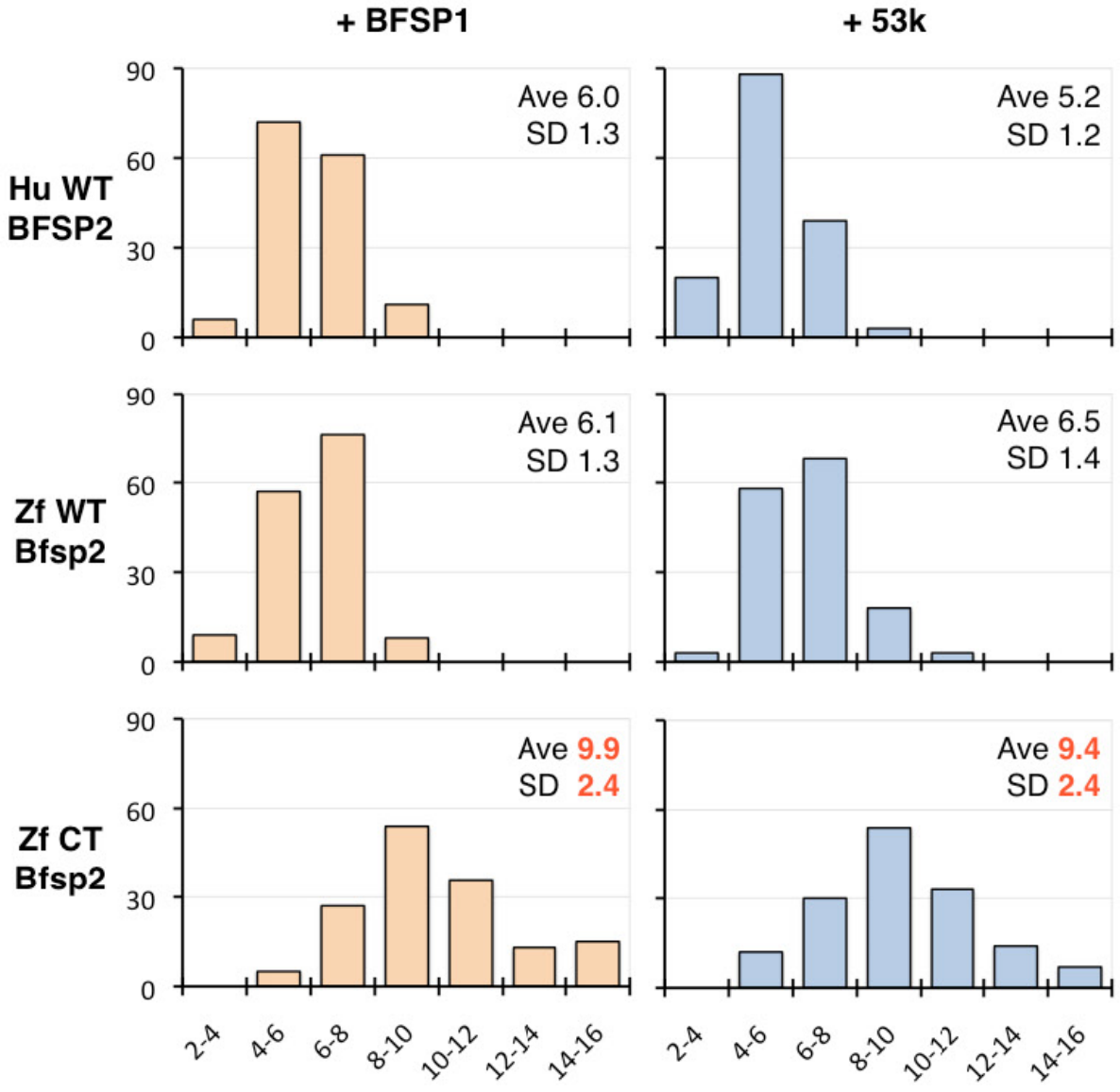

Fig 5.14. Beaded filament width distribution.

A total of 150 width measurements were made for each sample. The x axis show filament width categories (nm) and the y axis show frequency. Average (Ave) and standard deviation (SD) values are also shown for each sample. Measurements were made in randomly selected areas from 3 different TEM images. When Zf CT Bfsp2 is assembled with either BFSP1 or 53k, average filament width values are significantly higher (~1.5x) than values for Hu WT and Zf WT Bfsp2. Filaments formed by Zf CT Bfsp2 also have larger (~1.8x) standard deviations of width than values for Hu WT and Zf WT Bfsp2. Significance of difference was determined by P values <0.01 in an unpaired two-tailed Students t-test. For the complete data set, see supplementary data, Sup Fig 4.

RESULTS SUMMARY

Overall, data in this chapter indicate that the Zf Bfsp2 C-terminal tail significantly enhances protein solubility and can help to prevent the self association of Bfsp2 filament fragments, thus preventing aggregation (sedimentation data summarised in Table 5.15). In addition, this C-terminal tail is able to enhance the solubility and decrease aggregation of other proteins with which it assembles. The Zf Bfsp2 C-terminal tail can significantly reduce filament-filament interactions and prevent aggregation, when 53k is the assembly partner (Table 5.15). In addition, unlike Hu BFSP2, the Zf Bfsp2 C-terminal tail may play an important role in the formation of normal (5-6nm) filaments and may be important for the regulation of filament width. Interestingly, the C-terminal tail of BFSP1 also appears to significantly reduce filament-filament interactions and prevent aggregation when either Hu WT or Zf CT Bfps2 is the assembly partner. In addition, data suggests that BFSP1 may be capable of assembling with BFSP2 in a variety of different mass ratios.

	LOW SPEED		HIGH SPEED	
	Ave % in Pellet	SD	Ave % in Pellet	SD
Hu WT BFSP2	98	1	100	0
Zf WT Bfsp2	**9**	1	**15**	0
Zf CT Bfsp2	78	2	99	1
Hu WT BFSP2 + Zf WT Bfsp2	**19**	5	**55**	4
Hu WT BFSP2 + Zf CT Bfsp2	93	4	100	0
Zf WT Bfsp2 + Zf CT Bfsp2	**10**	2	**65**	4
Hu WT BFSP 2 + Bo BFSP1	10	2	69	10
Zf WT Bfsp2 + Bo BFSP1	6	1	73	3
Zf CT Bfsp2 + Bo BFSP1	7	2	74	5
Hu WT BFSP 2 + Bo 53k	59	14	80	2
Zf WT Bfsp2 + Bo 53k	**12**	4	78	1
Zf CT Bfsp2 + Bo 53k	78	1	92	1
Bo BFSP1	4	2	8	1
Bo 53k	7	2	9	2

Table 5.15. Summary of sedimentation characteristics of assembled Bfsp2 and BSFP1.

Summary of quantifications of high (80,000g) and low (2,500g) speed sedimentation characteristics of Bfsp2 and BFSP1 proteins. When assembled alone, Zf WT Bfsp2 remains soluble (top panel, blue values), unlike Hu WT or Zf CT Bfsp2. Zf WT Bfsp2 can also solublise Hu WT or Zf CT Bfsp2 when assembled in a 1:1 molar ratio (second panel, blue values). When assembled with Bo 53k, Zf WT Bfsp2 forms filaments which do not aggregate (fourth panel, blue value), unlike Hu WT or Zf CT Bfsp2. The amount of material pelleted is shown as a percentage of total material as quantified by gel densitometry. Average (Ave) values and standard deviations (SD) were calculated from 3 or 4 experimental repeats.

CHAPTER 6: EFFECTS OF THE DISEASE CAUSING R287W AND E233del BFSP2 MUTATIONS ON THE BEADED FILAMENT

AIM

To investigate the effects of the disease causing R287W and E233del BSFP2 mutations on the assembly of beaded filaments and their subsequent interactions and morphology.

INTRODUCTION

In the mammalian lens, beaded filaments are essential to lens optical properties, ensuring the correct cellular organisation and optimal plasma membrane profiles of the lens fiber cells (Perng et al., 2007; Song et al., 2009). Beaded filaments may also potentially interact with protein chaperones to help stabilise the high protein concentrations required for the high refractive index of the lens (Bloemendal et al., 2004).

Beaded filaments are composed of BFSP1 and BFSP2, and mutations in these proteins can cause cataract (Conley et al., 2000; Jakobs et al., 2000; Ma et al., 2008; Ramachandran et al., 2007). The R287W and R339H BFSP2 mutations both cause cataract in humans (Conley et al., 2000; Ma et al., 2008) and the E233del BFSP2 mutant causes cataract and myopia in humans (Cui et al., 2007; Jakobs et al., 2000; Zhang et al., 2004). However, to date, no studies have been done to determine the effect of these BFSP2 mutations on beaded filament assembly, morphology, or interaction with sHsps. Analysis these mutations could provide insight into the sHsp interaction and the mechanisms which lead to cataract formation.

Therefore, I investigated the *in vitro* effects of the R287W and E233del BFSP2 mutants (Fig 6.1) on beaded filament assembly, filament morphology, and interaction with aB crystallin. In this chapter, I show that although the R287W and E233del BFSP2 mutant proteins are assembly competent, the mutations effect filament morphology and also potentially alter the filament interaction with aB crystallin. In addition, I show that aB crystallin can actually inhibit beaded filament assembly, and that that post-translational modifications maybe important to beaded filament morphology.

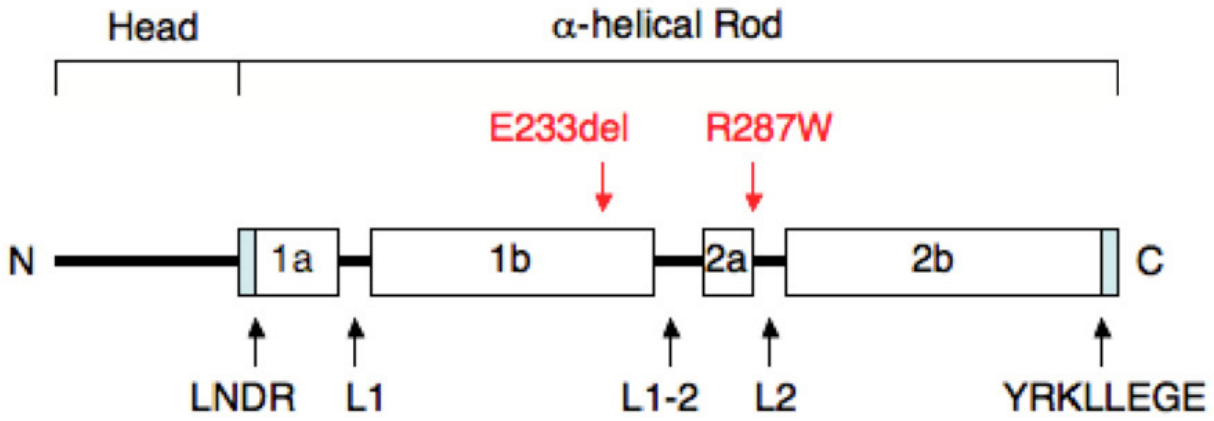

Fig 6.1. Predicted secondary structure for human BFSP2.

The boxes represent α-helical domains which are separated by the non-helical linkers, L1, L1-2 and L2. The blue boxes at the ends of helix 1a and 2b represent the highly conserved LNDR and YRKLLEGE motifs which are important for the assembly of IF proteins into filaments. The E233del mutation (point deletion) lies in the 1b helix while the R287W mutation lies at the start of the L2 linker. Both these mutations cause autosomal dominant cataract in humans.

METHODS

The R287W and E233del BFSP2 mutant constructs were created by PCR mutagenesis and confirmed by bi-directional DNA sequencing. Hu WT, R287W and E233del BFSP2 proteins were all expressed in *E. coli*, extracted from the water insoluble fraction and purified by anion then cation exchange chromatography, under denaturing conditions, to >98% purity (Fig 6.2, A). Notice the reduced electrophoretic mobility of the E233del BFSP2 compared with Hu WT and R287W BFSP2 (Fig 6.2, B). The mutation has seemingly caused a change in protein conformation which reduces its electrophoretic mobility. It is worth noting that SDS is used only to solubilise the proteins, which may not be completely unfolded and may retain secondary structure motifs that may affect the electrophoretic mobility. This has been observed previously for IF proteins, for example, a 4 residue truncation of GFAP results in significantly reduced electrophoretic mobility and 'apparently' increased molecular weight (Ralton et al., 1994).

For assembly, BF proteins at 0.2g/l were mixed (in the presence or absence of aB crystallin at 0.08g/l) and unfolded in 6M Urea buffer. Samples were then dialysed to reduce the Urea concentration to 4M, then 2M, then 0M over a period of 24h at 22°C. Samples were then dialysed into Tris-HCl pH 7.6, 50mM NaCl, 1mM $MgCl_2$ buffer at 22°C for 16h to finalise assembly. To assess filament morphology, filaments were analysed by TEM. Samples were prepared essentially using the Valentine method (Valentine et al., 1968).

To monitor assembly and quantify filament-filament interactions, two separate centrifugation assays were used. Samples were centrifuged at either 80,000g for 30min (high speed assay) or 2,500g for 15min (low speed assay). The pellets and supernatants were separated and solubilised in equal final volumes of SDS-PAGE sample buffer to allow direct comparison of the proportions of material in the supernatant and pellet. Results were then visualised via SDS-PAGE and quantified by gel densitometry.

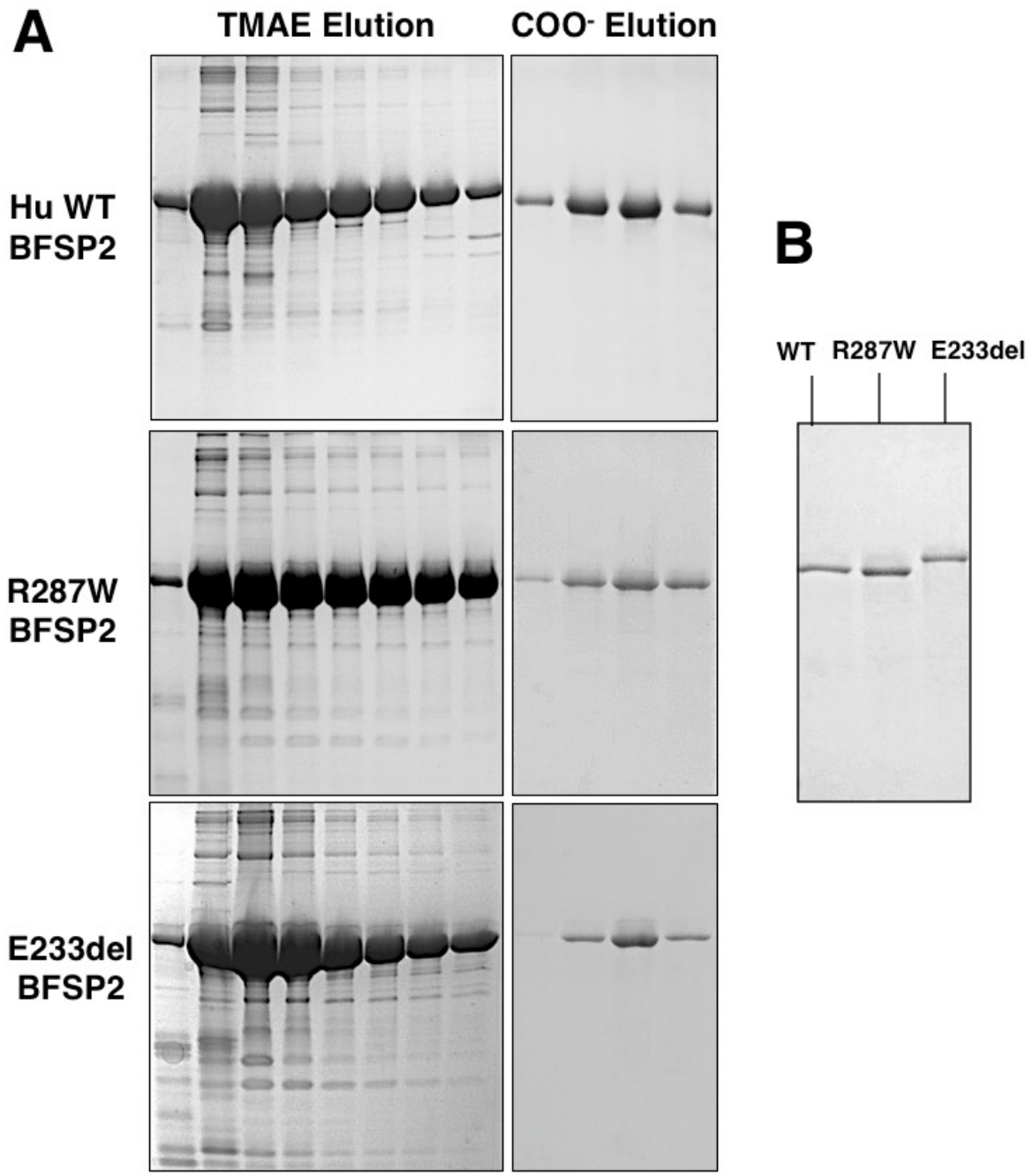

Fig 6.2. Purification of BFSP2 proteins.

Hu WT, R287W and E233del BFSP2 proteins were all expressed in *E. coli*, extracted from the water insoluble fraction and then purified by anion then cation exchange chromatography under denaturing conditions. (A) The SDS-PAGE gels show the TMAE anion exchange and COO- cation exchange chromatography purification elution profiles for the 3 BFSP2 proteins. (B) The final samples are >98% pure. The R287W and E233del mutant constructs were created by PCR mutagenesis and confirmed by bi-directional DNA sequencing.

RESULTS

Effect of the R287W and E233del mutations on the self assembly and solubility of BFSP2

To assess the effect of the R287W and E233del mutations on the self assembly and solubility of BFSP2, the low (2500g) and high (80,000g) speed sedimentation properties of Hu WT, R287W and E233del BFSP2 proteins were analysed by SDS-PAGE. Fig 6.3 shows 1 of 3 experimental repeats, which were quantified via gel densitometry, collated and averaged (Fig 6.3).

Results show that when assembled alone, all 3 BFSP2 proteins are completely pelleted at high speed (>99%), indicating that the R287W and E233del mutant BFSP2 proteins are still capable of assembling (Fig 6.3). At low speed, all 3 BFSP2 proteins are >80% pelleted, indicating aggregation of the assembled structures (Fig 6.3). There appears to be no significant difference between the solubility and aggregation of the mutant BFSP2 proteins compared to the Hu WT BFSP2 protein.

Fig 6.3. Sedimentation properties of self assembled Hu BSFP2 proteins.

(A) The high (80,000g) and low (2,500g) speed sedimentation of Hu WT, R287W and E233del BFSP2 assembled alone, analysed by SDS-PAGE. (B) Quantification of the sedimentation assay as determined by gel densitometry. Average values and standard deviations were calculated from 3 experimental repeats. When assembled alone, all 3 BSFP2 proteins are >99% pelleted at high speed and >80% pelleted at low speed. There is no significant difference between the solubility of the 3 self assembled BFSP2 proteins. Supernatant (S) and pellet (P).

(Figure on next page)

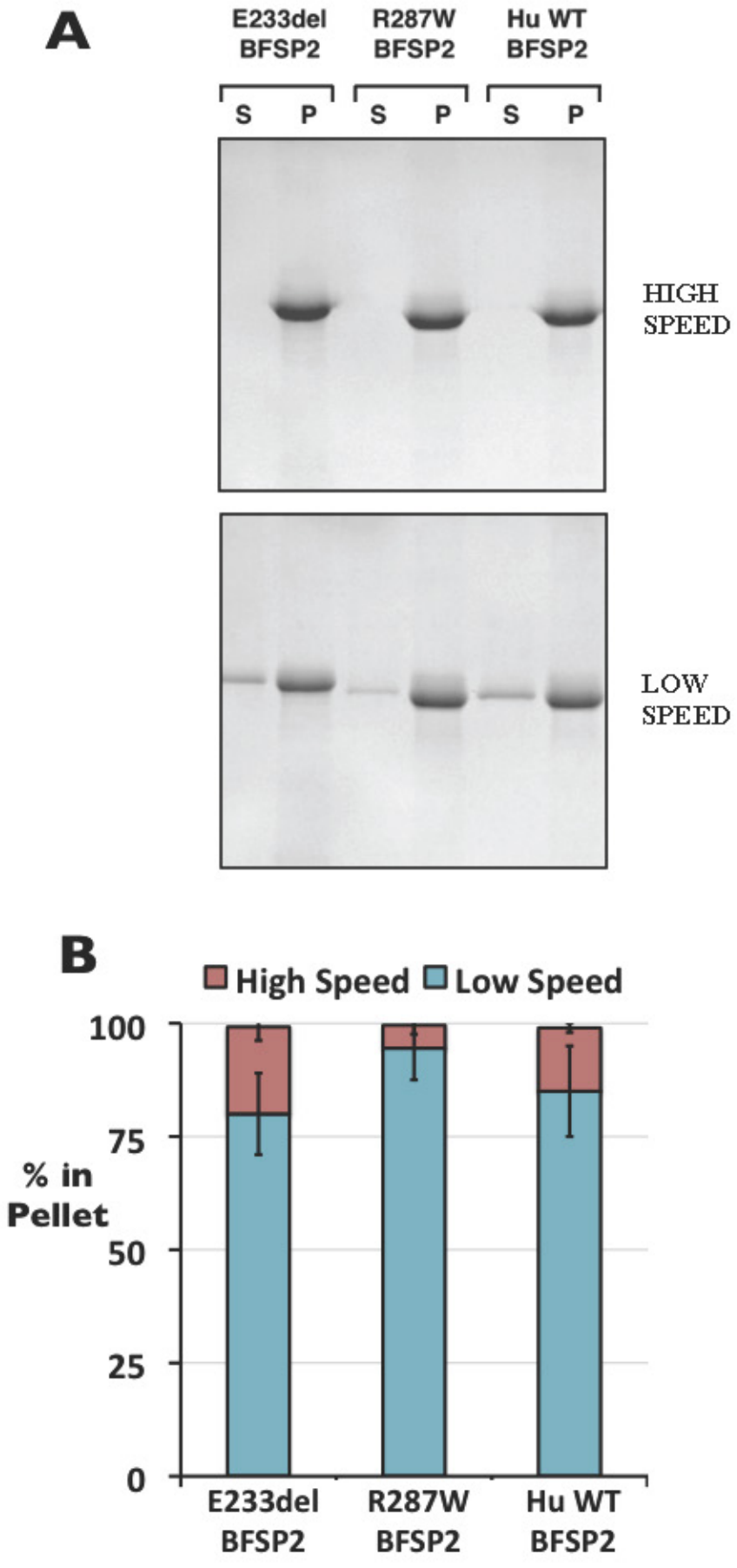

Fig 6.3 (Legend on previous page)

Purification of Hu WT BFSP1 and Hu WT 53k and assembly with Hu WT BFSP2

In the previous chapter, I showed that mixing BFSP2 with its BFSP1 or 53k assembly partner results in the formation of 5-6nm filaments. Therefore, in order to further analyse the effects of the BFSP2 mutations, the BFSP2 proteins were assembled with BFSP1 and 53k.

The previous chapter assembled Hu WT BFSP2 with 'native bovine' BFSP1 or 53k. However, in order to allow 'human' BFSP1 or 53k to be used for the assembly, rather than bovine, the recombinant expression constructs for Hu WT BFSP1 and Hu WT 53k were produced. These expression constructs were prepared by Antal Tapodi, in Professor Quinlan's lab at the University of Durham, UK. The proteins were then expressed in *E. coli*, extracted from the water insoluble fraction and purified by anion then cation exchange chromatography, under denaturing conditions, to >98% purity (Fig 6.4).

Assembly of Hu WT BFSP2 with Hu WT BFSP1 or Hu WT 53k

In order to confirm the assembly competence of the newly expressed 'recombinant human' BFSP1 and 53k proteins, the proteins were assembled with Hu WT BFSP2. The filaments formed were then compared to those formed by 'native bovine' BFSP1 and 53k proteins (Fig 6.5).

Results show that both the recombinant Hu BFSP1 and 53k are able to form filaments with Hu BFSP2, in both the presence and absence of Hu WT aB crystallin (Fig 6.5, right column). However, the filaments formed by Hu WT BFSP2 and the native bovine BFSP1 or 53k appear smoother and more uniform than those formed by Hu WT BFSP2 and the recombinant human BFSP1 or 53k (Fig 6.5, compare left and right columns). Filaments formed by the recombinant Hu BFSP1 or 53k appear to be less consistent in width with sharper turns (right column), in contrast to the more consistent width and gradual turns of the native bovine filaments (left column). Therefore, I decided to use 'native bovine' assembly partners, rather than the 'recombinant human', in the remainder of the chapter during comparison of the BFSP2 proteins.

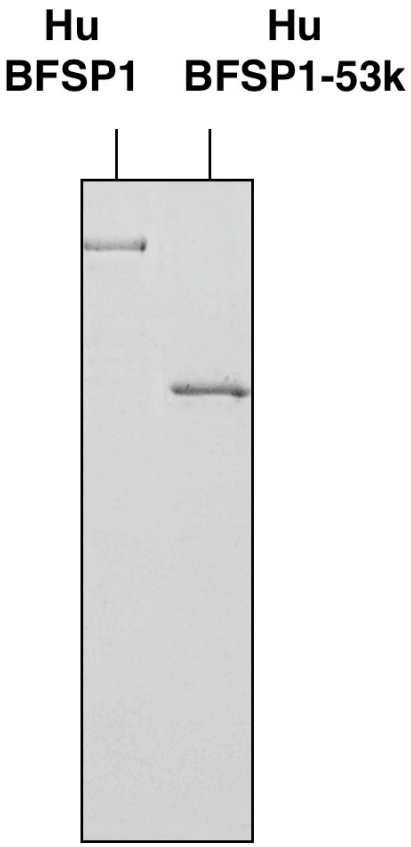

Fig 6.4. Purification of recombinant Hu BFSP1 and recombinant Hu 53k.

Recombinant human BFSP1 and recombinant human 53k were purified to >98% purity.

Fig 6.5. Analysis of assembly competence of recombinant human BFSP1 and 53k.

Comparison of the filaments formed when recombinant Hu WT BFSP2 is assembled with either 'native bovine' BFSP1/53k proteins (left column) or 'recombinant human' BFSP1/53k proteins (right column). All 8 assemblies contain the same Hu WT BFSP2. The bottom 2 rows also include recombinant Hu WT aB crystallin, an important interaction partner of beaded filaments. The filaments formed by the 'native bovine' BFSP1 and 53k appear smoother and more uniform in width than those formed by the 'recombinant human' BFSP1 and 53k (compare left and right columns).

(Figure on next page)

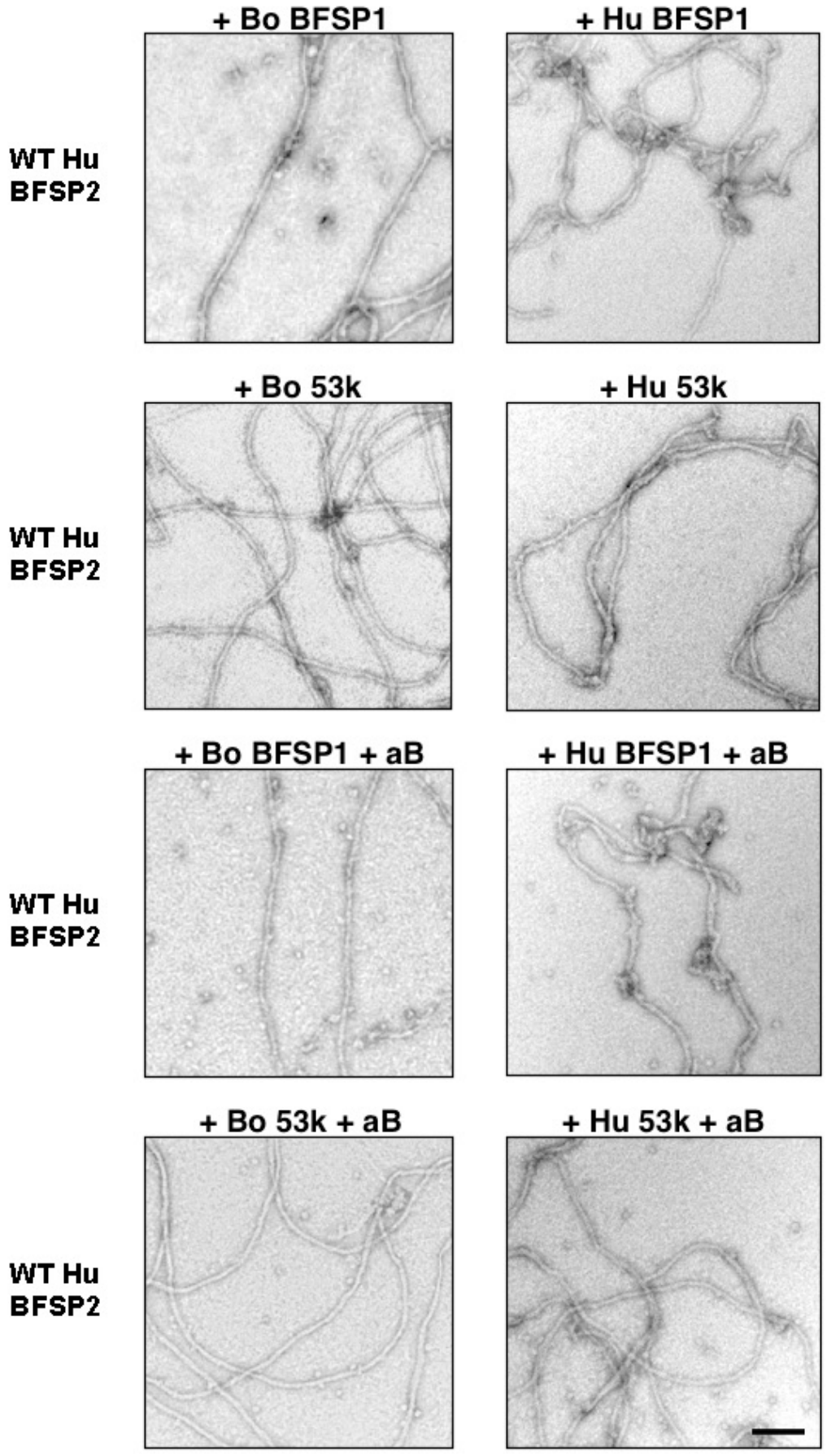

Fig 6.5 (Legend on previous page)

Sedimentation properties of Hu WT, R287W or E233del BFSP2 co-assembled with Bo BSFP1 or Bo 53k

In order to analyse any effect of the R287W and E233del BFSP2 mutations on filament assembly and interactions, the Hu WT, R287W or E233del BFSP2 proteins were assembled with Bo BFSP1 or Bo 53k, and the resulting filaments were analysed by high and low speed co-sedimentation (Fig 6.6). Fig 6.6 represents 1 of 3 experimental repeats, which were quantified via gel densitometry, collated and averaged (Fig 6.7).

When Hu WT, R287W or E233del BFSP2 proteins are co-assembled with either Bo BFSP1 or Bo 53k, >70% of material pellets at high speed for all assemblies, indicating comparable levels of assembly (Fig 6.7, red bars) and suggesting that the BFSP2 mutants are assembly competent.

In contrast, when assembled with Bo 53k, >70% of material pellets at low speed for all 3 BFSP2 proteins, indicating comparable, high levels of filament-filament interactions (Fig 6.7, blue bars). However, there appears to be no significant difference between the BFSP2 proteins, with regards to filament-filament interactions and aggregation, as detected by this assay.

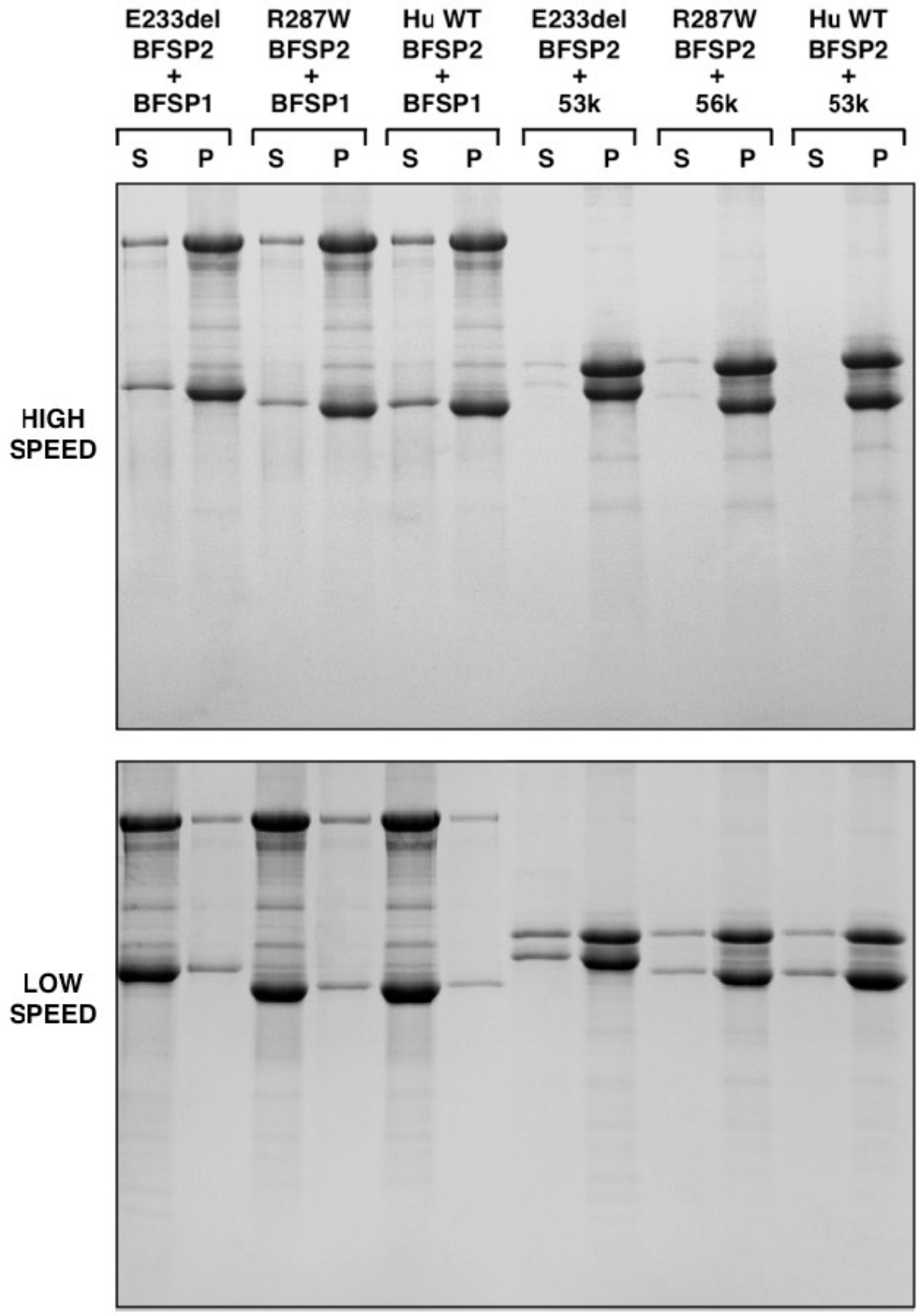

Fig 6.6. Co-sedimentation of Hu WT, R287W or E233del BFSP2 co-assembled with Bo BSFP1 or Bo 53k.

Low (2,500g) and high (80,000g) speed co-sedimentation of Hu WT, R287W and E233del BFSP2 proteins co-assembled in a 1:1 mass ratio with Bo BSFP1 or Bo 53k, analysed by SDS-PAGE. The above gels represent 1 of 3 repeats. Supernatant (S) and pellet (P).

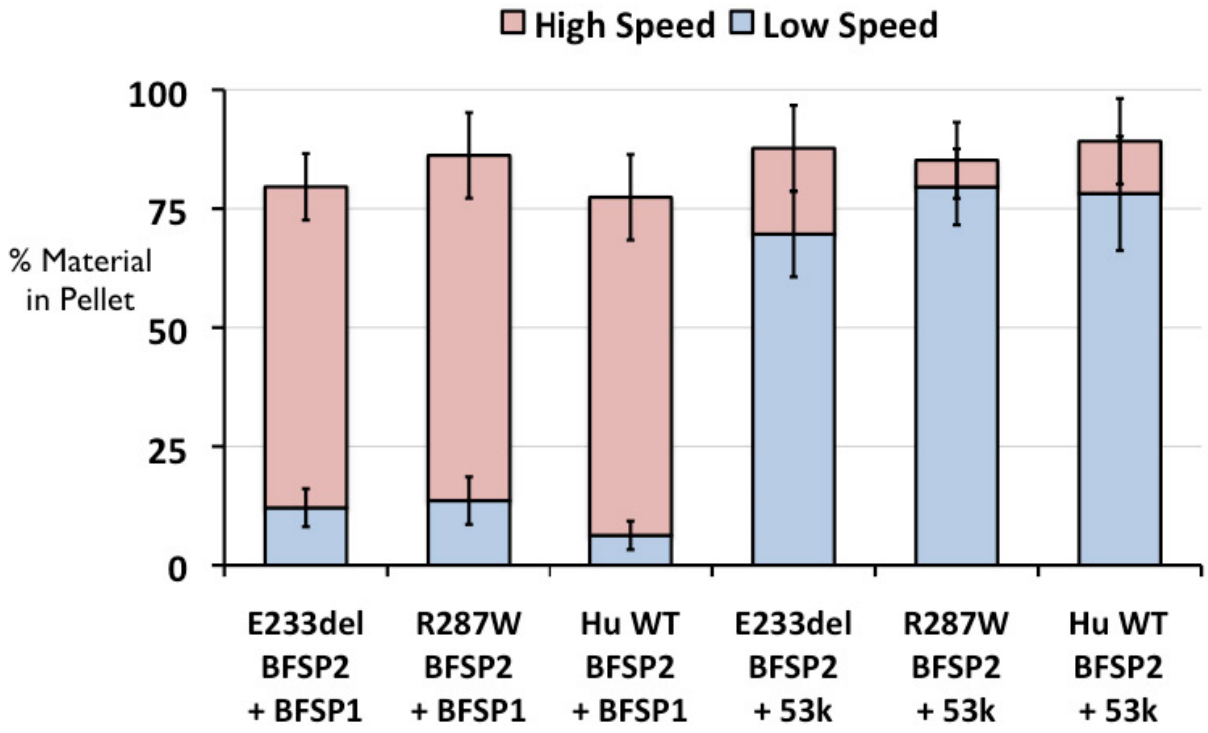

Fig 6.7. Quantification of co-sedimentation of Hu WT, R287W or E233del BFSP2 co-assembled with Bo BSFP1 or Bo 53k.

Bar chart of low (blue) and high (red) speed sedimentation of Hu WT, R287W and E233del BFSP2 co-assembled in a 1:1 mass ratio with Bo BSFP1 or Bo 53k. Filaments formed by BFSP2 and BFSP1 aggregate less then those formed by BFSP2 and 53k. However, there appears to be no significant difference between the BFSP2 proteins, with regards to filament-filament interactions and aggregation. The amount of material pelleted is shown as a percentage of total material as quantified by gel densitometry. Average values and standard deviations were calculated from 3 experimental repeats.

TEM analysis of Hu WT, R287W or E233del BFSP2 co-assembled with Bo BSFP1 or Bo 53k

In order to analyse any effect of the R287W and E233del BFSP2 mutations on filament morphology, the Hu WT, R287W and E233del BFSP2 proteins were assembled with Bo BFSP1 or Bo 53k, and the resulting filaments were analysed by TEM (Fig 6.8).

When Hu WT BFSP2 is mixed with Bo BFSP1 or Bo 53k, the proteins co-assemble into long, smooth 5-6nm filaments (Fig 6.8, top row). These filaments appear morphologically identical, despite the Hu WT BFSP2 and Bo 53k filaments showing significantly increased tendency to aggregate (~60% at low speed, see Fig 6.7, blue bars) compared to Hu WT BFSP2 and Bo BFSP1 filaments (~10% at low speed, see Fig 6.7, blue bars).

When R287W or E233del BFSP2 is mixed with Bo BFSP1, the proteins co-assemble into filaments (Fig 6.8), but these filaments appear morphologically different from those formed by Hu WT BFSP2 (Fig 6.8, compare down left column). The filaments formed by R287W or E233del BFSP2 and Bo BFSP1 appear less smooth, less consistent in width and less elongated, compared to equivalent filaments formed by Hu WT BFSP2.

When mixed with Bo 53k, the R287W and E233del BFSP2 mutants assemble into filamentous structures, but with dramatically altered morphology, compared to Hu WT BFSP2 (Fig 6.8, compare down right column). The filaments formed by R287W or E233del BFSP2 and Bo 53k appear less smooth, less elongated and far less consistent in width compared to equivalent filaments formed by WT BFSP2. Most strikingly, these filaments appear to have associated into aggregates (Fig 6.8).

Overall these data suggest that the disease causing R287W and E233del BFSP2 mutations result in altered filament morphology and these effects are most pronounced when 53k is the assembly partner.

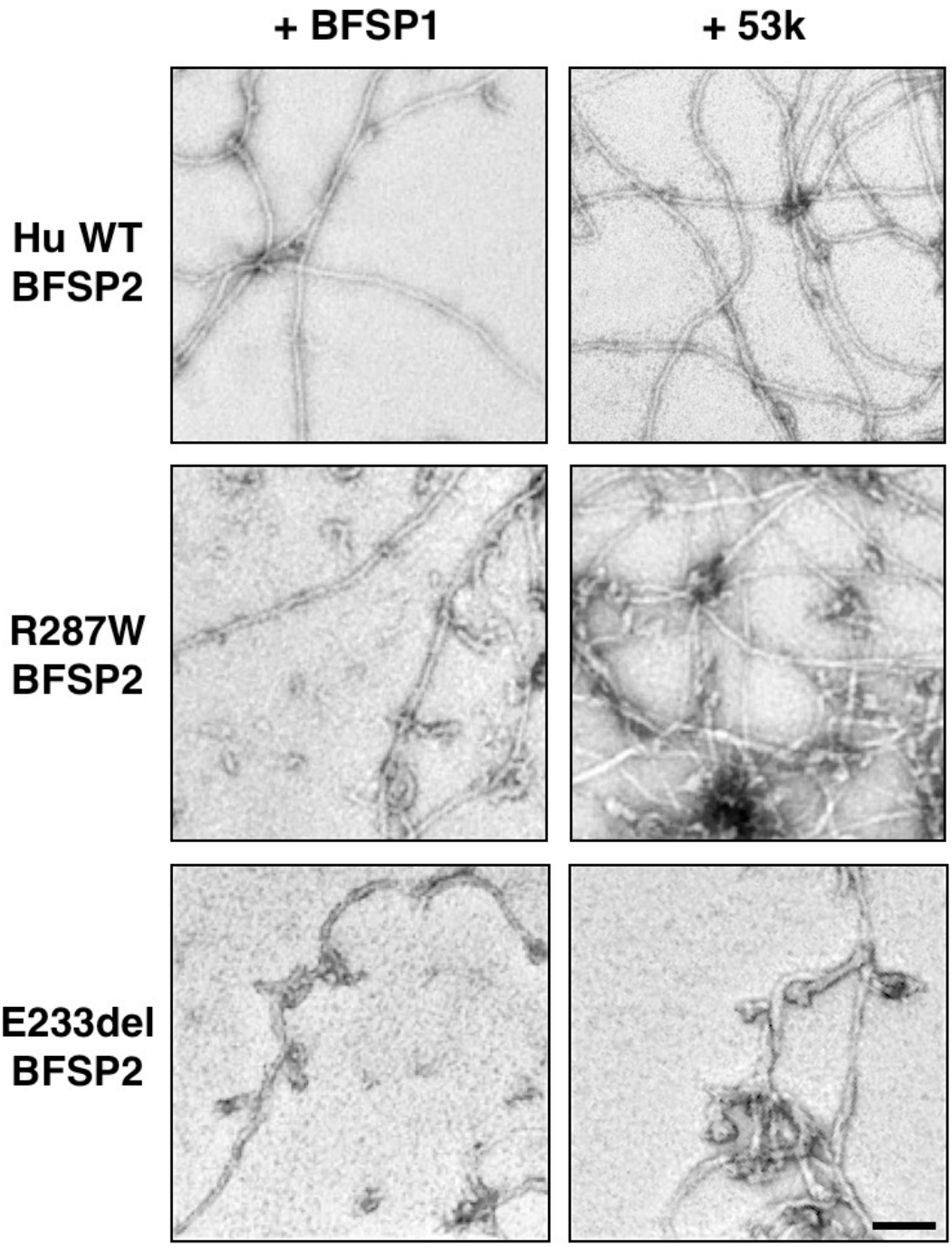

Fig 6.8. TEM analysis of Hu WT, R287W or E233del BFSP2 co-assembled with Bo BSFP1 or Bo 53k.

The left column shows Hu WT, R287W or E233del BFSP2 co-assembled with Bo BFSP1. The right column shows Hu WT, R287W or E233del BFSP2 co-assembled with Bo 53k. Scale bar represents 100nm.

Sedimentation properties of Hu WT, R287W or E233del BFSP2 co-assembled with Bo BSFP1 or Bo 53k, in the presence of aB crystallin

TEM analysis showed that the disease causing R287W and E233del BFSP2 mutations result in altered filament morphology (Fig 6.8). However, there was no apparent difference in filament assembly or filament-filament interactions, as detected by the high and low speed assay (Fig 6.7). I thus decided my analysis should include human aB crystallin, an important interaction partner of IFs, known to affect both filament-filament interactions and filament morphology (see later in this thesis).

Hu WT, R287W or E233del BFSP2 proteins were assembled with Bo BFSP1 or Bo 53k in the presence of Hu WT aB crystallin, and the resulting filaments were analysed by high and low speed co-sedimentation (Fig 6.9). Fig 6.9 represents 1 of 3 experimental repeats, which were quantified via gel densitometry, collated and averaged (Fig 6.10).

When the BFSP2 proteins are assembled with Bo 53k and aB crystallin, >80% of the BFSPs pellet at both low and high speed for all 3 BFSP2 proteins (R4H). These sedimentation characteristics are very similar to those seen for these filaments assembled in the absence of aB crystallin (Fig 6.7).

However, when the BFSP2 proteins are assembled with Bo BFSP1 and aB crystallin, ~65% of the R287W and E233del BFSP2 filaments pellet at high speed, whereas only 40% of Hu WT BFSP2 filaments pellet (Fig 6.10). Interestingly, these high speed sedimentation values of all 3 BFSP2 proteins are significantly lower than those obtained for these filaments assembled in the absence of aB crystallin (Fig 6.7). This comparison is shown in Fig 6.11, which compares the high speed sedimentation values for the 3 BFSP2 proteins assembled with Bo BFSP1 in both the presence and absence of aB crystallin (Fig 6.11).

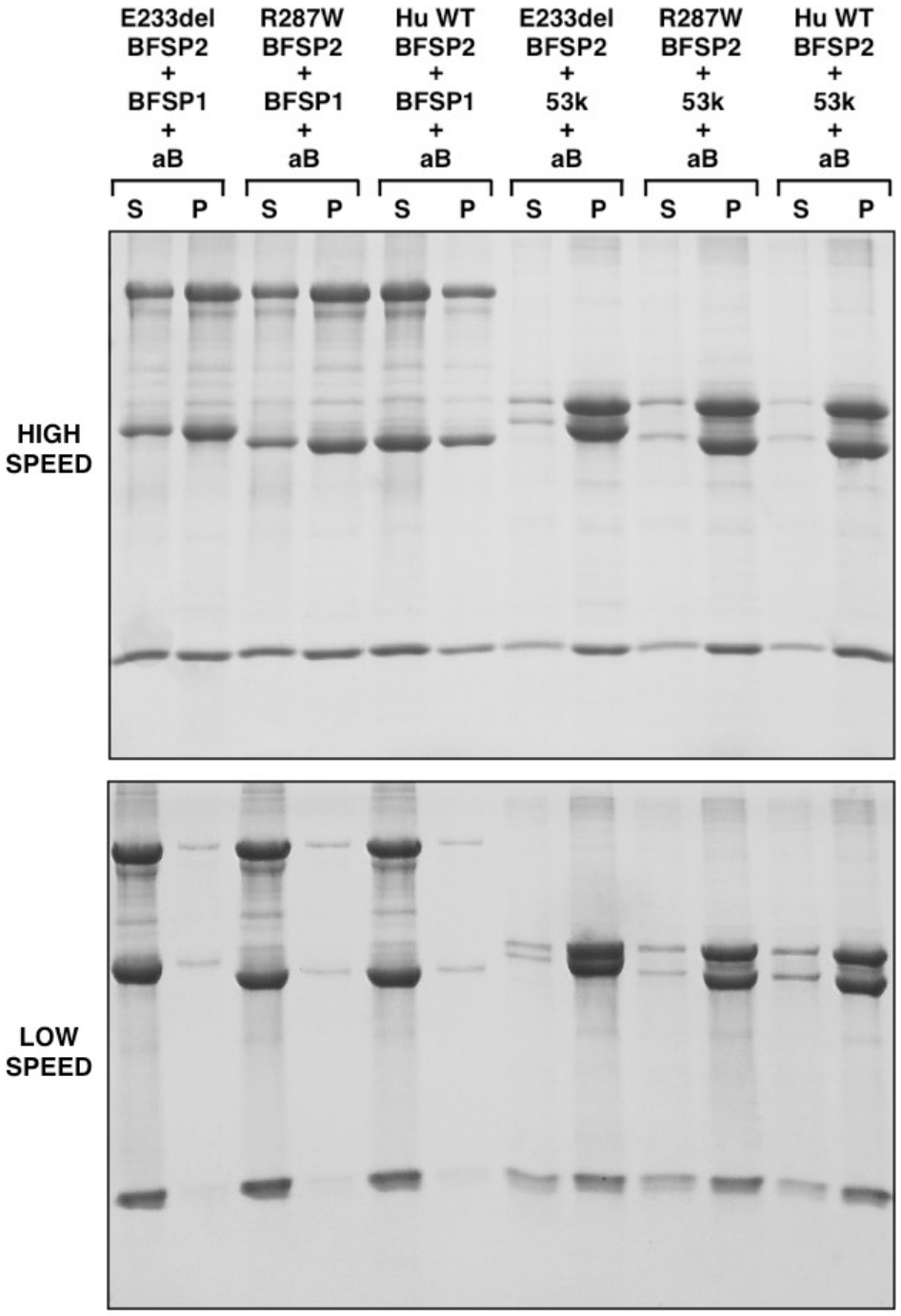

Fig 6.9. Co-sedimentation of Hu WT, R287W or E233del BFSP2 co-assembled with Bo BSFP1 or Bo 53k in the presence of aB crystallin.

Low (2,500g) and high (80,000g) speed co-sedimentation of Hu WT, R287W and E233del BFSP2 proteins co-assembled in a 1:1 mass ratio with Bo BSFP1 or Bo 53k in the presence of aB crystallin, analysed by SDS-PAGE. The above gels represent 1 of 3 repeats. Supernatant (S) and pellet (P).

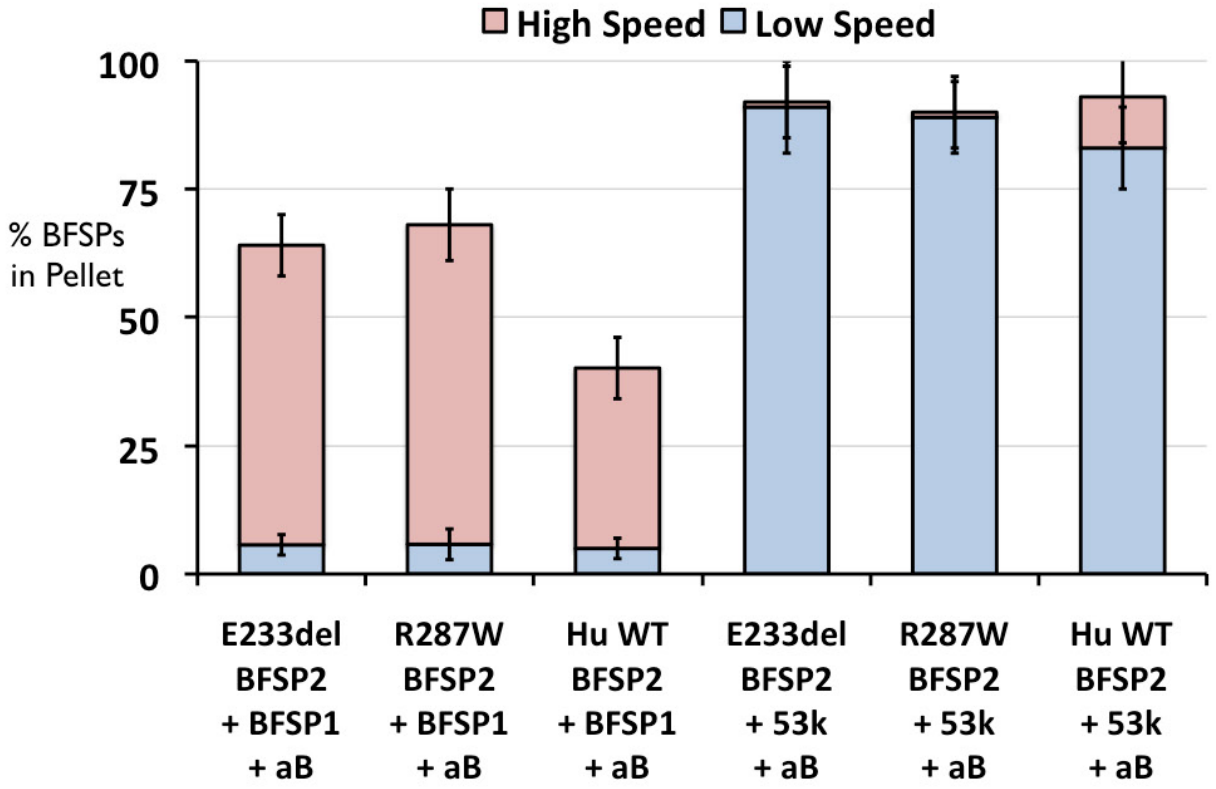

Fig 6.10. Quantification of co-sedimentation of Hu WT, R287W or E233del BFSP2 co-assembled with Bo BSFP1 or Bo 53k in the presence of aB crystallin.

Bar chart of low (blue) and high (red) speed sedimentation of Hu WT, R287W and E233del BFSP2 co-assembled in a 1:1 mass ratio with Bo BSFP1 or Bo 53k in the presence of aB crystallin. When the BFSP2 proteins are assembled with Bo BFSP1 and aB crystallin, 64% and 68% of the E233del and R287W BFSP2 filaments pellet at high speed respectively, whereas only 40% of Hu WT BFSP2 filaments pellet. The amount of material pelleted is shown as a percentage of total material as quantified by gel densitometry. Average values and standard deviations were calculated from 3 experimental repeats.

In the high speed sedimentation assay, the pellet (P) contains all the material which has assembled. The supernatant (S) contains any unassembled beaded filament proteins and any assembly intermediates. Therefore, a reduction in pelleted material indicates inhibition of assembly.

When aB crystallin is included in the assembly of the BFSP2 proteins with Bo BFSP1, there is a significant reduction in the high speed pelleted material (Fig 6.11). This indicates that aB crystallin may be inhibiting filament assembly. Interestingly, this effect is most pronounced for Hu WT BFSP2 filaments, which show a reduction in high speed pelleting from 78% to 40% upon addition of aB crystallin (Fig 6.11). The R287W and E233del BFSP2 mutants also show significant reductions of 86% to 68% and 80% to 64% respectively (Fig 6.11). Although this apparent aB crystallin inhibition of filament assembly is present for all 3 BFSP2 proteins, the effect is significantly reduced for the R287W and E233del BFSP2 mutants (Fig 6.11). This suggests that these mutations may have altered the interaction with aB crystallin.

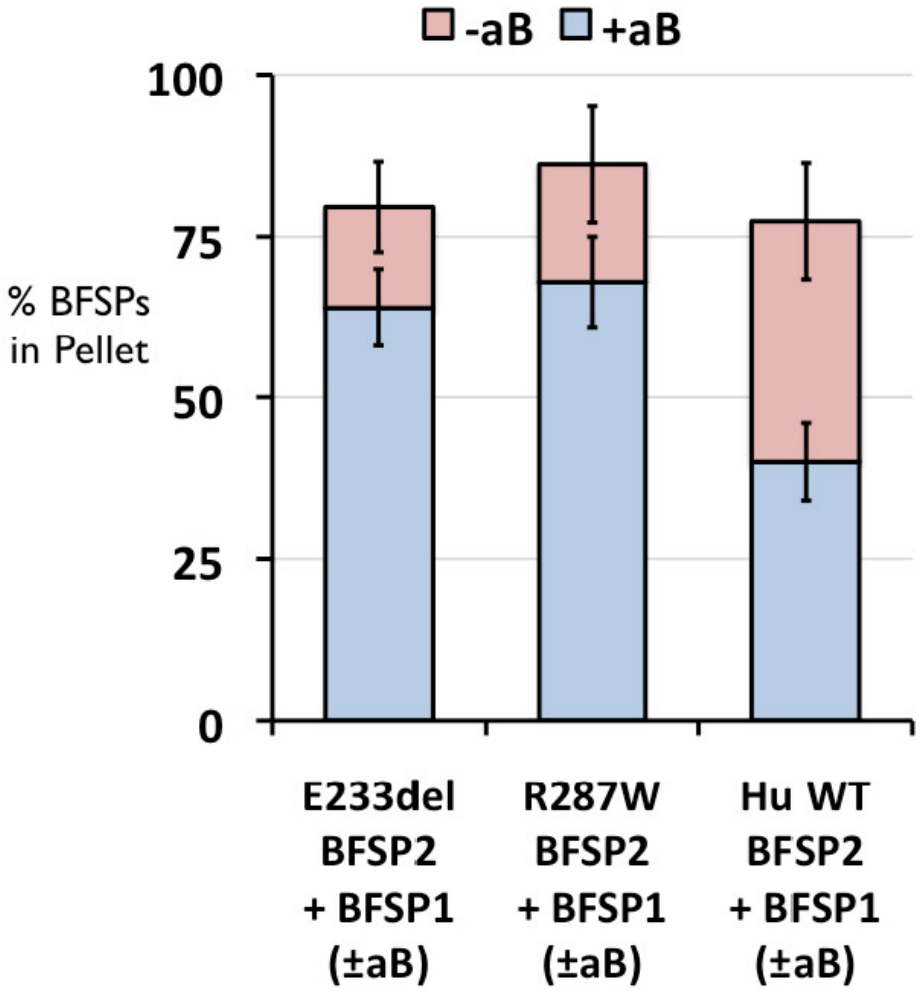

Fig 6.11. Comparison of high speed co-sedimentation of BFSP2 and BFSP1 proteins in the presence and absence of aB crystallin.

Comparison of high speed (80,000g) co-sedimentation of Hu WT, R287W or E233del BFSP2 co-assembled with Bo BSFP1 in both the presence (blue) and absence (red) of aB crystallin. Hu WT BFSP2 filaments show a reduction in high speed pelleting from 78% to 40% upon addition of aB crystallin. The R287W and E233del BFSP2 filaments also show significant reductions in pelleting of 86% to 68% and 80% to 64% respectively.

TEM Analysis of Hu WT, R287W or E233del BFSP2 co-assembled with Bo BSFP1 in the presence of aB crystallin

Co-sedimentation analysis showed that, when assembled with BFSP1, the R287W and E233del BFSP2 mutants may have affected the filament interactions with aB crystallin (Fig 6.11). In addition, aB crystallin is potentially capable of affecting filament morphology (see later in this thesis). Therefore, to further analyse this potentially altered interaction with aB crystallin, the Hu WT, R287W and E233del BFSP2 proteins were assembled with Bo BFSP1 in the presence of aB crystallin, and the resulting filaments were analysed by TEM (Fig 6.12).

When Hu WT BFSP2 is mixed with Bo BFSP1 in the presence of aB crystallin, the BFSPs co-assemble into long, smooth, 5-6nm filaments (Fig 6.12, top right). These filaments appear morphologically similar to those formed in the absence of aB crystallin (Fig 6.12, top left), despite a significant reduction in high speed pelleting of the sample upon aB crystallin addition (78% to 40%, Fig 6.11).

When R287W or E233del BFSP2 proteins are mixed with Bo BFSP1 in the presence of aB crystallin, the BFSPs co-assemble into 5-6nm filaments (Fig 6.12, centre right and bottom right). These filaments appear slightly smoother and more uniform than those formed in the absence of aB crystallin (Fig 6.12, compare left and right columns), but this is difficult to quantify and may not be significant. However, it is clear that these disease causing BFSP2 mutants are capable of forming filaments with BFSP1, and that these filaments do not aggregate.

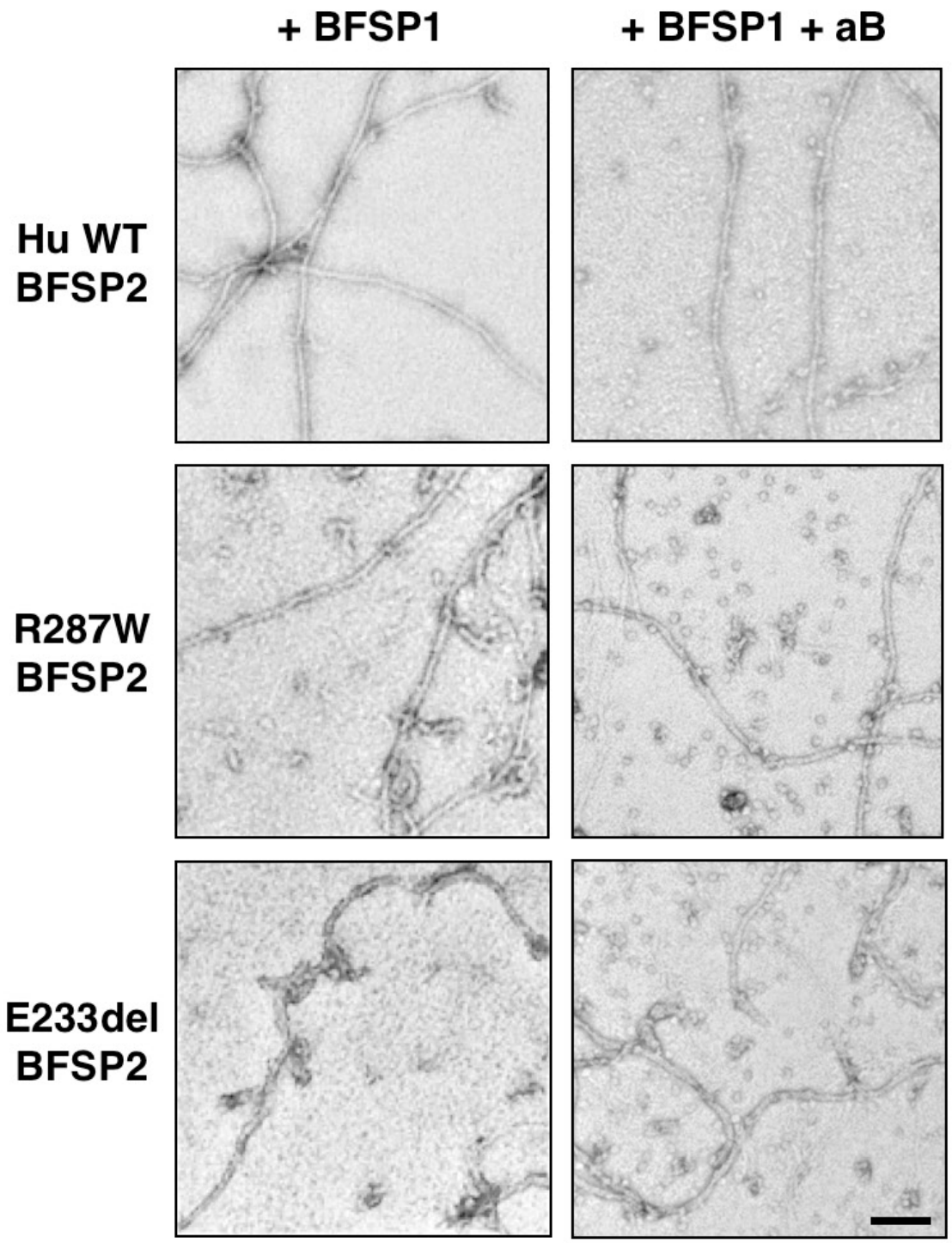

Fig 6.12. TEM analysis of Hu WT, R287W or E233del BFSP2 co-assembled with Bo BSFP1 in the presence or absence of aB crystallin.

The right column shows Hu WT, R287W and E233del BFSP2 proteins assembled with Bo BFSP1 in the presence of aB crystallin. The left column shows the BFSP2 proteins assembled with Bo BFSP1 in the absence of aB crystallin, and is taken from earlier figure (Fig 6.8), to allow comparison of the effects of aB crystallin addition. Scale bar represents 100nm.

RESULTS SUMMARY

Overall, data in this chapter indicate that the R287W and E233del BFSP2 mutants are assembly competent and can form filaments with Bo BFSP1 or 53k. However, these filaments appear less smooth, less consistent in width and less elongated, compared to equivalent filaments formed by Hu WT BFSP2.

Data in this chapter also suggest that, *in vitro*, aB crystallin may inhibit beaded filament assembly, and that this inhibition may be reduced by the R287W and E233del BFSP2 mutations.

In addition, data shows that filaments formed by Hu WT BFSP2 and 'native bovine' BFSP1 or 53k appear smoother and more uniform than those formed by Hu WT BFSP2 and 'recombinant human' BFSP1 or 53k. This may indicate that post-translational modifications are important in beaded filament assembly.

CHAPTER 7: DOMAINS IN aB CRYSTALLIN IMPORTANT FOR INTERACTION WITH DESMIN

AIM

To investigate the importance of the b3 and b8 strands and C-terminal residues 155-165 of aB crystallin in the interaction with desmin filaments.

PUBLICATION NOTE

The data presented in this chapter has been published in the PLoS ONE journal: Houck SA*, Landsbury A*, Clark JI, Quinlan RA. (2011). Multiple sites in αB-crystallin modulate interactions with desmin filaments assembled *in vitro*. PLoS ONE *6(11)*. (*Joint first author)

INTRODUCTION

aB crystallin modulates the assembly of IFs (Nicholl and Quinlan, 1994) and reduces filament-filament interactions in vitro (Perng et al., 1999a). In fact, over-expression of aB crystallin can reverse IF aggregation in transfected cells, suggesting that aB crystallin is involved in regulating the local associations of IFs (Koyama and Goldman, 1999).

aB crystallin is an important binding partner of the IF, desmin, (Perng et al., 1999b; Perng et al., 2004) and mutations in both desmin (Munoz-Marmol et al., 1998) and aB crystallin (Vicart et al., 1998) can cause myopathy. Indeed, the R120G aB crystallin mutation, which alters the interaction with desmin filaments (Perng et al., 2004), causes desmin related myopathy (DRM) characterised by aggregates of desmin and R120G aB crystallin (Vicart et al., 1998). Despite the inherent instability of R120G aB crystallin (Meehan et al., 2007; Treweek et al., 2005), the pathology is aB crystallin and desmin aggregates, rather than aB crystallin-only aggregates, demonstrating the importance of the sHsp-IF interaction (Vicart et al., 1998). Therefore, analysing the interaction of aB crystallin and desmin may provide important insights into the mechanisms which lead to disease.

Previous studies have attempted to identify the aB crystallin domains involved in the interaction with client proteins. The b3 and b8 strands and C-terminal residues 155-165 of aB crystallin have been identified by pin arrays as potential interaction sites for a variety of client proteins, including the filament proteins GFAP, actin and desmin (Fig 7.1) (Ghosh et al., 2007b). These regions have also been identified as potentially important for aB crystallin oligomerisation and chaperone activity (Fig 7.1) (Ghosh et al., 2005). Crystallisation (Laganowsky et al., 2010) and solution structural (Jehle et al., 2010; Peschek et al., 2009) studies suggest that all 3 sequences are surface exposed on the aB crystallin subunit and are potentially available to bind client proteins.

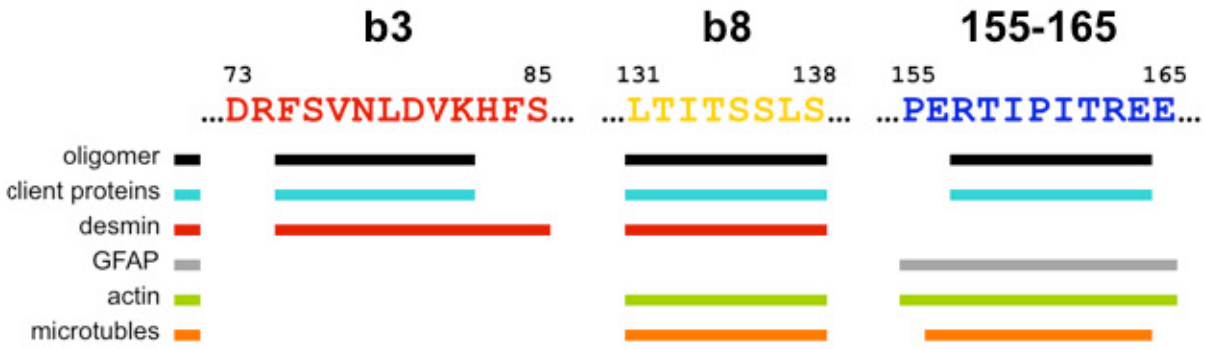

Fig 7.1. Interactions of the predicted b3 and b8 strands and C-terminal residues 155-165 in WT aB crystallin.

The predicted b3 strand (residues 73-85) and b8 strand (residues 131-138) and C-terminal residues 155-165 in aB crystallin have been been proposed as potential substrate interaction regions. The thick black lines below the residues indicate which residues in aB crystallin are proposed to be involved in assembly of aB crystallin into oligomers. The coloured lines indicate which residues in aB crystallin are proposed to be involved binding to client proteins (dark green), desmin (red), GFAP (grey), actin (lime) and microtubules (orange). All three regions are proposed to be important for assembly into oligomers (black lines) and binding of unfolding client proteins (turquoise lines). The b3 and b8 strand are proposed to be important for desmin binding (red lines). The b8 strand and 155-165 regions are proposed to be important for actin and microtubule binding (lime and orange lines, respectively). Refs: (Ghosh and Clark, 2005; Ghosh et al., 2005, 2006a; Ghosh et al., 2006b; Ghosh et al., 2007a, b; Ghosh et al., 2006d, 2007c).

The importance of these regions (b3, b8 and residues 155-165) of aB crystallin was investigated further by Ghosh et al. in 2006. Two chimeric b3 strand mutants (aAb3 and CEb3 aB crystallin) were generated by swapping the aB crystallin b3 strand (73-DRFSVNLDVKHFS-85) with the corresponding sequence from either human aA crystallin, DKFVIFLDVKHFS (aAb3 aB crystallin), or *C. elegans* HSP12.2, EKFEVGLDVQFFT (CEb3 aB crystallin) (Fig 7.2) (Ghosh et al., 2006b). Two chimeric b8 strand mutants (aAb8 and CEb8 aB crystallin) were generated by swapping the aB crystallin b8 strand (131-LTITSSLS-138) with the corresponding sequence from either human aA crystallin, SALSCSLS (aAb8 aB crystallin), or *C. elegans* HSP12.2, STVKSHLA (CEb8 aB crystallin) (Fig 7.2) (Ghosh et al., 2006a). A deletion mutant (d155 aB crystallin) was generated by deleting C-terminal residues 155-165 (155-PERTIPITREE-165) (Fig 7.2) (Ghosh et al., 2006d). The deleted C-terminal residues 155-165 contain the highly conserved IXI motif, predicted to be important for sHsp oligomer assembly and chaperone activity (Pasta et al., 2004; Saji et al., 2008).

Ghosh et al., 2006 found that the aAb3, CEb3, aAb8, CEb8 and d155 aB crystallin mutations have no significant effect on the secondary and tertiary structure of aB crystallin as determined by far and near UVCD spectroscopy and that all 5 mutants are thermostable upon heating to 50°C (Ghosh et al., 2006a; Ghosh et al., 2006b; Ghosh et al., 2006d). Size exclusion chromatography showed that at 22°C the oligomers formed by aAb3 aB crystallin and CEb3 aB crystallin are comparable to WT aB crystallin with ~24 subunits (Ghosh et al., 2006b) but those formed by aAb8 and CEb8 aB crystallin are ~32 subunits (Ghosh et al., 2006a). Oligomers formed by d155 aB crystallin are larger and more polydisperse (~24 to ~56 subunits) than WT aB crystallin, with poor solubility (Ghosh et al., 2006d).

Ghosh et al. also found that the aAb3 aB crystallin mutation does not affect chaperone activity for ADH or b-crystallin and is comparable to WT aB crystallin (Ghosh et al., 2006b). However, CEb3 aB crystallin chaperone activity for ADH and b-crystallin is reduced by 30% and 40% respectively. aAb8 aB crystallin chaperone activity for ADH and b-crystallin is reduced by 70% and 40% respectively while CEb8 aB crystallin promotes aggregation of b-crystallin more than 50-fold. CEb8 aB crystallin shows some chaperone activity for ADH, but activity is 6-fold less than WT aB crystallin (Ghosh et al., 2006a). d155 aB crystallin promotes aggregation of ADH and b-crystallin 3-fold and 11-fold respectively (Ghosh et al., 2006d).

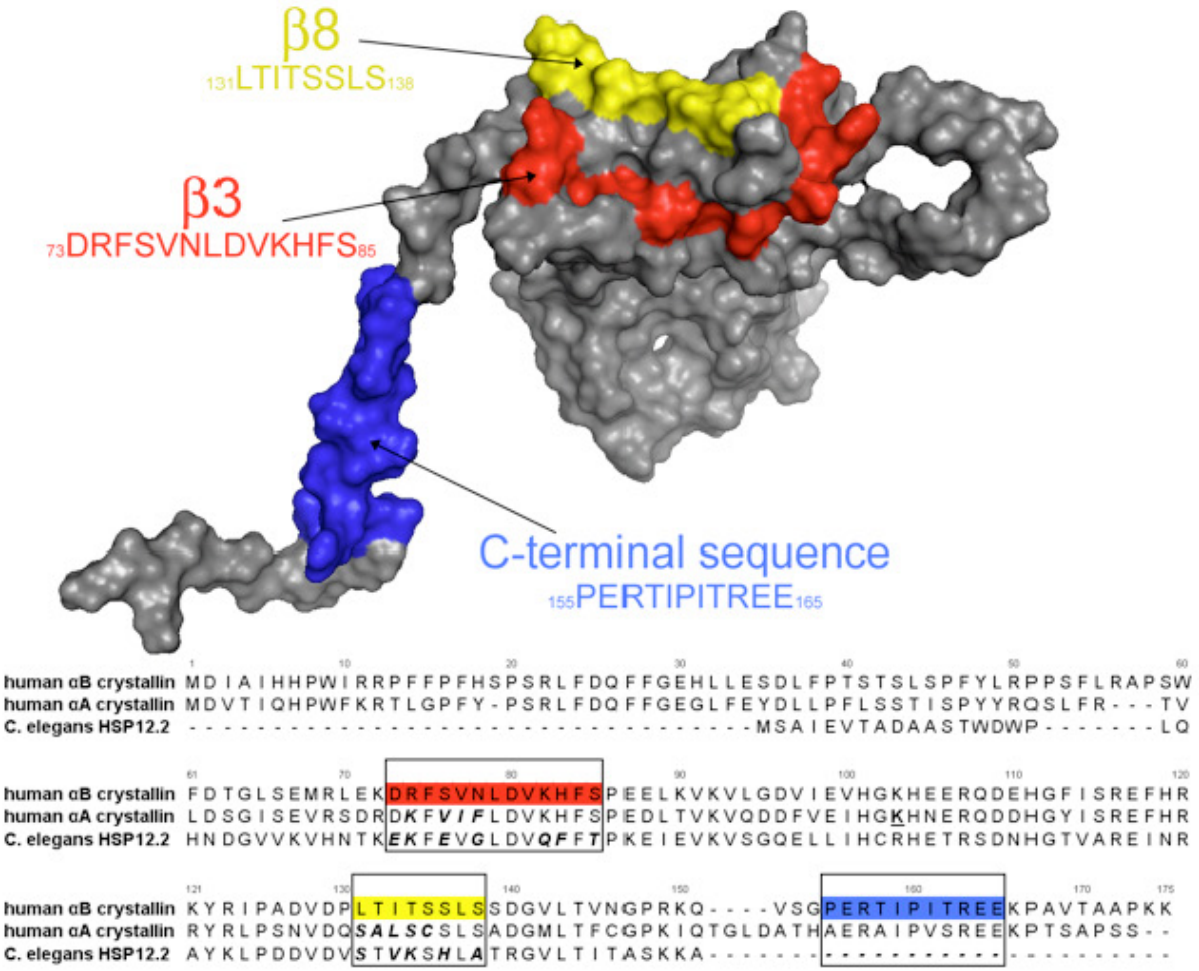

Fig 7.2. Predicted location of the b3 and b8 strands and C-terminal residues 155-165 in human WT aB crystallin.

The primary sequences for human WT aB crystallin, human WT aA crystallin and *C. elegans* WT HSP12.2 were aligned using the residue numbers for human aB crystallin in ClustalX. The colours in the aB crystallin sequence correspond with the interactive sequences labeled on the surface of the 3D model. The amino acid substitutions in the aB crystallin protein constructs are indicated by ***bold-italics***. The b3 strand (red) of aB crystallin, 73-DRFSVNLDVKHFS-85, was replaced with the corresponding sequences from aA crystallin, DKFVIFLDVKHFS (aAb3 aB crystallin), or HSP12.2, EKFEVGLDVQFFT (CEb3 aB crystallin). The b8 strand (yellow) of aB crystallin, 131-LTITSSLS-138, was replaced with the corresponding sequences in aA crystallin, SALSCSLS (aAb8 aB crystallin), or HSP12.2, STVKSHLA (CEb8 aB crystallin). The 155-165 residues (blue) were also deleted (d155 aB crystallin). This figure was prepared by Scott Houck at the University of Washington, USA.

Overall, Ghosh et al. found that the CEb3, aAb8, CEb8 and d155 aB crystallin mutations all had detrimental effects on aB crystallin activity, while no changes were detected for aAb3 aB crystallin. This suggests that the b3 strand, b8 strand and C-terminal residues 155-165 are all important in the interaction of aB crystallin with substrate proteins. However, aB crystallin ability (or lack of) to bind and chaperone unfolding client proteins does not necessarily correlate with the ability to bind assembled IFs and prevent filament-filament interactions. The interaction of aB crystallin with a denaturing, unfolding single client protein may be very different to the interaction with a fully assembled, unstressed filament polymer. In addition, pin-array assays do not consider the assembly status of filaments, a potentially crucial factor in interaction of aB crystallin with filaments. In pin arrays, the binding of the aB crystallin peptides to desmin reduces with increasing temperature (Ghosh et al., 2007b). However, the binding of the aB crystallin to desmin filaments (as measured by low speed co-sedimentation) increases with increasing temperature (Perng et al., 2004). Therefore, it is important to investigate these potential client protein interactive sequences in aB crystallin to determine the involvement in the interaction of aB crystallin with fully assembled desmin filaments.

In this chapter I show, using the 5 previously characterised aB crystallin mutants (aAb3, CEb3, aAb8, CEb8 and d155 aB), that altering the b3 strand, b8 strand and C-terminal sequences 155-165 in aB crystallin can significantly alter the interaction of aB crystallin with desmin filaments. I use TEM and sedimentation assays to characterise and quantify the mutant aB crystallin interactions with desmin filaments *in vitro*.

METHODS

The 5 aB crystallin mutants (aAb3, CEb3, aAb8, CEb8 and d155) were expressed and purified to >95% homogeneity (Fig 7.3) by Scott Houck at Professor John Clark's lab at the University of Washington USA and shipped to the Durham laboratories. Each protein was then quantified using BCA and the UV absorbance at 280nm.

To assess the effect of the aB crystallin mutations on interaction with desmin filaments, recombinant human desmin was expressed in *E. coli*, extracted from the water insoluble fraction and purified to homogeneity (>95%) in denaturing conditions via anion then cation exchange chromatography (Fig 7.4). Purified desmin was then mixed with WT or mutant aB crystallin and unfolded in 6M Urea buffer. Samples were and then dialysed to reduce the Urea concentration to 4M, then 2M, then 0M over a period of 24h at 22°C. Samples were then dialysed into Tris-HCl pH 7.4, 50mM NaCl buffer at either 22, 37 or 44°C for 16h to finalise filament assembly.

To quantify the interactions between desmin and the aB crystallin mutants, two separate centrifugation assays were used (Nicholl and Quinlan, 1994; Perng et al., 2004). The assays were originally developed by Bennardini et al in 1992. Samples were centrifuged at either 80,000g for 30min (high speed assay) or 2,500g for 15min (low speed assay). The pellets and supernatants were separated and solubilised in equal final volumes of SDS-PAGE sample buffer to allow direct comparison of the proportions of material in the supernatant and pellet. Results were then visualised via SDS-PAGE and quantified by gel densitometry.

For the high speed assay, the pellet (P) contains individual desmin filaments and any aggregates formed as a result of filament-filament interactions. Any aB crystallin that associates with these filaments or their aggregates will also be co-sedimented. The supernatant (S) contains soluble aB crystallin and also any or unassembled desmin or assembly intermediates. Therefore this assay measures filament assembly and aB crystallin binding to assembled filaments or aggregates.

For the low speed assay, individual desmin filaments are not pelleted, only those filaments which self associate into aggregates are pelleted. If aB crystallin binds to these aggregates,

then it too is co-sedimented. Unlike the high speed assay, it is only the aggregate associated aB crystallin which pellets rather than the aB crystallin associated with individual filaments. The supernatant (S) contains free desmin filaments, their associated aB crystallin, desmin assembly intermediates and the unassociated aB crystallin oligomers. Therefore, this assay measures filament-filament interaction and the ability of aB crystallin to prevent these filament-filament interactions.

To assess the effect of the aB crystallin mutants upon desmin filament morphology, filaments assembled in the presence of the mutant aB crystallins were analysed by TEM. Samples were prepared essentially using the Valentine method (Valentine et al., 1968).

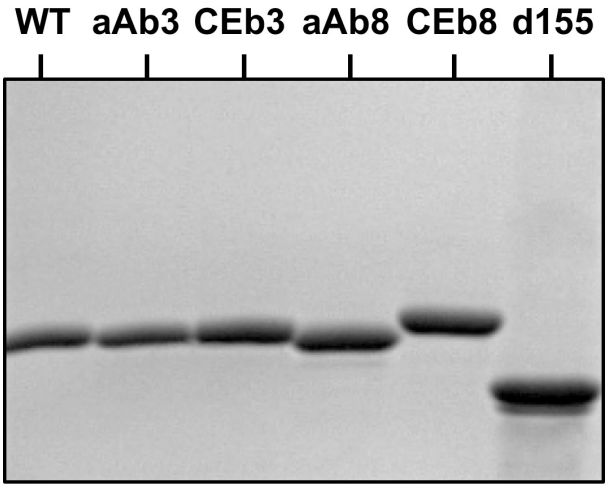

Fig 7.3. Purified WT and mutant aB crystallin proteins.

The 5 aB crystallin mutants (aAb3, CEb3, aAb8, CEb8 and d155) were expressed and purified to >95% homogeneity by Scott Houck at Professor John Clark's lab at the University of Washington USA and shipped to the Durham laboratories. Once in Durham, each protein was then quantified using BCA and the UV absorbance at 280nm. The WT desmin was purified by myself at the Durham laboratories (Fig 7.4).

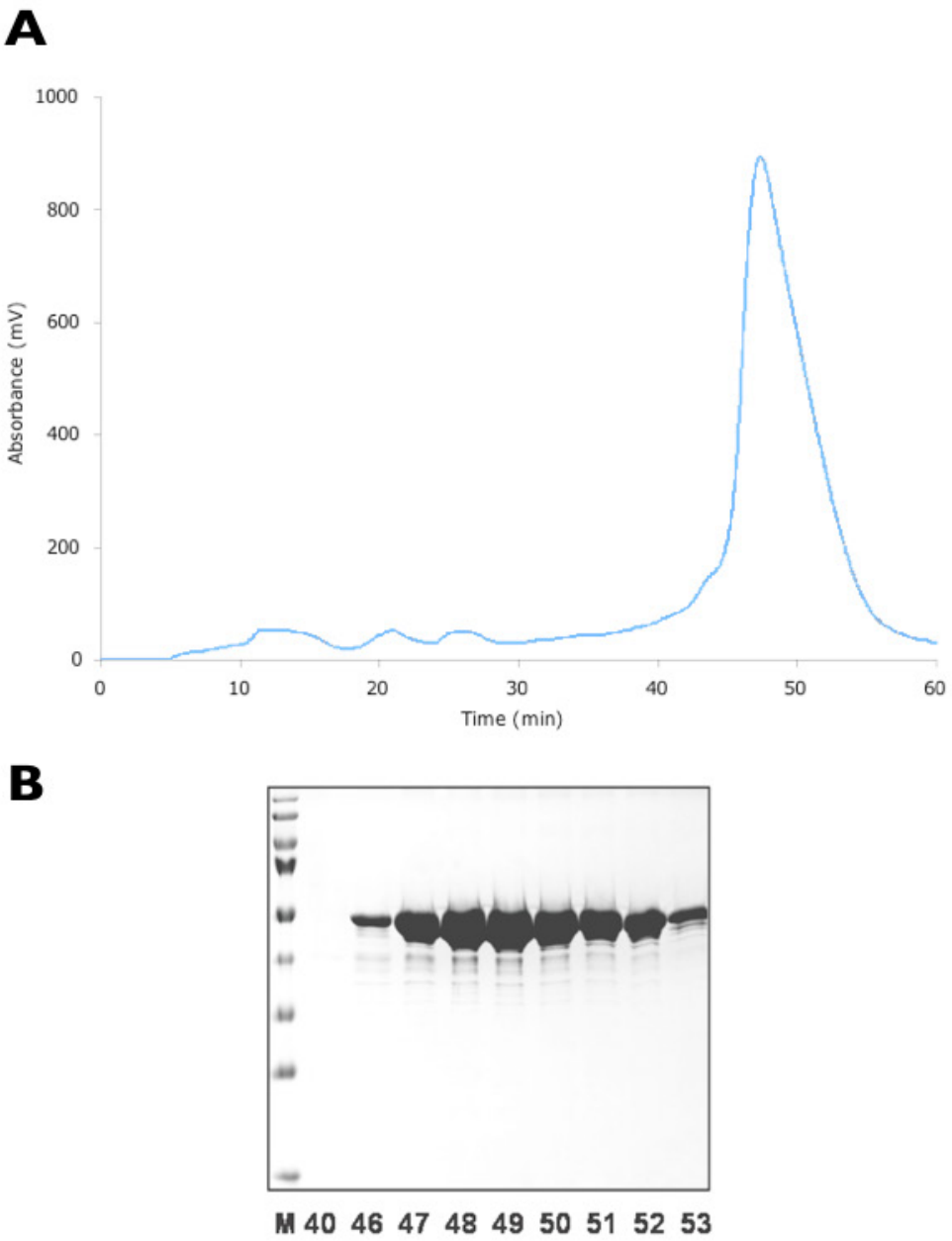

Fig 7.4. Cation exchange purification of recombinant human desmin.

Human WT desmin was purified by anion (data not shown) then cation exchange chromatography. The cation exchange chromatography elution profile (A) and corresponding SDS-PAGE gel (B) are shown. Desmin was applied at 1ml/min in 8M Urea, 20mM sodium formate pH 4, 1mM EDTA, 1mM DTT, 0.2mM PMSF and eluted with a linear gradient of 0-1M NaCl. Eluted material was collected as 1ml fractions and analysed on a 12% SDS-PAGE gel. Each gel lane is labelled with the corresponding chromatogram timescale. The desmin enriched fractions show a high level of homogeneity (>95%).

RESULTS

Effect of the aB crystallin mutations on oligomer solubility and morphology

To assess the effect of the aB crystallin mutations on aB crystallin oligomer solubility, the low and high speed sedimentation properties of WT and mutant aB crystallins at 22, 37 and 44°C were analysed by SDS-PAGE. Fig 7.5 represents 1 of 3 experimental repeats, which were quantified via gel densitometry, collated and averaged (Fig 7.6).

Results show that aAb3, CEb3, aAb8 and CEb8 aB crystallin mutants have solubility comparable to WT aB crystallin at all three temperatures. The mutant aB crystallins do not self aggregate and <15% pellets, even at high speed at 44°C (Fig 7.6). For d155 aB crystallin, solubility is comparable to WT aB at 22 and 37°C at both low and high speed. In contrast, at 44°C d155 aB self aggregates and ~30% pellets at low speed (Fig 7.6, dark blue bar). This ~3 fold increase in pelleting for d155 aB at 44°C compared with WT aB and the other 4 mutants demonstrates reduced solubility and an increased tendency to self aggregate. However, this effect is clearly temperature dependent.

To assess oligomer morphology, the mutant aB crystallins were then analysed via TEM after negative staining with uranyl acetate (Fig 7.7). All aB crystallins appear as polydisperse individual oligomers at 22, 37 and 44°C. For d155 aB at 44°C, the TEM image shows that the mutant is clearly capable of forming individual non-aggregated oligomers, despite its increased tendency to aggregate (Fig 7.6).

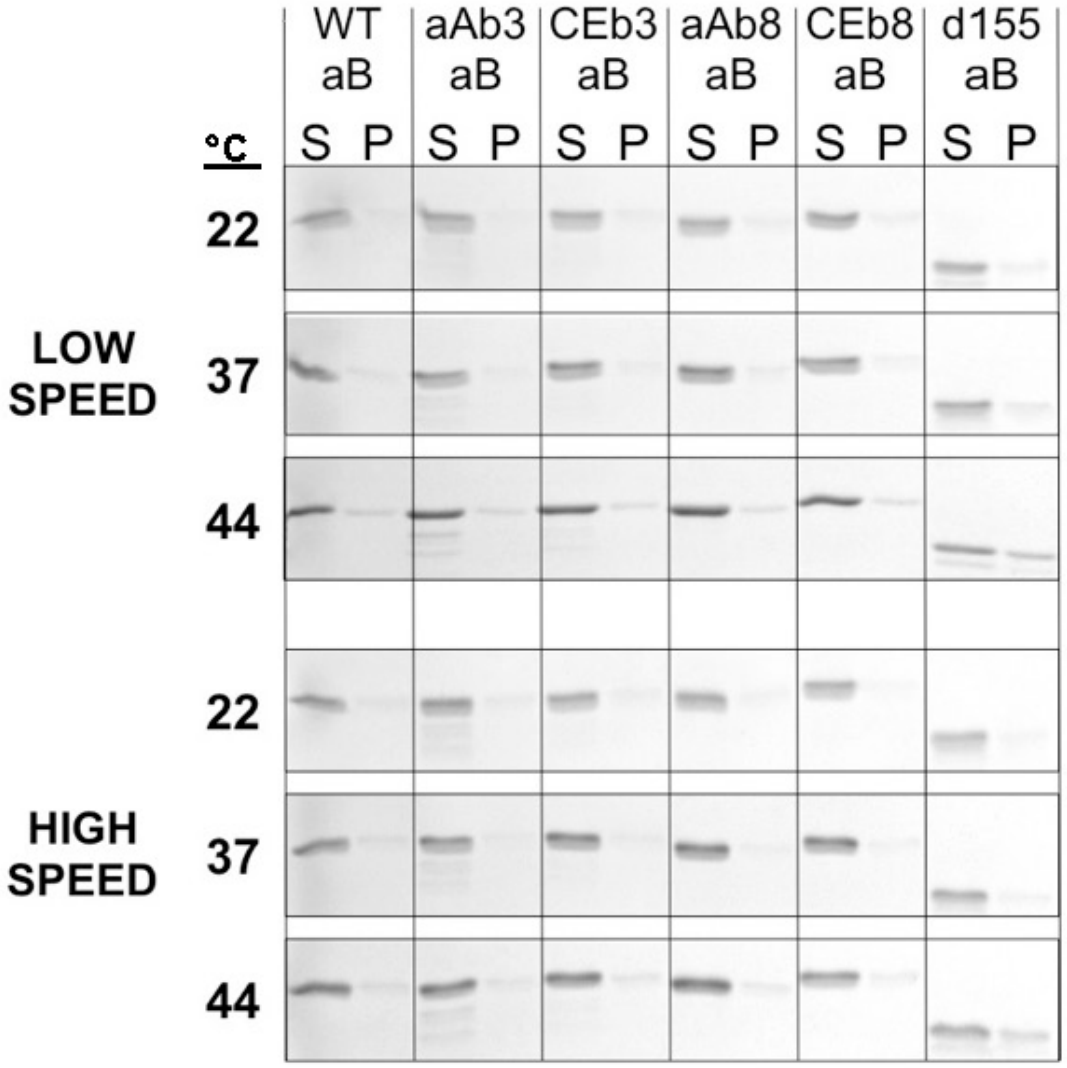

Fig 7.5. Sedimentation properties of WT and mutant aB crystallins.

The low and high speed sedimentation properties of each individual aB crystallin protein at 22, 37 and 44°C analysed by SDS-PAGE. For all the aB crystallins except d155 aB, <15% pellets at both low and high speed at all 3 temperatures. d155 aB crystallin shows a small increase in self aggregation at 44°C (30% pellets). The above gels represent 1 of 3 repeats. Supernatant (S) and pellet (P).

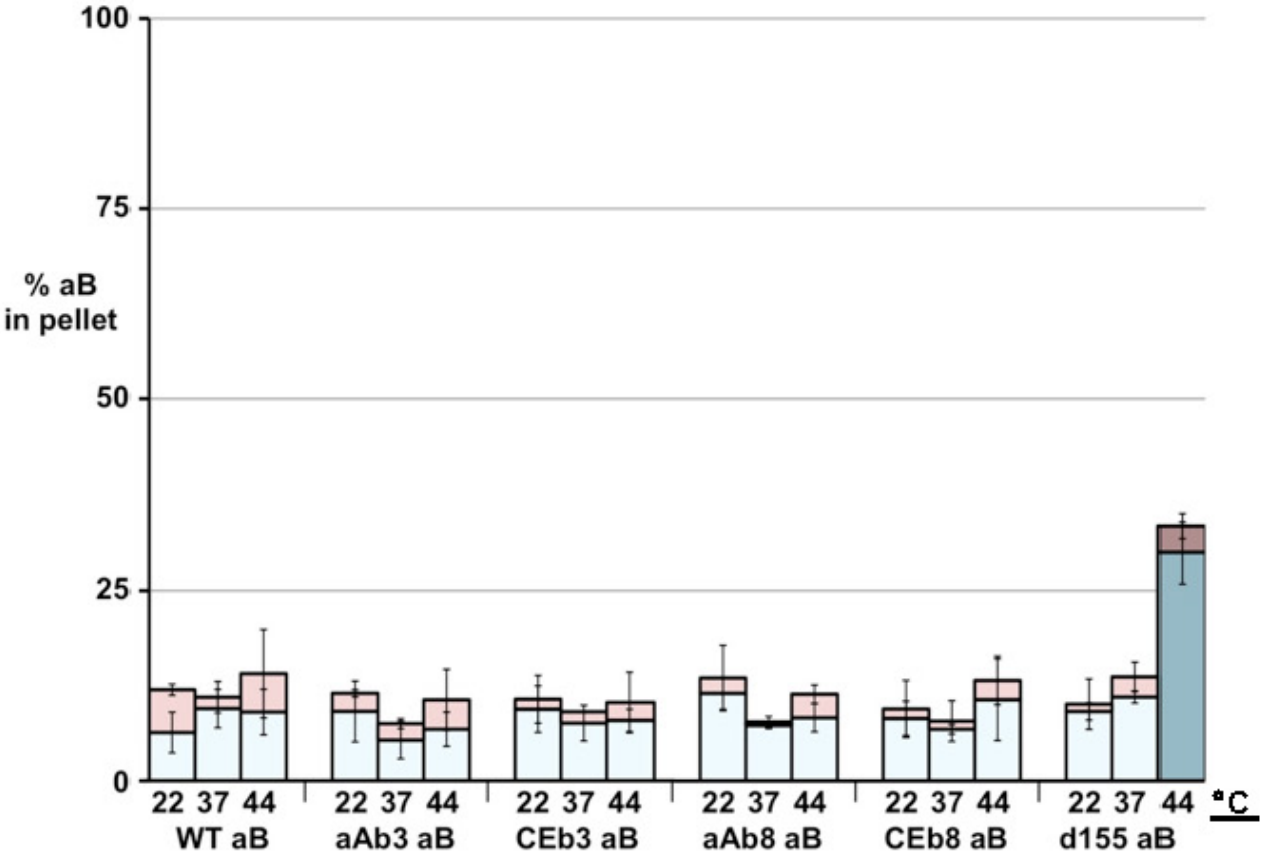

Fig 7.6. Quantification of sedimentation properties of WT and mutant aB crystallins.

Graph of the low speed (blue) and high speed (red) sedimentation data for the aB crystallins as quantified by gel densitometry. The percentage of aB crystallin in the pellet fractions at 22, 37 and 44°C was determined after both low and high speed sedimentation to quantify the self aggregation of the aB crystallins. All mutants showed similar sedimentation properties to the WT aB crystallin, except d155 aB crystallin at 44°C, which showed increased aggregation at both low (darker blue) and high speed (darker red). Average values and standard deviations were calculated from 3 or 4 experimental repeats.

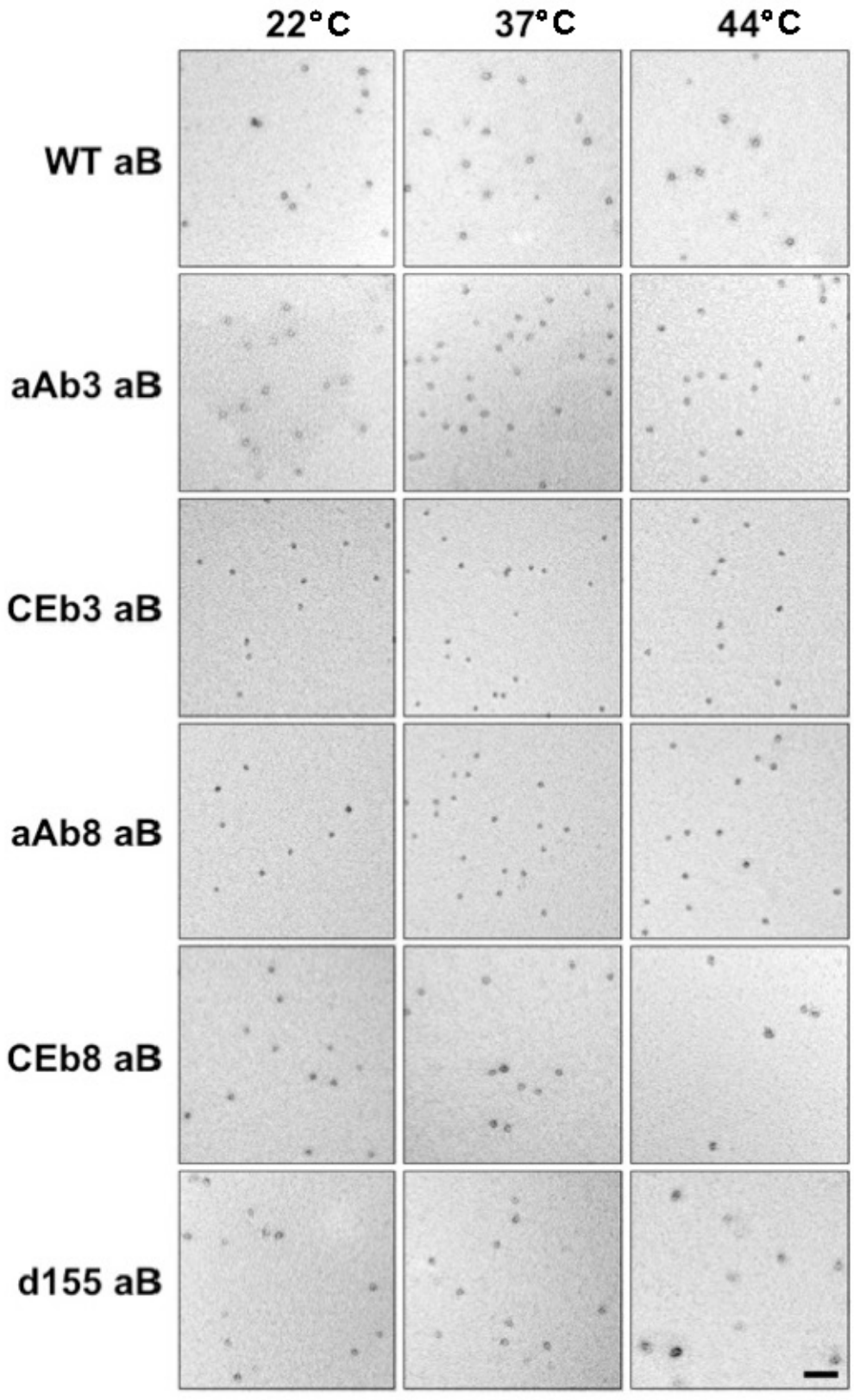

Fig 7.7. TEM characterisation of WT and mutant aB crystallins.

All aB crystallins appear as individual oligomers at 22, 37 and 44°C. Scale bar = 100nm.

Sedimentation properties and TEM characterisation of desmin filaments

To assess the solubility of desmin filaments in the absence of aB crystallin, the low (2,500g) and high (80,000g) speed sedimentation properties of desmin assembled at 22, 37 and 44°C were analysed by SDS-PAGE. Fig 7.8, A represents 1 of 3 experimental repeats, which were quantified via gel densitometry, collated and averaged (Fig 7.8, B).

At high speed, >90% of desmin pellets at all 3 temperatures (Fig 7.8, B, red bars), indicating successful assembly into filaments. At low speed, desmin shifts from 24% to 45% to 61% pelleted as the temperature increases from 22 to 37 to 44°C respectively (Fig 7.8, B, blue bars). This demonstrates that as temperature increases, filament-filament interactions increase, leading to filament self aggregation.

To assess morphology, the desmin filaments were then analysed by TEM (Fig 7.8, C). The desmin appears as long, smooth, constant width 10nm filaments at all 3 temperatures. There is no visible difference between the filaments at 22, 37 or 44°C despite an increasing tendency for the filaments to self aggregate with increasing temperature (Fig 7.8, B, blue bars).

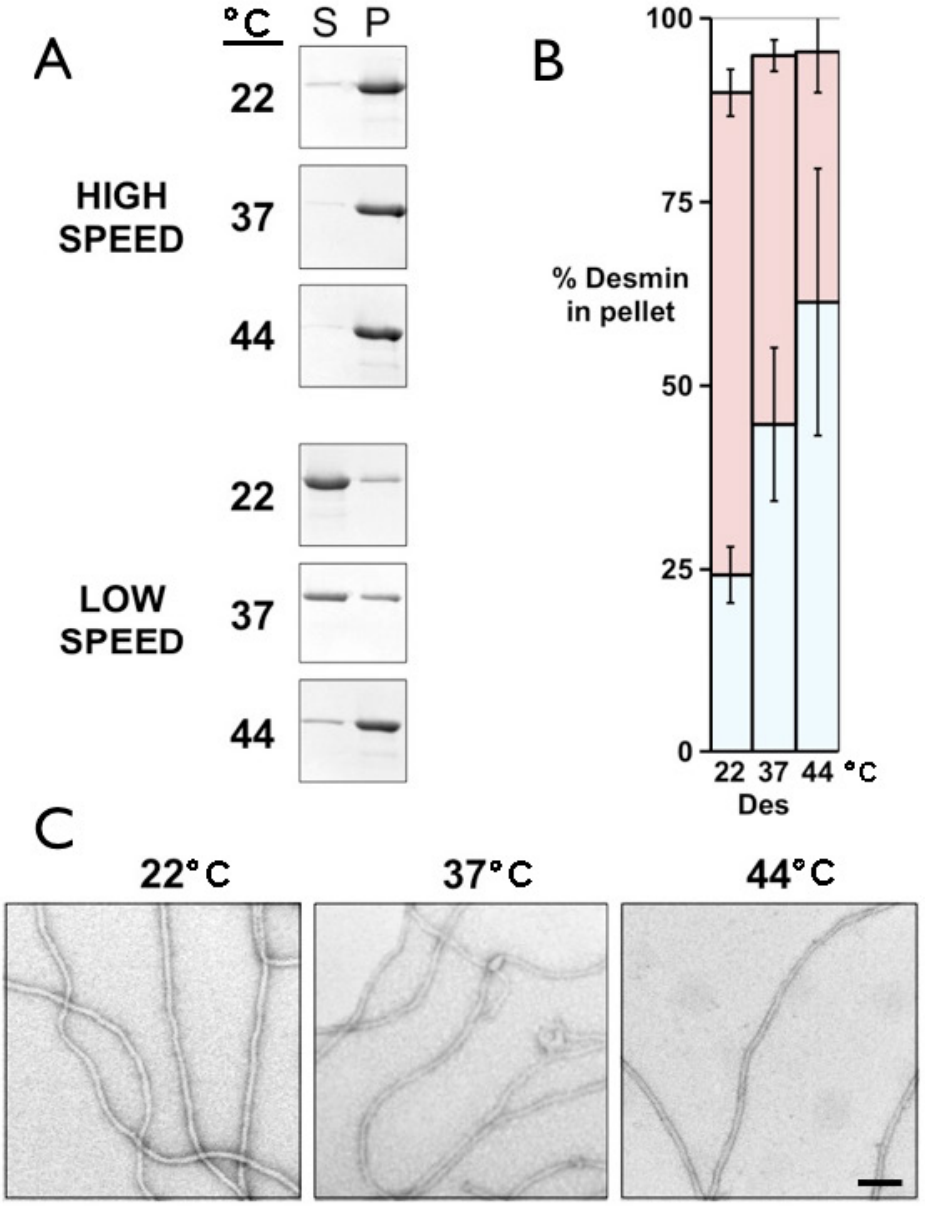

Fig 7.8. Sedimentation properties and TEM characterisation of desmin filaments.

(A) The low (2,500g) and high (80,000g) speed sedimentation properties of desmin assembled at 22, 37 and 44°C analysed by SDS-PAGE. At high speed, >90% of desmin pellets at all 3 temperatures. At low speed, desmin shifts from 24% to 45% to 61% pelleted as the temperature increases from 22 to 37 to 44°C respectively. (B) Bar chart of the low speed (blue) and high speed (red) sedimentation data for desmin as quantified by gel densitometry. Average values and standard deviations were calculated from 3 or 4 experimental repeats. (C) Morphology of desmin filaments analysed by TEM. The desmin appears as long, smooth, constant width 10nm filaments at all 3 temperatures. Scale bar represents 100nm.

High speed co-sedimentation properties of desmin and WT or mutant aB crystallins

To quantify the interaction of the aB crystallin mutants with desmin filaments, the high speed (80,000g) co-sedimentation properties of desmin assembled at 22, 37 and 44°C in the presence of WT or mutant aB crystallin were analysed by SDS-PAGE. Fig 7.9 represents 1 of 4 experimental repeats, which were quantified via gel densitometry, collated and averaged (Fig 7.10, red bars).

Note: In Fig 7.10, the % of desmin pelleted in both the high speed and low speed (see later) centrifugation assays are presented on the same bar. The values from the low speed assay are represented by the lower, blue portions of each bar while the values from the high speed assay are represented by the whole bar (i.e. top of the red portion). This allows comparison of the high and low speed sedimentation assays for each combination of aB crystallin mutant and desmin, which facilitates the analysis of results.

The high speed sedimentation results show that >90% of desmin pellets at all 3 temperatures when co-assembled with WT aB or any of the 5 mutants (Fig 7.9 and Fig 7.10, red bars). This indicates that the aB crystallin mutants do not inhibit desmin assembly as <10% of desmin remains unassembled, which is comparable with desmin assembled alone (Fig 7.8, B, red bars).

In addition to measuring desmin assembly, this high speed co-sedimentation assay also measures the binding of aB crystallin to the desmin filaments as any bound aB crystallin is pelleted. WT, aAb3, CEb3 and aAb8 aB crystallins remain soluble and <25% pellets at all 3 temperatures (Fig 7.9). In contrast, CEb8 and d155 aB crystallins show increased pelleting at all 3 temperatures relative to WT aB crystallin and are >95% pelleted at 44°C (Fig 7.9, bottom panel).

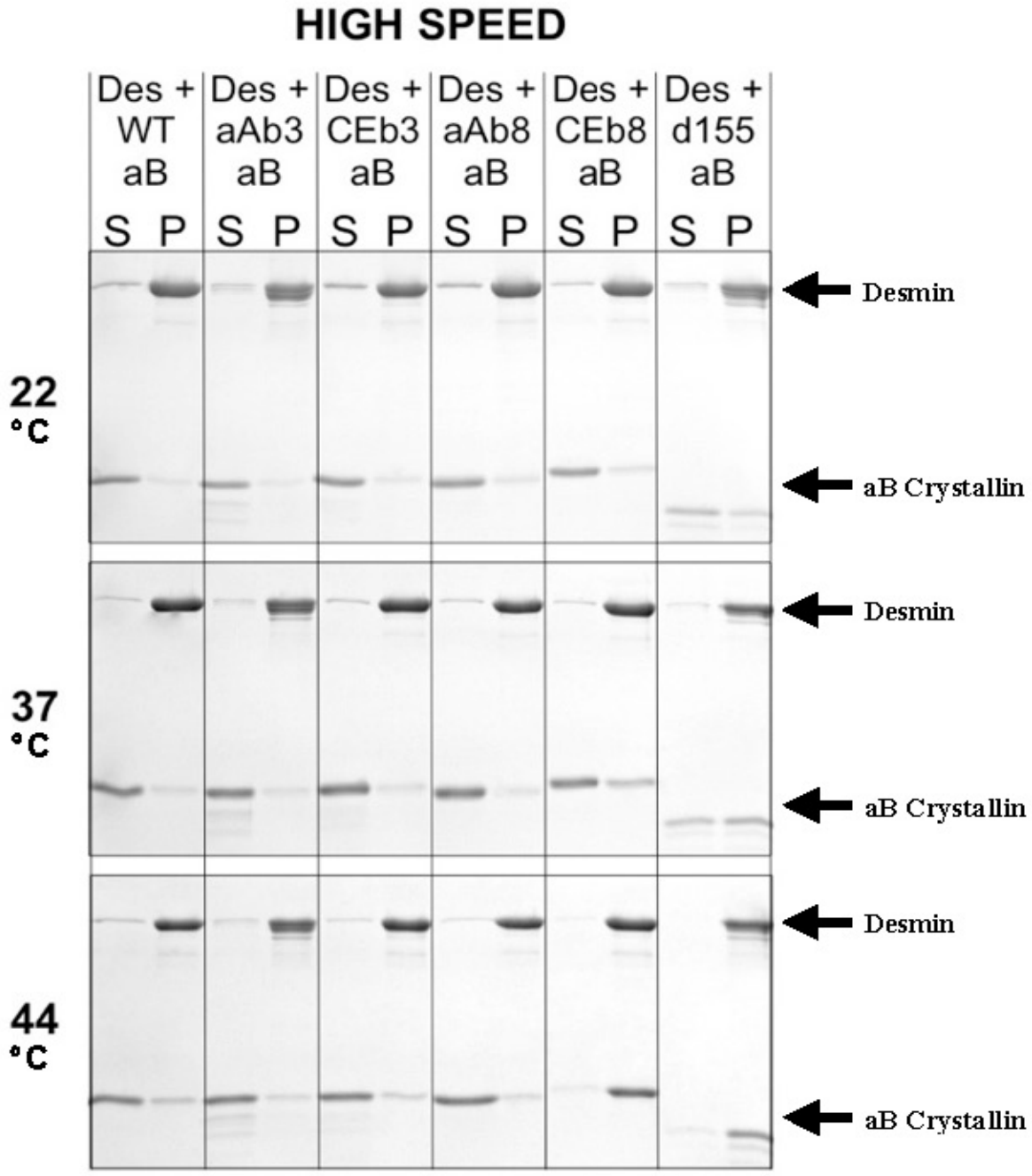

Fig 7.9. High speed co-sedimentation of desmin with WT or mutant aB crystallins.

High speed (80,000g) co-sedimentation of desmin and aB crystallin assembled at 22, 37 and 44°C analysed by SDS-PAGE. >90% of desmin pellets at all 3 temperatures when co-assembled with WT aB crystallin or any of the 5 mutants. WT, aAb3, CEb3 and aAb8 aB crystallins remain soluble and <25% pellets at all 3 temperatures. CEb8 and d155 aB crystallins show increased pelleting at all 3 temperatures relative to WT aB crystallin and are >95% pelleted at 44°C. The above gels represent 1 of 3 repeats. Supernatant (S) & pellet (P).

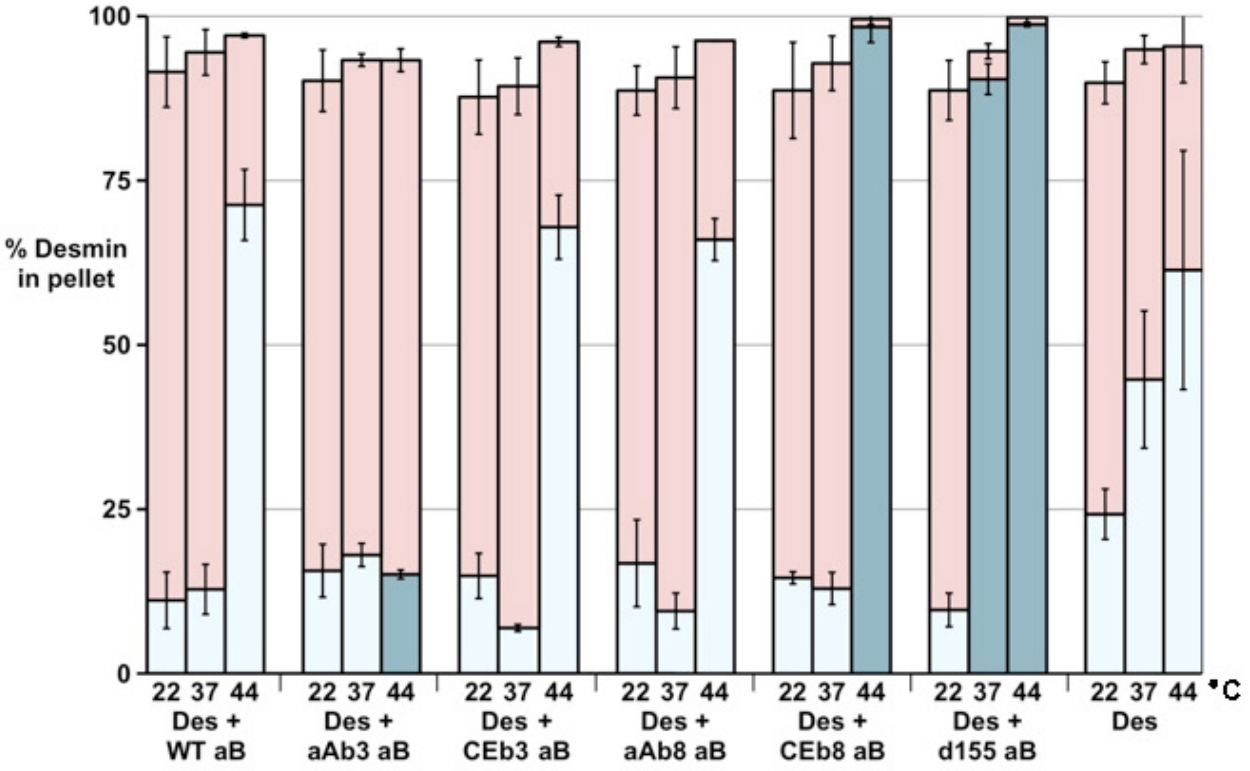

Fig 7.10. Quantification of desmin co-sedimentation with WT or mutant aB crystallins.

Bar chart of the low speed (light and dark blue) and high speed (red) pelleting of desmin when co-assembled with WT or mutant aB crystallin at 22, 37 and 44°C. At high speed, >90% of desmin pellets at all 3 temperatures when assembled alone, or when co-assembled with WT aB or any of the 5 mutants. At low speed at 44°C, aAb3 aB crystallin significantly reduces desmin pelleting (dark blue bar) relative to WT aB. Conversely, at low speed at 44°C, both the CEb8 and d155 aB crystallins significantly increase desmin pelleting (dark blue bars). d155 aB also significantly increases desmin pelleting at 37°C. The amount of material pelleted is shown as a percentage of total material as quantified by gel densitometry. Average values and standard deviations were calculated from 3 or 4 experimental repeats.

In order to quantify the extent of aB crystallin binding to desmin filaments, the amount of aB crystallin pelleting in the presence (Fig 7.9) and absence (Fig 7.5) of desmin was compared. This comparison is shown in Fig 7.11 which illustrates the increased pelleting of aB crystallin in the presence of desmin (Fig 7.11, red bars) compared with aB crystallin alone (Fig 7.11, blue bars). In the presence of desmin, WT aB crystallin shows no significant increase in pelleting at 22°C, but shows slightly increased pelleting at 37 and 44°C. This demonstrates that binding of WT aB crystallin to the desmin filaments is temperature dependent. CEb8 and d155 aB crystallins show significantly increased pelleting in the presence of desmin at all 3 temperatures relative to WT aB crystallin (Fig 7.11, red bars). This shows that aB crystallin filament binding has increased significantly for CEb8 and d155 aB and that this effect is temperature dependent. Conversely, pelleting of aAb3 is not affected by the presence of desmin at any of the 3 temperatures, indicating a complete lack of 'detectable' binding (Fig 7.11, red bars).

Overall, the high speed sedimentation results show that desmin assembly is not inhibited by WT aB crystallin or any of the 5 mutants. Filament binding of CEb3 and aAb8 aB crystallin is comparable with WT aB crystallin and is only detectable at 37 and 44°C. However, filament binding is significantly increased for CEb8 and d155 aB crystallins relative to WT aB crystallin. In contrast, no filament binding could be detected at any temperature for aAb3 aB crystallin.

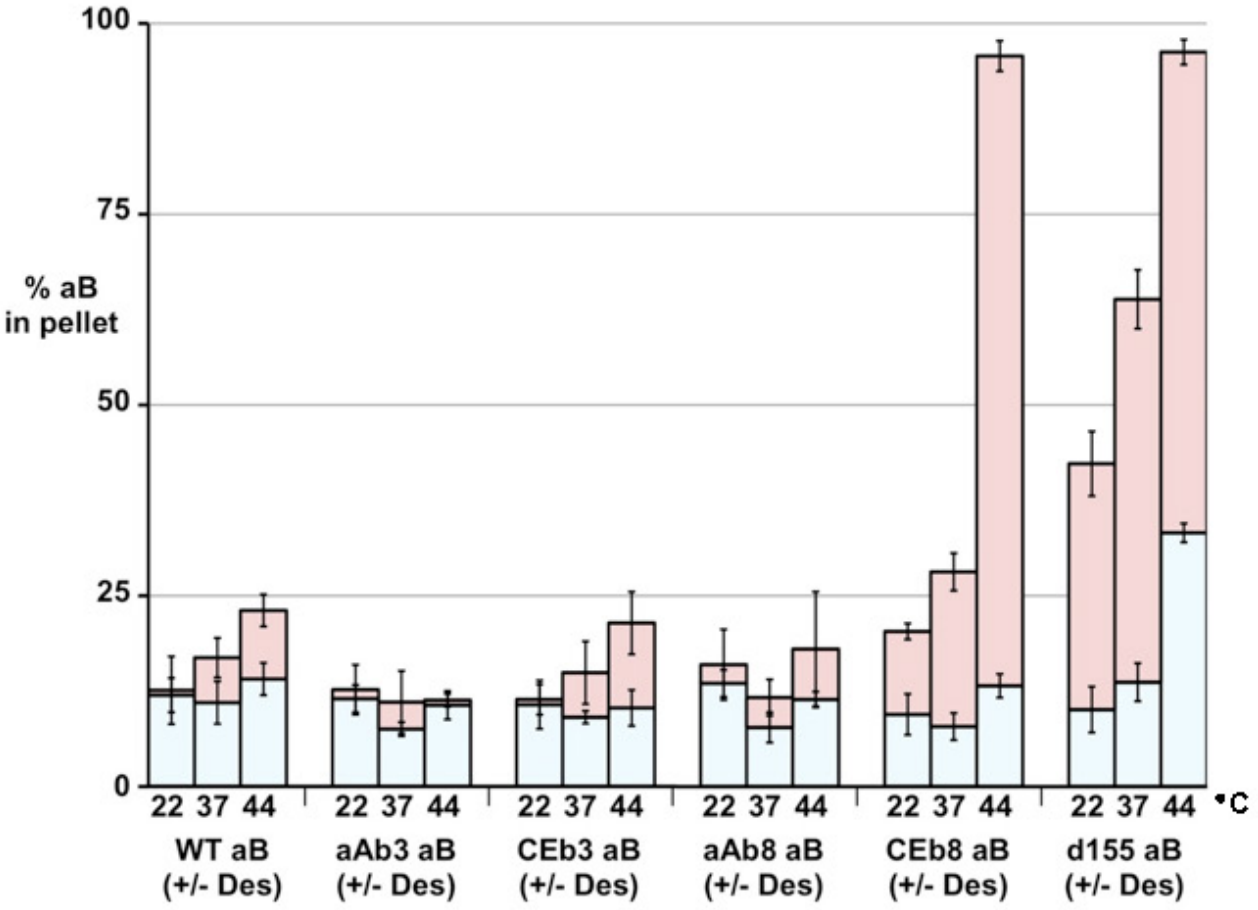

Fig 7.11. Comparison of WT or mutant aB crystallin sedimentation in the absence and presence of desmin.

Bar chart of the high speed pelleting of aB crystallin in the absence (blue) and presence (red) of desmin at 22, 37 and 44°C. The difference between the blue and red bars represents the increase in aB crystallin pelleting as a result of the presence of desmin. WT, CEb3 and aAb8 aB crystallins show slightly increased pelleting in the presence of desmin at 37 and 44°C. CEb8 and d155 aB crystallins show significantly increased pelleting in the presence of desmin at all 3 temperatures relative to WT aB crystallin. Conversely, pelleting of aAb3 is not affected by the presence of desmin at any of the 3 temperatures. The amount of material pelleted is shown as a percentage of total material as quantified by gel densitometry. Average values and standard deviations were calculated from 3 or 4 experimental repeats.

Low speed co-sedimentation properties of desmin and WT or mutant aB crystallins

To quantify further the interaction of the aB crystallin mutants with desmin filaments, the low speed (2,500g) co-sedimentation properties of desmin assembled at 22, 37 and 44°C in the presence of WT or mutant aB crystallin were analysed by SDS-PAGE. Fig 7.12 represents 1 of 4 experimental repeats, which were all quantified by gel densitometry, collated and averaged to generate the blue bars of the bar chart previously shown (Fig 7.10, blue bars).

At 22°C, <17% of desmin pellets when assembled with WT aB crystallin or any of the 5 mutants (Fig 7.12, top panel) compared with 24% of desmin pelleting alone (Fig 7.8, B). At low speed, only those filaments which self associate into aggregates are pelleted, hence at 22°C, WT aB crystallin and all 5 mutants are capable of reducing desmin filament-filament interactions which reduces desmin pelleting (Fig 7.10, 22°C, blue bars). This reduced desmin pelleting is not due to aB crystallin inhibiting desmin assembly as the high speed assay pelleted the same portion of assembled desmin both with and without aB crystallin (Fig 7.10, red bars).

At 37°C, <18% of desmin pellets when assembled with WT, aAb3, CEb3, aAb8 or CEb8 aB crystallin indicating significantly reduced filament-filament interactions compared with desmin assembled alone (Fig 7.10, 37°C, blue bars). In contrast, d155 aB crystallin causes 90% of desmin to pellet at 37°C, indicating that d155 aB crystallin promotes filament-filament interactions and causes aggregation (Fig 7.10, 37°C, dark blue bar).

At 44°C, >60% of desmin pellets when assembled with WT, CEb3 or aAb8 aB crystallins, which is comparable to desmin alone (Fig 7.10, 44°C, blue bars), indicating no effect on filament-filament interactions at 44°C. In contrast, both CEb8 and d155 aB crystallin cause >98% of desmin to pellet at 44°C, indicating promotion of filament-filament interactions leading to aggregation (Fig 7.10, 44°C, dark blue bars). Conversely, only 15% of desmin pellets when assembled with aAb3 aB crystallin at 44°C, indicating a significant reduction in filament-filament interactions which prevents aggregation. This represents ~5 fold reduction in filament aggregation compared with desmin alone or in the presence of WT aB crystallin (Fig 7.10, aAb8, 44°C, dark blue bar).

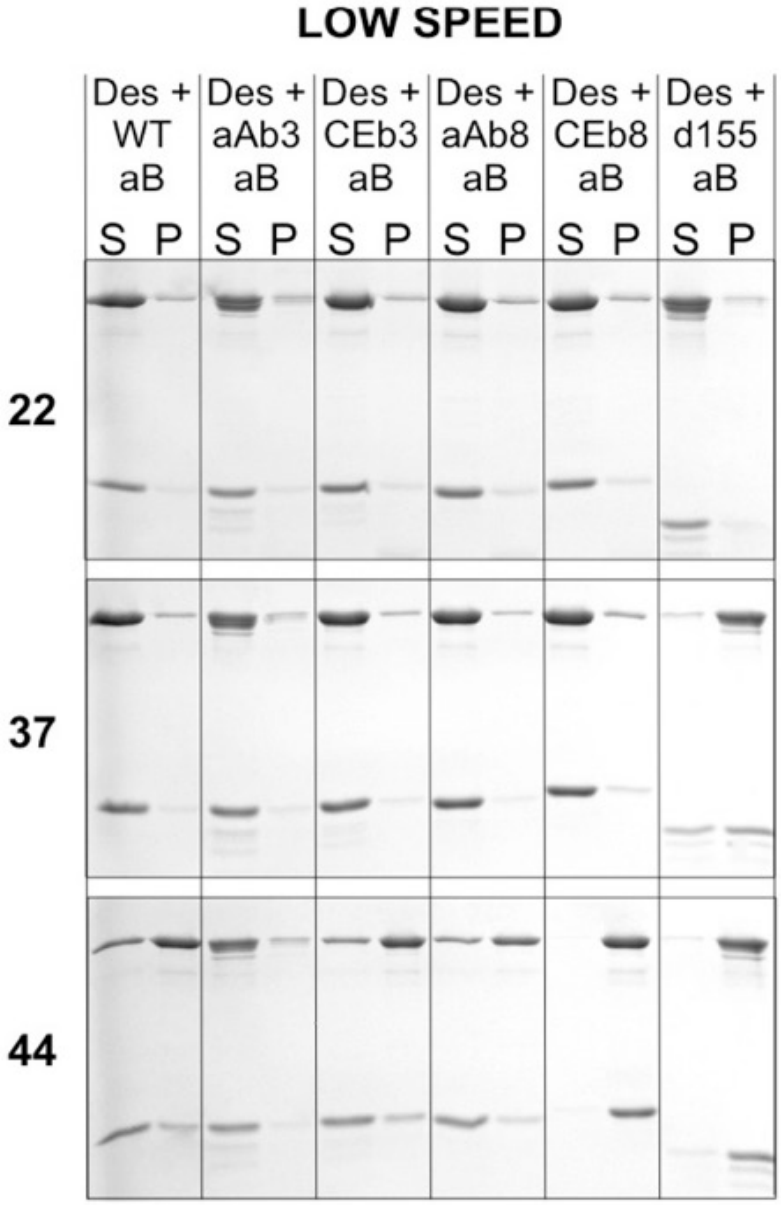

Fig 7.12. Low speed co-sedimentation of desmin and WT or mutant aB crystallins.

Low speed (2,500g) co-sedimentation of desmin and aB crystallin assembled at 22, 37 and 44°C analysed by SDS-PAGE. At 22 and 37°C, <20% of desmin pellets when assembled with WT aB crystallin or any of the mutants, except d155 which causes 90% of desmin to pellet at 37°C. At 44°C, >60% of desmin pellets when assembled with WT, CEb3 or aAb8 aB crystallins, but only 15% pellets when assembled with aAb3 aB crystallin. When assembled at 44°C in the presence of CEb8 or d155 aB crystallin, >98% of desmin pellets. WT, aAb3, CEb3 and aAb8 aB crystallins pellet <25% at all 3 temperatures. CEb8 and d155 aB crystallins show increased pelleting (>90%) relative to WT aB crystallin at 44°C. The gels represent 1 of 3 repeats. Supernatant (S) and pellet (P).

In addition to measuring filament-filament interactions, this low speed co-sedimentation assay also measures the binding of aB crystallin to any desmin filament aggregates, as any bound aB crystallin is also pelleted (Fig 7.12). The quantification of this data is shown in Fig 7.13 using blue bars. WT, aAb3, CEb3 and aAb8 aB crystallins remain soluble with <22% pelleting at all 3 temperatures (Fig 7.13, blue bars). In contrast, CEb8 and d155 aB crystallins are >95% pelleted at 44°C (Fig 7.13, dark blue bars). This shows that at 44°C, CEb8 and d155 aB crystallin not only cause desmin to aggregate, but also bind completely to these aggregates. d155 aB crystallin also shows binding to desmin aggregates at 37°C (Fig 7.13, 37°C, dark blue bar). In contrast, aAb3 aB crystallin shows a complete lack of 'detectable' binding to desmin aggregates, even at 44°C (Fig 7.13, 44°C, dark blue bar).

Overall, the low speed sedimentation results show that WT, aAb3, CEb3 and aAb8 aB crystallins are all able to reduce filament-filament interactions and therefore prevent aggregation at 22 and 37°C, but only aAb8 aB crystallin is able to reduce filament-filament interactions at 44°C. Conversely, while CEb8 and d155 aB crystallin reduce filament-filament interactions and aggregation at 22°C, at 44°C both mutants promote filament-filament interactions and cause aggregation and these aggregates contain bound aB crystallin.

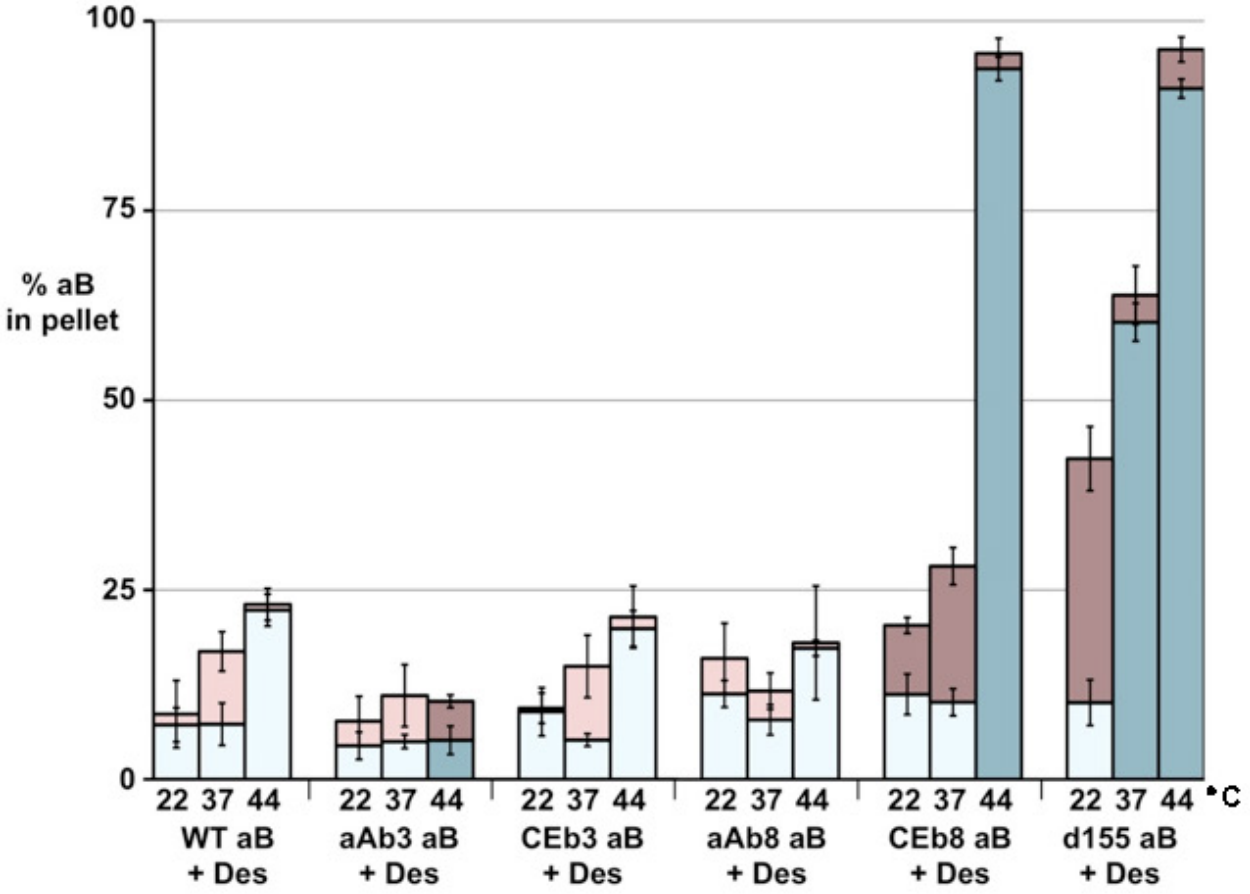

Fig 7.13. Quantification of WT or mutant aB crystallin co-sedimentation with desmin.

Bar chart of the low speed (light and dark blue) and high speed (light and dark red) pelleting of WT or mutant aB crystallin when co-assembled with desmin at 22, 37 and 44°C. At high speed, CEb8 and d155 aB crystallins show increased pelleting at all 3 temperatures (dark red bars) relative to WT aB crystallin and are >95% pelleted at 44°C. Conversely, at 44°C at both high and low speed, aAb3 aB crystallin shows reduced pelleting (<10%, dark blue and dark red bars) relative to WT aB crystallin. The amount of material pelleted is shown as a percentage of total material as quantified by gel densitometry. Average values and standard deviations were calculated from 3 or 4 experimental repeats.

Morphology of desmin filaments in the presence and absence of WT aB crystallin

To analyse the effect of WT aB crystallin on desmin filament morphology, desmin was assembled at 22, 37 or 44°C in the presence and absence of aB crystallin and samples were analysed by TEM. When assembled alone, WT aB crystallin forms oligomers at all 3 temperatures (Fig 7.14, top row). Desmin forms smooth, constant width 10nm filaments at all 3 temperatures when assembled alone (Fig 7.14, middle row). When desmin is co-assembled with WT aB crystallin, both the filaments and aB crystallin oligomers appear morphologically identical to those assembled alone (Fig 7.14, bottom row). The desmin filaments formed in both the presence and absence of aB crystallin are smooth and long (<2000nm) (Fig 7.15). However, while some aB crystallin oligomers remain unassociated (Fig 7.14, black arrows), some oligomers bind to the filament surface (Fig 7.14, black triangles). aB crystallin association with the filament surface can be clearly seen at all 3 temperatures (Fig 7.14, bottom row, black triangles). aB crystallin filament binding is clearly visible at 22°C, despite a complete lack of 'detectable' binding, as analysed by the low speed assay (Fig 7.11, red bar). These TEM results are visual confirmation that WT aB crystallin interacts with normal desmin filaments in the apparent absence of stress (Fig 7.14).

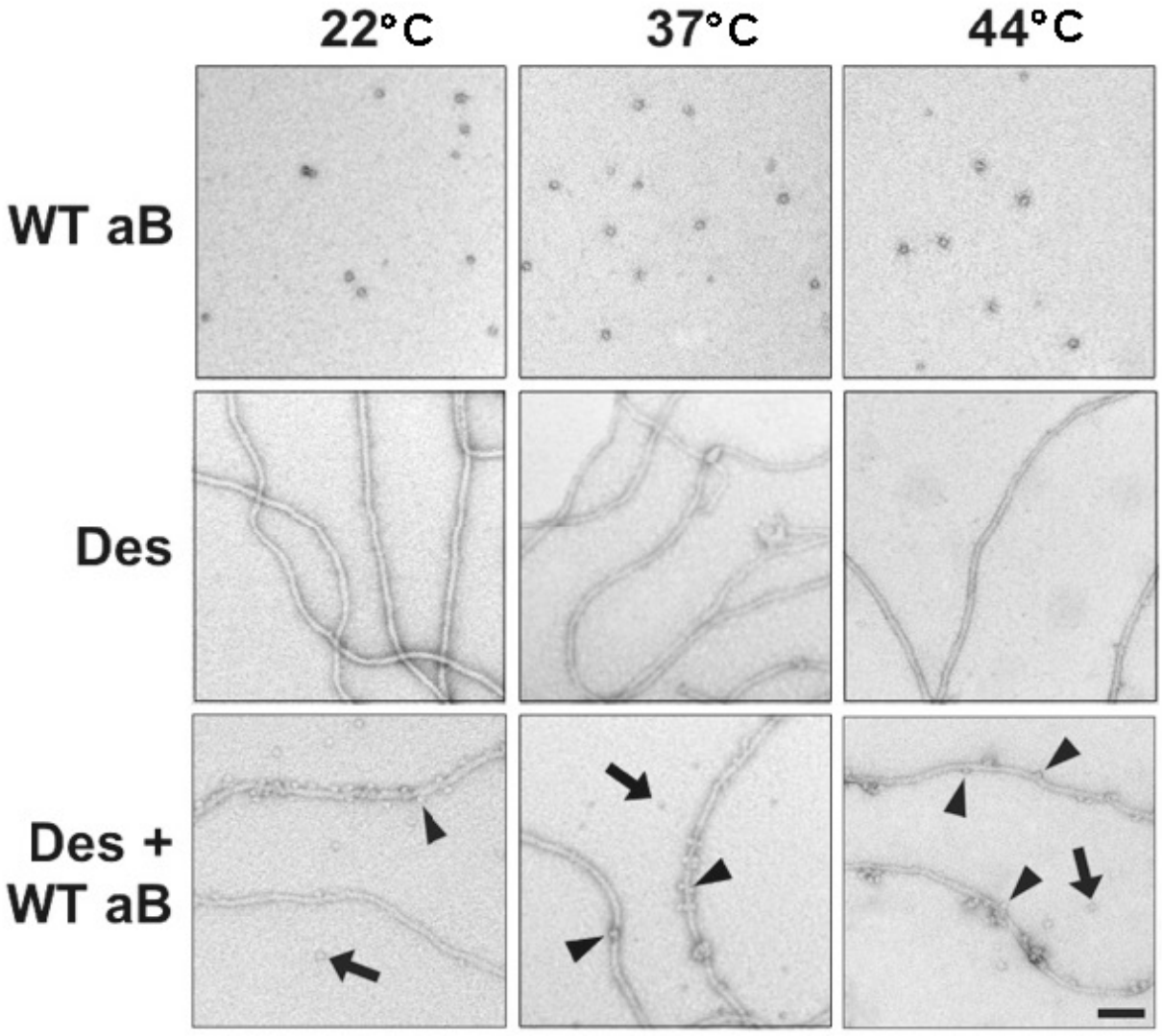

Fig 7.14. TEM analysis of desmin filaments and WT aB crystallin.

The morphology of the desmin filaments and WT aB assembled at 22, 37 or 44°C analysed by TEM. WT aB crystallin forms oligomers at all 3 temperatures. Desmin, when assembled alone or in the presence of WT aB crystallin, forms smooth, constant width 10nm filaments at all 3 temperatures. When desmin is assembled with WT aB crystallin, some aB crystallin oligomers associate with the filaments (black triangles) while some remained unassociated (black arrows). Scale bar represents 100nm.

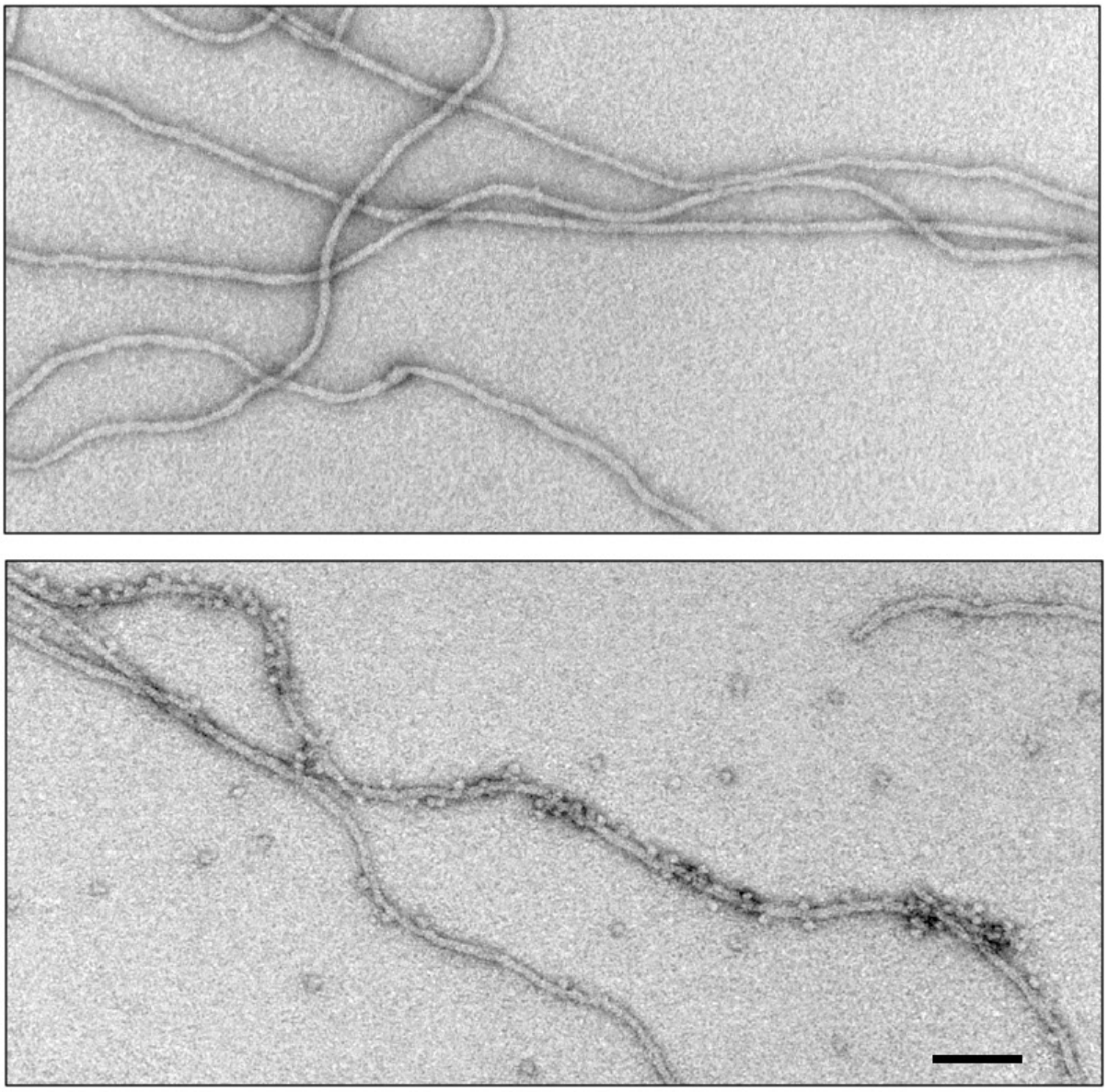

Fig 7.15. TEM analysis of desmin filaments in the presence and absence of WT aB crystallin at 22°C.

The micrographs show a small section of desmin filaments over 2000nm in length. The top pannel is desmin alone and the bottom panel is desmin with WT aB crystallin. These micrographs demonstrate the long filaments formed and are also visual confirmation that WT aB crystallin interacts with normal desmin filaments in the apparent absence of stress. aB crystallin can clearly be seen both binding to the filament surface, and unbound. Scale bar represents 100nm.

Morphology of desmin filaments in the presence of mutant aB crystallins

To analyse the effect of the aB crystallin mutants on desmin filament morphology, desmin was assembled at 22, 37 or 44°C in the presence and absence of the aB crystallins and samples were analysed by TEM. When assembled in the presence of aAb3 aB crystallin at 22, 37 or 44°C, desmin appears to form long, smooth, ~10nm filaments (Fig 7.16). At 44°C, despite aAb3 aB crystallin reducing filament-filament interactions 5 fold relative to WT aB crystallin (Fig 7.10), the filaments appear indistinguishable from those formed in the presence of WT aB crystallin (Fig 7.16). Although aAb3 aB crystallin can be seen binding to the surface of the filaments at all 3 temperatures (Fig 7.16, left column, black triangles), the amount of bound aAb3 aB crystallin appears significantly less than WT aB crystallin. This supports the high speed sedimentation data which did not detect any significant binding of aAb3 aB crystallin to the desmin filaments (Fig 7.11), even at 44°C.

When assembled in the presence of CEb3 or aAb8 aB at 22, 37 or 44°C, desmin also appears to form long, constant width 10nm filaments (Fig 7.17). Some aB crystallin oligomers associate with the filaments (black triangles) while some remained unassociated (black arrows). At all 3 temperatures, the filaments are seemingly indistinguishable from those formed in the presence of WT aB crystallin (Fig 7.14).

When assembled in the presence of CEb8 aB crystallin at 22 or 37°C, desmin appears to form long, smooth, constant width 10nm filaments (Fig 7.18) similar to those formed in the presence of WT aB crystallin. Some CEb8 aB crystallin oligomers associate with the filaments (Fig 7.18, black triangles) while some remain unassociated (Fig 7.18, black arrows). However at 44°C, CEb8 aB crystallin has a dramatic effect on the desmin filament morphology (Fig 7.18, bottom left panel). These filaments appear to be less consistent in width and many filament ends are visible, potentially indicating reduced average filament length. These filaments also appear to have sharp kinks, in contrast to the gradual curves of desmin filaments formed in the presence of WT aB crystallin (Fig 7.14). Most strikingly, these filaments have associated into larger structures which contain bound CEb8 aB crystallin (Fig 7.18, black triangles). There are no individual filaments visible, which explains the almost complete (98%) sedimentation of these filaments under low speed centrifugation (Fig 7.10, dark blue bar). Interestingly, these effects of CEb8 aB crystallin are highly temperature dependent and are not seen at 22 or 37°C (Fig 7.18).

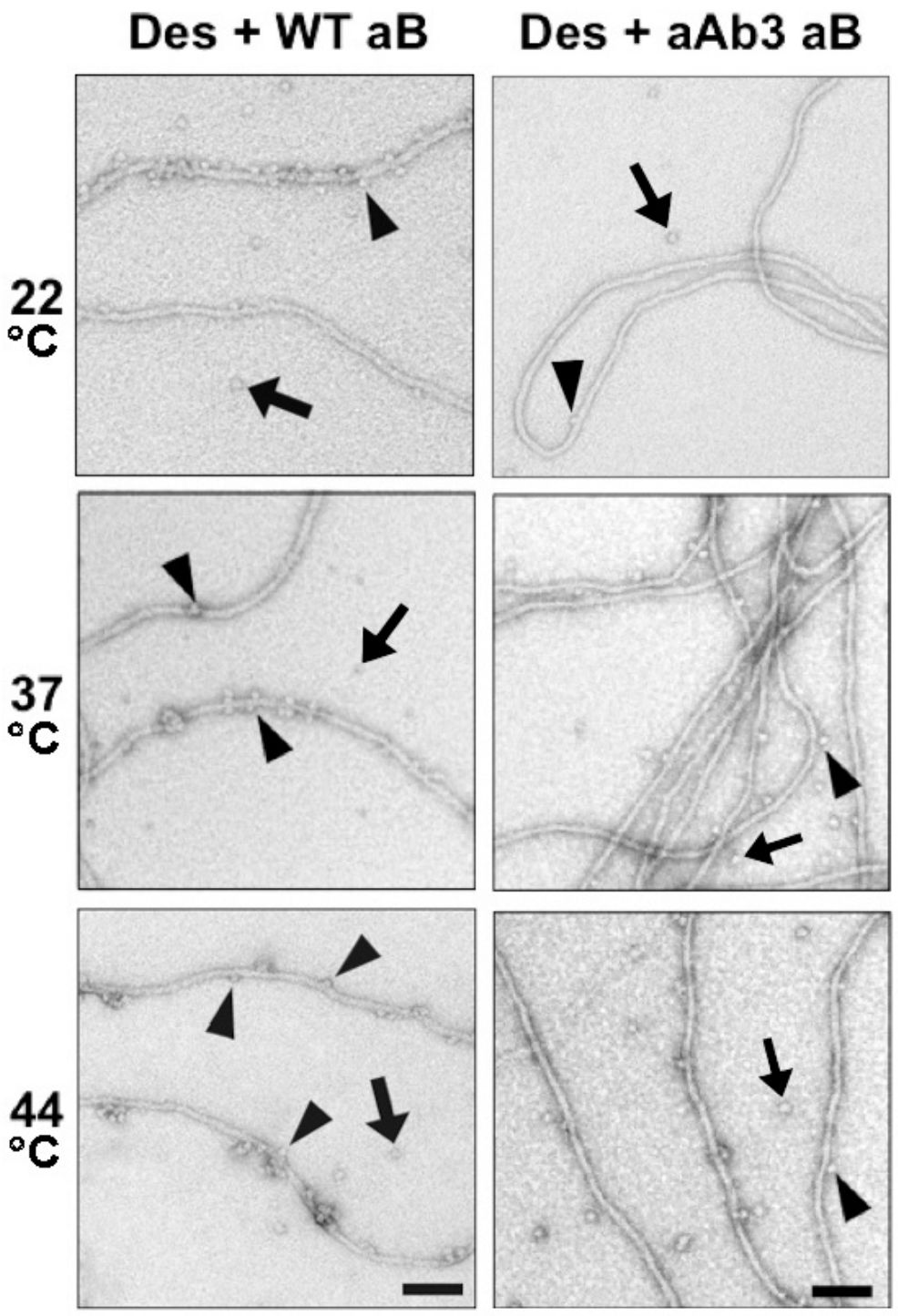

Fig 7.16. TEM comparison of desmin filaments assembled with WT or aAb3 aB crystallin.

Desmin forms long, smooth, constant width 10nm filaments when assembled with WT or aAb3 aB crystallins at 22, 37 or 44°C. Some aB crystallin oligomers associate with the filaments (black triangles) while some remained unassociated (black arrows). Scale bars represent 100nm.

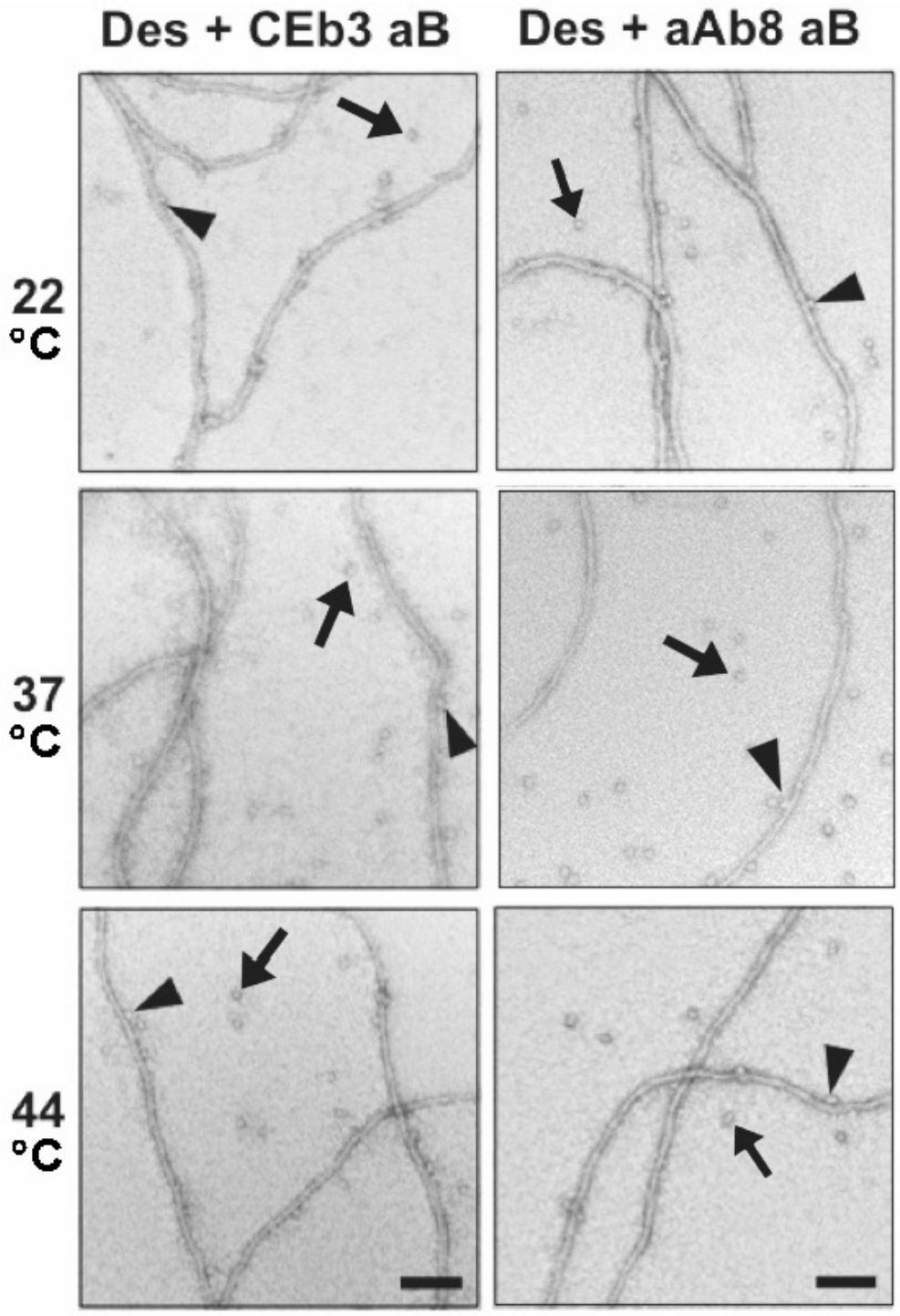

Fig 7.17. TEM comparison of desmin filaments assembled with CEb3 or aAb8 aB crystallin.

Desmin forms long, smooth, constant width 10nm filaments when assembled with CEb3 or aAb8 aB crystallins at 22, 37 or 44°C. Some aB crystallin oligomers associate with the filaments (black triangles) while some remained unassociated (black arrows). Scale bars represent 100nm.

When assembled in the presence of d155 aB at 22°C, desmin appears to form 10nm filaments (Fig 7.18, top right panel) similar to those formed in the presence of WT aB. Some d155 aB crystallin oligomers associate with the filaments (Fig 7.18, black triangle) while some remain unassociated (Fig 7.18, black arrow). However, at 37°C the d155 aB causes the desmin filaments to associate into larger structures which contain bound d155 aB crystallin (Fig 7.18, middle row, right panel, black triangles). Most filaments appear associated with the aggregate which explains the 90% sedimentation of these filaments under low speed centrifugation (Fig 7.10, dark blue bar). These effects become even more pronounced at 44°C as d155 aB appears to cause severe changes to filament morphology (Fig 7.18, bottom right panel). These filaments appear to have larger variations in width and many filament ends visible. All filaments appear associated with the aggregate, there are no individual filaments visible, which could explain the complete (99%) sedimentation of these filaments under low speed centrifugation (Fig 7.10, dark blue bar). There also appears to be no unbound d155 aB crystallin visible, which explains the 91% low speed co-sedimentation of aB with the aggregates (Fig 7.13).

Overall, TEM analysis shows that in the presence of aAb3, CEb3 and aAb8 aB crystallins, desmin appears to form normal 10nm filaments, comparable to those formed in the presence of WT aB crystallin. In contrast, CEb8 and d155 aB crystallins appear to increase desmin filament-filament interactions, but these effects are highly temperature dependent.

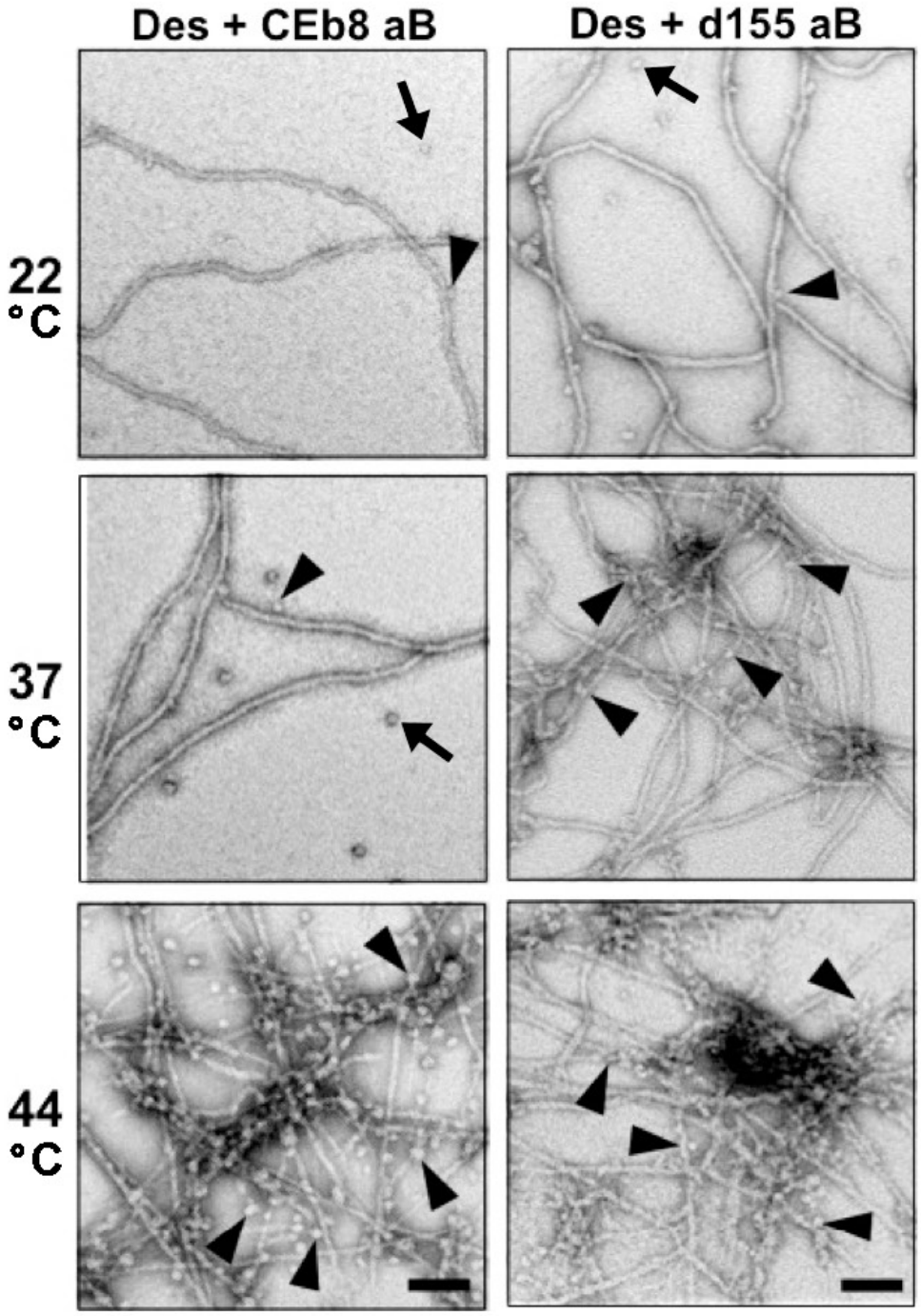

Fig 7.18. TEM comparison of desmin filaments assembled with CEb8 or d155 aB crystallin.

Desmin appears to form constant width 10nm filaments when assembled with CEb8 or d155 aB crystallins at 22°C. aB crystallin oligomers may associate with the filaments (black triangles) or remained unassociated (black arrows). However, at 44°C (and 37°C for d155 aB) the mutants cause filament aggregation along with seemingly increased aB crystallin oligomer association. Scale bars represent 100nm.

RESULTS SUMMARY

This data identifies, for the first time, sequences in aB crystallin that are important for interaction with desmin filaments. All 5 aB crystallin mutants assemble into individual oligomers which do not self aggregate (except d155 aB crystallin at 44°C) and do not inhibit desmin assembly. In the presence of WT, aAb3, CEb3 and aAb8 aB crystallins, desmin appears to form normal 10nm filaments (TEM data summarised in Fig 7.19). However, desmin filament binding is significantly increased for CEb8 and d155 aB crystallin at all 3 temperatures and at 44°C (and 37°C for d155 aB crystallin) both mutants promote filament-filament interactions and cause filament aggregation and these aggregates contain aB crystallin. Conversely, desmin filament binding, as detected by the high speed co-sedimentation assay, is significantly reduced for aAb3 aB crystallin at 44°C and this coincides with a significant reduction in desmin filament-filament interactions which prevents aggregation (sedimentation data summarised in Fig 7.20). Therefore, the ability to bind to desmin filaments does not necessarily correlate with the ability to prevent filament-filament interactions. Specifically, increased aB crystallin binding to desmin filaments, as detected by the high speed sedimentation assay, is not correlated with increased prevention of filament-filament interactions. Nevertheless, it is clear that b3 strand, b8 strand and c-terminal residues 155-165 in aB crystallin all play an important role in the interaction between aB crystallin and desmin filaments.

Fig 7.19. Summary of TEM analysis of desmin filaments assembled with WT or mutant crystallins.

Desmin forms long, smooth, constant width 10nm filaments when assembled with WT, aAb3, CEb3 and aAb8 aB crystallins at 22, 37 or 44°C. However at 44°C (and 37°C for d155 aB) CEb8 and d155 aB crystallins appear to cause a dramatic change in desmin filament morphology along with increased aB crystallin oligomer association which results in aggregation (red boxes). Some aB crystallin oligomers associate with the filaments (black triangles) while some remained unassociated (black arrows). Scale bars represent 100nm.

(Figure on next page)

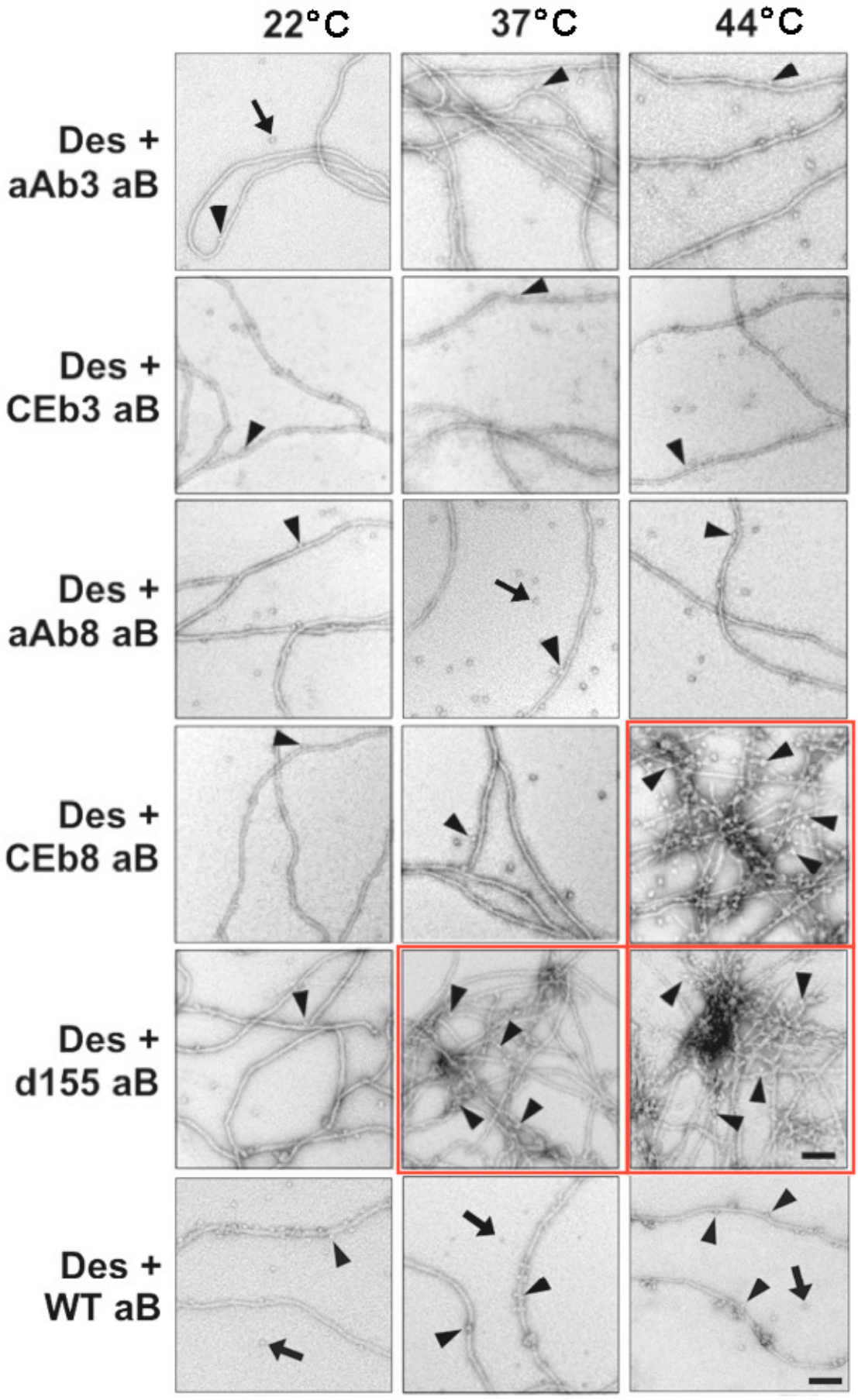

Fig 7.19 (Legend on previous page)

	LOW SPEED						HIGH SPEED					
	22°C		37°C		44°C		22°C		37°C		44°C	
	Ave % in Pellet	SD	Ave % in Pellet	SD	Ave % in Pellet	SD	Ave % in Pellet	SD	Ave % in Pellet	SD	Ave % in Pellet	SD
WT aB	6	3	10	3	9	3	12	1	11	2	14	6
aAb3 aB	9	4	5	2	7	2	12	0	8	1	11	4
CEb3 aB	9	3	8	2	8	1	11	3	9	0	10	4
aAb8 aB	12	2	7	0	8	2	14	4	8	1	11	1
CEb8 aB	8	2	7	1	11	5	9	4	8	3	13	3
del155 aB	9	1	11	1	30	4	10	3	14	2	33	2
Des	24	4	45	10	61	18	90	3	95	2	95	6
Des (+ WT aB)	11	4	13	4	71	5	92	5	94	3	97	0
Des (+ aAb3 aB)	16	4	18	2	15	1	90	5	93	1	93	2
Des (+ CEb3 aB)	15	3	7	1	68	5	88	6	89	4	96	1
Des (+ aAb8 aB)	17	7	10	3	66	3	89	4	91	5	96	0
Des (+ CEb8 aB)	15	1	13	2	98	2	89	7	93	4	100	1
Des (+ del155 aB)	10	3	90	2	99	0	89	5	95	1	100	1
WT aB (+ Des)	7	2	7	3	22	2	9	4	17	3	23	2
aAb3 aB (+ Des)	4	2	5	1	5	2	8	3	11	4	10	1
CEb3 aB (+ Des)	9	3	5	1	20	2	9	2	15	4	21	4
aAb8 aB (+ Des)	11	2	8	2	17	1	16	5	12	2	18	8
CEb8 aB (+ Des)	11	3	10	2	94	2	20	1	28	2	96	2
del155 aB (+ Des)	10	3	60	2	91	1	42	4	64	4	96	2

Fig 7.20. Summary of desmin and aB crystallin sedimentation characteristics.

Summary of high (80,000g) and low (2,500g) speed sedimentation characteristics of desmin and WT and mutant aB crystallins at 22, 37 and 44°C. The top section shows pelleting % values for WT and mutant aB crystallins and desmin when assembled alone. The middle section shows pelleting % values for desmin when co-assembled with WT or mutant aB crystallins. The bottom section shows pelleting % values for WT or mutant aB crystallin when co-assembled with desmin. Values significantly higher (red) or lower (blue) relative to WT aB crystallin values are highlighted. Average (Ave) values and standard deviations (SD) were calculated from 3 or 4 experimental repeats. Producing the data in this table required 58 SDS-PAGE gels and >1000 band quantifications.

CHAPTER 8: DOMAINS IN DESMIN IMPORTANT FOR INTERACTION WITH aB CRYSTALLIN

AIM

To investigate the importance of the desmin tail domain to filament morphology and the interaction with aB crystallin.

INTRODUCTION

The effect of disease causing aB crystallin mutations on the interaction with desmin filaments, and the subsequent aggregation leading to desmin related myopathy (DRM) has been well studied (Bova et al., 1999; Inagaki et al., 2006; Perng et al., 1999b; Perng et al., 2004; Reilich et al., 2010; Selcen and Engel, 2003; Treweek et al., 2005; Vicart et al., 1998). However, the effect of disease causing desmin mutations on the interaction with aB crystallin, has not yet been analysed.

To date, 53 disease causing desmin mutations have been identified, 12 of which are desminopathy causing point mutations in the tail domain (Goldfarb and Dalakas, 2009; Van Spaendonck-Zwarts et al., 2010). In contrast to the head domain, the tail domain of desmin is not essential for filament assembly (Geisler et al., 1982; Kaufmann et al., 1985). Previous investigations into 6 of these disease causing tail mutants (T442I, K449T, I451M, R454W, S460I and V469M) found that all but the R454W can assemble into filaments and all six mutants can integrate into the IF cytoskeleton *in vivo* (Bar et al., 2007). However, although most desminopathy causing tail mutants can assemble into filaments and associate into networks, these filaments associate into aggregates in patients (Bar et al., 2007).

It has been proposed that, although not essential for assembly, the tail domain of desmin is important for modulating interaction with aB crystallin and that mutations in the desmin tail domain may alter this interaction and cause filament aggregation (Sharma, 2011). To investigate this and identify which regions in the tail domain are important for sHsp interaction, Sharma, 2011 generated tail truncated desmin mutants of residues 1-409 (dTail des), 1-431 (d431 des) and 1-441 (d441 des). Another tail mutant was also generated to delete only the highly conserved 454-RDG-456 residues (RDG des). The sequence locations of these truncations and deletion are shown in Fig 8.1.

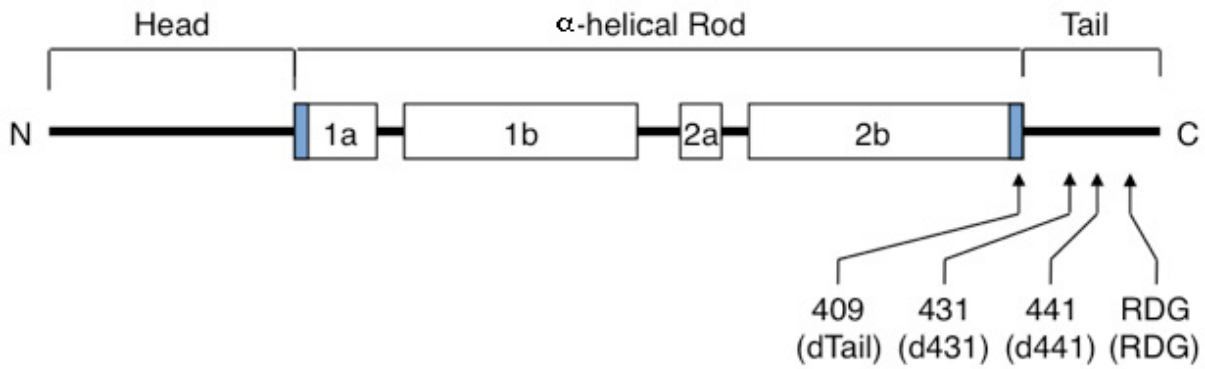

Fig 8.1. Diagram showing desmin secondary structure and location of tail mutations.

Diagram showing locations of desmin tail truncations to create mutants of residues 1-409 (dTail des), 1-431 (d431 des) and 1-441 (d441 des). Also shown is the location of the RDG motif, which was deleted to create RDG desmin. Desmin is composed of α-helical coiled coil domains flanked by a non-helical N- and C-termini head and tail. The boxes represent α-helical domains which are separated by the non-helical linkers. The blue boxes at the ends of helix 1a and 2b represent the highly conserved LNDR and YRKLLEGE motifs respectively which are important for the assembly of IF proteins into filaments.

Sharma, 2011 analysed the interaction of aB crystallin with the mutant desmin filaments *in vitro* using co-sedimentation, TEM and viscometry assays. TEM analysis confirmed that all 4 deletion mutants can form filaments *in vitro*. Sedimentation assays showed that binding of aB crystallin to RDG desmin was comparable with binding to WT desmin, but no aB crystallin binding was observed for d431, d441 or dTail desmin.

In addition, aB crystallin was able to significantly reduce WT desmin filament-filament interactions, but unable to prevent dTail filament-filament interactions, as determined by viscometry assays (Sharma, 2011). These data suggest that dTail desmin filaments are unable to interact with aB crystallin, which may lead to filament aggregation. However, it is known that aB crystallin interaction with IFs is highly dependent upon temperature and filament status (Perng et al., 2004). In addition, analytical ultra centrifugation showed co-sedimentation of aB crystallin with dTail desmin, indicating an interaction (Sharma, 2011).

Therefore, it is important to further investigate the role of the desmin tail domain in the interaction of aB crystallin with fully assembled desmin filaments. In this chapter I show, using 4 desmin mutants (d431, d441, RDG and dTail), that mutations in the desmin tail domain can significantly change filament morphology, filament-filament interactions and the interaction with aB crystallin. I use TEM and sedimentation assays to characterise the mutant desmin filaments and their interactions *in vitro*.

METHODS

The 4 desmin mutants (d431, d441, RDG and dTail Des) were expressed and purified to >95% homogeneity (Fig 8.2) by Sarika Sharma from Dr Harald Herrman's lab at the University of Heidelberg, Germany and shipped to the Durham laboratories. Each protein was then quantified using BCA and the UV absorbance at 280nm.

For assembly, the desmin mutants were mixed with aB crystallin and unfolded in 6M Urea buffer. Samples were then dialysed to reduce the Urea concentration to 4M, then 2M, then 0M over a period of 24h at 22°C. Samples were then dialysed into Tris-HCl pH 7.6, 50mM NaCl buffer at either 22, 37 or 44°C for 16h to finalise filament assembly. In contrast to the previous chapter, which finalises the assembly of the desmin filaments at pH 7.4, this chapter uses pH 7.6. This change was made to allow comparison with work already performed on these 4 desmin mutants by Sarika Sharma at the University of Heidelberg, Germany.

To quantify the interactions between the desmin mutant filaments and aB crystallin, two separate centrifugation assays were used. Samples were centrifuged at either 80,000g for 30min (high speed assay) or 2,500g for 15min (low speed assay). The pellets and supernatants were separated and solubilised in equal final volumes of SDS-PAGE sample buffer to allow direct comparison of the proportions of material in the supernatant and pellet. Results were then visualised via SDS-PAGE and quantified by gel densitometry.

For the high speed assay, the pellet (P) contains individual desmin filaments and any aggregates formed as a result of filament-filament interactions. Any aB crystallin that associates with these filaments or their aggregates will also be co-sedimented. The supernatant (S) contains soluble aB crystallin and also any or unassembled desmin or assembly intermediates. Therefore this assay measures filament assembly and aB crystallin binding to assembled filaments or aggregates.

For the low speed assay, individual desmin filaments are not pelleted, only those filaments which self associate into aggregates are pelleted. If aB crystallin binds to these aggregates, then it too is co-sedimented. Unlike the high speed assay, it is only the aggregate associated aB crystallin which pellets rather than the aB crystallin associated with individual filaments.

The supernatant (S) contains free desmin filaments, their associated aB crystallin, desmin assembly intermediates and the unassociated aB crystallin oligomers. Therefore, this assay measures filament-filament interaction and the ability of aB crystallin to prevent these filament-filament interactions.

To assess the effect of the desmin mutations upon filament morphology, filaments were assembled in the presence and absence of aB crystallin and analysed by TEM. Samples were prepared essentially using the Valentine method (Valentine et al., 1968). TEM images were also analysed to measure filament width. 50 measurements were made using three different images to give a total of 150 width measurements for each sample. Measurements were made at 100nm intervals along the length of the filaments in randomly selected areas.

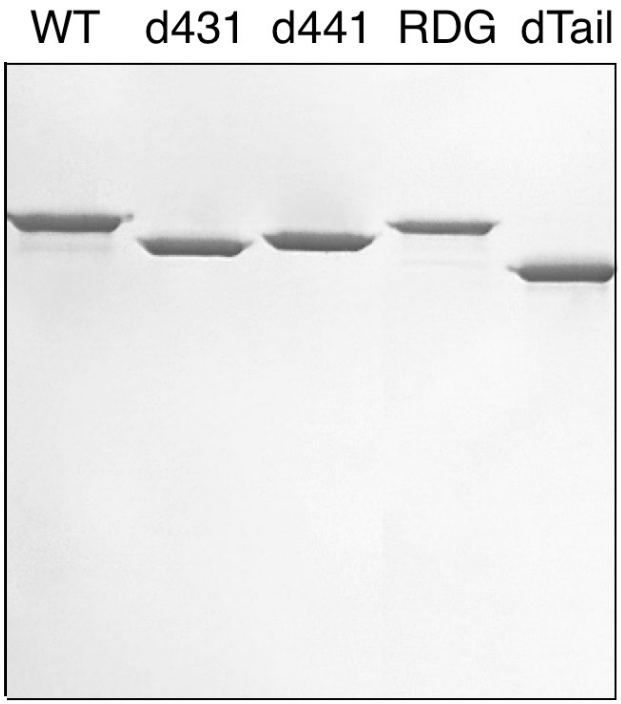

Fig 8.2. Purified WT and mutant desmin proteins.

The 4 desmin mutants (d431, d441, RDG and dTail) were expressed and purified to >95% homogeneity by Sarika Sharma at the German Cancer Research Centre in Germany and shipped to the Durham laboratories. Once in Durham, each protein was quantified using BCA and the UV absorbance at 280nm. WT desmin was purified by myself at the Durham laboratories.

RESULTS

Morphology of mutant desmin filaments changes with assembly speed

The assembly competence of the 4 desmin mutants (d431, d441, RDG and dTail) in the presence of aB crystallin was assessed previously by Sarika Sharma at the University of Heidelberg in 2010. In these experiments, filament assembly was finalised by addition of concentrated NaCl buffer, such that the NaCl concentration changed from 0mM to 50mM within a few seconds causing rapid filament assembly (Sharma, 2011). Samples were then incubated at 37°C for 1h before TEM analysis, which showed the formation of filaments (Fig 8.3, far right column in blue box). Some aB crystallin oligomers associated with the filaments (Fig 8.3, right column, black triangles) while some remained unassociated (Fig 8.3, right column, black arrows).

However, although the filaments formed by d431, d441 and dTail desmin are long and smooth (Fig 8.3, right column in blue box), they appear much wider than the ~10nm filaments formed by WT desmin (see previous results chapter, Fig 7.14). These filaments also appear to have large variations in width from ~15nm to ~30nm and appear to unfold and unravel at points along their length (Fig 8.3, blue arrows). The filaments formed by RDG desmin have failed to elongate and the short filament fragments appear to have assembled into larger branched structures (Fig 8.3, far right column). For further analysis of these images (Fig 8.3, right column in blue box), see Sharma, 2011.

To determine if the morphology of these mutant filaments could be improved, filaments were assembled using dialysis to gradually increase the NaCl concentration over a period of 16h hours (slow assembly), rather than seconds (rapid assembly) (Sharma, 2011). Filaments were assembled slowly for 16h at 22°C both with and without aB crystallin and then analysed by TEM (Fig 8.3, left and centre columns).

Results clearly show that when filaments are assembled slowly by dialysing, filament morphology is dramatically improved (Fig 8.3, compare centre and right columns). When assembled slowly, d431 and d441 desmin form radially compacted ~10nm filaments which more closely resemble WT desmin filaments, while dTail desmin forms filaments which appear much more even in width (Fig 8.3). However, the most dramatic effect of slow versus rapid assembly is seen for RDG desmin filaments which appear much longer, more radially compact and much more closely resemble WT desmin filaments (Fig 8.3, compare centre and right columns for RDG Des).

As seen in the previous results chapter, the filaments formed by WT desmin in the presence and absence of aB crystallin are indistinguishable (Fig 7.14). However, for d441, RDG and dTail desmin, filament morphology appears significantly improved by the addition of aB crystallin (Fig 8.3, compare left and centre columns). For these mutants, filaments formed in the presence of aB crystallin appear smoother and more closely resemble WT desmin filaments.

The morphology of these desmin mutant filaments will be analysed in more detail later in this chapter, but it is clear from this TEM data that the speed of assembly has a dramatic effect upon desmin filament morphology. The data also suggests that, for some desmin mutants, filament morphology maybe improved by the presence of aB crystallin during assembly.

Fig 8.3. Effect of assembly speed and aB crystallin addition on mutant desmin filament morphology.

When desmin mutants are assembled rapidly (right column in blue box), d431, d441 and dTail desmin form filaments with large variations in width from ~15nm to ~30nm and appear to unravel at points along their length (Fig 8.3, blue arrows). RDG desmin forms short filament fragments which aggregate. However, when assembled slowly, all mutant desmins appear to form filaments which more closely resemble WT desmin filaments. In addition, d441, RDG and dTail filament morphology appears improved by the presence of aB crystallin. Some aB crystallin oligomers associate with the filaments (black triangles) while some remained unassociated (black arrows). The images in the blue box (and their preceding filament assemblies) were produced by Sarika Sharma at the University of Heidelberg. Scale is the same for all images and the black bar represents 100nm.

(Figure on next page)

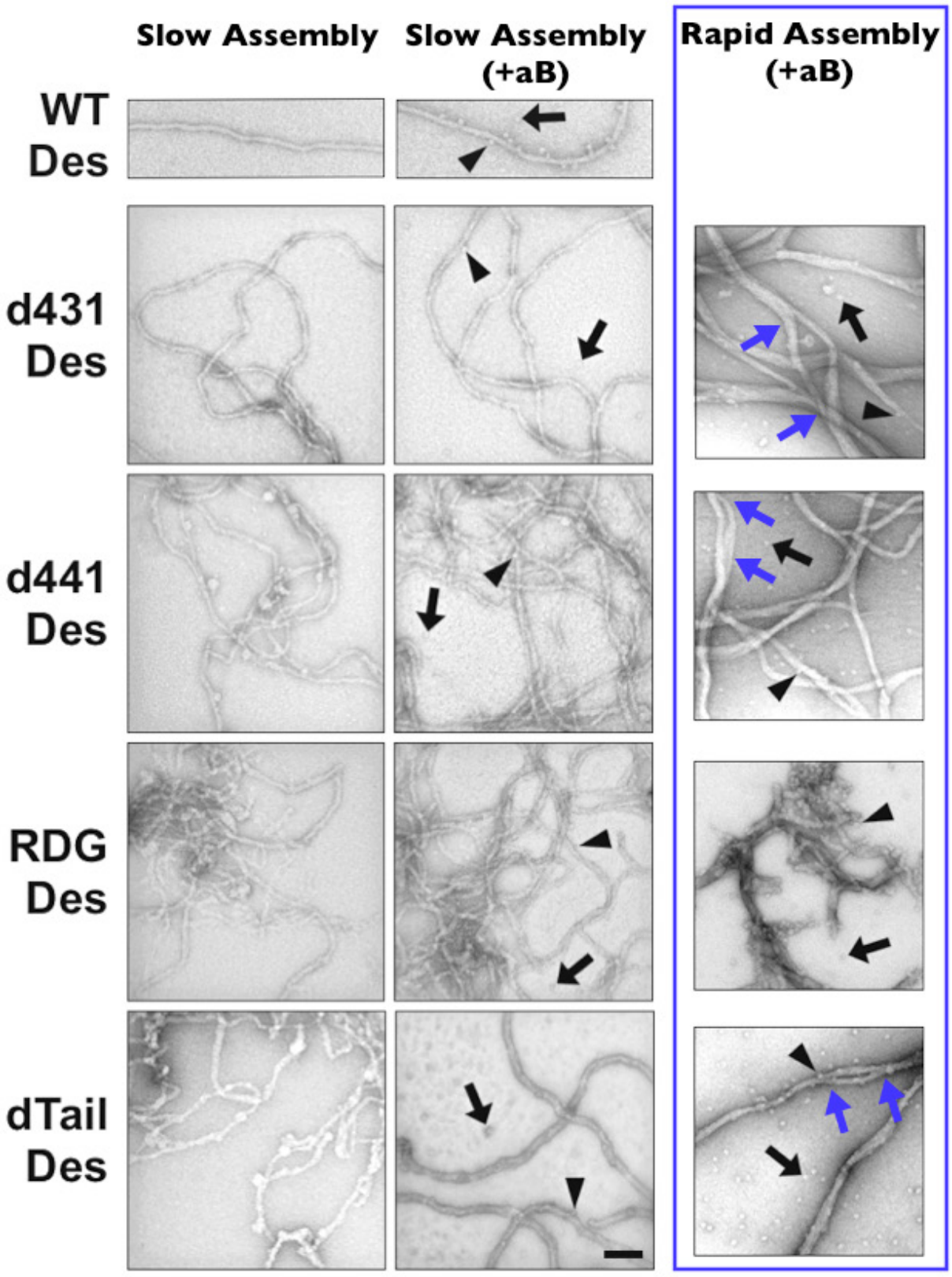

Fig 8.3 (Legend on previous page)

Filament width distributions of desmin mutants in the presence and absence of aB crystallin

To further analyse the morphology of the slow assembled filaments formed by the desmin mutants (d431, d441, RDG and dTail), the TEM images were analysed to determine filament width distributions in both the presence and absence of aB crystallin (Fig 8.4). The average values and standard deviations were calculated and differences were analysed using an unpaired two-tailed Students t-test to determine statistical significance (Fig 8.5).

WT, d431 and d441 desmin forms filaments of ~10nm average width in both the presence and absence of aB crystallin (Fig 8.5). In the absence of aB crystallin, RDG desmin forms filaments of 10.3nm average width, but in the presence of aB crystallin average filament width increases to 11.3nm, a significant increase compared to WT desmin filaments (10.5nm) (Fig 8.5). In both the presence and absence of aB crystallin, dTail desmin forms filaments of significantly larger average width (13.1 and 12.3nm respectively) compared to WT filaments (9.7 and 10.5nm respectively) (Fig 8.5).

All 4 desmin mutants (d431, d441, RDG and dTail) show significantly increased filament width distribution profiles (Fig 8.4) with significantly larger standard distributions of width (Fig 8.5) compared to WT desmin (1.5-2.5x larger than WT). Although the filaments formed by d431 and d441 desmin have an average width comparable to WT desmin filaments, the standard deviation of widths are larger (~2.8nm) compared to WT (1.3nm and 1.9nm) in both the presence and absence of aB crystallin (Fig 8.5). This suggests that the desmin tail mutations have affected filament width control. Interestingly, for WT, d441, RDG and dTail desmin filaments, the standard distribution of filament width decreases upon aB crystallin addition (Fig 8.5). Furthermore, both RDG and dTail desmin average filament widths increase significantly upon aB crystallin addition (Fig 8.5). This may suggest that aB crystallin can affect filament width and that the RDG and dTail desmin mutations may have altered the interaction with aB crystallin.

Overall, results show that all 4 desmin tail mutations (d431, d441, RDG and dTail) cause increased filament width distributions, and that dTail desmin (and RDG desmin in the presence of aB crystallin) have increased average filament widths. In addition, results suggest that aB crystallin has the potential to affect desmin filament morphology.

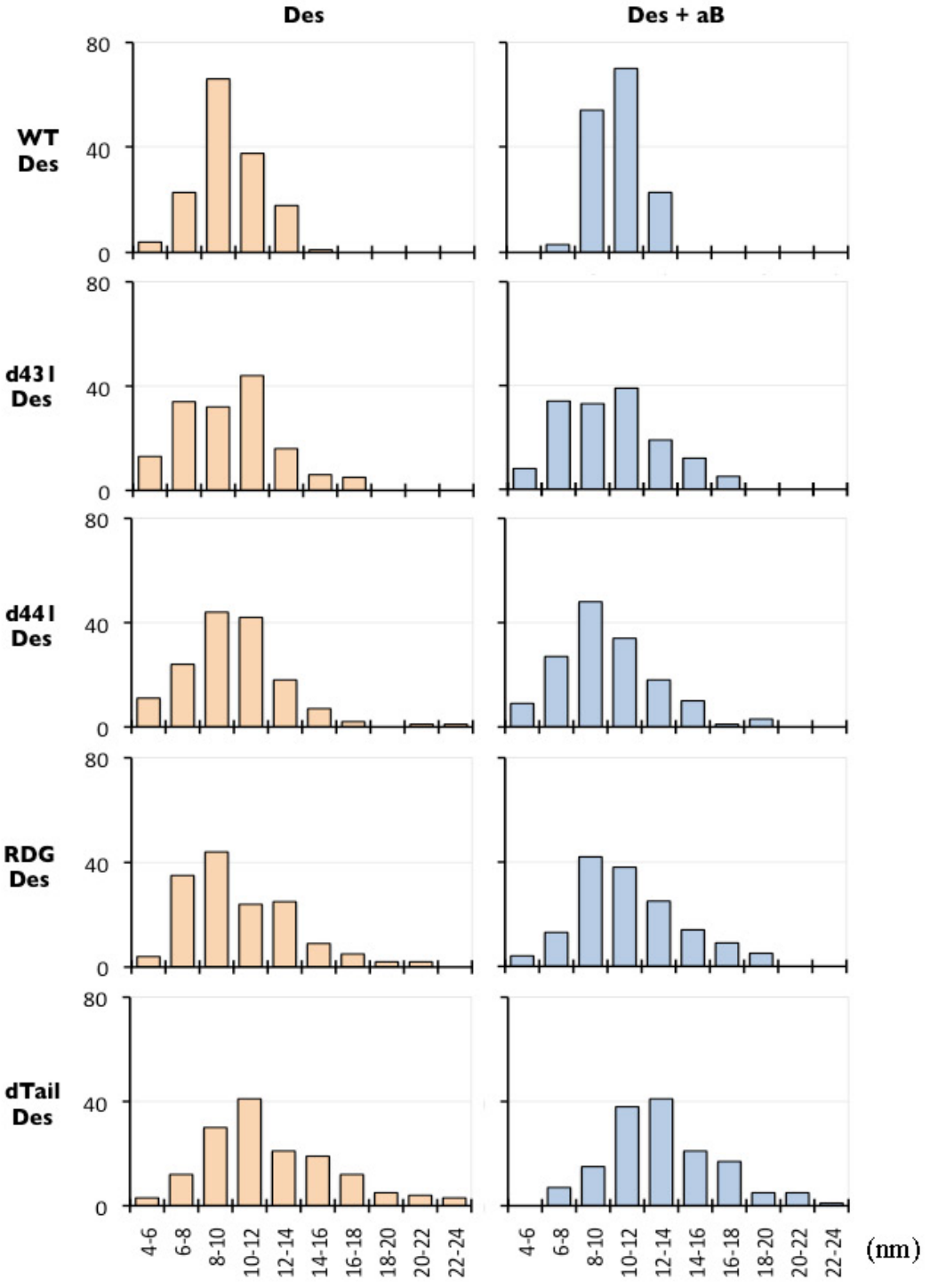

Fig 8.4. TEM measurements of WT and mutant desmin filament width distributions in the presence and absence of aB crystallin at 22°C.

The x axis shows filament width categories (nm) and the y axis shows the raw frequency. A total of 150 width measurements were made for each desmin mutant in randomly selected areas from 3 different TEM images. For the complete data set, see supplementary data, Sup Fig 5.

	Des		Des + aB	
	Ave	**SD**	**Ave**	**SD**
WT Des	9.7	1.9	10.5	1.3
d431 Des	9.8	**2.8**	10.1	**2.8**
d441 Des	9.9	**3.0**	9.9	**2.8**
RDG Des	10.3	**3.3**	**11.3**	**3.1**
dTail Des	**12.3**	**3.8**	**13.1**	**3.3**

Fig 8.5. Summary of TEM measurements of WT and mutant desmin filament width.

Summary of WT and mutant desmin filament widths (nm) in the presence and absence of aB crystallin at 22°C. Average (Ave) values highlighted in red are statistically different from WT values as determined by *P* values <0.01 in an unpaired two-tailed Students t-test. Standard deviation (SD) values larger than WT are also highlighted in green. dTail desmin filaments are, on average, significantly wider than WT desmin filaments in both the presence and absence of aB crystallin. RDG desmin filaments are, on average, significantly wider than WT desmin filaments in the presence of aB crystallin. All 4 mutants have greater standard deviations of filament width than WT (1.5-2.5x larger than WT).

pH induced changes in sedimentation properties of WT desmin filaments

The solubility of desmin filaments in the absence of aB crystallin was investigated previously (previous results chapter, Fig 7.8, B). However, in this current chapter, filaments are assembled at pH 7.6, whereas in the previous chapter filaments are assembled at pH 7.4. This change was made to allow comparison with work already performed on the 4 desmin mutants by Sarika Sharma at the University of Heidelberg, Germany. Therefore, it was necessary to re-assess the co-sedimentation properties of WT desmin at pH 7.6, rather than pH 7.4.

The high speed sedimentation results show that at both pH 7.6 and 7.4, WT desmin pellets >90% at all 3 temperatures (Fig 8.6, red bars). This confirms that changing the pH from 7.4 to 7.6 does not affect desmin assembly into filaments.

The low speed sedimentation results (Fig 8.6, blue bars) show that at both pH 7.6 and 7.4, WT desmin remains soluble at 22°C (~25% pellets). This indicates that changing the pH from 7.4 to 7.6 does not change filament-filament interactions at 22°C. However at 37°C, 68% (±10%) of WT desmin pellets at pH 7.6 but only 45% (±10%) pellets at pH 7.4 (Fig 8.6, 37°C, blue bars). Although the standard deviations of these values are unusually high, this difference is still statistically significant. Most strikingly, at 44°C only 16% (±6%) of desmin pellets at pH 7.6 whereas 61% (±18%) pellets at pH 7.4 (Fig 8.6, 44°C, blue bars). This suggests that changing the pH from 7.4 to 7.6 slightly increases filament-filament interactions at 37°C, but significantly decreases filament-filament interactions at 44°C. In order to analyse the desmin mutations in this chapter, all mutant desmin values at pH 7.6 will be compared to WT desmin values at pH 7.6.

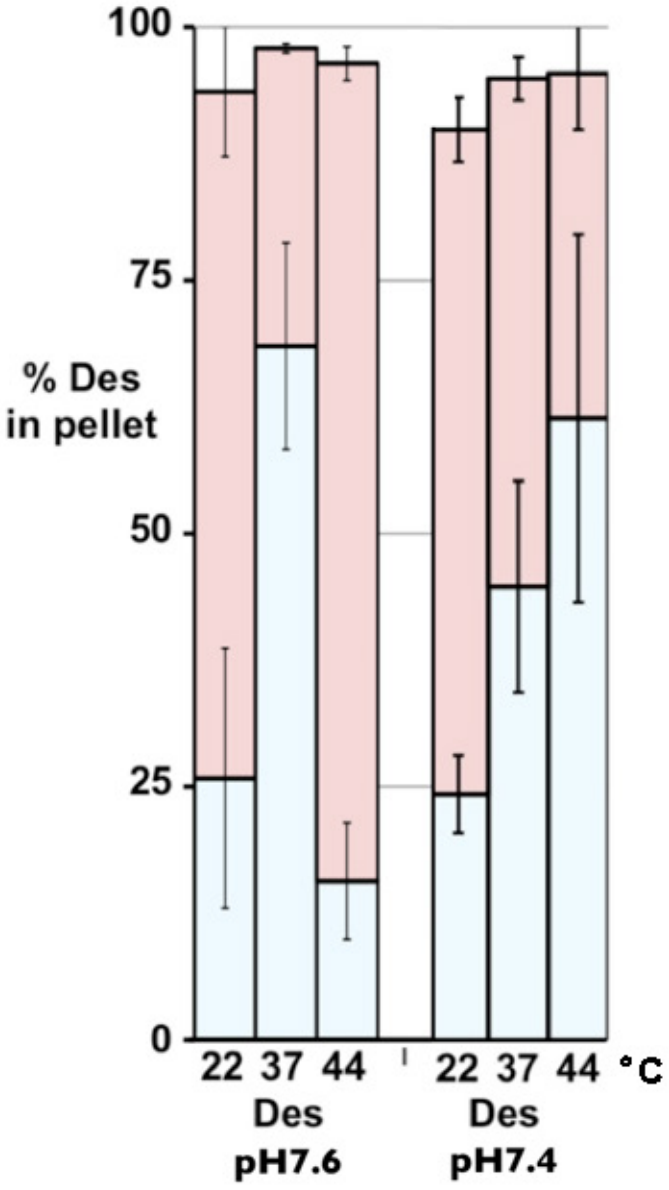

Fig 8.6. Sedimentation properties of WT desmin assembled at pH 7.6 and 7.4.

The low (blue bars) and high (red bars) speed sedimentation properties of WT desmin assembled at 22, 37 and 44°C at either pH 7.6 or 7.4. At high speed, >90% of desmin pellets at all 3 temperatures at both pH 7.6 and 7.4. At low speed at 22°C, desmin remains soluble at both pH 7.6 and 7.4 (~25% pellets). However, at low speed, at 37°C pH 7.6 increases filament-filament interactions, and at 44°C pH 7.6 decreases filament-filament interactions, relative to pH 7.2. The amount of material pelleted is shown as a percentage of total material as quantified by gel densitometry. Average values and standard deviations were calculated from 3 experimental repeats.

High speed co-sedimentation properties of desmin mutants in the presence and absence of aB crystallin

To quantify the interaction of the desmin mutants with aB crystallin, the high speed (80,000g) co-sedimentation properties of the desmin mutants assembled at 22, 37 and 44°C in the presence and absence of aB crystallin was analysed by SDS-PAGE. Fig 8.7 represents 1 of 4 experimental repeats, which were quantified via gel densitometry, collated and averaged (Fig 8.8). The pellet (P) contains individual desmin filaments and any aggregates formed as a result of filament-filament interactions. The supernatant (S) contains unassembled desmin or assembly intermediates. Therefore this assay measures filament assembly.

The high speed sedimentation results show that for WT desmin and all 4 mutants, >90% of the sample pellets at all 3 temperatures when assembled with or without aB crystallin. (Fig 8.7). This shows that all 4 desmin mutants are assembly competent in both the presence and absence of aB crystallin as there is no remaining unassembled desmin or assembly intermediates (Fig 8.7).

In the presence of aB crystallin, WT desmin and all 4 mutants show slightly reduced pelleting (Fig 8.8, compare blue and red bars), perhaps indicating a slight inhibition of assembly. The largest difference is seen for WT desmin at 37°C (Fig 8.8) as the addition of aB crystallin reduces pelleting from 98% to 88%. This effect is also seen for WT desmin at 44°C (96% to 89%), RDG desmin at 44°C (100% to 95%) and dTail at 22°C (99% to 94%). However, these differences are small and very close to the margin of error. For the other desmin mutants and additional temperatures, the reduction in desmin pelleting due to aB crystallin addition is not statistically significant (Fig 8.8).

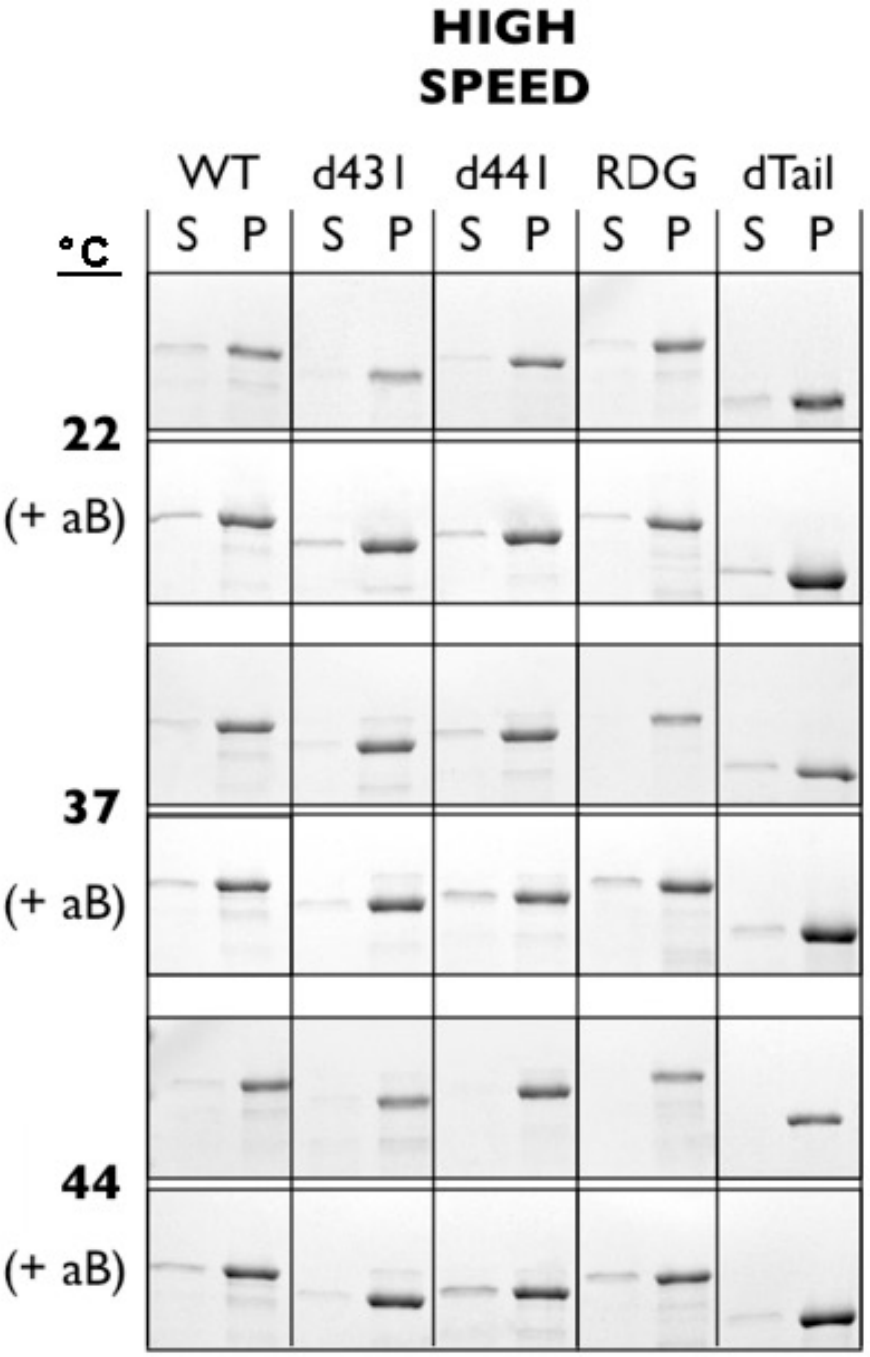

Fig 8.7. High speed sedimentation of WT or mutant desmin assembled in the presence and absence of aB crystallin.

High speed (80,000g) sedimentation of WT or mutant desmin, assembled at 22, 37 or 44 °C in the presence and absence of aB crystallin, analysed by SDS-PAGE. For WT desmin and all 4 mutants, >90% of desmin pellets at all 3 temperatures in both the presence and absence of aB crystallin. The above gels represent 1 of 4 repeats. Supernatant (S) and pellet (P). Note that the aB crystallin bands are not shown in this figure.

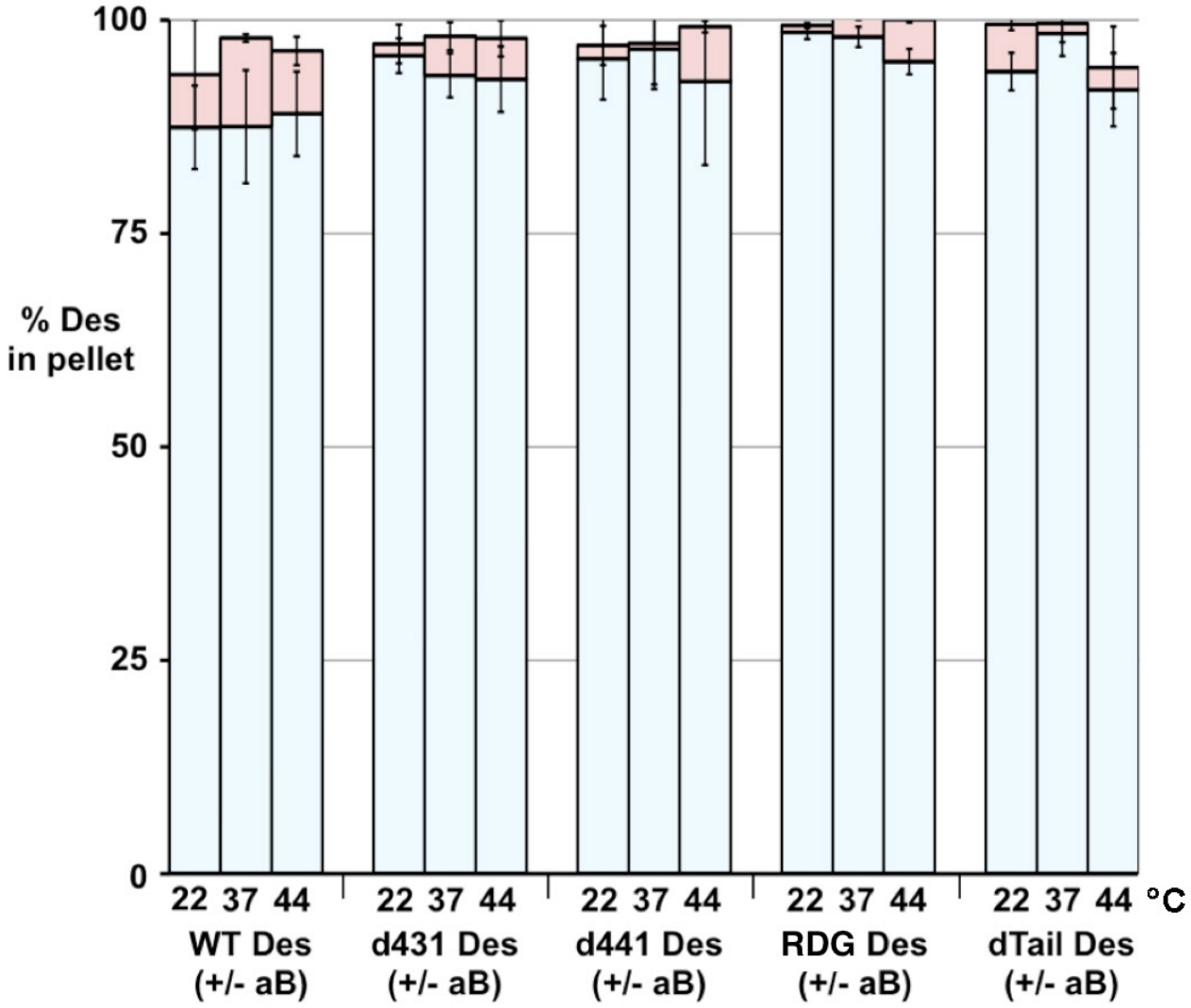

Fig 8.8. Comparison of WT or mutant desmin high speed sedimentation in the absence and presence of aB crystallin.

Bar chart of the high speed pelleting of desmin in the presence (blue) and absence (red) of aB crystallin at 22, 37 and 44°C. The difference between the blue and red bars represents the reduction in desmin pelleting as a result of the presence of aB crystallin. For WT desmin and all 4 mutants, >90% of desmin pellets at all 3 temperatures when assembled both with and without aB crystallin. The amount of material pelleted is shown as a percentage of total material as quantified by gel densitometry. Average values and standard deviations were calculated from 4 experimental repeats.

Low speed co-sedimentation properties of desmin mutants in the presence and absence of aB crystallin

To further quantify the interaction of the desmin mutants with aB crystallin, the low speed (2,500g) co-sedimentation properties of the desmin mutants assembled at 22, 37 and 44°C in the presence and absence of aB crystallin was analysed by SDS-PAGE. Fig 8.9 represents 1 of 4 experimental repeats, which were quantified via gel densitometry, collated and averaged (Fig 8.10). The pellet (P) contains only those filaments which have self associated into aggregates. Individual desmin filaments remain in the supernatant (S). Therefore, this assay measures filament-filament interaction and hence the ability of aB crystallin to prevent these filament-filament interactions.

The low speed sedimentation results show significant differences between WT desmin and all 4 mutants. When assembled in the absence of aB crystallin (Fig 8.10, red bars), WT desmin is soluble at 22 and 44°C (<26% pellets), but aggregates at 37°C (68% pellets). Conversely, desmin mutants d431 and d441 are most soluble at 37°C (39% and 24% pellets respectively) and aggregate at 22 and 44°C (>61% pellets). This indicates that filament-filament interactions are highest at 37°C for WT desmin and lowest at 37°C for d431 and d441 desmin. However, the addition of aB crystallin (Fig 8.10, blue bars) is able to reduce filament-filament interactions for WT, d431 and d441 desmin at all 3 temperatures such that these filaments are all soluble (<21% pellets) and do not aggregate (Fig 8.10, blue bars). This indicates that although the d431 and d441 desmin mutations have altered the filament-filament interactions, the filaments are still able to interact with aB crystallin to reduce these filament-filament interactions and prevent aggregation.

When assembled in the absence of aB crystallin, dTail desmin has similar sedimentation characteristics to d431 and d441 desmin, aggregating most at 22 and 44°C (Fig 8.10, red bars). However, although addition of aB crystallin is able to reduce dTail desmin filament-filament interactions and increase filament solubility at all 3 temperatures, this effect is significantly smaller than that seen for d431 and d441 desmin. At 22°C, addition of aB crystallin only reduces dTail filament pelleting from 68% to 58% (Fig 8.10). At 37 and 44°C, addition of aB crystallin reduces dTail desmin pelleting from 57% to 29% and from 87% to 29% respectively, but this pelleting is still ~2 fold higher than WT, d431 and d441 desmin in

the presence of aB crystallin (Fig 8.10, blue bars). In addition, the ability of aB crystallin to prevent dTail filament-filament interactions is highly temperature dependant. At 44°C, aB crystallin reduces dTail pelleting from 87% to 29%, but at 22°C pelleting is only reduced from 68% to 58% (Fig 8.10). This suggests that the dTail mutation has not only altered filament-filament interactions, but also the filament interaction with aB crystallin, such that the ability of aB crystallin to prevent these filament-filament interactions is reduced, and filaments aggregate.

The RDG deletion dramatically increases filament-filament interactions, such that in the absence of aB crystallin, >95% pellets at all 3 temperatures (Fig 8.10, red bars). Although addition of aB crystallin is able to reduce RDG desmin filament-filament interactions and increase filament solubility at all 3 temperatures (>95% to <77% pelleting), this effect is significantly smaller than that seen for WT desmin or any of the other 3 mutants (Fig 8.10). This suggests that the RDG mutation has not only increased filament-filament interactions, but has also altered the filament interaction with aB crystallin, such that the ability of aB crystallin to prevent filament-filament interactions is reduced, and filaments aggregate.

Overall, the low speed sedimentation results show that all 4 desmin mutations (d431, d441, RDG and dTail) affect filament-filament interactions, and that this effect is highly temperature dependant. In addition, RDG and dTail desmin also alter the filament interaction with aB crystallin, such that the ability of aB crystallin to prevent filament-filament interactions is reduced.

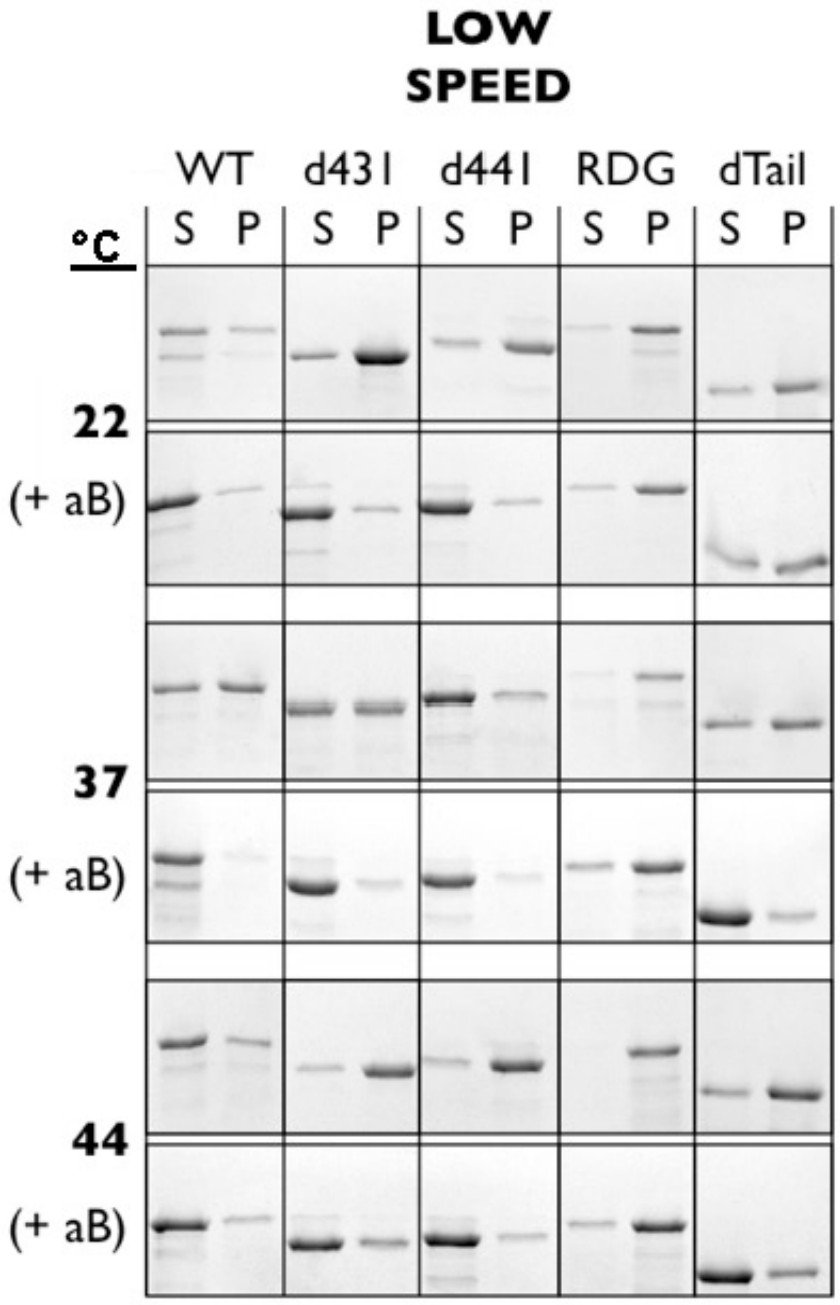

Fig 8.9. Low speed sedimentation of WT or mutant desmin assembled in the presence and absence of aB crystallin.

Low speed (2,500g) sedimentation of WT or mutant desmin, assembled at 22, 37 or 44°C in the presence and absence of aB crystallin, analysed by SDS-PAGE. For WT desmin and all 4 mutants, the addition of aB crystallin decreases desmin pelleting at all 3 temperatures. The largest effect of aB crystallin addition is the solubilisation of d431 desmin at 22°C. The above gels represent 1 of 4 repeats. Supernatant (S) and pellet (P). Note that the aB crystallin bands are not shown in this figure.

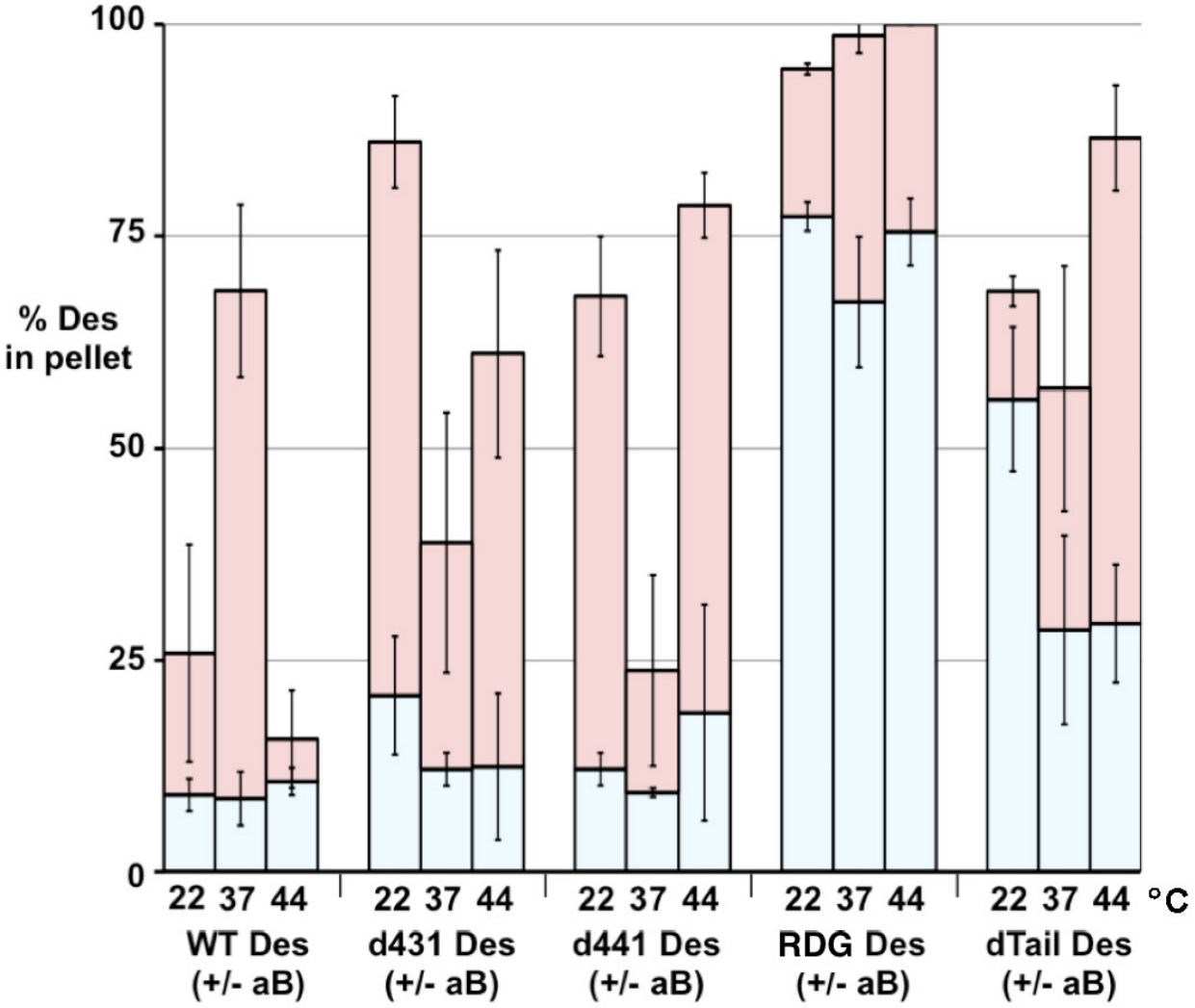

Fig 8.10. Comparison of WT and mutant desmin low speed sedimentation in the presence and absence of aB crystallin.

Bar chart of the low speed pelleting of WT or mutant desmin in the presence (blue) and absence (red) of aB crystallin at 22, 37 and 44°C. The difference between the blue and red bars represents the decrease in desmin pelleting as a result of aB crystallin addition which reduces filament-filament interactions. (Red Bars) When assembled alone, d431, d441 and dTail desmin filaments are all more soluble than WT desmin filaments at 37°C, but less soluble at 22 and 44°C. RDG desmin aggregates at all 3 temperatures. (Blue Bars) Addition of aB crystallin is able to reduce filament-filament interactions for WT and all 4 mutants at all 3 temperatures, however, this effect is smaller for RDG and dTail desmin. The amount of material pelleted is shown as a percentage of total material as quantified by gel densitometry. Average values and standard deviations were calculated from 4 experimental repeats.

Binding of aB crystallin to WT or mutant desmin filaments

To assess the effect of the desmin mutations on the binding of aB crystallin, the low (2,500g) and high (80,000g) speed co-sedimentation properties of aB crystallin in the presence of the desmin mutants at 22, 37 and 44°C was analysed. At high speed, any aB crystallin that binds individual filaments or their aggregates is co-sedimented, but at low speed, only the aggregate bound aB crystallin pellets. Fig 8.11 shows the average of 3 experimental repeats.

When assembled alone, aB crystallin remains soluble at all 3 temperatures with <10% and <14% pelleting at low and high speed respectively (Fig 8.11). In the presence of WT desmin, aB crystallin shows no significant increase in pelleting at 22°C, but shows slightly increased high speed pelleting at 37 and 44°C (Fig 8.11), indicating temperature dependant binding. In the presence of d431 and d441 desmin, aB crystallin pelleting is similar to that seen with WT desmin, although for the mutants, binding at 22°C can be detected.

Interestingly, in the presence of dTail desmin, aB crystallin does not show any increase in pelleting at low or high speed at any of the 3 temperatures and is comparable with aB crystallin assembled alone (Fig 8.11). This indicates a complete lack of 'detectable' binding, despite aB crystallin significantly reducing dTail desmin filament-filament interactions (R2D). Conversely, in the presence of RDG desmin, aB crystallin pelleting increases ~1.5 fold relative to WT desmin at both low and high speed and at all 3 temperatures, indicating an increase in aB crystallin binding to RDG desmin filaments.

Overall, sedimentation results show that RDG desmin has increased (~1.5 fold) aB crystallin binding at all 3 temperatures while dTail desmin has a complete lack of 'detectable' aB crystallin binding. d431 and d441 desmin show slightly increased aB crystallin binding at 22°C, but otherwise have similar aB crystallin binding characteristics to WT desmin.

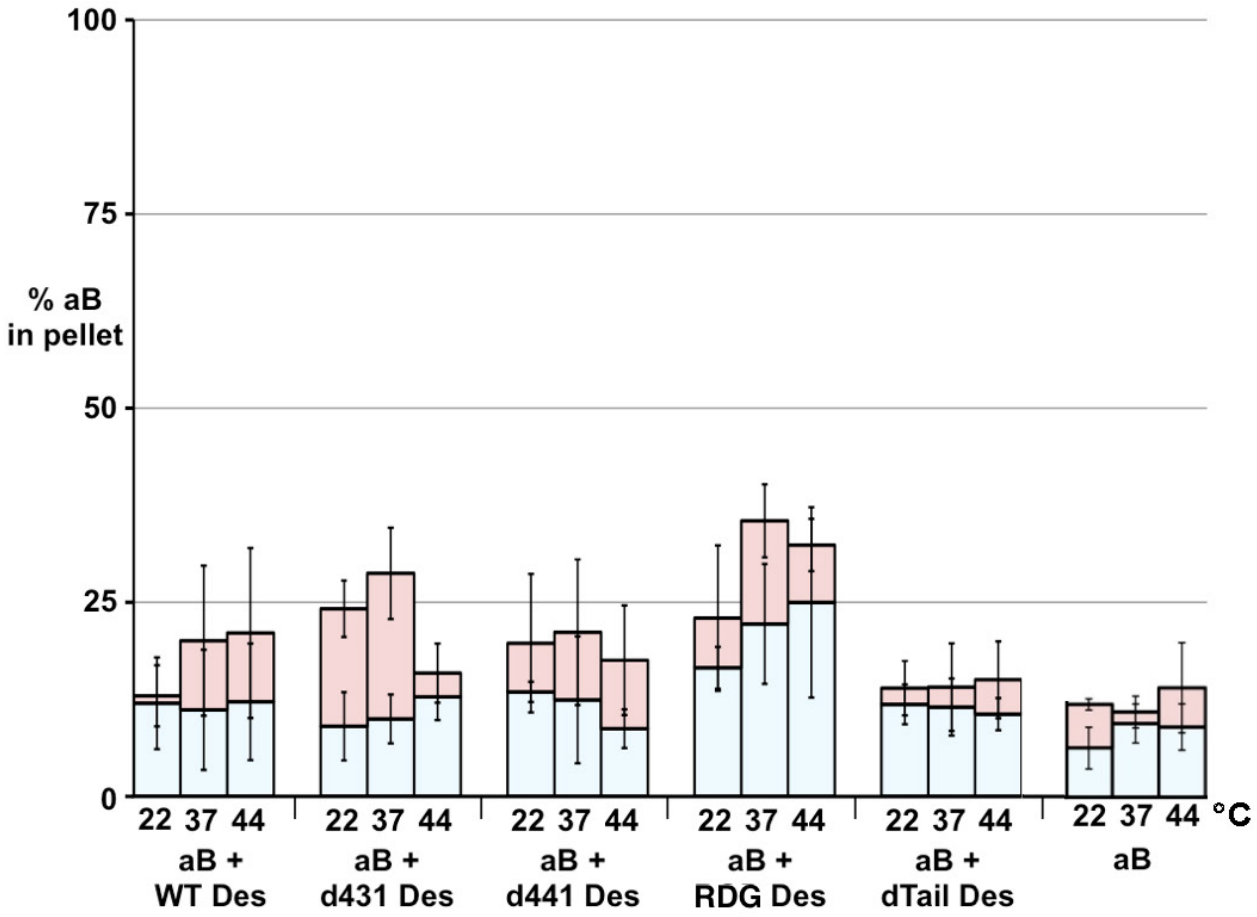

Fig 8.11. Quantification aB crystallin co-sedimentation with WT or mutant desmin.

Bar chart of the low speed (blue) and high speed (red) pelleting of aB crystallin in the presence of WT or mutant desmin at 22, 37 and 44°C. In the presence of WT desmin, aB crystallin shows no significant increase in pelleting at 22°C, but shows slightly increased high speed pelleting at 37 and 44°C. RDG desmin has increased (~1.5 fold) aB crystallin binding at all 3 temperatures at both low and high speed, while dTail desmin has a complete lack of 'detectable' aB crystallin binding. d431 and d441 show slightly increased binding at 22°C, but otherwise have similar aB crystallin binding characteristics to WT desmin. The amount of material pelleted is shown as a percentage of total material as quantified by gel densitometry. Average values and standard deviations were calculated from 4 experimental repeats.

Morphology of mutant desmin filaments in the presence of aB crystallin

To analyse the effect of the desmin mutations on filament morphology, the mutants were assembled at 22, 37 or 44°C in the presence of aB crystallin and samples were analysed by TEM. When WT desmin is assembled in the presence of aB crystallin, the filaments formed at all 3 temperatures are long, smooth, constant width ~10nm filaments (see previous results chapter, Fig 7.14). Some aB crystallin oligomers associate with the filaments while some remained unassociated.

When d431, d441, RDG and dTail desmin are assembled in the presence of aB crystallin, both mutants are able to form filaments at all 3 temperatures (Fig 8.12 and Fig 8.13). Some aB crystallin oligomers associate with the mutant filaments (black triangles) while some remained unassociated (black arrows). However, these mutant filaments appear less smooth than WT desmin filaments and appear to have sharp kinks (see red arrows for examples) and large variations in width (compare green arrows) (Fig 8.12 and Fig 8.13).

Despite these apparent changes in filament morphology, d431 and d441 filaments do not aggregate in the presence of aB crystallin at any of the 3 temperatures (R2D, blue bars). In addition, although the dTail filaments show significantly increased tendency to aggregate in the presence of aB crystallin at 22°C compared with 37 and 44°C (R2D, red bars), there are no obvious changes in morphology at 22°C compared with 37 or 44°C (Fig 8.13).

Overall, TEM analysis shows that the d431, d441, RDG and dTail desmin mutants are all capable of assembling into filaments at 22, 37 and 44°C, but all mutations appear to have affected filament morphology.

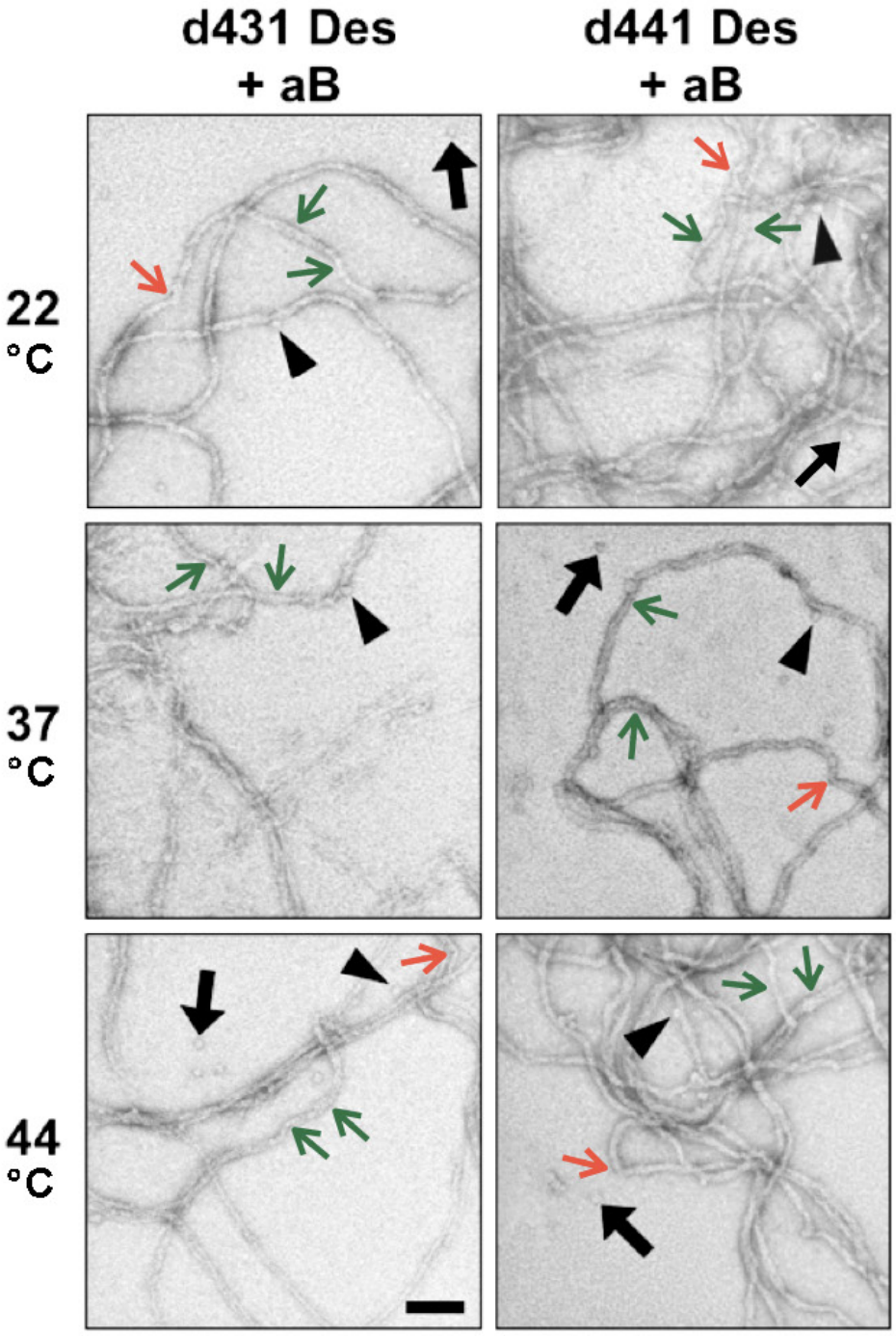

Fig 8.12. TEM analysis of d431 and d441 desmin filaments assembled with aB crystallin.

In the presence of aB crystallin, d431 and d441 desmin are able to form ~10nm filaments at all 3 temperatures. However, these filaments appear less smooth than WT filaments and appear to have sharp kinks (see red arrows for examples) and large variations in width (compare green arrows). Some aB crystallin oligomers associate with the filaments (black triangles) while some remained unassociated (black arrows). Scale bar represents 100nm.

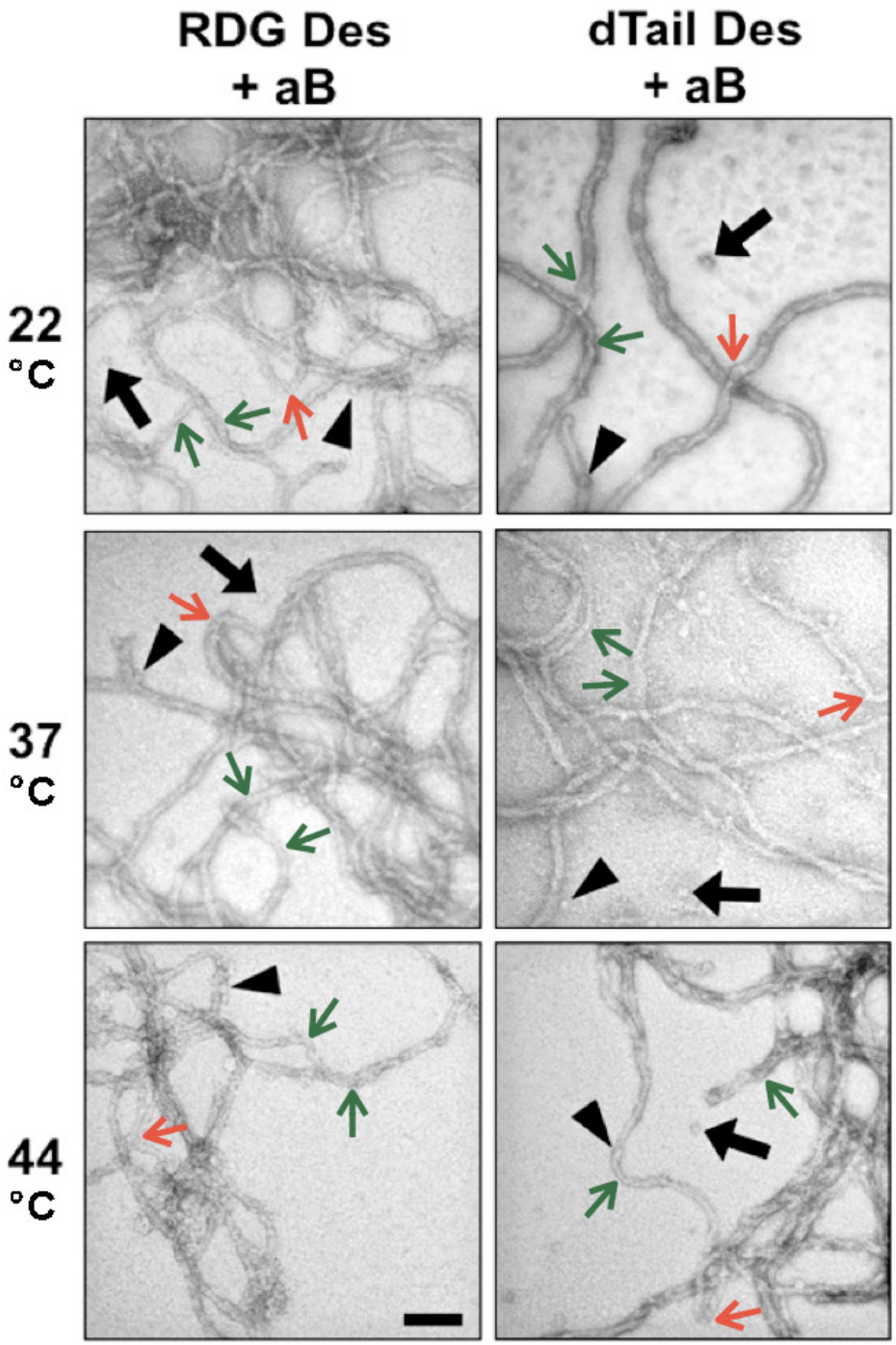

Fig 8.13. TEM analysis of RDG and dTail desmin filaments assembled with aB crystallin.

In the presence of aB crystallin, RDG and dTail desmin are able to form filaments at all 3 temperatures. However, these filaments appear less smooth than WT filaments and appear to have sharp kinks (see red arrows for examples) and large variations in width (compare green arrows). Some aB crystallin oligomers associate with the filaments (black triangles) while some remained unassociated (black arrows). Scale bar represents 100nm.

Filament width distributions of desmin mutants in the presence of aB crystallin at 22, 37 and 44°C

To further analyse the morphology of the mutant desmin filaments and investigate the apparent large deviations in mutant filament width (Fig 8.12 and Fig 8.13), TEM images were analysed to determine filament width distributions in the presence of aB crystallin at 22, 37 and 44°C (Fig 8.14). The average values and standard deviations were calculated and differences were analysed using an unpaired, two-tailed Students t-test to determine statistical significance (Table 8.15).

WT, d431 and d441 desmin form filaments of ~10-11nm average width at all 3 temperatures (Table 8.15). However, RDG and dTail desmin form filaments with significantly larger average width (~11-13nm) at all 3 temperatures compared to WT desmin filaments (Table 8.15).

All 4 desmin mutants (d431, d441, RDG and dTail) show significantly increased filament width distribution profiles (Fig 8.14) with significantly larger standard distributions of width at all 3 temperatures compared to WT desmin (1.8-2.6x larger than WT) (Table 8.15). Although the filaments formed by d431 and d441 desmin have an average width comparable to WT desmin filaments, the standard deviations of width are larger (2.8-3.3nm) compared to WT (1.3-1.7nm) (Fig 8.5). This suggests that the desmin tail mutations have affected filament width control. Interestingly, for WT and all 4 mutants, the standard distribution of filament width increases with temperature (Fig 8.5). This may suggest that temperature can affect filament width.

Overall, results show that all 4 desmin tail mutations (d431, d441, RDG and dTail) cause increased filament width distributions, and that RDG and dTail mutations cause increased average filament widths. Results also suggest that temperature may play a role in desmin filament morphology.

Fig 8.14. TEM measurements of WT and mutant desmin filament width distribution in the presence of aB crystallin at 22, 37 and 44°C.

The x axis shows filament width categories (nm) and the y axis shows raw frequency. A total of 150 width measurements were made for each desmin mutant in randomly selected areas from 3 different TEM images. For complete data sets, see supplementary data, Sup Fig 6, Sup Fig 7 and Sup Fig 8.

(Figure on next page)

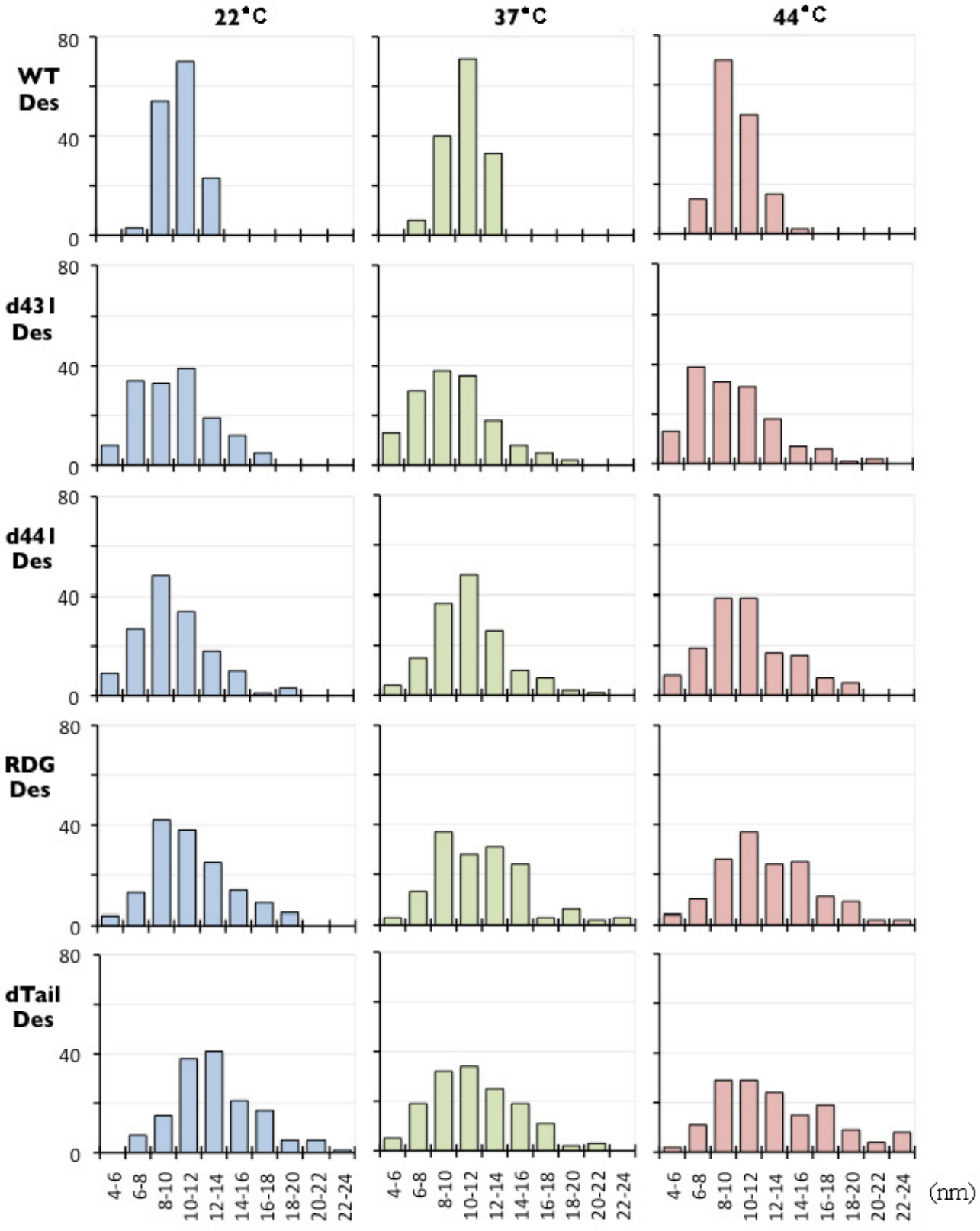

Fig 8.14 (Legend on previous page)

	22°C		37°C		44°C	
	Ave	**SD**	**Ave**	**SD**	**Ave**	**SD**
WT Des (+ aB)	10.5	1.3	10.6	1.6	10.1	1.7
d431 Des (+ aB)	10.1	**2.8**	9.9	**3.1**	9.9	**3.3**
d441 Des (+ aB)	9.9	**2.8**	11.0	**2.9**	10.8	**3.3**
RDG Des (+ aB)	**11.3**	**3.1**	**11.9**	**3.6**	**12.5**	**3.7**
dTail Des (+ aB)	**13.1**	**3.3**	**11.4**	**3.5**	**13.1**	**4.5**

Table 8.15. Summary of TEM measurements of WT and mutant desmin filament width distribution in the presence of aB crystallin.

The table shows the average (Ave) and standard distribution (SD) of filament widths (nm). A total of 150 width measurements were made for each sample. Measurements were made in randomly selected areas from 3 different TEM images. Average (Ave) values highlighted in red are statistically different from WT values as determined by *P* values <0.01 in an unpaired two-tailed Students t-test. Standard deviation (SD) values larger than WT are highlighted in green. All 4 mutants have greater standard deviations of filament width than WT (1.9-2.5x larger than WT, green values in table) and RDG and dTail desmin filaments have significantly higher average width values at all temperatures, compared to WT desmin (red values in table).

RESULTS SUMMARY

These data identify sequences in the desmin tail domain that are important for filament morphology, solubility and interaction with aB crystallin. All desmin tail mutants (d431, d441, RDG and dTail) are capable of assembling into filaments in both the presence and absence of aB crystallin, but all these mutations appear to have affected desmin filament morphology (TEM data summarised in Fig 8.16).

Results show that all 4 desmin tail mutations (d431, d441, RDG and dTail) cause increased filament width distributions, and that RDG and dTail mutations cause increased average filament widths. Results also suggest that both aB crystallin and temperature may play a role in desmin filament morphology. In the absence of aB crystallin, all 4 desmin mutations affect filament-filament interactions and filament aggregation, and this effect is highly temperature dependant (sedimentation data summarised in Table 8.17).

Although the d431 and d441 mutations affect filament morphology, aB crystallin is still able to interact with these mutant filaments to prevent filament-filament interactions and aggregation. Conversely, RDG and dTail desmin alter the filament interaction with aB crystallin, such that the ability of aB crystallin to prevent filament-filament interactions is reduced. However, results also show that while RDG desmin causes increased aB crystallin binding at all temperatures, dTail desmin causes a complete lack of 'detectable' aB crystallin binding. Therefore, as observed in the previous chapter with aB crystallin mutants aAb3 and d155 aB, the ability of aB crystallin to co-sediment with desmin filaments does not necessarily correlate with the ability to prevent filament-filament interactions. In this chapter, both increased and decreased aB crystallin co-sedimenting is linked to a reduced ability of aB crystallin to prevent filament-filament interactions.

Data in the chapter also suggests that the speed of filament assembly may have a dramatic effect upon the filament morphology. In addition, although changing the pH from 7.4 to 7.6 does not appear to affect WT desmin filament morphology, at pH 7.6 filament-filament interactions are increased at 37°C, but reduced at 44°C compared to pH 7.4. This suggests that filament-filament interactions maybe highly pH and temperature dependant.

Fig 8.16. TEM comparison of WT and mutant desmin filaments assembled with aB crystallin.

In the presence of aB crystallin, WT desmin forms, smooth ~10nm filaments at 22, 37 and 44°C. All desmin tail mutants (d431, d441, RDG and dTail) are capable of assembling into filaments in the presence of aB crystallin, but all these mutations appear to have affected filament morphology. Some aB crystallin oligomers associate with the WT and mutant filaments (black triangles) while some remained unassociated (black arrows). Scale bar represents 100nm.

(Figure on next page)

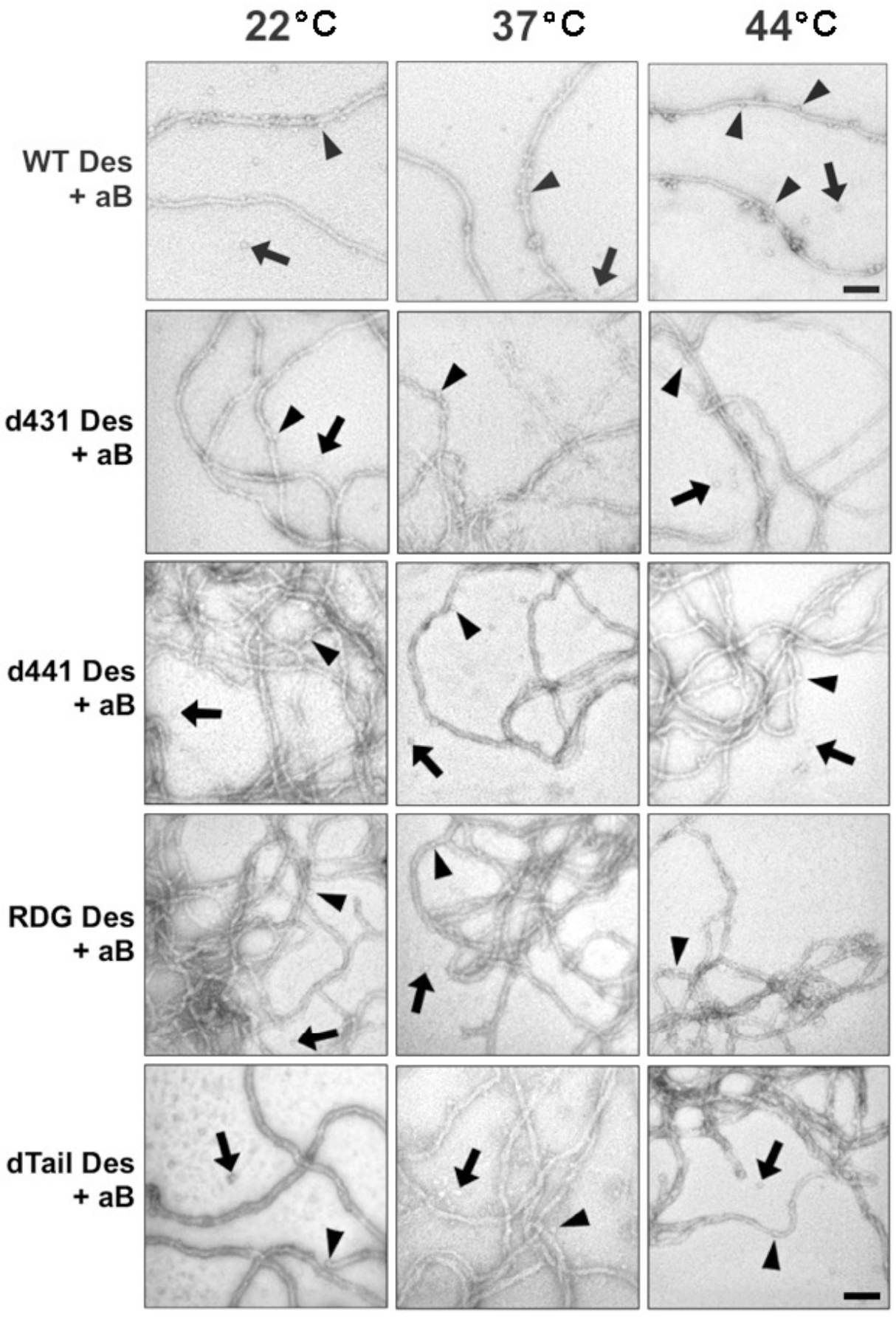

Fig 8.16 (Legend on previous page)

	LOW SPEED						HIGH SPEED					
	22°C		37°C		44°C		22°C		37°C		44°C	
	Ave % in Pellet	SD	Ave % in Pellet	SD	Ave % in Pellet	SD	Ave % in Pellet	SD	Ave % in Pellet	SD	Ave % in Pellet	SD
WT Des	26	13	68	10	16	6	94	6	98	0	96	2
d431 Des	86	5	39	15	61	12	97	2	98	2	98	2
d441 Des	68	7	24	11	79	4	97	2	95	5	99	1
RDG Des	95	1	99	2	100	0	99	0	100	0	100	0
dTail Des	68	2	57	14	87	6	99	1	98	2	94	5
WT Des (+ aB)	9	2	9	3	11	2	87	5	88	7	89	5
d431 Des (+ aB)	21	7	12	2	12	9	96	2	94	3	93	4
d441 Des (+ aB)	12	2	9	1	19	13	95	5	97	4	93	10
RDG Des (+ aB)	77	2	67	8	75	4	99	1	98	1	95	1
dTail Des (+ aB)	56	8	29	11	29	7	94	2	98	3	92	4
aB (+ WT Des)	12	6	11	8	12	8	13	4	20	10	21	11
aB (+ d431 Des)	9	4	10	3	13	3	24	4	29	6	16	4
aB (+ d441 Des)	13	1	12	8	9	2	20	9	21	9	18	7
aB (+ RDG Des)	17	3	22	8	25	12	23	9	35	5	32	3
aB (+ dTail Des)	12	3	12	4	11	2	14	3	14	6	15	5

Table 8.17. Summary of desmin and aB crystallin sedimentation characteristics.

Summary of high (80,000g) and low (2,500g) speed sedimentation characteristics of WT and mutant desmin with aB crystallin at 22, 37 and 44°C. The top section shows pelleting % values for WT and mutant desmin when assembled alone. The middle section shows pelleting % values for WT and mutant desmin when co-assembled with aB crystallin. The bottom section shows pelleting % values for aB crystallin when co-assembled with WT or mutant desmin. Values significantly higher (red) or lower (blue) relative to WT desmin values are highlighted. Average (Ave) values and standard deviations (SD) were calculated from 4 experimental repeats. Producing the data in this table required 52 SDS-PAGE gels and >900 band quantifications.

CHAPTER 9: THE EFFECT OF IN VITRO ASSEMBLY CONDITIONS ON INTERMEDIATE FILAMENT PROPERTIES

AIM

Compare two distinct, previously published methods of *in vitro* filament assembly with respect to IF morphology, filament-filament interactions and filament interactions with aB crystallin. In addition, investigate the effects of pH of assembly on desmin filament morphology, filament-filament interactions and filament interactions with aB crystallin.

INTRODUCTION

Previously published *in vitro* IF assemblies have used two distinct methods of filament assembly (Perng et al., 1999b; Perng et al., 2004). Both assembly methods begin by unfolding the IF protein in 6M Urea buffer (6M Urea, 20mM Tris-HCl pH 8, 1mM DTT, 1mM EDTA, 0.2mM PMSF), then dialysing to reduce the Urea concentration to 4M, then 2M, then 0M over a period of 24h at 22°C. There are then two distinct methods of finalising filament assembly. The first method is used throughout this thesis to assemble desmin and involves slow dialysis into 20mM Tris-HCl pH 7.6 or 7.4, 50mM NaCl buffer at either 22, 37 or 44°C for 16h. In this chapter, this method will be referred to as the 'slow assembly' method. The second method of finalising filament assembly involves the instant addition of a 20-fold concentrated assembly buffer to give a final concentration of 100mM Imidazole-HCl pH 6.8, followed by incubated for 1h at 22, 37 or 44°C (Hayes et al., 2008; Perng et al., 2004). In this chapter, this method will be referred to as the 'fast assembly' method.

These methods differ in the buffer type and ionic strength ('20mM Tris, 50mM NaCl' vs '100mM Imidazole'), pH (7.6/7.4 vs 6.8) and speed of buffer exchange (slow dialysis vs instant addition). Both methods are used in the published literature (Hayes et al., 2008; Perng et al., 1999b; Perng et al., 2004; Sharma, 2011) to analyse filament assembly and subsequent filament-filament interactions and filament interactions with aB crystallin. It is therefore important to determine if the method of *in vitro* assembly itself will affect the outcome of such experiments. To investigate this, desmin was assembled using the 'fast assembly' method and then analysed by high and low speed sedimentations assays and TEM, to allow comparison with the 'slow assembly' method used in previous results chapters throughout this thesis.

In addition, in the earlier results chapter analysing desmin tail mutations, results suggested that filament-filament interactions and filament aggregation maybe affected by pH (Fig 8.6). In order to investigate this further, desmin was assembled (using the 'slow assembly' method only) at pH 8.0, 7.6, 7.2 or 6.8 and resulting filaments were analysed by sedimentation assays and TEM.

To quantify filament assembly and filament-filament interactions, two separate centrifugation assays were used as described in previous results chapters. Samples were centrifuged at either 80,000g for 30min (high speed assay) or 2,500g for 15min (low speed assay). The pellets and supernatants were separated and solubilised in equal final volumes of SDS-PAGE sample buffer to allow direct comparison of the proportions of material in the supernatant and pellet. Results were then visualised via SDS-PAGE and quantified by gel densitometry. The high speed assay measures filament assembly and aB crystallin binding to assembled filaments or aggregates, while the low speed assay measures filament-filament interaction and the ability of aB crystallin to prevent these filament-filament interactions. To assess the effect upon filament morphology, samples were analysed by TEM.

In this chapter, I show that method of *in vitro* filament assembly, including the assembly pH, can significantly affect desmin filament morphology and subsequent filament-filament interactions and filament interactions with aB crystallin.

RESULTS

Effect of assembly method on desmin filament sedimentation properties

Desmin was assembled using the 'fast assembly' method at 22, 37 or 44°C in the presence or absence of WT aB crystallin, and analysed by high and low speed sedimentation assays and SDS-PAGE. Fig 9.1 represents 1 of 3 experimental repeats, which were all quantified by gel densitometry, collated and averaged (Fig 9.2). These experiments were performed in collaboration with Scott Houck from Professor John Clark's lab at the University of Washington.

When desmin is assembled alone, there is no significant difference between the high and low speed sedimentation characteristics at 22, 37 or 44°C (Fig 9.2). These sedimentation characteristics are almost identical to those observed in a previous results chapter using the 'slow assembly' method (see Fig 8.11, far right triplicate). When aB crystallin is assembled with desmin, there is a temperature dependent increase in aB crystallin pelleting at both low and high speed, indicating filament binding (Fig 9.2). These characteristics are also similar to those observed in previous results chapters using the 'slow assembly' method (see Fig 7.13 and Fig 8.11, far left triplicates).

At high speed, >90% of desmin pellets at 22, 37 and 44°C in both the presence and absence of aB crystallin (Fig 9.1). At low speed, >80% of desmin pellets at 22, 37 and 44°C in absence of aB crystallin (Fig 9.1). However, in the presence of aB crystallin at low speed, 95% of desmin is pelleted at 22°C, whereas only 53% and 46% is pelleted at 37 and 44°C respectively (Fig 9.2, blue bars). At 22°C, there is no significant difference between desmin low speed pelleting in the presence and absence of aB crystallin. However, at 37 and 44°C, the addition of aB crystallin reduces desmin low speed pelleting from 80% to 53%, and 89% to 46% respectively (Fig 9.2, blue bars). This indicates that aB crystallin has caused a significant reduction in filament-filament interactions which reduces desmin filament aggregation, but this effect is temperature dependent.

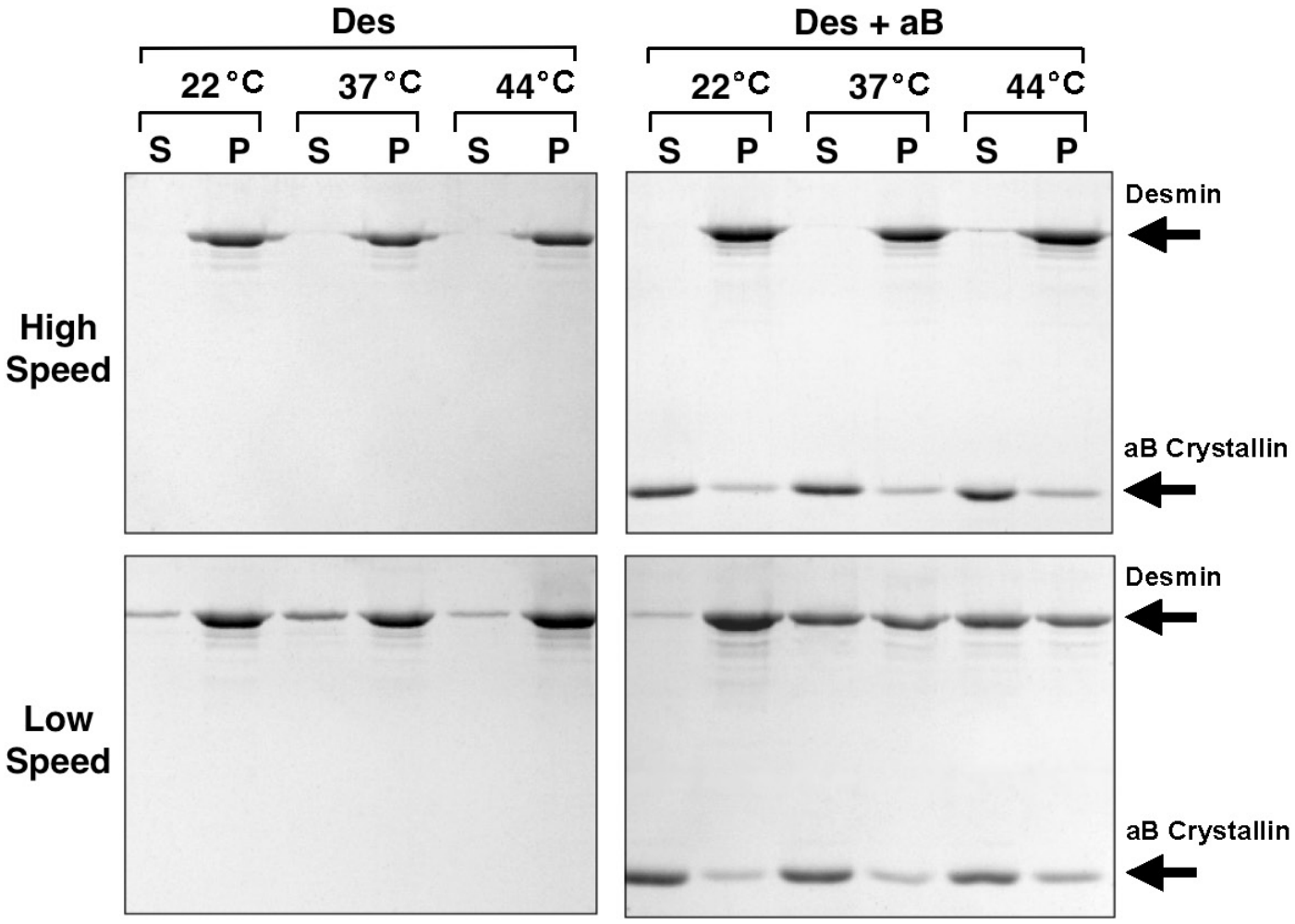

Fig 9.1. Sedimentation properties of desmin assembled using the 'fast assembly' method at 22, 37 or 44°C in the presence or absence of WT aB crystallin.

The low (2,500g, bottom two gels) and high (80,000g, top two gels) speed ssedimentation of desmin using the 'fast assembly' method at 22, 37 or 44°C in the presence or absence of WT aB crystallin, analysed by SDS-PAGE. The left hand gels show desmin assembled alone, and the right hand gels show desmin assembled with aB crystallin. The above gels represent 1 of 3 repeats. Supernatant (S) and pellet (P). These experiments were performed in collaboration with Scott Houck from the University of Washington.

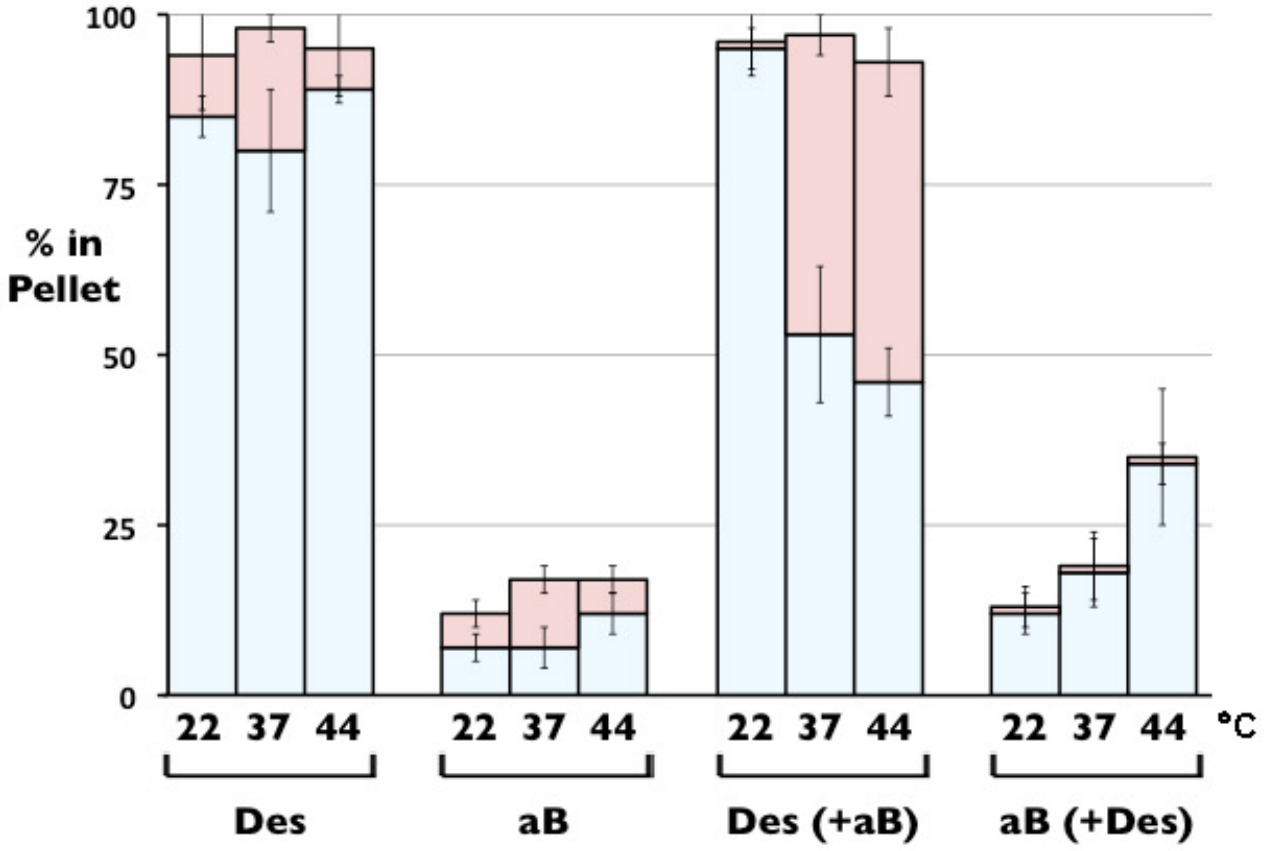

Fig 9.2. Quantification of sedimentation of desmin assembled using the 'fast assembly' method at 22, 37 or 44° C in the presence or absence of WT aB crystallin.

The bar chart shows the quantification of the low speed (blue) and high speed (red) sedimentation data for WT desmin assembled alone (Des), or in the presence of WT aB crystallin (Des (+aB)). The aB crystallin sedimentation is also shown for aB crystallin assembled alone (aB) and in the presence of desmin (aB (+ Des)). The amount of material pelleted is shown as a percentage of total material as quantified by gel densitometry. Average values and standard deviations were calculated from 3 experimental repeats. These experiments were performed in collaboration with Scott Houck from the University of Washington.

The desmin low speed sedimentation characteristics were compared for the 'fast assembly' (Fig 9.2, blue bars) and 'slow assembly' (earlier results chapter, Fig 8.10, far left triplicate) methods in both the presence and absence of aB crystallin, at 22, 37 and 44°C (Fig 9.3).

In the absence of aB crystallin, desmin pelleting is lower for 'slow assembly' than 'fast assembly' at all 3 temperatures (Fig 9.3), indicating reduced filament-filament interactions. In fact, assembling filaments via the 'slow assembly' compared to the 'fast assembly' method, reduces desmin low speed pelleting from 85% and 89%, to 26% and 16% at 22 and 44°C respectively (Fig 9.3). These data suggest that the 'fast assembly' method may result in filaments which are significantly more likely to self associate and aggregate.

In the presence of aB crystallin, the difference between 'slow assembly' and 'fast assembly' methods is even more apparent. The 'fast assembly' method results in desmin low speed pelleting of 95%, 53% and 46% at 22, 37 and 44°C respectively, compared to 'slow assembly' desmin pelleting of 9%, 9% and 11% at 22, 37 and 44°C respectively (Fig 9.3). These data suggest that the 'fast assembly' method may significantly impair the ability of aB crystallin to reduce filament-filament interactions and prevent filament aggregation.

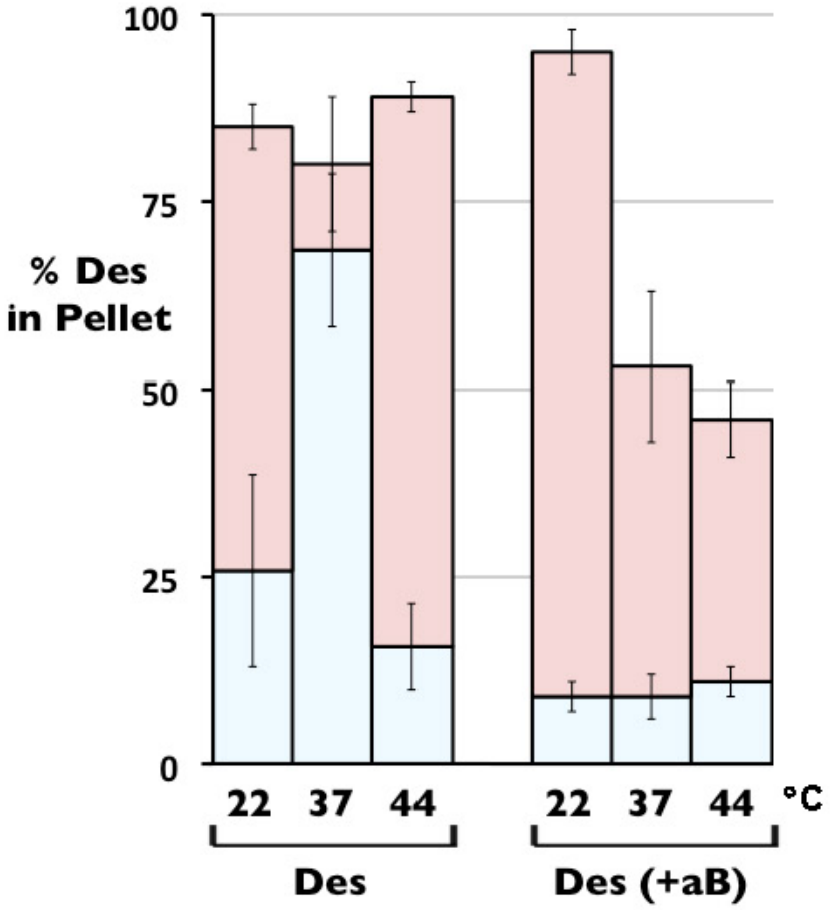

Fig 9.3. Comparison of desmin low speed sedimentation characteristics for 'slow assembly' and 'fast assembly'.

Comparison of desmin low speed (2,500g) sedimentation characteristics for 'slow assembly' (blue) and 'fast assembly' (red) in the presence or absence of aB crystallin at 22, 37 or 44°C. The amount of material pelleted is shown as a percentage of total material as quantified by gel densitometry. Average values and standard deviations were calculated from 3 experimental repeats.

Effect of assembly method on desmin filament morphology

To investigate if filament morphology is affected, desmin was assembled using either the 'fast assembly' or 'slow assembly' method at 22°C, and the resulting filaments were analysed by TEM (Fig 9.4). The filaments formed using the 'slow assembly' method appear as long, smooth ~10nm filaments, which do not aggregate. In striking contrast, the filaments formed using the 'fast assembly' method appear less elongated and appear to have associated into aggregates, which explains the 85% low speed pelleting (Fig 9.3).

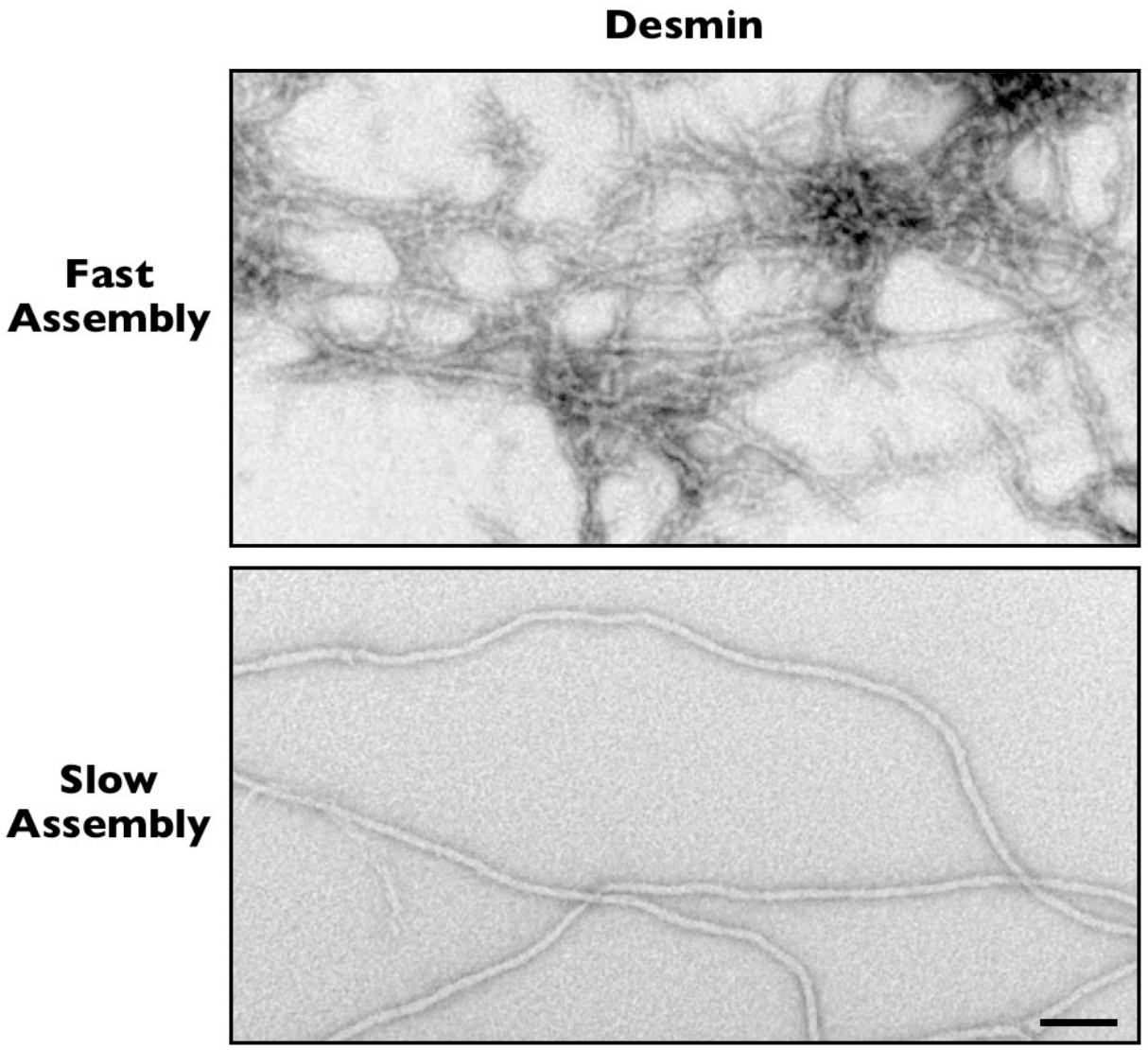

Fig 9.4. TEM comparison of 'slow assembly' and 'fast assembly' of desmin filaments.

Desmin was assembled using either the 'fast assembly' or 'slow assembly' method at 22°C and the resulting filaments were analysed by TEM. The filaments formed using the 'fast assembly' method appear less elongated and have associated into aggregates. In contrast, the filaments formed using the 'slow assembly' method appear as long, smooth ~10nm filaments, which do not aggregate. Scale bar represents 100nm.

Effect of pH on desmin filament sedimentation properties

To assess the effect of pH on desmin assembly and filament-filament interactions, desmin was assembled (using the 'slow assembly' method only) at pH 8.0, 7.6, 7.2, or 6.8 at 37°C in the presence or absence of WT aB crystallin, and analysed by high and low speed sedimentation assays and SDS-PAGE. Fig 9.5 represents 1 of 3 experimental repeats, which were all quantified by gel densitometry, collated and averaged (Fig 9.6).

At high speed, >85% of desmin is pelleted at all 4 pH values, in both the presence and absence of aB crystallin (Fig 9.6, red bars). This indicates that desmin can assemble at all 4 pH values.

Al low speed, in the absence of aB crystallin, 77%, 70%, 55% and 83% of desmin is pelleted at pH 8.0, 7.6, 7.2 and 6.8 respectively (Fig 9.6). Upon aB crystallin addition, the proportion of pelleted desmin does not change significantly at pH 7.2 or 6.8 with 51% and 92% pelleting. At pH 8.0, aB crystallin addition causes a small decrease in desmin low speed pelleting from 77% to 59%. However, most strikingly, at pH 7.6, aB crystallin addition reduces desmin low speed pelleting from 70% to 20%, without an significant change in high speed pelleting (Fig 9.6). This suggests that aB crystallin has caused a significant decrease in desmin filament-filament interactions and that this effect is highly pH dependent. However, there does not appear to be any significant change in aB crystallin pelleting, in the presence or absence of desmin, at any of the 4 pH values (Fig 9.6).

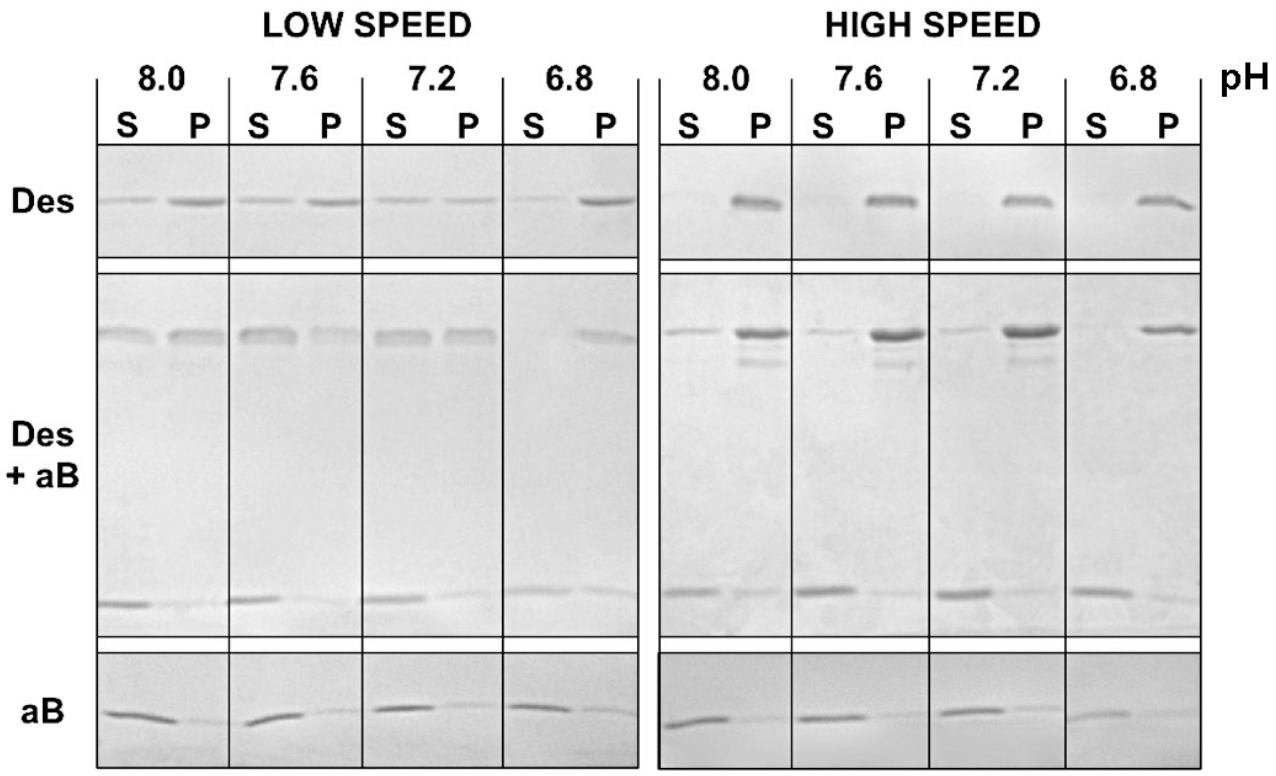

Fig 9.5. Sedimentation properties of desmin assembled at various pH at 37°C in the presence or absence of WT aB crystallin.

The low (2,500g) and high (80,000g) speed sedimentation of desmin assembled at pH 8.0, 7.6, 7.2, or 6.8 at 37°C in the presence or absence of WT aB crystallin, analysed by SDS-PAGE. The top gels show desmin assembled alone, the middle gels show desmin assembled with aB crystallin, and the bottom gels show aB crystallin assembled alone. The above gels represent 1 of 3 repeats. Supernatant (S) and pellet (P).

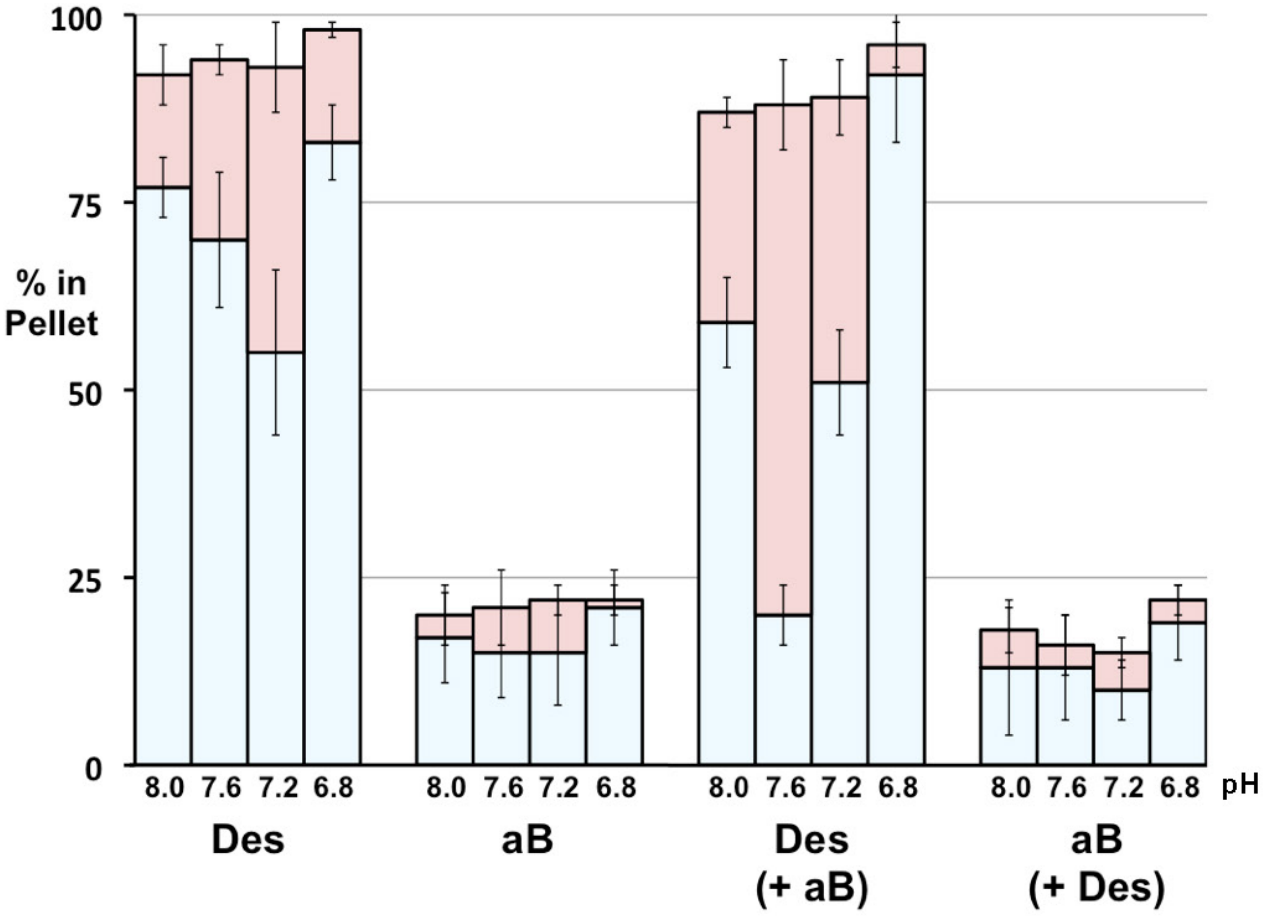

Fig 9.6. Quantification of sedimentation of desmin assembled at various pH at 37°C in the presence or absence of WT aB crystallin.

The bar chart shows the quantification of the low speed (blue) and high speed (red) sedimentation data for WT desmin assembled alone (Des), or in the presence of WT aB crystallin (Des (+aB)). The aB crystallin sedimentation is also shown for aB crystallin assembled alone (aB) and in the presence of desmin (aB (+ Des)). At 37°C, at pH 8.0, 7.2 and 6.8 aB crystallin does not significantly reduce filament-filament interactions. However, at pH 7.6 aB crystallin reduces desmin pelleting from 70% to 20%. This suggests that pH may play an important role in the interaction between sHsps and IFs. The amount of material pelleted is shown as a percentage of total material as quantified by gel densitometry. Average values and standard deviations were calculated from 3 or 4 experimental repeats.

Effect of pH on desmin filament morphology

To assess the effect of pH on desmin filament morphology, desmin was assembled at pH 8.0, 7.6 or 6.8 at 37°C, in the presence or absence of aB crystallin, and analysed by TEM (Fig 9.7).

At pH 7.6 and 6.8, in both the presence and absence of aB crystallin, desmin appears to form long, smooth, constant width 10nm filaments (Fig 9.7, top and middle rows). At pH 7.6, filaments in the presence of aB crystallin appear indistinguishable from those formed in the absence of aB crystallin (Fig 9.7, middle row, compare left and right image), despite significantly increased tendency to aggregate at low speed (70% compared to 20%) (Fig 9.6, blue bars). Furthermore, filaments formed in the presence of aB crystallin at pH 6.8 appear indistinguishable from those formed in the presence of aB crystallin at pH 7.6, despite dramatically increased sedimentation at low speed (83% compared to 20%).

At pH 8.0, in the absence of aB crystallin, desmin appears to form filament fragments which have aggregated into large structures (Fig 9.7, bottom left). These structures, formed at pH 8.0, are dramatically different from the smooth ~10nm filaments formed at pH 7.6 (Fig 9.7, middle row, left), illustrating the pH sensitivity of desmin filament formation. Interestingly, at pH 8.0, the addition of aB crystallin appears to improve morphology such that the filament fragments appear longer and more filamentous (Fig 9.7, bottom row, compare left and right image).

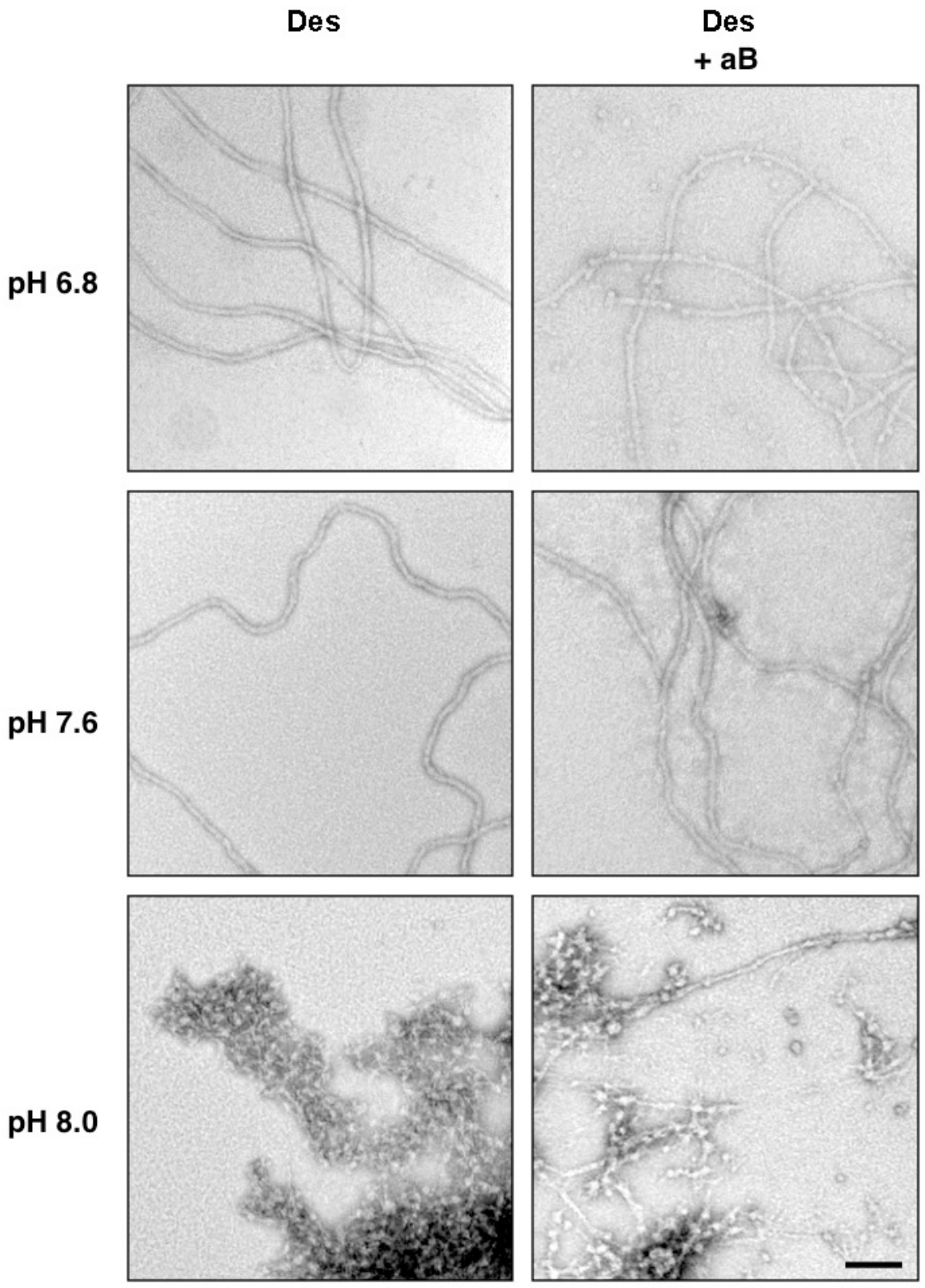

Fig 9.7. TEM analysis of desmin assembled at pH 8.0, 7.6 or 6.8 at 37°C in the presence or absence of aB crystallin.

Scale bar represents 100nm.

Additional pH effects

It is worth noting that pH sensitivity of filament formation can also be observed for beaded filaments assembled *in vitro* from recombinant human BFSP1, BFSP2 and aB crystallin (see supplementary data, Sup Fig 9). At pH 7.6 the BFSPs assemble into ~5-6nm filaments, but at pH 6.8 and 8.0, the morphology changes dramatically and aggregates appear to form (Sup Fig 9).

It is also worth noting that WT aB crystallin was analysed to determine if pH values 8.0, 7.6, 7.2 and 6.8 would affect protein stability. Differential scanning fluorimetry was used to analyse aB crystallin at the 4 pH values and no difference in thermostability was detected, in the buffer conditions used (see supplementary data, Sup Fig 10).

RESULTS SUMMARY

Overall, data in this chapter suggests that, when desmin is assembled alone, the 'fast assembly' method may result in filaments which are significantly more likely to self associate and aggregate, compared to filaments assembled using the 'slow assembly' method. The 'fast assembly' method may also significantly impair the ability of aB crystallin to reduce filament-filament interactions and prevent filament aggregation. In addition, filaments formed using the 'fast assembly' method appear less elongated and appear to have associated into aggregates.

Data in this chapter also suggests that pH may play an important role in desmin filament assembly, filament-filament interactions and the interaction between desmin filaments and aB crystallin. In addition, these data suggest that the ability of aB crystallin to prevent desmin filament-filament interactions maybe pH dependent.

CHAPTER 10: DISCUSSION

THE R107G MUTATION IN Hsp16.5 DOES NOT AFFECT STRUCTURE OR CHAPERONE ACTIVITY IN VITRO

The R120G aB crystallin mutation causes cataract and myopathy in humans (Vicart et al., 1998). R120G aB crystallin itself forms protein amyloid (Meehan et al., 2007), which inhibits the proteasome (Chen et al., 2005) and induces autophagy (Tannous et al., 2008). In addition, proteasome inhibition causes accumulation of aB crystallin into aggresomes (Ito et al., 2002) which can cause IF aggregation (Bardag-Gorce et al., 2004). The mutation also causes mitochondrial toxicity (Maloyan et al., 2005) and a state of reductive stress (Bova et al., 1999; Gupta and Srivastava, 2004; Rajasekaran et al., 2007; Treweek et al., 2005). The mutation, which alters the charge within the conserved a-crystallin domain, reduces chaperone activity and causes formation of larger, more polydisperse oligomers (Bova et al., 1999). Studies have also shown that R120G aB crystallin causes increased desmin and vimentin filament binding, increased filament-filament interactions and subsequently, filament aggregation (Perng et al., 1999b; Perng et al., 2004; Song et al., 2008; Vicart et al., 1998). In patients, R120G aB crystallin induces DRM and muscle fibres contain aggregates of desmin and R120G aB crystallin (Vicart et al., 1998) and muscle cell lines transfected with R120G aB crystallin cDNA form intracellular aggregates containing both desmin and R120G aB crystallin. In a mouse model, R120G aB crystallin induces cardiomyopathy and autophagy (Tannous et al., 2008). Interestingly, despite the inherent instability of R120G aB crystallin (Meehan et al., 2007; Treweek et al., 2005), the pathology is aB crystallin and desmin aggregates, rather than aB crystallin-only aggregates, demonstrating the crucial importance of the sHsp-IF interaction (Vicart et al., 1998).

Studies have shown that aB crystallin oligomers are polydisperse and in dynamic equilibrium with sub-assembly species (Aquilina et al., 2003; Bloemendal et al., 2004; Haley et al., 2000; Haley et al., 1998; Horwitz, 2008; McHaourab et al., 2009), making crystallisation of the full length protein unattainable to date. Therefore, at the time of undertaking the studies in this thesis, it was not known how or why the R120G mutation affected the structure of aB crystallin, and how this altered structure might lead to altered IF interactions, and disease. Indeed, it has been suggested that the R120 residue may lie in an IF binding domain (Ghosh et al., 2007b). Understanding the structural effects of the R120G aB crystallin mutation may

provide insight into the sHsp-IF interaction (which is altered by the mutant) and the potential mechanisms which lead to disease.

At the undertaking of the studies in this thesis, there was no published crystallographic data available for aB crystallin or any of its domains. In addition, the role of the Arginine residue, which is highly conserved throughout sHsps (Kim et al., 1998), was unknown. However, a crystal structure was available for the sHsp Mj Hsp16.5, as discussed in the introduction of this thesis. Therefore, I worked with the crystallographer Ehmke Pohl and produced and re-crystallised the sHsp Mj WT Hsp16.5, improving the resolution (2.5Å) compared to the previously published crystal structure (Van Montfort et al., 2001b). We can confirm that the Mj Hsp16.5 assembles into a 24-subunit hollow sphere with eight triangular and six square pores arranges in octahedral symmetry, as previously described (Van Montfort et al., 2001b). I then produced the R107G Hsp16.5 mutant, an equivalent to R120G aB crystallin, and we crystallised the mutant protein (2.9Å), to allow analysis of the structural changes caused by the mutation.

Surprisingly, I found that the R107G mutation in Hsp16.5 did not cause any structural changes. The mutation was confirmed by mass spectrometry and was clearly visible in structural models produced from the crystallisation data, confirming the presence of the R107G mutation. The high quality resolutions we collected for both WT and R107 Hsp16.5 (2.5 and 2.9Å, respectively) confirm that the proteins are isostructural, and that the R107G mutation in Hsp16.5 does not have any detectable structural effects. Further investigation also showed that, unlike the R120G aB crystallin mutation, the R107G Hsp16.5 mutation does not appear to affect *in vitro* chaperone activity.

These data were initially surprising, but the very recent crystallisation of the a-crystallin domain (ACD) from R120G aB crystallin (Clark et al., 2011) provides insight into important structural differences between Hsp16.5 and aB crystallin. In Hsp16.5, dimer formation requires ACD b2 and b6 strand exchange between monomers (Van Montfort et al., 2001b). However, in animals, there are fewer residues between strands b5 and b7, causing the b6 strand to become part of the b7 strand, forming the 'b6+7' strand (Clark et al., 2011). The highly conserved arginine residue (R120 in human aB crystallin) lies in the b6+7 strand and forms an interchain ion pair with a conserved aspartic acid (R120–D109 in human aB crystallin), helping to form a hydrophobic groove created by the b4 and b8 strand edges at the

dimer interface (Bagneris et al., 2009; Laganowsky et al., 2010; Laganowsky and Eisenberg, 2010). However, the disease causing R120G (and D109H) aB crystallin mutations both remove the R120-D109 ion pair and cause formation of a pair of salt bridges between H83 and D80, not seen in WT aB crystallin, which causes closure of the hydrophobic b4-b8 groove (Clark et al., 2011).

Therefore in humans, dimer formation occurs when monomers exchange the b6+7 strand, which contains the R120 residue, and mutating this residue affects an important interchain ion pair with D109. However, Hsp16.5 dimer formation requires b2 and b6 strand exchange, not the b7 strand, which contains the R107 residue. In fact, in the Hsp16.5 crystal structure, no intra- or inter-chain interactions were predicted for the R107 residue.

The altered dimer formation caused by the R120G mutation in aB crystallin is thus predicted to effect the oligomer, which may affect subunit dynamics and availability of substrate binding sites, leading to altered chaperone activity and altered IF interactions. Indeed, the mutation has been shown to cause formation of larger, more polydisperse oligomers with reduced chaperone activity and increased IF binding (Bova et al., 1999; Perng et al., 2004). In contrast to the R120 residue in aB crystallin, the R107 residue of Hsp16.5 is not predicted to play the same essential role in dimer formation, and indeed we confirm that the R107G mutation does not affect the Hsp16.5 protein structure. These data suggest that even highly conserved residues may have dramatically different structural roles within different sHsps.

This poses the question of why the arginine residue in the ACD is so highly conserved throughout sHsps. Data in this thesis suggests that R107G Hsp16.5 has chaperone activity comparable to WT Hsp16.5. However, only one substrate was tested (citrate synthase) and sHsp mutations have previously been shown to cause increased *in vitro* chaperone activity for one substrate, yet decreased chaperone activity for another (Hayes et al., 2008). In addition, the chaperone assay was performed at 44°C, but the archaeon *Methanococcus jannaschii* (Mj) is a hyperthermophile and lives in hyperthermal oceanic vents, which experience temperatures of ~50-95°C. Previous studies have shown that the sHsp oligomer:subunit equilibrium (Aquilina et al., 2003; Aquilina et al., 2005; Bova et al., 2000) is shifted to favor smaller subunits at elevated temperature (Giese and Vierling, 2002; Stromer et al., 2004; Van Montfort et al., 2001a; Van Montfort et al., 2001b; Wintrode et al., 2003) and that rate of subunit exchange increases with temperature (Friedrich et al., 2004). In addition, regulation of

chaperone activity by subunit exchange dynamics has been reported for a range of sHsp, for example, human aB crystallin (Liu et al., 2006c), bovine a-crystallin (Srinivas et al., 2005), human Hsp27 (Shashidharamurthy et al., 2005), mycobacterium Hsp16.3 (Fu et al., 2003) and synechocystis Hsp16.6 (Giese and Vierling, 2002). Therefore, although the R107 Hsp16.5 mutant showed comparable chaperone activity to WT Hsp16.5 at 44°C, at elevated temperatures the mutation may alter subunit dynamics and uncover differences in chaperone activity between these proteins. However, the role of this conserved arginine in Hsp16.5 remains to be determined.

THE C-TERMINAL TAIL OF Hsp16.5 AFFECTS OLIGOMERISATION AND CHAPERONE ACTIVITY IN VITRO

The myopathy causing Q151X aB crystallin (Selcen and Engel, 2003) removes the entire C-terminal tail and despite its inherent instability (Hayes et al., 2008), the muscle pathology is aB crystallin and desmin aggregates, rather than aB crystallin-only aggregates, further demonstrating the critical importance of the sHsp-IF interaction. In fact, the Q151X mutation has been shown to cause increased interactions with IFs (Hayes et al., 2008). Studies of Q151X may thus provide further insights into the sHsp interaction with IFs.

As previously discussed, at the time of undertaking the studies in this thesis, there was no published crystallographic data available for aB crystallin or any of its domains. Therefore, it was not confirmed how or why the Q151X mutation affected the structure of aB crystallin, and how this altered structure might lead to altered IF interactions, and subsequent disease. Previous studies have shown that the Q151X is unable to oligomerise (Hayes et al., 2008) and it has been suggested that loss of the conserved C-terminal IXI motif prevents the aB crystallin higher order assembly (Pasta et al., 2004). Indeed, crystal structures for both Mj Hsp16.5 and Ta Hsp16.9 show that the oligomers are stabilised by the C-terminal IXI motif (Kim et al., 1998; Van Montfort et al., 2001b). In Hsp16.5 and Hsp16.9, the IXI motif of one subunit interacts with a hydrophobic groove created by the b4 and b8 strand edges of the a-crystallin domain of another subunit, which allows higher order oligomer formation (Kim et al., 1998; Van Montfort et al., 2001b).

Understanding the structural effects of the Q151X aB crystallin mutation may provide insight into the sHsp-IF interaction (which is altered by the mutant) and the potential mechanisms which lead to disease. In the absence of atomic level structural data for aB crystallin, Hsp16.5 was used to model the Q151X mutation and analyse any structural effects. I therefore produced the I140X Hsp16.5, a mutant equivalent to Q151X aB crystallin. I also produced the G143X Hsp16.5, which is truncated just before the IXI motif, to allow investigation into the structural effects of removing this highly conserved domain. In collaboration with Ehmke Pohl, I then crystallised the mutant proteins, to allow analysis of the structural changes caused by the mutations.

The I140X and G143X Hsp16.5 proteins formed crystals and X-ray diffraction showed altered unit cell dimensions and a potentially altered space group, compared to the WT

Hsp16.5. This may indicate a possible change in overall structure, but the resolution (~4Å) of the data is not high enough to verify this intriguing possibility. Analysis of our WT Hsp16.5 crystal data suggest that the I140X and G143X Hsp16.5 mutants remove backbone hydrogen bonds at residues N145 and E147, which may be involved in intersubunit contacts. The I140X Hsp16.5 truncation also removes the side chain interactions between K141-E78 and backbone hydrogen bond at residues K142. However, despite my efforts of purifying and attempting to crystallise both the I140X and G143X proteins on more than 10 separate occasions, I could not obtain crystals that provided the diffraction resolution necessary to confirm the potential structural changes.

Throughout the I140X and G143X Hsp16.5 purifications, I found that the these C-terminal truncations had dramatically altered purification characteristics and were difficult to separate from contaminating proteins, perhaps suggesting increased binding to the contaminating 'substrate' proteins. Indeed, previous studies have shown that the Q151X aB crystallin also shows increased substrate binding (Hayes et al., 2008). The C-terminal IXI motif may regulate the accessibility of the b4-b8 substrate binding site and mutations which remove or disturb the IXI domain may result in constantly exposed hydrophobic surfaces at the b4-b8 groove, which could increase interactions with substrates. This may explain the difficulty in purifying the I140X and G143X Hsp16.5 proteins, as described in the results chapter. During the I140X and G143X Hsp16.5 purifications, I also observed dramatically reduced solubility, even though the proteins are thermostable at 80°C for 30 minutes. Interestingly, the Q151X aB crystallin also shows dramatically reduced protein solubility with only slightly decreased thermostability (Hayes et al., 2008). Thermostability is a function of the protein's secondary structure and folding state, whereas sHsp solubility has been suggested to depend upon the presence of the polar and highly flexible C-terminal tail (Carver et al., 1992; Hayes et al., 2008; Jiao et al., 2005). These observations with the I140X and G143X Hsp16.5 proteins support the role of the C-terminal tail in sHsp solubility.

Previous studies have suggested that Mj Hsp16.5 oligomer formation requires the C-terminal IXI motif of one dimer to interact with the b4 and b8 hydrophobic groove of another dimer (Kim et al., 1998). Indeed, I found that G143X Hsp16.5, which lacks the IXI motif, was unable to oligomerise and only formed dimers, as determined by analytical SEC. In addition, these results also confirm that Hsp16.5 dimer formation does not require the C-terminal tail. I also found the I140X and G143X Hsp16.5 mutations to cause significantly increased

chaperone activity *in vitro* (~2 fold increase), compared to WT Hsp16.5. Similarly, the Q151X aB crystallin, which is also unable to oligomerise, has been shown to cause a ~7 fold increase in chaperone activity for citrate synthase *in vitro*, relative to WT aB crystallin (Hayes et al., 2008). The decreased oligomerisation and increased chaperone activity of G143X Hsp16.5 reported in this thesis is consistent with previous studies in which no correlation between complex assembly and chaperone activity is observed for aA or aB crystallin mutants (Ghosh et al., 2006a; Ghosh et al., 2006b; Hayes et al., 2008; Raju et al., 2011; Saha and Das, 2004). WT aB crystallin and the del41-58 deletion mutant have similar chaperone activities but different complex sizes, while the del41-58 and del155-165 aB crystallin mutants have different chaperone activities but similar complex sizes (Ghosh et al., 2006d). In another example, CEb3 aB crystallin oligomer size is comparable to WT aB crystallin but chaperone activity for ADH and b-crystallin is reduced by 30% and 40% respectively (Ghosh et al., 2006b). Furthermore, in the absence of both N- and C-termini, the ACD retains significant chaperone activity but is unable to oligomerise (Feil et al., 2001). The G143X Hsp16.5 data presented in this thesis support the theory that chaperone activity is not dependant upon oligomer assembly and is not correlated with oligomer size.

In both aB crystallin and Hsp16.5, the C-terminal tail appears to act as a cap on the hydrophobic groove created by the b4 and b8 strand edges of the a-crystallin domain, binding via the conserved IXI motif to allow oligomerisation. Truncation of the C-terminal tail removes the IXI motif from the hydrophobic groove, which prevents oligomerisation and exposes the hydrophobic substrate binding groove. This appears to increase substrate binding and enhance chaperone activity, but without the hydrophilic C-terminal tail, protein solubility is greatly reduced. The increased chaperone activity of G143X and I140X Hsp16.5 and Q151X aB crystallin may therefore be due to an increase in the number of sites available for client protein binding due to the loss of sHsp oligomerisation. The I140X and G143X Hsp16.5 data presented in this chapter therefore support the theory that destabilisation and loss of solubility, rather than loss of chaperone activity, may be the major factor in sHsp C-terminal mutant disease development. However, as previously discussed, the Q151X aB crystallin muscle pathology is aB crystallin and desmin aggregates, rather than aB crystallin-only aggregates, further demonstrating the critical importance of the sHsp-IF interaction (Hayes et al., 2008). Further details of the structural changes which occur upon C-terminal tail mutations and IXI motif truncations may provide insight into the differences observed *in vitro* and *in vivo*.

The human cataract causing D140N aB crystallin point mutation (Liu et al., 2006e) substitutes a negative charged aspartic acid by a neutral asparagine residue at codon 140 within the highly conserved a-crystallin domain. The charged aspartic acid residue at position 140 is conserved in many different species of mammals and other vertebrates (Avivi et al., 2001) which suggests an important role in maintaining the structure and functions of aB crystallin. It has also been reported that maintenance of the net charge is critical for the chaperone activity of a-crystallins and site-directed mutation studies have suggested that chaperone activity of a-crystallins will be affected whenever charged residues are mutated (Plater et al., 1996).

The D140 residue lies between the b8 and b9 strands, and is not predicted to be involved in oligomer formation (Ghosh and Clark, 2005). Indeed, results in this thesis show that D140N aB crystallin oligomers are comparable to WT aB crystallin in both average size (~28 subunits) and polydispersity, as shown by analytical SEC. However, it has been suggested the D140N mutation may affect a putative intermolecular salt bridge with R56 in the N-terminal region (Jehle et al., 2011). This could affect oligomer subunit dynamics and chaperone activity and thus affect interactions with IFs. The pathology of the D140N mutation is restricted to the lens, yet aB crystallin is highly expressed in muscle tissue. This suggests that tissue specific interactions of aB crystallin may underlie the disease phenotypes. The D140 residue may be important for interactions with the lens specific BFs, which are not present in muscle. The D140 residue of a-crystallins was conserved through evolution (de Jong et al., 1984) which suggests this residue has a critical function *in vivo*.

In a previous study, Liu et al. 2006 reported the D140N mutation to cause alterations in tertiary structure and surface hydrophobicity causing lower thermal stability and a significant loss of chaperone activity (Liu et al., 2006e). It was also reported that the D140N mutant behaves as a dominant negative which inhibits the chaperone activity of WT aB crystallin (Liu et al., 2006e). Liu et al. 2006 proposed that an altered tertiary and quaternary structure in D140N results in reduced chaperone activity and thermostability which underlies the molecular mechanisms of the cataractogenesis (Liu et al., 2006e). However, the findings presented in this thesis suggest that D140N aB crystallin retains chaperone activity *in vitro*, even surpassing the protection of WT aB crystallin for the tested client proteins. Such a

situation has been observed previously for the myopathy causing Q151X and 464delCT aB crystallins and the cataract causing 450delA aB crystallin, which all show significantly increased chaperone activity for some substrates *in vitro* (Hayes et al., 2008), compared to WT aB crystallin. Hayes et al., 2008 suggested altered interaction with IFs, rather than loss of chaperone function, as a possible mechanism of the disease phenotype. Indeed, it may be the case the D140N causes altered interactions with the lens specific beaded filaments, which could explain the lack of a muscle phenotype.

I also found the D140N mutant aB crystallin was only slightly less thermostable than the WT aB crystallin. I found both WT and D140N aB crystallin retained solubility at 65°C for 80 minutes, while Liu et al. 2006 found D140N aB crystallin to aggregate after only 12 minutes under these conditions, while WT aB crystallin remained soluble (Liu et al., 2006e). It is important to note that heat stability is a function of the protein's secondary structure and folding state, while chaperone activity is primarily a function of factors at the tertiary and quaternary levels of organisation (Carver and Lindner, 1998). Indeed, CD data in this thesis shows that D140N aB crystallin has a slight loss of secondary structure which would be expected to cause a slight decrease in thermostability.

It is important to consider that experiments in this thesis used identical extraction and purification methods for both WT and D140N aB crystallin. Both proteins were extracted from the soluble fraction and purified via ion exchange and size exclusion chromatography, without any denaturation of the protein. In contrast, Liu et al. 2006 extracted the D140N aB crystallin protein from insoluble inclusion bodies and purified the protein under denaturing conditions, after which the protein was refolded. This may account for the differences being observed in chaperone activity and thermostability. If D140N aB crystallin failed to refold correctly this could affect oligomerisation. Indeed, Liu et al. 2006 observed large alterations in D140N tertiary and quaternary structure and found the mutant to assemble into larger oligomers than the WT aB crystallin. In contrast, the D140N analysed in this study was not denatured at any point during extraction or purification and no change in oligomer size was detected.

Therefore, I suggest that D140N cataractogenesis may not be caused by lowered chaperone activity or lower thermostability, but may involve another mechanism, for example, altered interactions with IFs. The pathology of the D140N mutation is restricted to the lens, yet aB

crystallin is highly expressed in muscle tissue. However, D140N may be more rapidly degraded in muscles, which have active proteolytic systems, which could prevent a muscle phenotype. aB crystallin has been shown to interact with a ubiquitin ligase component and stimulate protein ubiquitination (den Engelsman et al., 2003) suggesting a role for aB crystallin in the ubiquitin proteosome pathway (Hoffman, 2003). Protein aggregate formation impairs the function of the ubiquitin-proteosome system (Bence et al., 2001) and results in the accumulation of aB crystallin in aggresomes (Ito et al., 2002) along with IFs. It may be that the active proteolytic systems in muscles are able to effectively degrade the mutant D140N thus preventing a phenotype, while in the lens the mutant results in protein aggregation. In muscle, the effects of D140N aB crystallin may also be inhibited by chaperone proteins such as HSP27 (Ito et al., 2003) or the presence of IF networks (Perng et al., 2004). Alternatively, the D140N aB crystallin mutation may affect interactions with the lens specific BFs, which are not present in muscle. Indeed, there may be multiple specific conditions which cause the D140N aB crystallin mutation to result in a lens only phenotype. Transient transfection of the mutants and into MCF7 cells, where there is no endogenous aB crystallin, may provide further insight into the mechanisms by which D140N aB crystallin causes disease.

BFs are essential to lens optical properties (Alizadeh et al., 2003, 2004; Alizadeh et al., 2002; Sandilands et al., 2003; Sandilands et al., 2004). They are thought to contribute to the highly specialised cellular organisation of fibre cells (Augusteyn, 2007; Maddala et al., 2011) and the precise alignment of fibre cell membranes which minimises intercellular spaces and maintains the high refractive index of the lens (Michael et al., 2003). Cytoplasmic protein concentrations in the lens are extremely high (>300 g/l) (Bloemendal et al., 2004) and protein crowding must be regulated by chaperones to preventing aggregation (Ellis and Minton, 2006). It has been suggested that BF may help to stabilise these high protein concentrations through interactions with protein chaperones (Song et al., 2009). Indeed, *in vivo* BFs are found with 12-15nm a-crystallin 'beads' extensively bound along their length (FitzGerald and Casselman, 1991; Maisel and Perry, 1972). sHsps interaction has been demonstrated for all IF proteins *in vitro* and *in vivo*, but the interaction with BFs is unusual because a-crystallin association is so extensive that the 5-6nm BFSP1 and BFSP2 filament backbone (Goulielmos et al., 1996; Merdes et al., 1993) is almost completely obscured (Carter et al., 1995; Quinlan et al., 1996). The reasons for this unusual interaction of BFs and a-crystallin and the subsequent functional significance are unknown, but understanding this interaction may provide important insight into the sHsp-IF interaction.

Before analysing the interaction with sHsps, it is important understand the interaction of BSFP1 and BFSP2, which co-assemble to form the filament backbone, potentially providing a scaffold for a-crystallin (Song et al., 2009). However, the assembly mechanism of BFSP1 and BFSP2 to form the 5-6nm BFs (Goulielmos et al., 1996; Merdes et al., 1993) is unknown. Furthermore, the impact of the different domains of the BFSP1 and BFSP2 proteins to filament properties has yet to be analysed in detail, and will likely be critical to a-crystallin association.

In all mammals and birds, BFSP2 and keratin 19 are the only IF proteins which lack a C-terminal tail domain (Sawada et al., 1995; Stasiak and Lane, 1987). In contrast, teleost fish Bfsp2 proteins are predicted to have a C-terminal tail domain (Binkley et al., 2002). Zebrafish have a single *bfsp2* gene which is in contrast to other single copy mammalian genes which are duplicated in zebrafish due to a genome wide duplication event (Postlethwait et al., 2004).

bfsp2 expression has been confirmed in the zebrafish lens using a polyclonal antibody generated to residues 407-419 common to both splice variants (Landsbury et al., awaiting publication). The functional significance of this unusual 'tailed' BFSP2 protein was unknown, and it is clear that analysis may provide insight into BF assembly and the BFSP protein domains which contribute to BF filament properties. Therefore, I analysed the tailed zebrafish WT Bfsp2 protein in comparison with a C-terminally truncated (CT) 'tail-less' zebrafish BFSP2 and also with human WT BFSP2, which lacks a C-terminal tail (Sawada et al., 1995). Both BFSP1 and its 53kDa fragment (53k) (Masaki and Quinlan, 1997; Quinlan et al., 1992; Wang et al., 2009) have been shown to be competent assembly partners of BFSP2, forming 5-6nm filaments (Carter et al., 1995; Goulielmos et al., 1996; Song et al., 2009). However, since the cDNA was not available for zebrafish *bfsp1* or *bfsp1-53k*, native bovine BFSP1 and its 53kDa fragment were selected as surrogate assembly partners for the recombinantly produced Bfsp2 proteins. The protein assembly properties and subsequent filament properties were analysed to determine the role of both the BFSP2 and BFSP1 C-terminal tails.

Data in this thesis shows that the zebrafish C-terminal tail greatly increases BFSP2 solubility, and removal of the tail causes the protein to aggregate. Indeed, It has previously been shown that bovine BFSP2 forms filamentous structures that have a strong tendency to self associate and then aggregate (Carter et al., 1995). Interestingly, when assembled with bovine 53k, the zebrafish C-terminal tail changes filament properties, such that filament-filament interactions are reduced and filaments are much less likely to aggregate. In addition, my data shows that the BFSP1 C-terminal tail reduces filament-filament interactions and prevents aggregation when a tail-less Bfps2 is the assembly partner. Previous studies on the IFs vimentin, keratin 14 and desmin have suggested that the C-terminal tail may play an important role in filament-filament interactions (Bar et al., 2010; Bousquet et al., 2001; Lin et al., 2010), but the mechanism remains to be determined.

Unlike the N-terminal head domain, the C-terminal tail domain of IFs is not thought to be required for filament assembly. Indeed, I found that truncating the C-terminal tail from zebrafish BFSP2 did not prevent assembly with either bovine BFSP1 or 53k. These data further demonstrate the flexibility tolerated in domain structure when it comes to the *in vitro* assembly of BF proteins (Perng et al., 2007; Wallace et al., 1998). However, type III IF proteins contain a RDG-motif in the C-terminal tail domain and this feature is partially present in zebrafish Bfsp2 tail (426-TDG-428), perhaps suggesting a role in filament

assembly. Indeed, my data also clearly shows that when assembled with BFSP1 or 53k, the zebrafish C-terminal tail plays an important role in regulation of the filament width. Data in this thesis on desmin assembly also clearly shows that the C-terminal tail plays an important role in filament width control. In addition, previous studies with vimentin have also implicated the IF C-terminal tail in regulation of filament width (Herrmann et al., 1996). However, since BFs are co-assembled using two different proteins, there will be fundamental differences compared to assembly of vimentin or desmin. In addition, my data suggests that BFs may be capable of forming from a range of different BFSP1:BFSP2 ratios, a feature of BFs which has also been observed previously (Merdes et al., 1993) and adds to the complexity of the BF assembly mechanism.

Data in this thesis suggests that for BFs assembled *in vitro*, filament-filament interaction and aggregation is reduced if a C-terminal tail is present on either BFSP1 or Bfsp2. The lack of a BFSP2 C-terminal tail in mammals and birds, which reduces BFSP2 protein solubility, may be compensated for by the C-terminal tail of its assembly partner BFSP1, which reduces filament-filament interactions and prevents aggregation. For zebrafish, the ENSEMBL database was updated in July 2011 (after completion of the experimental work in this thesis) to include the zebrafish *bfsp1* transcript (ENSEMBL: ENSDART00000114655). Interestingly, the Zf Bfsp1 protein is predicted to possess a C-terminal tail domain much shorter than its mammalian orthologues, truncated by some 50 residues (~4.5kDa). Therefore, it maybe the case that in zebrafish, it is the C-terminal tailed Bfsp2 which reduces filament-filament interactions and prevents aggregation, rather than Bfsp1. Further characterisation of the zebrafish lens specific cytoskeleton will be required to fully understand these differences.

MUTATIONS IN BFSP2 CAN AFFECT BEADED FILAMENT MORPHOLOGY

In the mammalian lens, BFs are essential to lens optical properties (Alizadeh et al., 2003, 2004; Alizadeh et al., 2002; Sandilands et al., 2003; Sandilands et al., 2004), ensuring the correct cellular organisation and optimal plasma membrane profiles of the lens fiber cells (Perng et al., 2007; Song et al., 2009). BFs may also potentially interact with protein chaperones to help stabilise the high protein concentrations required for the high refractive index of the lens (Bloemendal et al., 2004). The potential roles of BFs has been discussed previously in this thesis, including the unusual interaction with the sHsp, a-crystallin. Indeed, BFs may be involved in the mechanism by which the previously discussed D140N aB crystallin causes disease.

BFs are composed of the IF proteins BFSP1 and BFSP2 (Masaki and Watanabe, 1992; Sawada et al., 1995), and mutations in these proteins can cause cataract (Conley et al., 2000; Jakobs et al., 2000; Ma et al., 2008; Ramachandran et al., 2007). The R287W BFSP2 mutation, which lies at the start of the L2 linker, causes cataract in humans (Conley et al., 2000; Ma et al., 2008) and the E233del BFSP2 mutation, which lies in the 1b helix, causes cataract and myopia in humans (Cui et al., 2007; Jakobs et al., 2000; Zhang et al., 2004). However, to date, no studies have been done to determine the effect of these BFSP2 mutations on BF assembly, morphology, or interaction with sHsps. To investigate the potential functional consequences of these mutations and gain insights into the sHsp-IF interaction and the mechanisms which lead to cataract formation, I investigated the *in vitro* assembly properties of the R287W and E233del BFSP2 mutants and the subsequent filament properties and interactions with aB crystallin.

The data in this thesis clearly shows that the R287W and E233del BFSP2 mutations both affect filament morphology when assembled with bovine BFSP1 or 53k. This could significantly affect the BF cytoskeleton network, which is vital for fibre cell organisation at the lens suture and for lens transparency (Michael et al., 2003). Indeed, although the major phenotype of the E233del BFSP2 is myopia, a Y-shaped cataract is also present, caused by altered lens organisation (Zhang et al., 2004).

My data also suggest that aB crystallin may actually inhibit BF assembly *in vitro*, an effect observed previously for other IFs, for example GFAP and vimentin (Nicholl and Quinlan, 1994; Perng et al., 1999a). In addition the R287W and E233del BFSP2 mutations reduced the effect of aB crystallin inhibition, perhaps suggesting altered interactions with aB crystallin. The unusual relationship of BF with sHsps makes this an intriguing observation, and further analysis may provide additional insight into the sHsp-IF interaction.

In vivo, BFs are found with 12-15nm a-crystallin 'beads' bound extensively along their length (FitzGerald and Casselman, 1991; Maisel and Perry, 1972) (See Fig 10.1). Indeed, the inclusion of a-crystallin with BFSP1 and BFSP2 during *in vitro* assembly has previously been shown to result in filaments morphologically similar to the native beaded filament (Carter et al., 1995), with extensive sHsp association. a-crystallin is a molecular chaperone which comprises aA crystallin and aB crystallin, assembled in a 3:1 ratio (Borkman and McLaughlin, 1995; Carver et al., 1994; Horwitz, 1992; Rao et al., 1993). Interestingly, my data show that inclusion of aB crystallin with BFSP1 and BFSP2 does not form BFs which resemble those found *in vivo*. The BFs formed in the presence of aB crystallin, rather than a-crystallin, appear to show much lower levels of sHsp association. This suggests that the presence of aA crystallin, which is almost entirely lens specific, is critical to the BF-sHsp interaction. Interestingly, when vimentin is coassembled with a-crystallin *in vitro*, the a-crystallin particles also decorate the 10nm IFs (Nicholl and Quinlan, 1994), but the association is greatly reduced compared to BFs. This further demonstrates the unusual relationship between BFs and sHsps.

Interestingly, data in this thesis also suggest that post-translational (PT) modifications of BFSPs may play an important role in BF assembly. When human BFSP2 was assembled with native bovine BFSP1 rather than recombinant human BFSP1, the filaments formed appeared smoother and more consistent in width. This suggests that the presence of PT modifications on the native bovine BFSP1 are more important to filament morphology that the sequences differences, caused by using a bovine protein rather than human. Interestingly, previous studies have identified PT modifications in both bovine BFSP1 and BFSP2 (Wang et al., 2009). Studies found that Met-1 of BFSP2 was removed and Ser-2 was acetylated. Nine phosphorylation sites were identified on BFSP1 and seven on BFSP2. Most of the identified phosphorylation sites of BFSP1 are located in the tail domain, whereas those of BFSP2 are mostly in the head domain, but no phosphorylation sites were identified in the central rod

domains. BFSP1 was also found to be myristoylated (Wang et al., 2009) and it has been suggested that post-translational myristoylation may be involved in the regulation of cytoskeletal structure during apoptosis (Utsumi et al., 2003). Myristoylation can cause alterations in protein-protein interactions, membrane binding, and targeting (Cross et al., 1984; Peitzsch and McLaughlin, 1993; Zha et al., 2000). The significance of these PT modifications to the BFSPs, and the subsequent effect on filament properties remains to be determined, but results in this thesis suggest they may have significant effects on filament morphology. In addition, if PT modifications affects filament morphology and the filament surface, this may affect the interaction with a-crystallin. Further analysis of the BF assembly mechanism is required to understand the functional significance of these changes.

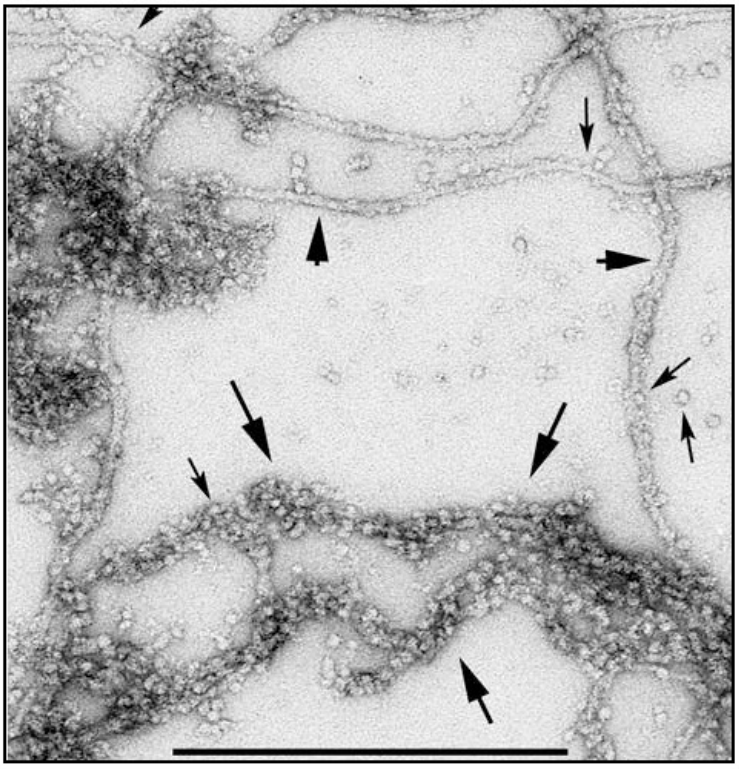

Fig 10.1. TEM of Native filaments extracted from the lens.

The image shows native filaments extracted from the lens. Two types of filament are visible: Smooth, 10nm filaments (arrowheads) decorated with a-crystallin particles (small arrows); Beaded filaments (large arrows) with extensive a-crystallin particle association causing the filament backbone to be almost totally obscured. Scale bar: 500 nm. Adapted from Song et al., 2009.

MUTATION IN THE DESMIN C-TERMINAL TAIL CAN AFFECT FILAMENT PROPERTIES

The importance of the sHsp-IF interaction has been discussed previously and is also supported by results in this thesis. A previous study by Sharma, 2011 suggested that mutations in the desmin C-terminal tail may affect interaction with aB crystallin, and subsequently affect filament aggregation (Sharma, 2011). In addition, results suggested that removal of the desmin C-terminal tail domain resulted in filaments unable to bind aB crystallin, suggesting the desmin tail as a potential aB crystallin binding site. Further investigation of this intriguing possibility required analysis of the effects of C-terminal tail mutations on desmin filament properties. Indeed, identification of altered filament properties may provide insight into the potentially altered interaction with aB crystallin. Tail truncated desmin mutants of residues 1-409 (dTail des), 1-431 (d431 des) and 1-441 (d441 des) were used. Another tail mutant was also generated to delete only the highly conserved 454-RDG-456 residues (RDG des).

My analysis showed that the desmin C-terminal tail domain is not required for filament assembly. Indeed, all 4 desmin tail mutants analysed, including the dTail desmin mutant which truncates the entire C-terminal tail, were able to form filaments. Previous studies have also reported that, in contrast to the head domain, the tail domain of desmin is not essential for filament assembly (Geisler et al., 1982; Kaufmann et al., 1985). In addition, a previous analysis of 6 disease causing desmin tail mutants (T442I, K449T, I451M, R454W, S460I and V469M) found that all but the R454W can assemble into filaments and all six mutants can integrate into the IF cytoskeleton *in vivo* (Bar et al., 2007). However, my results clearly show that all 4 tail mutants analysed in this thesis (d431, d441, RDG and dTail) have significant effects on filament morphology. All 4 tail mutants cause a loss of filament width control, such that filament width distributions are significantly increased. Furthermore, I found that for the dTail desmin mutant which removes the entire tail, the average filament width was also significantly increased. Indeed, previous studies have suggested that IF C-terminal tail domains are involved in regulation of filament width (Herrmann et al., 1996). I also observed loss of BF width control upon truncating the zebrafish BFSP2 C-terminal tail, as discussed earlier in this thesis. Clearly, the C-terminal tail plays an important role in filament

morphology. Indeed deletion of the C-terminal tail domain from GFAP has also been shown to alter filament morphology (Chen and Liem, 1994).

All 4 desmin mutants analysed in this thesis (d431, d441, RDG and dTail desmin) remove the highly conserved RDG motif and interestingly, previous studies have shown that disturbance of the RDG motif can alter IF filament morphology, both *in vitro* and *in vivo* (McCormick et al., 1993). In addition, a synthetic nonapeptide corresponding to this motif has been reported to bind the desmin tail and cause altered filament morphology (Birkenberger and Ip, 1990). Furthermore, the R416W point mutation in the C-terminal tail RDG motif of GFAP causes IF aggregates and the neurodegenerative disease, Alexander disease (Der Perng et al., 2006; Quinlan et al., 2007). Overall, data in this thesis strongly support the role of the IF C-terminal tail and the RDG motif in filament morphology and width control and suggest that truncation or mutation within this domain will increase filament width distribution and change filament morphology, which in turn will likely affect interaction with sHsps.

Interestingly, I also found that the desmin C-term tail mutations (d431, d441, RDG and dTail desmin) all affected desmin filament-filament interactions and aggregation, and that this effect was highly temperature dependent. Indeed, previous studies have shown that although most desminopathy causing tail mutants can assemble into filaments and associate into networks, these filaments subsequently associate into aggregates in patients (Bar et al., 2007). Previous studies on desmin C-terminal tail mutants have implicated the tail in filament-filament interactions (Bar et al., 2010). In addition, previous studies on the IFs vimentin and keratin 14 have also suggested that the C-terminal tail may indeed play an important role in filament-filament interactions (Bousquet et al., 2001; Lin et al., 2010). Interestingly, of the 4 tail mutants (d431, d441, RDG and dTail desmin), I found that RDG desmin, which deletes only the RDG motif from the C-terminal tail and leaves the rest of the tail in tact, caused the greatest change in filament-filament interactions. Indeed, the RDG mutant desmin caused a significant increase in filament-filament interactions such that these filaments aggregated and were completely pelleted in the low speed sedimentation assay. Although the desmin truncations d431, d441 and dTail all remove tail sections containing the RDG motif, these truncations do not cause the same increase in filament-filament interactions as the RDG desmin mutant. These data may suggest that, in the absence of the RDG motif, the C-terminal tail is actually becomes detrimental to filament morphology and filament-filament interactions.

These data clearly show that the C-terminal tail domain of desmin is crucial to filament morphology and subsequent filament-filament interactions. Indeed, of the 53 disease causing desmin mutations identified to date, 12 are desminopathy causing mutations in the tail domain (Goldfarb and Dalakas, 2009; Van Spaendonck-Zwarts et al., 2010). These changes in filament morphology will subsequently affect the filament interaction with sHsps, which is demonstrated and discussed in the next section.

BUFFER CONDITIONS CAN AFFECT FILAMENT PROPERTIES AND INTERACTION WITH aB CRYSTALLIN

Analysing the sHsp-IF interaction *in vitro* requires filament assembly. Previously published *in vitro* IF assemblies have used two distinct methods of finalising assembly (Perng et al., 1999b; Perng et al., 2004). The first method is used throughout this thesis to finalise desmin assembly and involves slow dialysis into Tris-HCl pH 7.6 or 7.4, 50mM NaCl buffer for 16h. This method will be referred to as 'slow assembly'. The second method of finalising filament assembly involves the rapid addition of a 20-fold concentrated assembly buffer to give a final concentration of 100mM Imidazole-HCl pH 6.8, followed by incubation for 1h (Hayes et al., 2008; Perng et al., 2004). This method will be referred to as 'fast assembly'. These methods of filament assembly differ in buffer type, buffer pH and buffer exchange speed, but both methods have previously been used to analyse filament assembly and subsequent filament-filament interactions and filament interactions with aB crystallin (Perng et al., 1999b; Perng et al., 2004). It was thus important to determine if the method of *in vitro* assembly could affect the outcome of such experiments. Indeed, results in this thesis show that filaments assembled using the 'fast assembly' method are more likely to self associate and aggregate, compared to filaments assembled using the 'slow assembly' method. Results in this thesis also show that the 'fast assembly' method impairs the ability of aB crystallin to reduce filament-filament interactions and prevent filament aggregation, perhaps indicating altered sHsp-IF interaction. Interestingly, studies have suggested that an increased rate of substrate aggregation may cause decreased sHsp chaperone activity (Carver et al., 2002; Jaya et al., 2009). Indeed, filaments formed using the 'fast assembly' method appear aggregated when viewed using TEM. A study by Sharma 2011 also found the 'fast assembly' method to cause altered IF morphology and increased filament aggregation (Sharma, 2011).

The 'fast assembly' and 'slow assembly' methods differ in buffer type, buffer pH and buffer exchange speed, resulting in dramatically different IF properties, and altered sHsp-IF interaction. In fact, each of these factors has been shown separately to affect filament morphology and subsequent interactions with aB crystallin. Sharma, 2011 found that the buffer type (Imidazole, Tris or Potassium Phosphate) has significant effect on filament morphology and binding of aB crystallin (Sharma, 2011). The effect of buffer exchange speed can also be observed to cause dramatic changes in filament morphology. Sharma, 2011

finalised filament assembly of desmin mutants (d431, d441, RDG and dTail desmin) by rapid addition of NaCl, whereas I finalised filament assembly of the same mutants by slow dialysis addition of NaCl, with dramatic differences to resulting filament morphology (see Fig 8.3).

Results in this thesis also clearly demonstrate the effect of pH on desmin filament morphology and filament-filament interactions, which was analysed using the 'slow assembly method' at different pH values. I found that increasing the pH from 6.8 to 7.2 causes a significant decrease in desmin filament-filament interactions and filament aggregation, while a pH increase from 7.6 to 8.0 causes dramatic changes to filament morphology. In addition, I also found that beaded filament morphology changes dramatically as the pH changes from 6.8 to 7.6 to 8.0 (See Sup Fig 9). My data also show that pH can significantly affect the ability of aB crystallin to prevent filament-filament interactions and filament aggregation. Desmin filaments assembled alone at pH 6.8 or 7.6 appear morphologically identical and have comparable levels of filament-filament interactions and aggregation. However, when assembled in the presence of aB crystallin, although filaments still appear morphologically identical at pH 6.8 and 7.6, filament-filament interaction and aggregation is significantly reduced by aB crystallin at pH 7.6, but remains unchanged at pH 6.8. Indeed, previous studies have also suggested that the sHsp-IF interaction may be pH dependant (Bennardini et al., 1992). Furthermore, NMR and SAXS studies have shown that interaction between the C-terminal IXI motif and the b4-b8 hydrophobic substrate binding groove in aB crystallin is pH dependant (Jehle et al., 2010). The C-terminal IXI motif may thus regulate the accessibility of the b4-b8 substrate binding site depending upon cellular conditions. At pH 7.6, the IXI motif appears to bind the b4-b8 hydrophobic groove, while pH 6.8 appears to cause release and exposure of the IXI motif from the b4-b8 groove, along with a substantial change in quaternary structure of the aB crystallin oligomer (Jehle et al., 2010). It maybe the case that dissociation of the C-terminal IXI motif both exposes a potential substrate binding site and partially destabilises the oligomer, causing altered interactions with IFs.

These data clearly demonstrate that the buffer conditions of *in vitro* filament assembly can significantly affect filament morphology, filament-filament interactions and aggregation, and filament interactions with aB crystallin. This has important implications for *in vitro* studies of sHsp-IF interactions. Further analysis is required to understand the functional significance of these important changes, but it is clear that future studies of sHsp-IF interactions should include careful analysis of buffer conditions and their subsequent effects.

THE INTERACTION BETWEEN DESMIN FILAMENTS AND aB CRYSTALLIN CAN BE AFFECTED BY MUTATION IN EITHER PROTEIN

The b3 strand (residues 73-85) and b8 strand (residues 131-138) and C-terminal residues 155-165 of aB crystallin have previously been identified by pin arrays as potential interaction sites for a variety of client proteins, including the IF, desmin (Ghosh et al., 2007b). These regions have also been identified as potentially important for aB crystallin chaperone activity and oligomerisation (Ghosh et al., 2005). Crystallisation (Laganowsky et al., 2010) and solution structural (Jehle et al., 2010; Peschek et al., 2009) studies suggest that all 3 sequences are surface exposed on the aB crystallin subunit and are potentially available to bind client proteins and IFs. A previous study by Sharma, 2011 suggested that mutations in the desmin C-terminal tail may affect interaction with aB crystallin, and subsequently affect filament aggregation (Sharma, 2011). In addition, results suggested that removal of the desmin C-terminal tail domain results in filaments unable to bind aB crystallin, suggesting the desmin tail as a potential aB crystallin binding site. Therefore, to gain insight into the sHsp-IF interaction, I used aB crystallins with mutations in the b3 strand, b8 strand and C-terminal residues 155-165 to assess the effect on the interaction with desmin. In addition, I used desmin proteins with mutations in the tail domain to assess the effect on interaction with aB crystallin.

Two chimeric b3 strand aB crystallin mutants were analysed, where the aB crystallin b3 strand was swapped with the aA crystallin b3 strand (aAb3 aB) or the *C. elegans* Hsp12.2 b3 strand (CEb3 aB) (Ghosh et al., 2006b). Two chimeric b8 strand aB crystallin mutants were analysed, where the aB crystallin b8 strand was swapped with the aA crystallin b8 strand (aAb8 aB) or the *C. elegans* Hsp12.2 b8 strand (CEb8 aB) (Ghosh et al., 2006a). A deletion mutant was also used, which lacked C-terminal residues 155-165 (d155 aB) (Ghosh et al., 2006d). It was previously shown that aAb3, CEb3, aAb8, CEb8 and d155 aB crystallin mutations have no significant effect on the secondary and tertiary structure of aB crystallin as determined by far and near UVCD spectroscopy and all 5 mutants are thermostable upon heating to 50°C (Ghosh et al., 2006a; Ghosh et al., 2006b; Ghosh et al., 2006d). Tail truncated desmin mutants of residues 1-409 (dTail des), 1-431 (d431 des) and 1-441 (d441 des) were analysed, along with another tail mutant generated to delete only the highly conserved 454-RDG-456 residues (RDG des).

Results show that the d155 aB crystallin mutant increases binding to desmin filaments and increases filament-filament interactions, causing aggregation. These effects are highly temperature dependent and were observed at 37 and 44°C, but not 22°C. Interestingly, the polar and highly flexible C-terminal tail (Carver et al., 1992; Jiao et al., 2005), which is disturbed in d155 aB crystallin, is thought to be important for solubility of sHsp oligomers and sHsp-substrate complexes (Carver, 1999; Ghosh et al., 2006d). Residues 155-165 may also be critical for solubility, such that d155 aB substrate complexes are prone to aggregation. Indeed, results show that d155 aB crystallin significantly increases desmin filament-filament interactions and filament aggregation. Previous studies have also shown that the mutant promotes aggregation of ADH and b-crystallin 3-fold and 11-fold respectively (Ghosh et al., 2006d). The sHsp C-terminal tail is also thought to form both inter- and intramolecular tertiary interactions, which are important to sHsp function (Pasta et al., 2002; Saji et al., 2008). In fact, the recent model of aB crystallin (Jehle et al., 2011) predicts that the C-terminal IXI motif of one dimer interacts with the b4-b8 hydrophobic groove of another dimer, an interaction essential for correct oligomer assembly (Jehle et al., 2010; Jehle et al., 2011; Laganowsky et al., 2010; Pasta et al., 2004). Indeed, the d155 aB crystallin mutation, which removes the IXI domain, was previously shown to form larger, more polydisperse oligomers (~24 to ~56 subunits) (Ghosh et al., 2006d). The mutant also disturbs the 163-REEK-166 motif, thought to participate in inter subunit interactions (Rajan et al., 2006) and solubility (Treweek et al., 2007). Indeed, the d155 aB crystallin oligomers were previously reported to have reduced solubility (Ghosh et al., 2006d). The data also shows that d155 aB significantly increases desmin filament binding. It may be the case that deletion of the IXI motif leaves the hydrophobic b4-b8 substrate binding groove exposed, thus increasing substrate binding. Similarly, the myopathy causing Q151X aB crystallin (Selcen and Engel, 2003), which removes the entire C-terminal tail including the IXI motif, was also reported to cause increased desmin filament binding (Hayes et al., 2008).

Previous results have shown the CEb8 and aAb8 aB crystallin mutants both form larger oligomers and have reduced chaperone activity, compared to WT aB crystallin (Ghosh et al., 2006a). Data in this thesis show that the CEb8 aB crystallin increases binding to desmin filaments and increases filament-filament interactions, causing aggregation. Similarly to the d155 aB crystallin, the effects of the CEb8 aB crystallin are highly temperature dependant and observed at 44°C, but not 22 or 37°C. In contrast, results show that the aAb8 aB crystallin is

comparible to WT aB crystallin with respect to desmin filament binding and regulation of filament-filament interactions, at all temperatures. Results also show that the aAb3 aB crystallin decreases binding to desmin filaments and decreases filament-filament interactions, preventing aggregation. In contrast, the CEb3 aB crystallin is comaprable to WT aB crystallin with respect to desmin filament binding and regulation of filament-filament interactions, at all temperatures. These data show that mutation in the aB crystallin b3 or b8 strands can have highly diverse effects on interaction with desmin filaments.

In addition, data in this thesis also show that mutation in the desmin C-terminal tail can affect the interaction with aB crystallin. The RDG desmin mutant, which removes only the RDG motif, causes increased aB crystallin binding and reduces the ability of aB crystallin to prevent filament-filament interactions. Interestingly, the d431 and d441 desmin mutants, which truncate the C-terminal tail and hence remove the RDG domain, show interaction with aB crystallin comparable to WT desmin. However, dTail desmin, which truncates the entire tail, shows reduced binding to aB crystallin and also reduces the ability of aB crystallin to prevent filament-filament interactions. Indeed, Sharma 2011, found that WT aB crystallin was able to significantly reduce WT desmin filament-filament interactions, but unable to prevent dTail filament-filament interactions, as determined by viscometry assays (Sharma, 2011). It has previously been suggested that the desmin C-terminal tail is important for modulating interaction with aB crystallin (Sharma, 2011).

The data presented in this thesis show that mutating the aB crystallin b3 strand, b8 strand and C-terminal residues 155-165 may affect the interaction with desmin filaments. In addition, data also show that mutating the C-terminal tail domain of desmin may affect the interaction with aB crystallin. This data can be interpreted in two ways; the domains are involved directly in binding, or the domains have other roles which indirectly affects the protein interactions. In the case of the latter, mutations in desmin domains may affect filament morphology or filament surface geometry, which could affect interaction with sHsps. Mutations in aB crystallin domains may affect sHsp oligomerisation or subunit dynamics, which could indirectly affect interaction with desmin filaments. Indeed, I suggested earlier in this thesis that there may in fact be a complete lack of a specific sHsp substrate binding surface. sHsps may instead rely on multiple, variable contact sites distributed throughout the sHsp. The fact that substrate binding domains have been predicted throughout the aB crystallin sequence supports this theory (See Fig 1.9). Furthermore, the highly diverse filament interaction effects

observed for the aAb3, CEb3, aAb8 and CEb8 aB crystallins may also suggest that these domains are not definitive binding sites, but can affect the aB crystallin oligomer subunit dynamics to indirectly cause differential binding and interactions. Very recently, solid state NMR, SAXS, and EM data was used to produce an atomic-level model of full-length aB crystallin (Jehle et al., 2011). In the full-length aB crystallin 24-mer model, almost all residues are solvent exposed somewhere on the oligomer, which may explain the huge diversity in predicted binding sites spread throughout the aB crystallin sequence. Overall, these data may suggest that sHsps may rely on multiple, variable contact sites distributed throughout the sHsp and there may in fact be a complete lack of a specific sHsp substrate binding surface. Indeed, I also suggest that desmin filaments may not contain a definitive aB crystallin binding site, but that interaction may instead be driven by the geometry of the filament surface. Results in this thesis demonstrate that mutations in desmin domains, as well as environmental conditions, can affect filament morphology, but also filament-filament interactions and propensity to aggregate, which is likely driven by exposed hydrophobic residues on the filament surface. Indeed, the highly diverse aB crystallin interactions observed for the d431, d441, RDG and dTail desmin tail mutants may suggest that these domains are not definitive binding sites, but can affect filament assembly, morphology and subsequently the filament surface, indirectly causing altered interaction with aB crystallin. Closer analysis of the filament surface, perhaps using isothermal calorimetry (ITC) or fluorescent hydrophobic probes (e.g. BisANS), may provide further insight into this intriguing possibility.

aB CRYSTALLIN 'BINDING' DOES NOT CORRELATE WITH REGULATION OF FILAMENT-FILAMENT INTERACTIONS

Studies analysing the sHsp-IF interaction require methods to quantify the extent of aB crystallin interaction with the filament. In this thesis, and in previous studies cited (Bennardini et al., 1992; Djabali et al., 1997; Hayes et al., 2008; Perng et al., 1999b; Perng et al., 2004), aB crystallin 'binding' to IFs is measured by aB crystallin co-pelleting with IFs at 80,000-150,000g for 30 minutes. When binding is measured using this experimental technique, results in this thesis and results from previous studies show that aB crystallin 'binding' to IFs does not correlate with regulation of filament-filament interactions. Both the CEb8 and d155 aB crystallin mutants analysed in this thesis cause increased desmin filament binding along with increased filament-filament interactions. This situation has also been observed previously for the R120G aB crystallin mutation which causes increased binding to GFAP and desmin filaments along with increased filament-filament interactions (Perng et al., 1999b; Perng et al., 2004). In these situations, increased binding of aB crystallin to the IF accompanies increased filament-filament interactions. Indeed, the aAb3 aB crystallin mutation analysed in this thesis causes a complete lack of filament binding along with decreased filament-filament interactions. These data suggest that aB crystallin binding is correlated with filament-filament interactions and aggregation. Of course, this poses the question of how filament-filament interactions can be prevented in the absence of aB crystallin binding to the filament surface. However, a previous study showed the Q151X aB crystallin mutation causes increased binding to desmin filaments along with decreased filament-filament interactions (Hayes et al., 2008). Overall, these data show that aB crystallin 'binding', as detected by high speed centrifugation, does not correlate with regulation of filament-filament interactions.

I propose that the widely used 'high speed co-sedimentation assay' is not capable of detecting fast, transitory interactions between sHsps and IFs, and as such a lack of co-pelleting of the sHsp with the IFs does not necessarily indicate a lack of interaction or 'binding'. In fact, studies have suggested that complete subunit exchange in aB crystallin oligomers can occur within 30 minutes (Ahmad et al., 2008), in an exponential pattern (Bova et al., 1997), suggesting that half of the subunits within the oligomer may be exchanged within a 5 minute period. In addition, hydrogen-deuterium exchange (HX) studies show that sHsps in complex

with a substrate exchange amide hydrogens at the same rate as sHsps in the absence of the substrate (Cheng et al., 2008), suggesting either transient sHsp-substrate interactions or identical regions of oligomerisation and substrate binding, or both. HX studies also show that both termini of the substrate, maltose dehydrogenase in this case, are solvent exposed (Cheng et al., 2008), even while interacting with sHsps, possibly suggesting rapid, transient sHsp-substrate interactions. It maybe that within sHsp-substrate complexes, interactions between the sHsp and substrate are energetically weak with fast on/off kinetics. Therefore, although the complex as a whole is stable, the individual interactions may be transient, and stable secondary structures may not be formed between sHsp and substrate.

Due to the highly variable and dynamic nature of sHsp-substrate interactions, there is limited thermodynamic and kinetic data. However, two modes of sHsp-substrate interaction have been proposed for aA crystallin and aB crystallin binding to early or late unfolding substrate intermediates (McHaourab et al., 2002; Rajaraman et al., 2001; Sathish et al., 2003). Measurement of forward and reverse rate constants for a-crystallin-substrate complex formation also shows two dissociation constants (Latham et al., 2009). sHsps interacting with the early unfolding intermediates form a transient, unstable complex while the sHsps interacting with the late unfolding intermediates form a stable, soluble complex (Rajaraman et al., 2001). Indeed, it maybe the case that under normal conditions, WT aB crystallin never forms a stable bond with the desmin filament surface, but instead continuously interacts with energetically weak, fast on/off kinetics. In this case, aB crystallin may be able to prevent filament-filament interactions and filament aggregation, but would not be co-pelleted with the desmin filament in the 30 minute 'high speed co-sedimentation assay'. Indeed, this could also explain the results I observed for aAb3 aB crystallin, which is more effective than WT aB crystallin at preventing desmin filament-filament interactions, even though the protein does not co-pellet with the filaments. If the aAb3 aB crystallin mutation weakens the aB crystallin filament interaction, with a corresponding increase in on/off kinetics, this could be more effective at preventing filament-filament interactions, but the interaction would be undetectable by high speed co-sedimentation. Conversely, this could also explain the effects of the CEb8, d155 and R120G aB crystallins which promote desmin filament-filament interactions and show increased co-pelleting with the filaments. If the CEb8, d155 or R120G aB crystallin mutations strengthen the aB crystallin filament interaction, with a corresponding decreased in on/off kinetics, this could result in the aB crystallin complexes being bound to multiple filaments simultaneously, which could promote filament-filament interactions and

filament aggregation. This would also potentially be detected by the high speed co-sedimentation assay. This theory could also explain the effects of the Q151X mutation, which reduces desmin filament-filament interactions and shows increased co-pelleting with the filament. The Q151X aB crystallin mutation may strengthen the aB crystallin filament interaction, thus protecting exposed hydrophobic regions on the filament surface, but lack of ability to oligomerise would prevent binding to multiple filaments simultaneously. Indeed, Hayes et al, 2008 found that Q151X aB crystallin was more effective than WT aB crystallin at preventing filament-filament interactions. This may result from increased numbers of aB crystallin subunits able to bind the filament surface due to loss of oligomerisation. Interestingly, a previous study showed that WT aB crystallin did not co-pellet with the dTail desmin mutant during the 'high speed centrifugation assay', a result confirmed by work in this thesis, but analytical ultra centrifugation showed co-sedimentation of aB crystallin with dTail desmin, indicating an interaction (Sharma, 2011). However, insufficient experimental evidence means the validity of this theory of sHsp-IF interaction remains to be determined.

BIOLOGICAL IMPLICATIONS OF sHsp-IF INTERACTIONS

Intermediate filaments (IFs) form dynamic networks which are essential for cell mechanical properties, cell signaling, the stress response and cell integration into tissues (D'Alessandro et al., 2002; Herrmann et al., 2009; Janmey et al., 2009; Kim and Coulombe, 2007; Quinlan, 2002; Vogel and Sheetz, 2009). While IFs can be membrane associated (Franke et al., 1987a; Sandilands et al., 1995a; Song et al., 2009), they can also traverse the cell cytoplasm (Janmey et al., 2009; Kim and Coulombe, 2007) and therefore require mechanisms to prevent unwanted filament-filament interactions which may lead to aggregation (Perng et al., 1999a; Quinlan, 2002). sHsps interact with IF networks (Carter et al., 1995; Nicholl and Quinlan, 1994; Quinlan et al., 1996) to modulate filament-filament interactions (Perng et al., 1999a; Quinlan, 2002), stabilise IF assembly intermediates (Perng et al., 1999b) and assist in the assembly, organisation and stabilisation of the filament network (Bennardini et al., 1992; Djabali et al., 1999; Ghosh et al., 2007a; Muchowski et al., 1999b; Nicholl and Quinlan, 1994; Perng et al., 2004). Indeed, studies have demonstrated that sHsps can prevent IF aggregation in vivo (Koyama and Goldman, 1999; Wang et al., 2003). Mutation in either sHsp (Inagaki et al., 2006; Sacconi et al., 2011; Selcen and Engel, 2003) or IF (Goldfarb and Dalakas, 2009; Levin et al., 2010; Munoz-Marmol et al., 1998) can cause disease in humans, characterised by aggregates containing both sHsps and IFs (Der Perng et al., 2006; Evgrafov et al., 2004; Goldfarb and Dalakas, 2009; Goldfarb et al., 2008; Irobi et al., 2004; Iwaki et al., 1993; Iwaki et al., 1989; Li et al., 2005; Quinlan et al., 2007; Schroder and Schoser, 2009; Taylor et al., 2007; Vicart et al., 1998). This clearly demonstrates the vital importance of the relationship between sHsp and IFs. Indeed, this relationship may in fact be symbiotic, with sHsps providing stability to filaments, and filaments providing a scaffold for a reservoir of sHsps.

The sHsp-IF interaction can be induced by stress (Chiesi et al., 1990; Djabali et al., 1997; Golenhofen et al., 1999; Iwaki et al., 1993; Iwaki et al., 1989; Kato et al., 1993; Lowe et al., 1992; Muchowski et al., 1999b). Indeed, disruption to sHsp-IF interactions can reduce the ability of cells to resist stress (Head et al., 1994; Iwaki et al., 1994; Perng et al., 1999a) and prevent apoptosis (Mehlen et al., 1995). However, sHsp-IF interactions also play a vital role in unstressed cells (Perng et al., 1999a; Wisniewski and Goldman, 1998). In fact, both sHsps and IFs have been linked to the proteasome (Arcangeletti et al., 1997; den Engelsman et al.,

2004). Indeed, mutations in both sHsps (Chen et al., 2005; Liu et al., 2006b) and IFs (Cho and Messing, 2009; Harada et al., 2008; Liu et al., 2006a; Liu et al., 2006b) have been reported to impair the proteosome system. Studies have shown that IF aggregation (Messing et al., 1998) compromises the proteosome system (Tang et al., 2006), since IF proteins are turned over by the proteasome (Ku and Omary, 2000). Interestingly, studies have shown that inhibition of the proteasome can lead to further aggregation of sHsps (Ito et al., 2002) and IFs (Bardag-Gorce et al., 2004). In fact, recent evidence suggests a direct correlation between the rate of protein turnover by the proteasome and the level of IF protein (Nitahara-Kasahara et al., 2009). This suggests that the relationship between IFs, sHsps and the proteasome machinery is critical to cell function. Indeed, mutations which affect the sHsp-IF interaction can cause aggregation (Perng et al., 1999b; Perng et al., 2004; Song et al., 2008; Vicart et al., 1998), and this may have downstream consequences, leading to impairment of the proteosome system. This may in turn lead to further mutant protein aggregation, which can increase autophagy (Tannous et al., 2008) and disease severity (Tang et al., 2008). Indeed, once the balance has shifted in favour of these processes, the system may become self-perpetuating, increasing the stress load experienced by the cell (Fig 10.2). This further demonstrates the vital importance of sHsp-IF interactions to the cell.

Data in this thesis provide insight into the sHsp-IF interaction, but the molecular details remain to be determined. Further investigations into sHsp subunit dynamics and filament architecture, which likely modulate the interaction, will provide further insight into the vital sHsp-IF interaction. This may allow development of new therapeutic approaches to restore normal cellular function by maintaining the physiological sHsp-IF interaction and therefore inhibiting the formation of the pathological aggregates which cause disease.

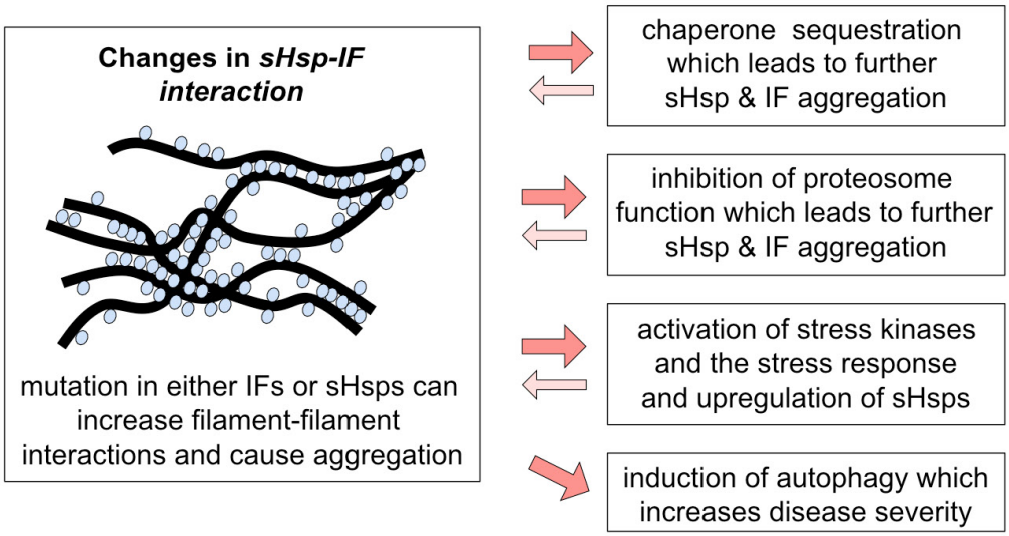

Fig 10.2. The effects of altered sHsp-IF interactions.

Mutations in either IFs or sHsps can change the sHsp-IF interaction and cause aggregation, which can cause activation of stress kinases, proteasome inhibition, oxido-reductive stress and the induction of autophagy. Once the balance has shifted in favor of these processes, then the system becomes self-perpetuating increasing the stress.

APPENDIX: SUPPLEMENTARY FIGURES

SUPPLEMENTARY FIGURES

The following supplementary figures provide supporting materials for the results chapters. These figures should be referred to when references are made at relevant points throughout the results chapters.

	WT	G143X	I140X	R107G
UNIT CELL				
a = b [Å]	171.58	126.9	126.1	172.14
c [Å]	102.22	179.29	180.0	102.48
α = β = 90°, = 120[°]				
resolution range [Å]	100-2.5	30-4	30-3.5	100-3.0
completeness [%]	98.6 (98.3)	95.8 (67.0)	98.7 (96.6)	99.3 (99.9)
I/σ(I)	26 (2.6)	6.7 (1.8)	8.5 (1/2)	18 (3.6)
Rsym	0.034 (0.66)	0.094 (0.48)	0.083 (0.65)	0.054 (0.47)
unique reflections	33 049			22054
R	0.25			
Rfree	0.27*			
bond length rmsd [Å]	0.017			
bond angles rmsd [°]	1.65			

(numbers in brackets refer to the last resolution shell)
* Rfree calculated with 5% of all reflections (Brunger 1991)

Sup Table 1. Crystallographic data collection and refinement statistics for WT, G143X, I140X and R107G Hsp16.5.

The R107G Hsp16.5 is isostructural to WT Hsp16.5, which was previously reported by Kim et al., 1998. Data collected for I140X and G143X Hsp16.5 shows that the unit cell dimension and the potential space group have changed, compared to the WT Hsp16.5. This may indicate a possible change in overall organisation, however the resolution of the data is not sufficient to verify this intriguing possibility. Note: Data statistics of the preliminary data processing are shown, but because the data was still being processed by Dr Ehmke Pohl at the time of writing. X-ray diffraction data collection and processing was performed by Dr Ehmke Pohl.

Sup Fig 2. Analytical SEC calibration.

Analytical SEC was performed using a 24ml Superose 6 SEC column at a flow rate of 0.2ml/min. (A) SEC elution profile of the calibration proteins; thyroglobulin (669kDa), ferritin (440kDa), aldolase (158kDa), conalbumin (75kDa) and ovalbumin (44kDa). Blue Dextran (2000kDa) was used to determine the void volume of the column (not shown). (B) Plot of the separation constant (K(av)) of the calibration proteins against log of their molecular weight. (C) K(av) calculation formula.

(Figure next page)

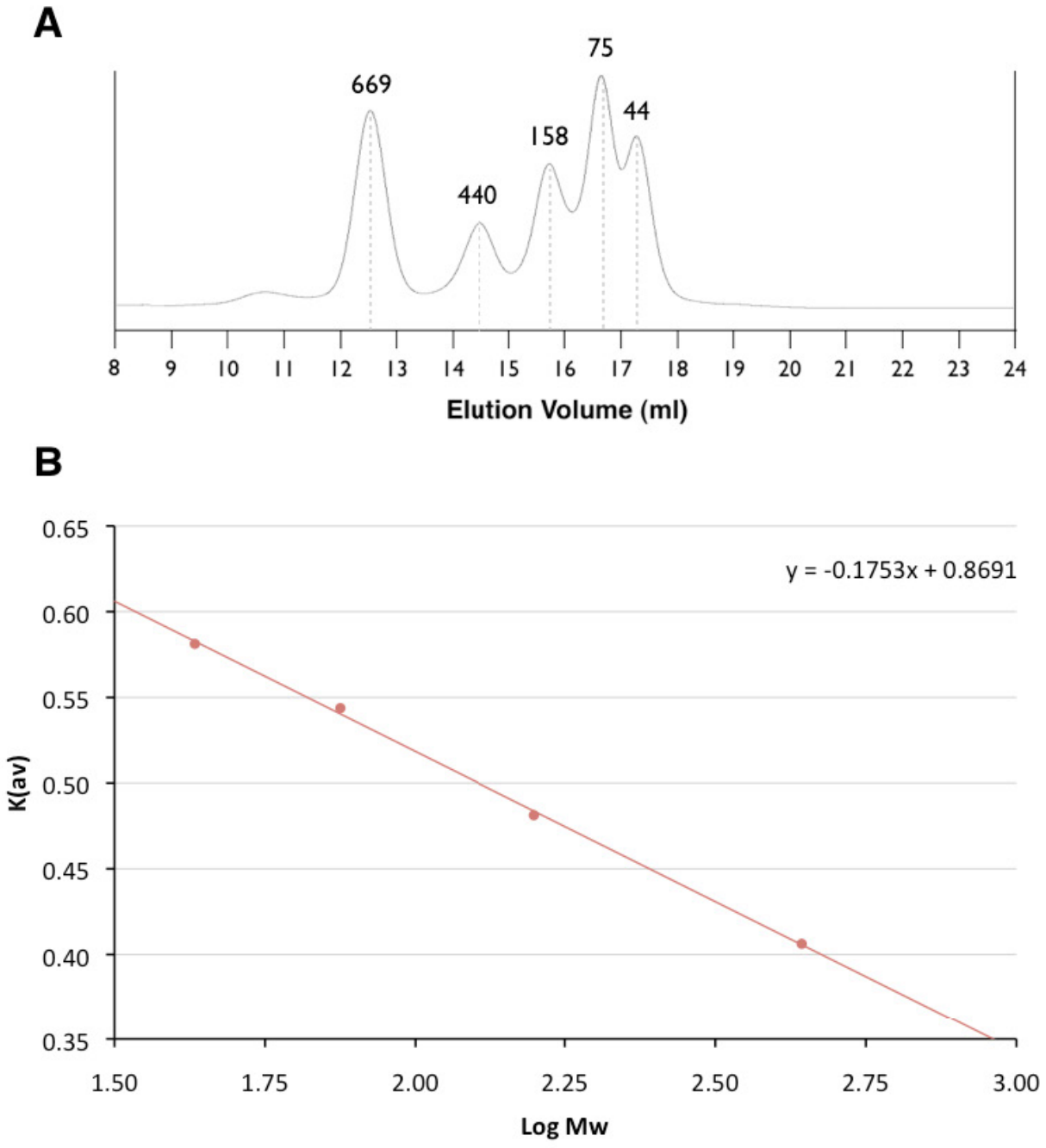

Sup Fig 2 (Legend on previous page)

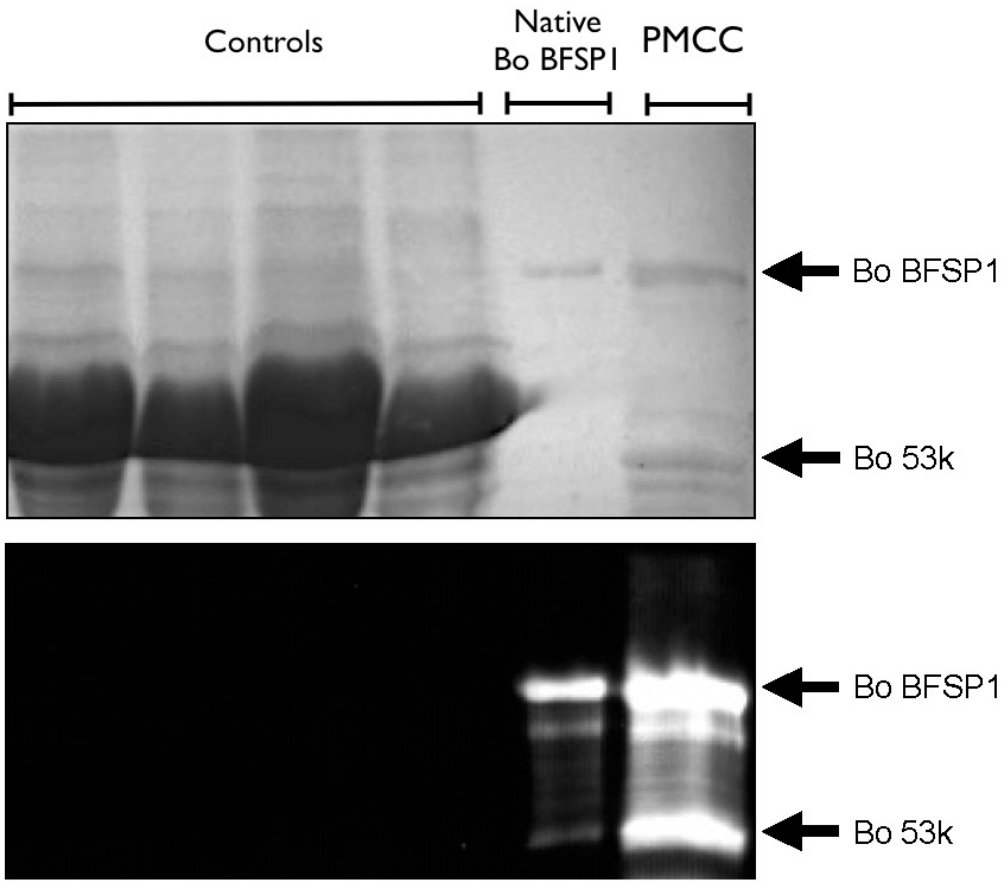

Sup Fig 3. Western blot confirmation of native bovine BFSP1

The soluble protein extracts (Controls) and the insoluble bovine plasma membrane cytoskeleton complex (PMCC) were used as negative and positive controls respectively. The PMCC contains BFSP1 and its breakdown product (53k). This western blot confirms the isolation and purification of Native Bo BFSP1.

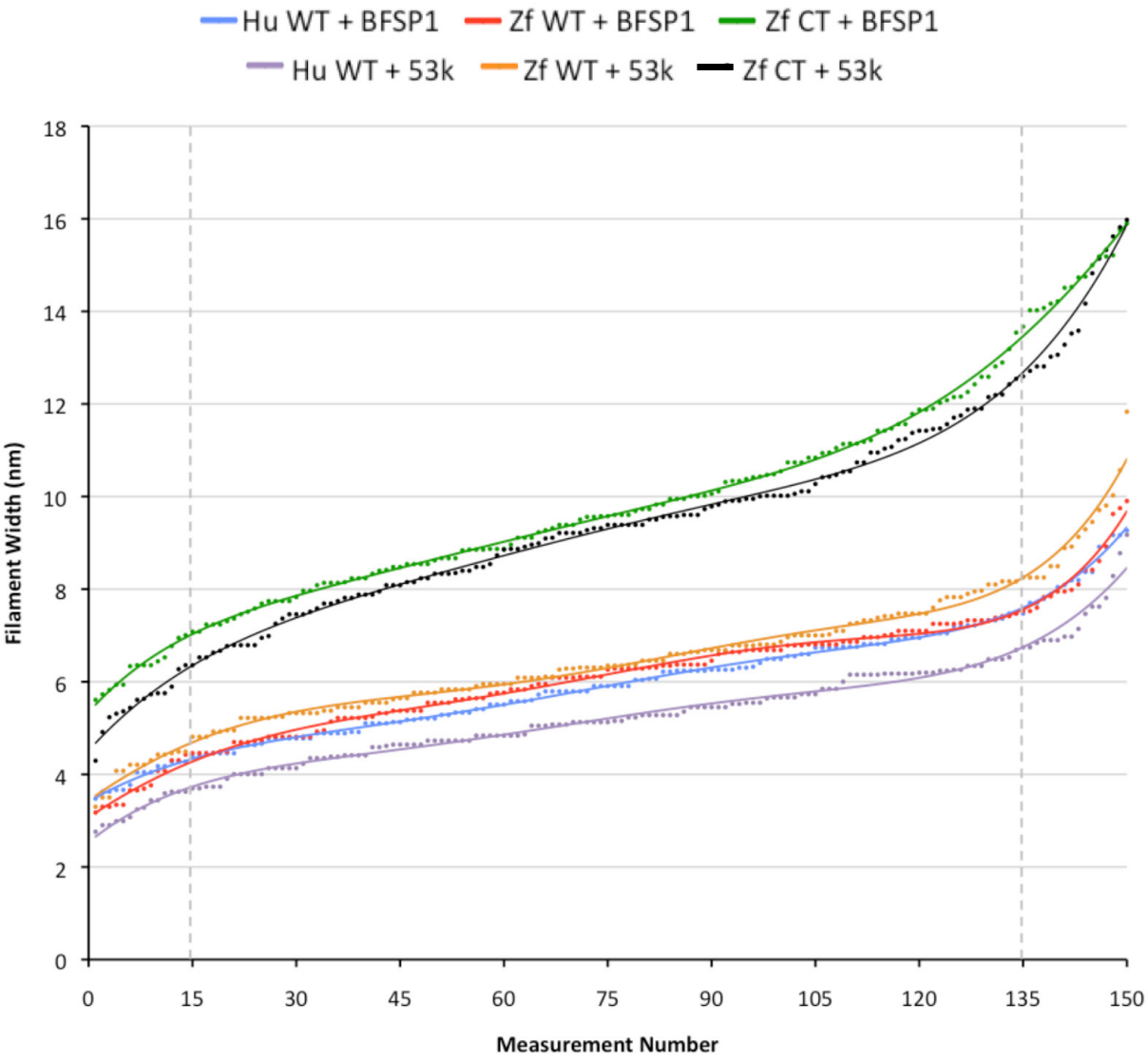

Sup Fig 4. TEM measurements of beaded filament width.

Filaments were assembled using the following proteins: Hu WT BFSP2 and Bo WT BFSP1 (Blue); Zf WT Bfsp2 and Bo WT BFSP1 (Red); Zf CT Bfsp2 and Bo WT BFSP1 (Green); Hu WT BFSP2 and Bo WT 53k (Purple); Zf WT Bfsp2 and Bo WT 53k (Orange); Zf CT Bfsp2 and Bo WT 53k (Black). A total of 150 filament width measurements were then made for each sample in randomly selected areas from 3 different TEM images. The values were then arranged in ascending order and plotted. The dotted lines indicate the top and bottom 10% of values.

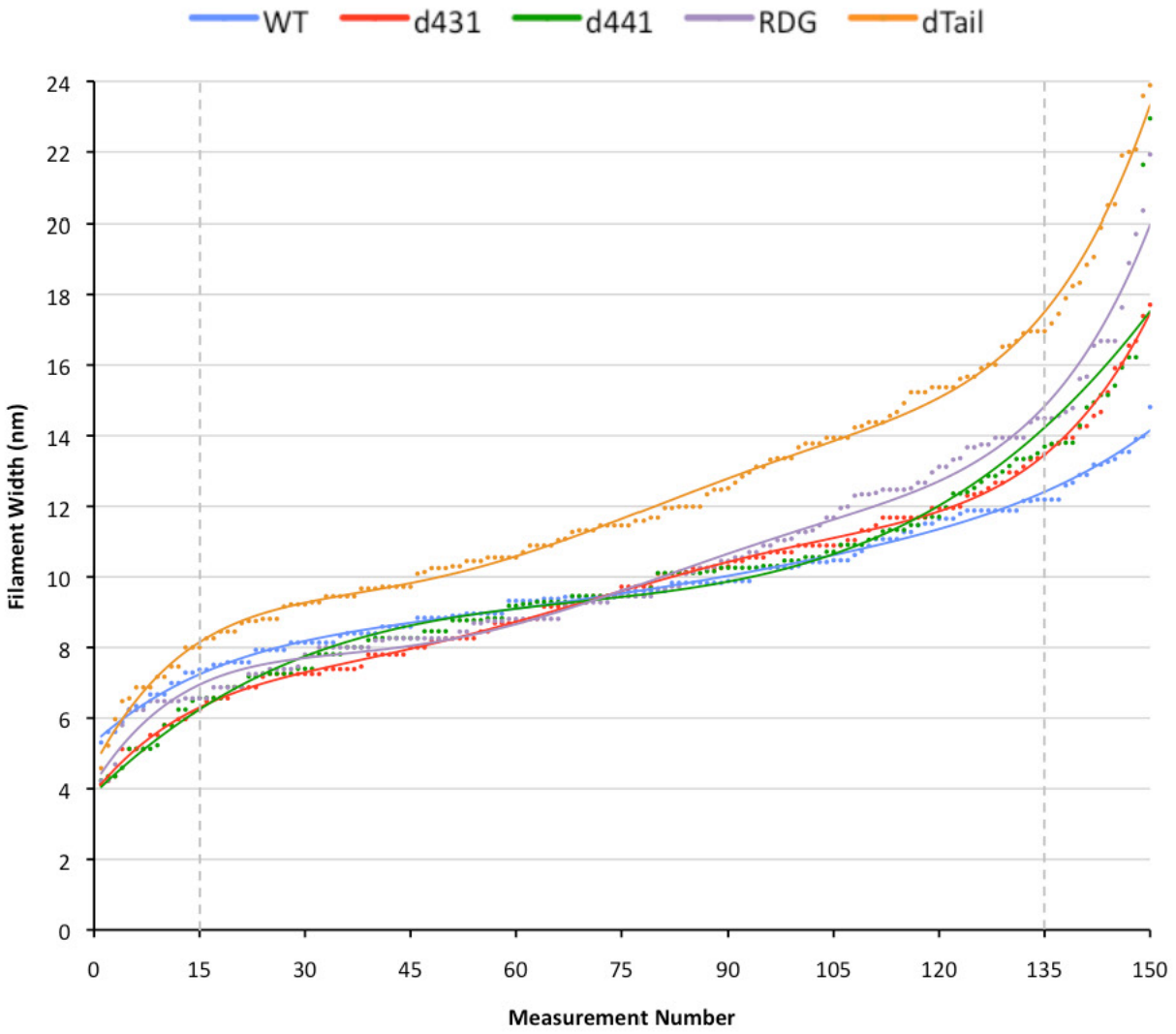

Sup Fig 5. TEM measurements of WT and mutant desmin filament width at 22°C.

Desmin was assembled into filaments and 150 filament width measurements were made for each sample in randomly selected areas from 3 different TEM images. The values were then arranged in ascending order and plotted. The dotted lines indicate the top and bottom 10% of values. Filament widths for WT desmin (Blue), d431 desmin (Red), d441 desmin (Green), RDG desmin (Purple) and dTail desmin (Orange) are shown.

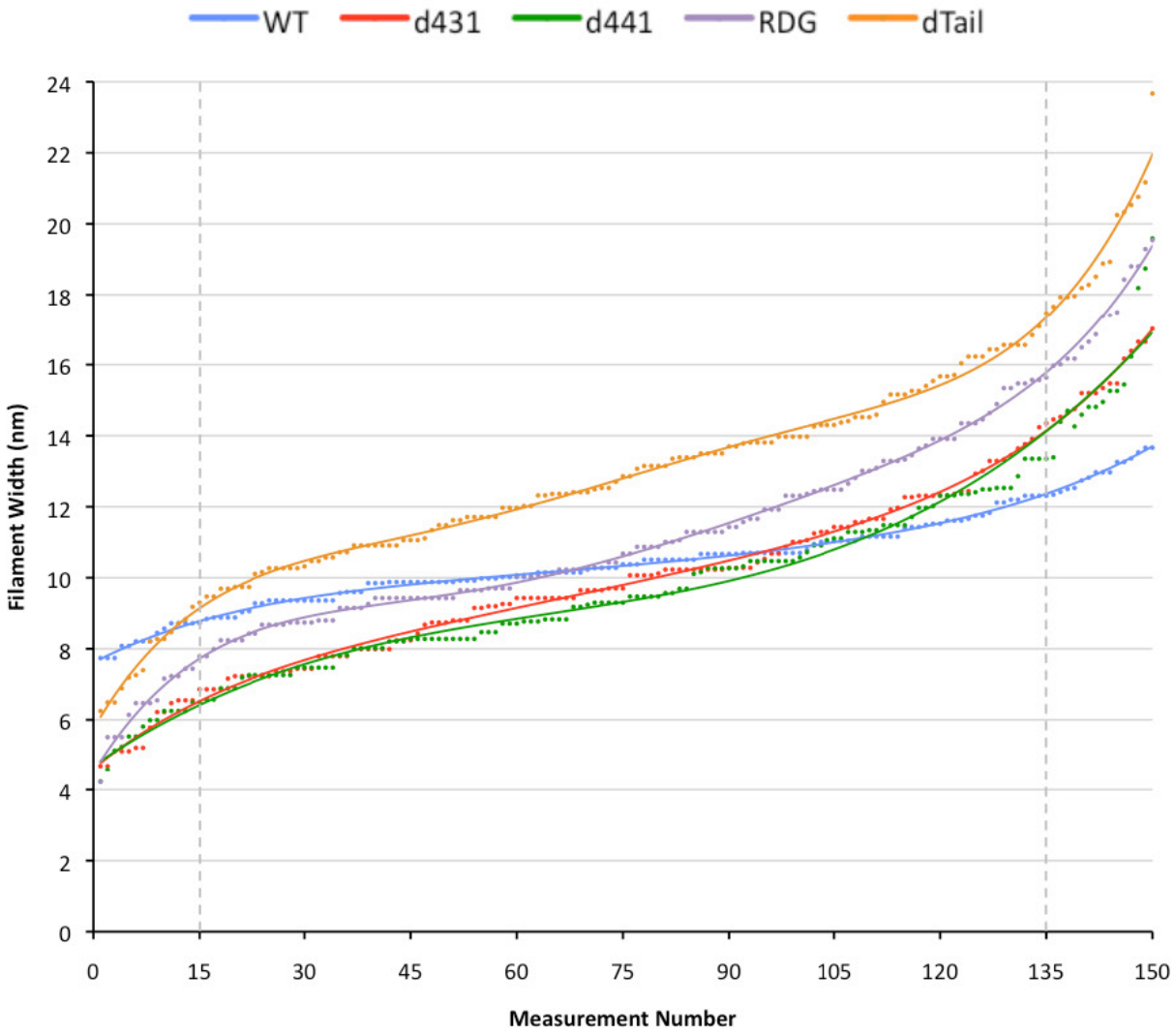

Sup Fig 6. TEM measurements of WT and mutant desmin filament width in the presence of aB crystallin at 22°C.

Desmin was assembled into filaments in the presence of aB crystallin and 150 filament width measurements were made for each sample in randomly selected areas from 3 different TEM images. The values were then arranged in ascending order and plotted. The dotted lines indicate the top and bottom 10% of values. Filament widths for WT desmin (Blue), d431 desmin (Red), d441 desmin (Green), RDG desmin (Purple) and dTail desmin (Orange) are shown.

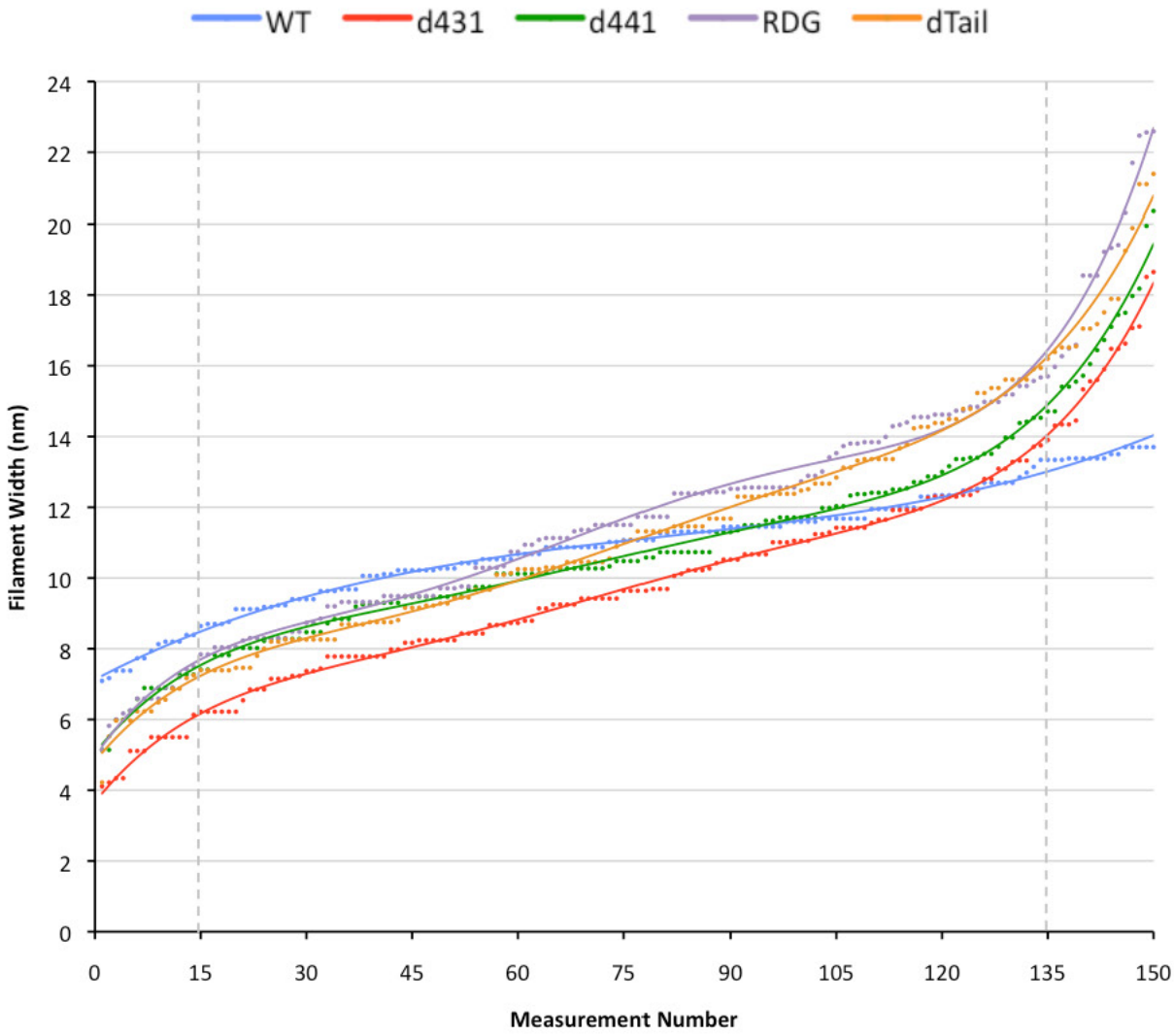

Sup Fig 7. TEM measurements of WT and mutant desmin filament width in the presence of aB crystallin at 37°C.

Desmin was assembled into filaments in the presence of aB crystallin and 150 filament width measurements were made for each sample in randomly selected areas from 3 different TEM images. The values were then arranged in ascending order and plotted. The dotted lines indicate the top and bottom 10% of values. Filament widths for WT desmin (Blue), d431 desmin (Red), d441 desmin (Green), RDG desmin (Purple) and dTail desmin (Orange) are shown.

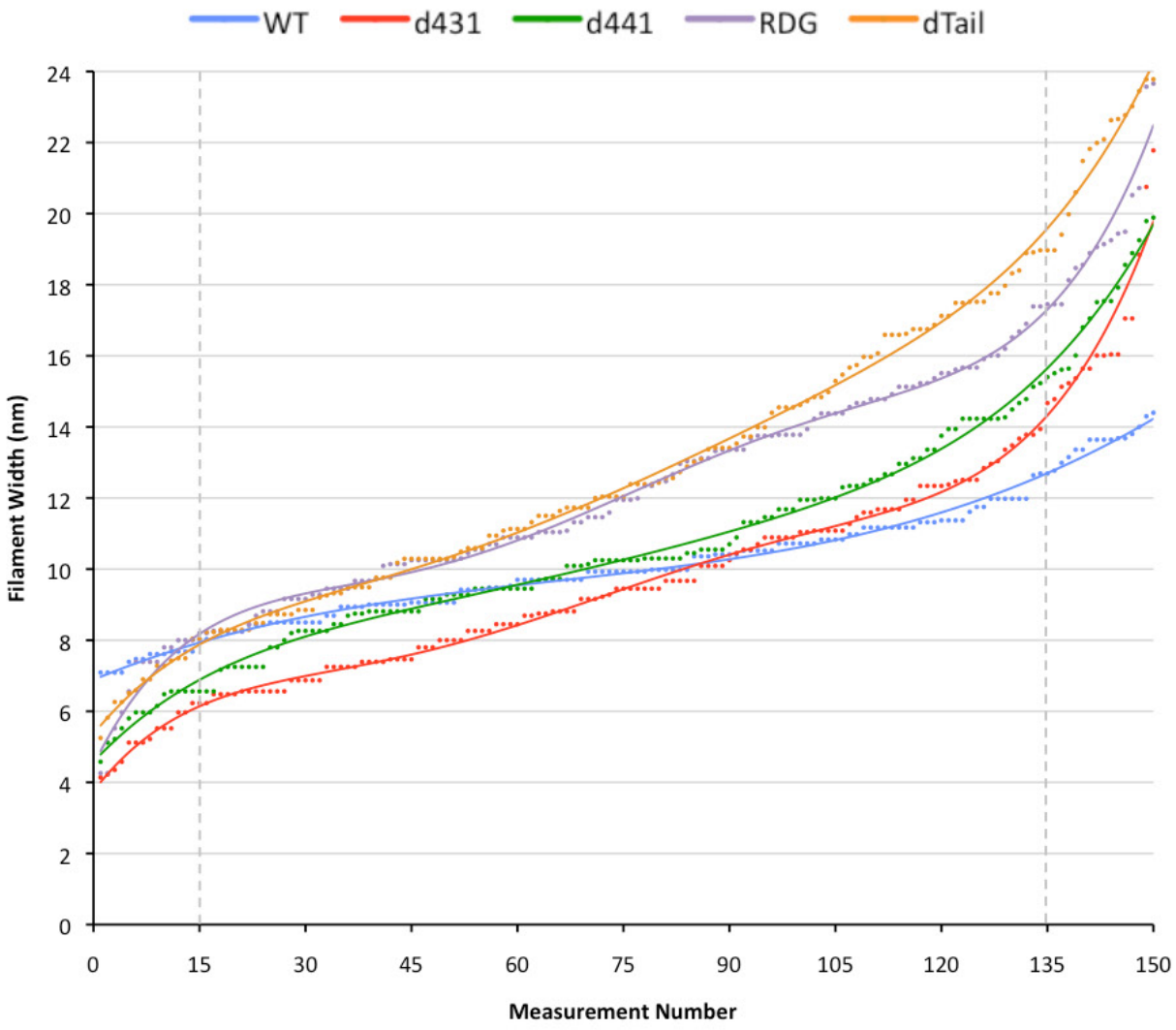

Sup Fig 8. TEM measurements of WT and mutant desmin filament width in the presence of aB crystallin at 44°C.

Desmin was assembled into filaments in the presence of aB crystallin and 150 filament width measurements were made for each sample in randomly selected areas from 3 different TEM images. The values were then arranged in ascending order and plotted. The dotted lines indicate the top and bottom 10% of values. Filament widths for WT desmin (Blue), d431 desmin (Red), d441 desmin (Green), RDG desmin (Purple) and dTail desmin (Orange) are shown.

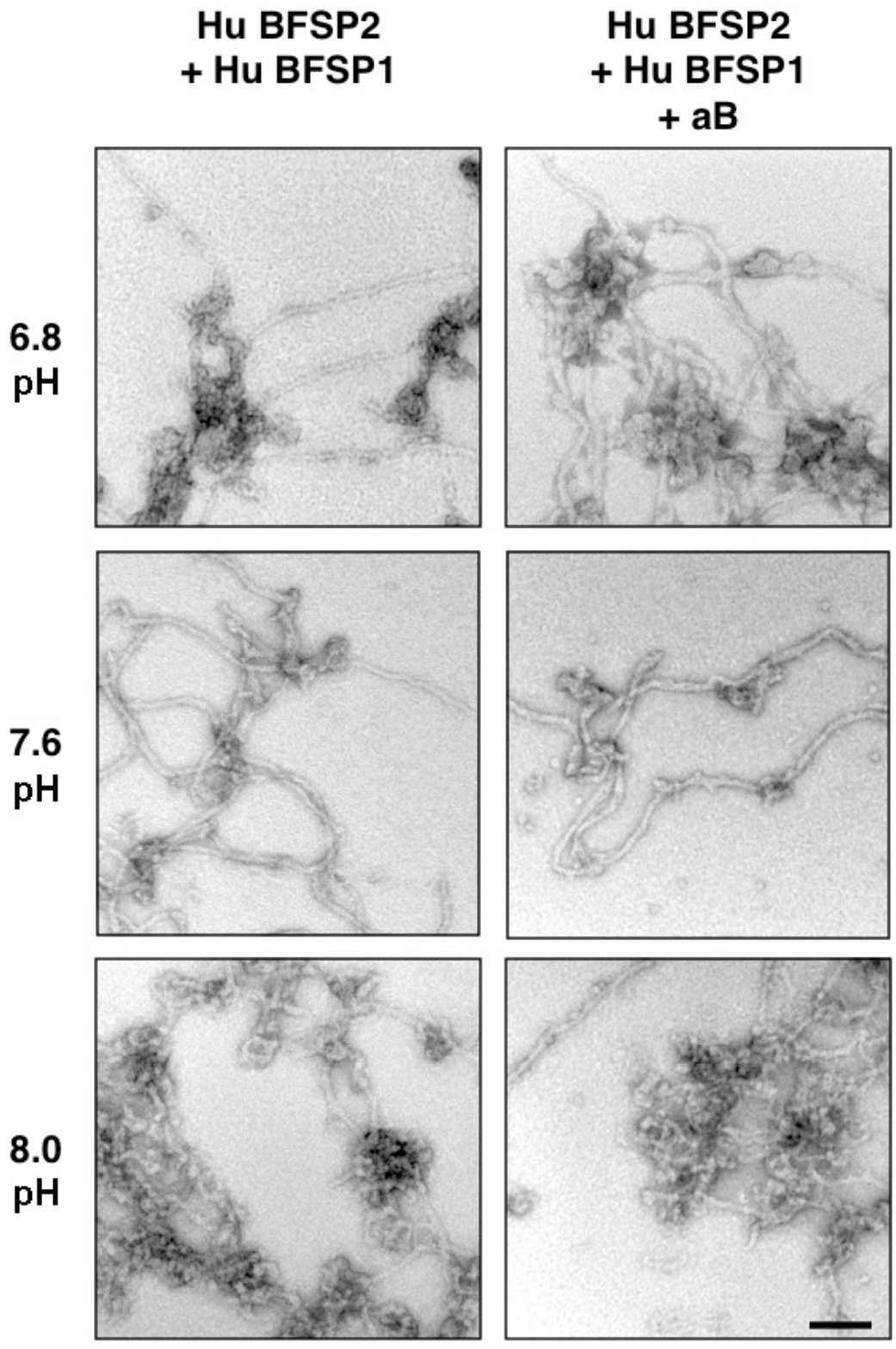

Sup Fig 9. TEM analysis of pH dependance of *in vitro* beaded filament assembly.

Recombinant human BFSP1 and BFSP1 were assembled in the presence or absence of aB crystallin at 22°C at pH 6.8, 7.6 or 8.0. Scale bar represents 100nm.

Sup Fig 10. pH dependance of WT aB crystallin thermostability.

The graphs show the thermostability of WT aB crystallin at pH 8.0, 7.6, 7.2 or 6.8, measured indirectly via differential scanning fluorimetry. (A) WT aB crystallin in 20mM Tris-HCl pH 8.0, 7.6, 7.2 or 6.8 was incubated with SYPRO Orange dye at increasing temperature and the fluorescence monitored. The control shows SYPRO Orange dye alone, and is identical to the aB crystallin alone controls (not shown). (B) The first derivative of the raw fluorescence (F) and temperature (T) data (dF/dT). The peak inflection point indicates the protein melting point temperature. The graphs are the average of 3 independent repeats and the standard deviations of melting point values are shown. All fluorescence values were corrected using a buffer only control (not shown). WT aB crystallin thermostability does not appear to be affected by pH, in these buffer conditions.

(Figure next page)

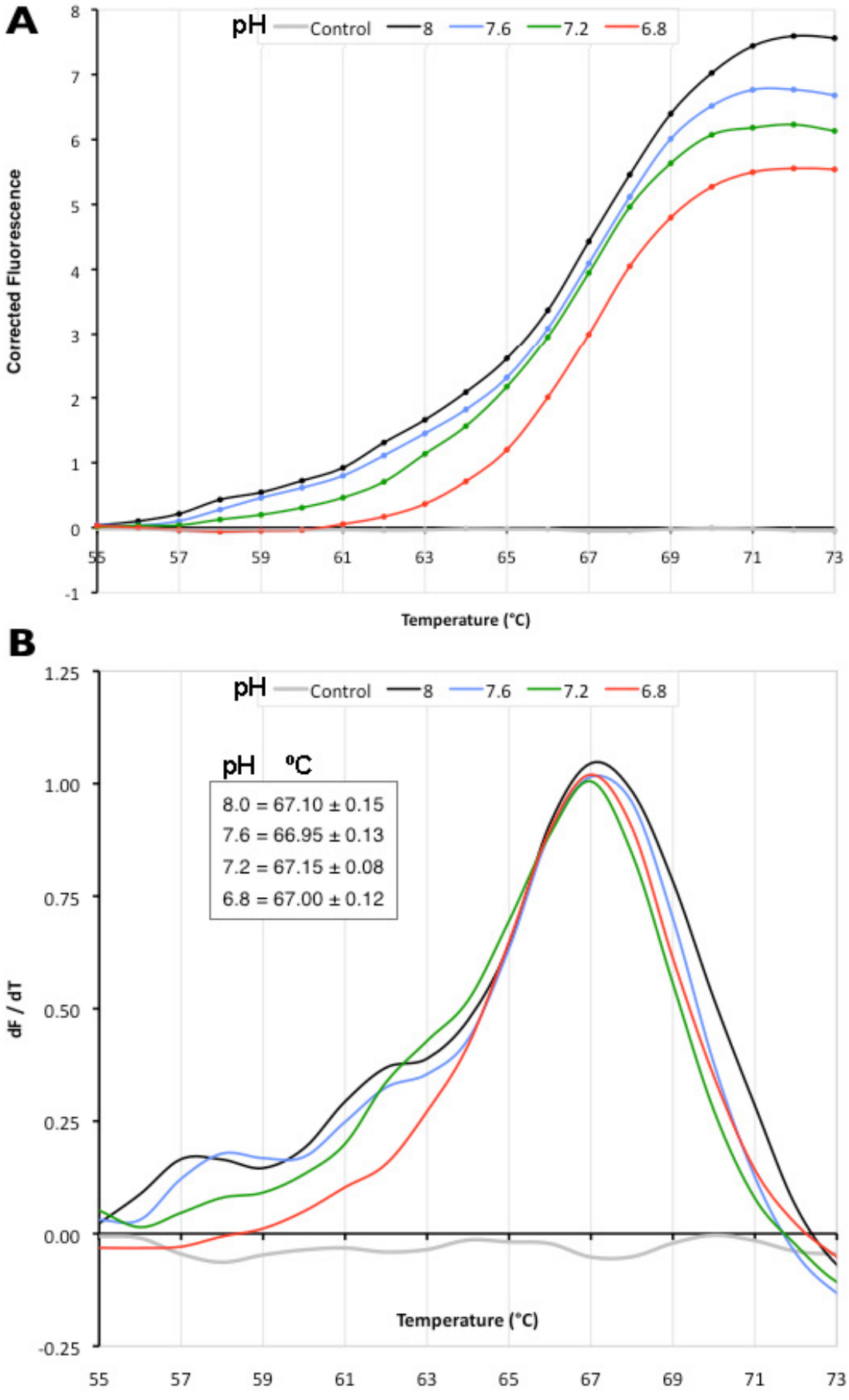

Sup Fig 10 (Legend on previous page)

APPENDIX: REFERENCES

Ahmad, M.F., Raman, B., Ramakrishna, T., and Rao Ch, M. (2008). Effect of phosphorylation on alpha B-crystallin: differences in stability, subunit exchange and chaperone activity of homo and mixed oligomers of alpha B-crystallin and its phosphorylation-mimicking mutant. J Mol Biol *375*, 1040-1051.

Ahrman, E., Lambert, W., Aquilina, J.A., Robinson, C.V., and Emanuelsson, C.S. (2007). Chemical cross-linking of the chloroplast localized small heat-shock protein, Hsp21, and the model substrate citrate synthase. Protein Sci *16*, 1464-1478.

Alizadeh, A., Clark, J., Seeberger, T., Hess, J., Blankenship, T., and FitzGerald, P.G. (2003). Targeted deletion of the lens fiber cell-specific intermediate filament protein filensin. Invest Ophthalmol Vis Sci *44*, 5252-5258.

Alizadeh, A., Clark, J., Seeberger, T., Hess, J., Blankenship, T., and FitzGerald, P.G. (2004). Characterization of a mutation in the lens-specific CP49 in the 129 strain of mouse. Invest Ophthalmol Vis Sci *45*, 884-891.

Alizadeh, A., Clark, J.I., Seeberger, T., Hess, J., Blankenship, T., Spicer, A., and FitzGerald, P.G. (2002). Targeted genomic deletion of the lens-specific intermediate filament protein CP49. Invest Ophthalmol Vis Sci *43*, 3722-3727.

Aquilina, J.A., Benesch, J.L., Bateman, O.A., Slingsby, C., and Robinson, C.V. (2003). Polydispersity of a mammalian chaperone: mass spectrometry reveals the population of oligomers in alphaB-crystallin. Proc Natl Acad Sci U S A *100*, 10611-10616.

Aquilina, J.A., Benesch, J.L., Ding, L.L., Yaron, O., Horwitz, J., and Robinson, C.V. (2004). Phosphorylation of alphaB-crystallin alters chaperone function through loss of dimeric substructure. J Biol Chem *279*, 28675-28680.

Aquilina, J.A., Benesch, J.L., Ding, L.L., Yaron, O., Horwitz, J., and Robinson, C.V. (2005). Subunit exchange of polydisperse proteins: mass spectrometry reveals consequences of alphaA-crystallin truncation. J Biol Chem *280*, 14485-14491.

Aquilina, J.A., and Watt, S.J. (2007). The N-terminal domain of alphaB-crystallin is protected from proteolysis by bound substrate. Biochem Biophys Res Commun *353*, 1115-1120.

Arai, H., and Atomi, Y. (1997). Chaperone activity of alpha B-crystallin suppresses tubulin aggregation through complex formation. Cell Struct Funct *22*, 539-544.

Arbustini, E., Pasotti, M., Pilotto, A., Pellegrini, C., Grasso, M., Previtali, S., Repetto, A., Bellini, O., Azan, G., Scaffino, M., *et al.* (2006). Desmin accumulation restrictive cardiomyopathy and atrioventricular block associated with desmin gene defects. Eur J Heart Fail *8*, 477-483.

Arcangeletti, M.C., Pinardi, F., Missorini, S., De Conto, F., Conti, G., Portincasa, P., Scherrer, K., and Chezzi, C. (1997). Modification of cytoskeleton and prosome networks in relation to protein synthesis in influenza A virus-infected LLC-MK2 cells. Virus research *51*, 19-34.

Arrigo, A.P., Simon, S., Gibert, B., Kretz-Remy, C., Nivon, M., Czekalla, A., Guillet, D., Moulin, M., Diaz-Latoud, C., and Vicart, P. (2007). Hsp27 (HspB1) and alphaB-crystallin (HspB5) as therapeutic targets. FEBS Lett *581*, 3665-3674.

Atomi, Y., Yamada, S., Strohman, R., and Nonomura, Y. (1991). Alpha B-crystallin in skeletal muscle: purification and localization. J Biochem *110*, 812-822.

Augusteyn, R.C. (1998). alpha-Crystallin polymers and polymerization: the view from down under. Int J Biol Macromol *22*, 253-262.

Augusteyn, R.C. (2004a). alpha-crystallin: a review of its structure and function. Clin Exp Optom *87*, 356-366.

Augusteyn, R.C. (2004b). Dissociation is not required for alpha-crystallin's chaperone function. Exp Eye Res *79*, 781-784.

Augusteyn, R.C. (2007). Growth of the human eye lens. Molecular vision *13*, 252-257.

Avilov, S.V., Aleksandrov, N.A., and Demchenko, A.P. (2004). Quaternary structure of alpha-crystallin is necessary for the binding of unfolded proteins: a surface plasmon resonance study. Protein Pept Lett *11*, 41-48.

Avivi, A., Joel, A., and Nevo, E. (2001). The lens protein alpha-B-crystallin of the blind subterranean mole-rat: high homology with sighted mammals. Gene *264*, 45-49.

Bagneris, C., Bateman, O.A., Naylor, C.E., Cronin, N., Boelens, W.C., Keep, N.H., and Slingsby, C. (2009). Crystal structures of alpha-crystallin domain dimers of alphaB-crystallin and Hsp20. J Mol Biol.

Bar, H., Fischer, D., Goudeau, B., Kley, R.A., Clemen, C.S., Vicart, P., Herrmann, H., Vorgerd, M., and Schroder, R. (2005). Pathogenic effects of a novel heterozygous R350P desmin mutation on the assembly of desmin intermediate filaments in vivo and in vitro. Hum Mol Genet *14*, 1251-1260.

Bar, H., Goudeau, B., Walde, S., Casteras-Simon, M., Mucke, N., Shatunov, A., Goldberg, Y.P., Clarke, C., Holton, J.L., Eymard, B., *et al.* (2007). Conspicuous involvement of desmin tail mutations in diverse cardiac and skeletal myopathies. Hum Mutat *28*, 374-386.

Bar, H., Schopferer, M., Sharma, S., Hochstein, B., Mucke, N., Herrmann, H., and Willenbacher, N. (2010). Mutations in desmin's carboxy-terminal "tail" domain severely modify filament and network mechanics. J Mol Biol *397*, 1188-1198.

Bardag-Gorce, F., Vu, J., Nan, L., Riley, N., Li, J., and French, S.W. (2004). Proteasome inhibition induces cytokeratin accumulation in vivo. Exp Mol Pathol *76*, 83-89.

Basha, E., Friedrich, K.L., and Vierling, E. (2006). The N-terminal arm of small heat shock proteins is important for both chaperone activity and substrate specificity. J Biol Chem *281*, 39943-39952.

Basha, E., Lee, G.J., Breci, L.A., Hausrath, A.C., Buan, N.R., Giese, K.C., and Vierling, E. (2004a). The identity of proteins associated with a small heat shock protein during heat stress in vivo indicates that these chaperones protect a wide range of cellular functions. J Biol Chem *279*, 7566-7575.

Basha, E., Lee, G.J., Demeler, B., and Vierling, E. (2004b). Chaperone activity of cytosolic small heat shock proteins from wheat. Eur J Biochem *271*, 1426-1436.

Bence, N.F., Sampat, R.M., and Kopito, R.R. (2001). Impairment of the ubiquitin-proteasome system by protein aggregation. Science *292*, 1552-1555.

Bennardini, F., Wrzosek, A., and Chiesi, M. (1992). Alpha B-crystallin in cardiac tissue. Association with actin and desmin filaments. Circ Res *71*, 288-294.

Bergman, J.E., Veenstra-Knol, H.E., van Essen, A.J., van Ravenswaaij, C.M., den Dunnen, W.F., van den Wijngaard, A., and van Tintelen, J.P. (2007). Two related Dutch families with a clinically variable presentation of cardioskeletal myopathy caused by a novel S13F mutation in the desmin gene. Eur J Med Genet *50*, 355-366.

Berry, V., Francis, P., Reddy, M.A., Collyer, D., Vithana, E., MacKay, I., Dawson, G., Carey, A.H., Moore, A., Bhattacharya, S.S., *et al.* (2001). Alpha-B crystallin gene (CRYAB) mutation causes dominant congenital posterior polar cataract in humans. Am J Hum Genet *69*, 1141-1145.

Bhat, S.P., Horwitz, J., Srinivasan, A., and Ding, L. (1991). Alpha B-crystallin exists as an independent protein in the heart and in the lens. Eur J Biochem *202*, 775-781.

Bhattacharyya, J., Padmanabha Udupa, E.G., Wang, J., and Sharma, K.K. (2006). Mini-alphaB-crystallin: a functional element of alphaB-crystallin with chaperone-like activity. Biochemistry *45*, 3069-3076.

Binkley, P.A., Hess, J., Casselman, J., and FitzGerald, P. (2002). Unexpected variation in unique features of the lens-specific type I cytokeratin CP49. Invest Ophthalmol Vis Sci *43*, 225-235.

Birkenberger, L., and Ip, W. (1990). Properties of the desmin tail domain: studies using synthetic peptides and antipeptide antibodies. J Cell Biol *111*, 2063-2075.

Biswas, A., and Das, K.P. (2004). Role of ATP on the interaction of alpha-crystallin with its substrates and its implications for the molecular chaperone function. J Biol Chem *279*, 42648-42657.

Blankenship, T.N., Hess, J.F., and FitzGerald, P.G. (2001). Development- and differentiation-dependent reorganization of intermediate filaments in fiber cells. Invest Ophthalmol Vis Sci *42*, 735-742.

Bloemendal, H., de Jong, W., Jaenicke, R., Lubsen, N.H., Slingsby, C., and Tardieu, A. (2004). Ageing and vision: structure, stability and function of lens crystallins. Prog Biophys Mol Biol *86*, 407-485.

Bluhm, W.F., Martin, J.L., Mestril, R., and Dillmann, W.H. (1998). Specific heat shock proteins protect microtubules during simulated ischemia in cardiac myocytes. Am J Physiol *275*, H2243-2249.

Borkman, R.F., and McLaughlin, J. (1995). The molecular chaperone function of alpha-crystallin is impaired by UV photolysis. Photochem Photobiol *62*, 1046-1051.

Bousquet, O., Ma, L., Yamada, S., Gu, C., Idei, T., Takahashi, K., Wirtz, D., and Coulombe, P.A. (2001). The nonhelical tail domain of keratin 14 promotes filament bundling and enhances the mechanical properties of keratin intermediate filaments in vitro. J Cell Biol *155*, 747-754.

Bova, M.P., Ding, L.L., Horwitz, J., and Fung, B.K. (1997). Subunit exchange of alphaA-crystallin. J Biol Chem *272*, 29511-29517.

Bova, M.P., McHaourab, H.S., Han, Y., and Fung, B.K. (2000). Subunit exchange of small heat shock proteins. Analysis of oligomer formation of alphaA-crystallin and Hsp27 by fluorescence resonance energy transfer and site-directed truncations. J Biol Chem *275*, 1035-1042.

Bova, M.P., Yaron, O., Huang, Q., Ding, L., Haley, D.A., Stewart, P.L., and Horwitz, J. (1999). Mutation R120G in alphaB-crystallin, which is linked to a desmin-related myopathy, results in an irregular structure and defective chaperone-like function. Proc Natl Acad Sci U S A *96*, 6137-6142.

Boyle, D.L., Takemoto, L., Brady, J.P., and Wawrousek, E.F. (2003). Morphological characterization of the Alpha A- and Alpha B-crystallin double knockout mouse lens. BMC Ophthalmol *3*, 3.

Bozanic, D., Bocina, I., and Saraga-Babic, M. (2006). Involvement of cytoskeletal proteins and growth factor receptors during development of the human eye. Anatomy and embryology *211*, 367-377.

Brady, J.P., Garland, D., Duglas-Tabor, Y., Robison, W.G., Jr., Groome, A., and Wawrousek, E.F. (1997). Targeted disruption of the mouse alpha A-crystallin gene induces cataract and cytoplasmic inclusion bodies containing the small heat shock protein alpha B-crystallin. Proc Natl Acad Sci U S A *94*, 884-889.

Brunkener, M., and Georgatos, S.D. (1992). Membrane-binding properties of filensin, a cytoskeletal protein of the lens fiber cells. J Cell Sci *103 (Pt 3)*, 709-718.

Bullard, B., Ferguson, C., Minajeva, A., Leake, M.C., Gautel, M., Labeit, D., Ding, L., Labeit, S., Horwitz, J., Leonard, K.R., *et al.* (2004). Association of the chaperone alphaB-crystallin with titin in heart muscle. J Biol Chem *279*, 7917-7924.

Bult, C.J., White, O., Olsen, G.J., Zhou, L., Fleischmann, R.D., Sutton, G.G., Blake, J.A., FitzGerald, L.M., Clayton, R.A., Gocayne, J.D., *et al.* (1996). Complete genome sequence of the methanogenic archaeon, Methanococcus jannaschii. Science *273*, 1058-1073.

Capetanaki, Y., and Milner, D.J. (1998). Desmin cytoskeleton in muscle integrity and function. Subcell Biochem *31*, 463-495.

Carlsson, L., Fischer, C., Sjoberg, G., Robson, R.M., Sejersen, T., and Thornell, L.E. (2002). Cytoskeletal derangements in hereditary myopathy with a desmin L345P mutation. Acta Neuropathol *104*, 493-504.

Carter, J.M., Hutcheson, A.M., and Quinlan, R.A. (1995). In vitro studies on the assembly properties of the lens proteins CP49, CP115: coassembly with alpha-crystallin but not with vimentin. Exp Eye Res *60*, 181-192.

Carver, J.A. (1999). Probing the structure and interactions of crystallin proteins by NMR spectroscopy. Prog Retin Eye Res *18*, 431-462.

Carver, J.A., Aquilina, J.A., Cooper, P.G., Williams, G.A., and Truscott, R.J. (1994). Alpha-crystallin: molecular chaperone and protein surfactant. Biochim Biophys Acta *1204*, 195-206.

Carver, J.A., Aquilina, J.A., Truscott, R.J., and Ralston, G.B. (1992). Identification by 1H NMR spectroscopy of flexible C-terminal extensions in bovine lens alpha-crystallin. FEBS Lett *311*, 143-149.

Carver, J.A., and Lindner, R.A. (1998). NMR spectroscopy of alpha-crystallin. Insights into the structure, interactions and chaperone action of small heat-shock proteins. Int J Biol Macromol *22*, 197-209.

Carver, J.A., Lindner, R.A., Lyon, C., Canet, D., Hernandez, H., Dobson, C.M., and Redfield, C. (2002). The interaction of the molecular chaperone alpha-crystallin with unfolding alpha-lactalbumin: a structural and kinetic spectroscopic study. J Mol Biol *318*, 815-827.

Chen, Q., Liu, J.B., Horak, K.M., Zheng, H., Kumarapeli, A.R., Li, J., Li, F., Gerdes, A.M., Wawrousek, E.F., and Wang, X. (2005). Intrasarcoplasmic amyloidosis impairs proteolytic function of proteasomes in cardiomyocytes by compromising substrate uptake. Circ Res *97*, 1018-1026.

Chen, Q., Ma, J., Yan, M., Mothobi, M.E., Liu, Y., and Zheng, F. (2009). A novel mutation in CRYAB associated with autosomal dominant congenital nuclear cataract in a Chinese family. Mol Vis *15*, 1359-1365.

Chen, W.J., and Liem, R.K. (1994). The endless story of the glial fibrillary acidic protein. J Cell Sci *107 (Pt 8)*, 2299-2311.

Cheng, G., Basha, E., Wysocki, V.H., and Vierling, E. (2008). Insights into small heat shock protein and substrate structure during chaperone action derived from hydrogen/deuterium exchange and mass spectrometry. J Biol Chem *283*, 26634-26642.

Chiesi, M., Longoni, S., and Limbruno, U. (1990). Cardiac alpha-crystallin. III. Involvement during heart ischemia. Mol Cell Biochem *97*, 129-136.

Cho, W., and Messing, A. (2009). Properties of astrocytes cultured from GFAP over-expressing and GFAP mutant mice. Exp Cell Res *315*, 1260-1272.

Ciocca, D.R., and Calderwood, S.K. (2005). Heat shock proteins in cancer: diagnostic, prognostic, predictive, and treatment implications. Cell Stress Chaperones *10*, 86-103.

Clark, A.R., Naylor, C.E., Bagneris, C., Keep, N.H., and Slingsby, C. (2011). Crystal Structure of R120G Disease Mutant of Human alphaB-Crystallin Domain Dimer Shows Closure of a Groove. J Mol Biol. 2011 Apr 22;408(1):118-34.

Conley, Y.P., Erturk, D., Keverline, A., Mah, T.S., Keravala, A., Barnes, L.R., Bruchis, A., Hess, J.F., FitzGerald, P.G., Weeks, D.E., *et al.* (2000). A juvenile-onset, progressive cataract locus on chromosome 3q21-q22 is associated with a missense mutation in the beaded filament structural protein-2. Am J Hum Genet *66*, 1426-1431.

Cross, F.R., Garber, E.A., Pellman, D., and Hanafusa, H. (1984). A short sequence in the p60src N terminus is required for p60src myristylation and membrane association and for cell transformation. Mol Cell Biol *4*, 1834-1842.

Cui, X., Gao, L., Jin, Y., Zhang, Y., Bai, J., Feng, G., Gao, W., Liu, P., He, L., and Fu, S. (2007). The E233del mutation in BFSP2 causes a progressive autosomal dominant congenital cataract in a Chinese family. Mol Vis *13*, 2023-2029.

D'Alessandro, M., Russell, D., Morley, S.M., Davies, A.M., and Lane, E.B. (2002). Keratin mutations of epidermolysis bullosa simplex alter the kinetics of stress response to osmotic shock. J Cell Sci *115*, 4341-4351.

Dagvadorj, A., Goudeau, B., Hilton-Jones, D., Blancato, J.K., Shatunov, A., Simon-Casteras, M., Squier, W., Nagle, J.W., Goldfarb, L.G., and Vicart, P. (2003). Respiratory insufficiency in desminopathy patients caused by introduction of proline residues in desmin c-terminal alphα-helical segment. Muscle Nerve *27*, 669-675.

Dalakas, M.C., Park, K.Y., Semino-Mora, C., Lee, H.S., Sivakumar, K., and Goldfarb, L.G. (2000). Desmin myopathy, a skeletal myopathy with cardiomyopathy caused by mutations in the desmin gene. N Engl J Med *342*, 770-780.

Datta, S.A., and Rao, C.M. (1999). Differential temperature-dependent chaperone-like activity of alphaA- and alphaB-crystallin homoaggregates. J Biol Chem *274*, 34773-34778.

de Jong, W.W., Zweers, A., Versteeg, M., and Nuy-Terwindt, E.C. (1984). Primary structures of the alpha-crystallin A chains of twenty-eight mammalian species, chicken and frog. Eur J Biochem *141*, 131-140.

del Valle, L.J., Escribano, C., Perez, J.J., and Garriga, P. (2002). Calcium-induced decrease of the thermal stability and chaperone activity of alpha-crystallin. Biochim Biophys Acta *1601*, 100-109.

den Engelsman, J., Bennink, E.J., Doerwald, L., Onnekink, C., Wunderink, L., Andley, U.P., Kato, K., de Jong, W.W., and Boelens, W.C. (2004). Mimicking phosphorylation of the small heat-shock protein alphaB-crystallin recruits the F-box protein FBX4 to nuclear SC35 speckles. Eur J Biochem *271*, 4195-4203.

den Engelsman, J., Keijsers, V., de Jong, W.W., and Boelens, W.C. (2003). The small heat-shock protein alpha B-crystallin promotes FBX4-dependent ubiquitination. J Biol Chem *278*, 4699-4704.

Der Perng, M., Su, M., Wen, S.F., Li, R., Gibbon, T., Prescott, A.R., Brenner, M., and Quinlan, R.A. (2006). The Alexander disease-causing glial fibrillary acidic protein mutant, R416W, accumulates into Rosenthal fibers by a pathway that involves filament aggregation and the association of alpha B-crystallin and HSP27. Am J Hum Genet *79*, 197-213.

Devi, R.R., Yao, W., Vijayalakshmi, P., Sergeev, Y.V., Sundaresan, P., and Hejtmancik, J.F. (2008). Crystallin gene mutations in Indian families with inherited pediatric cataract. Mol Vis *14*, 1157-1170.

Djabali, K., de Nechaud, B., Landon, F., and Portier, M.M. (1997). AlphaB-crystallin interacts with intermediate filaments in response to stress. J Cell Sci *110 (Pt 21)*, 2759-2769.

Djabali, K., Piron, G., de Nechaud, B., and Portier, M.M. (1999). alphaB-crystallin interacts with cytoplasmic intermediate filament bundles during mitosis. Exp Cell Res *253*, 649-662.

Duncan, G., and Jacob, T.J. (1984). Calcium and the physiology of cataract. Ciba Found Symp *106*, 132-152.

Dyson, H.J., and Wright, P.E. (2005). Intrinsically unstructured proteins and their functions. Nat Rev Mol Cell Biol *6*, 197-208.

Eftink, M.R. (1995). Use of multiple spectroscopic methods to monitor equilibrium unfolding of proteins. Methods Enzymol *259*, 487-512.

Ehrnsperger, M., Graber, S., Gaestel, M., and Buchner, J. (1997). Binding of non-native protein to Hsp25 during heat shock creates a reservoir of folding intermediates for reactivation. EMBO J *16*, 221-229.

Ehrnsperger, M., Lilie, H., Gaestel, M., and Buchner, J. (1999). The dynamics of Hsp25 quaternary structure. Structure and function of different oligomeric species. J Biol Chem *274*, 14867-14874.

Ellis, R.J., and Minton, A.P. (2006). Protein aggregation in crowded environments. Biological chemistry *387*, 485-497.

Emsley, P., and Cowtan, K. (2004). Coot: model-building tools for molecular graphics. Acta Crystallogr D Biol Crystallogr *60*, 2126-2132.

Englander, S.W., Mayne, L., and Krishna, M.M. (2007). Protein folding and misfolding: mechanism and principles. Q Rev Biophys *40*, 287-326.

Eswar, N., Eramian, D., Webb, B., Shen, M.Y., and Sali, A. (2008). Protein structure modeling with MODELLER. Methods Mol Biol *426*, 145-159.

Evgrafov, O.V., Mersiyanova, I., Irobi, J., Van Den Bosch, L., Dierick, I., Leung, C.L., Schagina, O., Verpoorten, N., Van Impe, K., Fedotov, V., *et al.* (2004). Mutant small heat-shock protein 27 causes axonal Charcot-Marie-Tooth disease and distal hereditary motor neuropathy. Nat Genet *36*, 602-606.

Favre, B., Schneider, Y., Lingasamy, P., Bouameur, J.E., Begre, N., Gontier, Y., Steiner-Champliaud, M.F., Frias, M.A., Borradori, L., and Fontao, L. (2011). Plectin interacts with the rod domain of type III intermediate filament proteins desmin and vimentin. Eur J Cell Biol *90*, 390-400.

Feil, I.K., Malfois, M., Hendle, J., van Der Zandt, H., and Svergun, D.I. (2001). A novel quaternary structure of the dimeric alpha-crystallin domain with chaperone-like activity. J Biol Chem *276*, 12024-12029.

Fidzianska, A., Kotowicz, J., Sadowska, M., Goudeau, B., Walczak, E., Vicart, P., and Hausmanowa-Petrusewicz, I. (2005). A novel desmin R355P mutation causes cardiac and skeletal myopathy. Neuromuscul Disord *15*, 525-531.

Fischer, R.S., Quinlan, R.A., and Fowler, V.M. (2003). Tropomodulin binds to filensin intermediate filaments. FEBS Lett *547*, 228-232.

FitzGerald, P.G. (1990). Methods for the circumvention of problems associated with the study of the ocular lens plasma membrane-cytoskeleton complex. Curr Eye Res *9*, 1083-1097.

FitzGerald, P.G., and Casselman, J. (1991). Immunologic conservation of the fiber cell beaded filament. Current eye research *10*, 471-478.

Franck, E., Madsen, O., van Rheede, T., Ricard, G., Huynen, M.A., and de Jong, W.W. (2004). Evolutionary diversity of vertebrate small heat shock proteins. J Mol Evol *59*, 792-805.

Franke, W.W., Hergt, M., and Grund, C. (1987a). Rearrangement of the vimentin cytoskeleton during adipose conversion: formation of an intermediate filament cage around lipid globules. Cell *49*, 131-141.

Franke, W.W., Kapprell, H.P., and Cowin, P. (1987b). Plakoglobin is a component of the filamentous subplasmalemmal coat of lens cells. Eur J Cell Biol *43*, 301-315.

Franzmann, T.M., Menhorn, P., Walter, S., and Buchner, J. (2008). Activation of the chaperone Hsp26 is controlled by the rearrangement of its thermosensor domain. Mol Cell *29*, 207-216.

Franzmann, T.M., Wuhr, M., Richter, K., Walter, S., and Buchner, J. (2005). The activation mechanism of Hsp26 does not require dissociation of the oligomer. J Mol Biol *350*, 1083-1093.

Friedrich, K.L., Giese, K.C., Buan, N.R., and Vierling, E. (2004). Interactions between small heat shock protein subunits and substrate in small heat shock protein-substrate complexes. J Biol Chem *279*, 1080-1089.

Fu, X., Liu, C., Liu, Y., Feng, X., Gu, L., Chen, X., and Chang, Z. (2003). Small heat shock protein Hsp16.3 modulates its chaperone activity by adjusting the rate of oligomeric dissociation. Biochem Biophys Res Commun *310*, 412-420.

Fu, X., Zhang, H., Zhang, X., Cao, Y., Jiao, W., Liu, C., Song, Y., Abulimiti, A., and Chang, Z. (2005). A dual role for the N-terminal region of Mycobacterium tuberculosis Hsp16.3 in self-oligomerization and binding denaturing substrate proteins. J Biol Chem *280*, 6337-6348.

Fuchs, E., and Weber, K. (1994). Intermediate filaments: structure, dynamics, function, and disease. Annu Rev Biochem *63*, 345-382.

Fuchs, E., and Yang, Y. (1999). Crossroads on cytoskeletal highways. Cell *98*, 547-550.

Fujita, Y., Ohto, E., Katayama, E., and Atomi, Y. (2004). alphaB-Crystallin-coated MAP microtubule resists nocodazole and calcium-induced disassembly. J Cell Sci *117*, 1719-1726.

Ganadu, M.L., Aru, M., Mura, G.M., Coi, A., Mlynarz, P., and Kozlowski, H. (2004). Effects of divalent metal ions on the alphaB-crystallin chaperone-like activity: spectroscopic evidence for a complex between copper(II) and protein. J Inorg Biochem *98*, 1103-1109.

Geeves, M.A., Fedorov, R., and Manstein, D.J. (2005). Molecular mechanism of actomyosin-based motility. Cell Mol Life Sci *62*, 1462-1477.

Geisler, N., Kaufmann, E., and Weber, K. (1982). Proteinchemical characterization of three structurally distinct domains along the protofilament unit of desmin 10 nm filaments. Cell *30*, 277-286.

Ghosh, J.G., and Clark, J.I. (2005). Insights into the domains required for dimerization and assembly of human alphaB crystallin. Protein Sci *14*, 684-695.

Ghosh, J.G., Estrada, M.R., and Clark, J.I. (2005). Interactive domains for chaperone activity in the small heat shock protein, human alphaB crystallin. Biochemistry *44*, 14854-14869.

Ghosh, J.G., Estrada, M.R., and Clark, J.I. (2006a). Structure-based analysis of the beta8 interactive sequence of human alphaB crystallin. Biochemistry *45*, 9878-9886.

Ghosh, J.G., Estrada, M.R., Houck, S.A., and Clark, J.I. (2006b). The function of the beta3 interactive domain in the small heat shock protein and molecular chaperone, human alphaB crystallin. Cell Stress Chaperones *11*, 187-197.

Ghosh, J.G., Houck, S.A., and Clark, J.I. (2007a). Interactive domains in the molecular chaperone human alphaB crystallin modulate microtubule assembly and disassembly. PLoS ONE *2*, e498.

Ghosh, J.G., Houck, S.A., and Clark, J.I. (2007b). Interactive sequences in the stress protein and molecular chaperone human alphaB crystallin recognize and modulate the assembly of filaments. Int J Biochem Cell Biol *39*, 1804-1815.

Ghosh, J.G., Houck, S.A., and Clark, J.I. (2008). Interactive sequences in the molecular chaperone, human alphaB crystallin modulate the fibrillation of amyloidogenic proteins. Int J Biochem Cell Biol.

Ghosh, J.G., Houck, S.A., Doneanu, C.E., and Clark, J.I. (2006c). The beta4-beta8 groove is an ATP-interactive site in the alpha crystallin core domain of the small heat shock protein, human alphaB crystallin. J Mol Biol *364*, 364-375.

Ghosh, J.G., Shenoy, A.K., Jr., and Clark, J.I. (2006d). N- and C-Terminal motifs in human alphaB crystallin play an important role in the recognition, selection, and solubilization of substrates. Biochemistry *45*, 13847-13854.

Ghosh, J.G., Shenoy, A.K., Jr., and Clark, J.I. (2007c). Interactions between important regulatory proteins and human alphaB crystallin. Biochemistry *46*, 6308-6317.

Giese, K.C., Basha, E., Catague, B.Y., and Vierling, E. (2005). Evidence for an essential function of the N terminus of a small heat shock protein in vivo, independent of in vitro chaperone activity. Proc Natl Acad Sci U S A *102*, 18896-18901.

Giese, K.C., and Vierling, E. (2002). Changes in oligomerization are essential for the chaperone activity of a small heat shock protein in vivo and in vitro. J Biol Chem *277*, 46310-46318.

Giese, K.C., and Vierling, E. (2004). Mutants in a small heat shock protein that affect the oligomeric state. Analysis and allele-specific suppression. J Biol Chem *279*, 32674-32683.

Goldfarb, L.G., and Dalakas, M.C. (2009). Tragedy in a heartbeat: malfunctioning desmin causes skeletal and cardiac muscle disease. J Clin Invest *119*, 1806-1813.

Goldfarb, L.G., Olive, M., Vicart, P., and Goebel, H.H. (2008). Intermediate filament diseases: desminopathy. Adv Exp Med Biol *642*, 131-164.

Goldfarb, L.G., Park, K.Y., Cervenakova, L., Gorokhova, S., Lee, H.S., Vasconcelos, O., Nagle, J.W., Semino-Mora, C., Sivakumar, K., and Dalakas, M.C. (1998). Missense mutations in desmin associated with familial cardiac and skeletal myopathy. Nat Genet *19*, 402-403.

Goldfarb, L.G., Vicart, P., Goebel, H.H., and Dalakas, M.C. (2004). Desmin myopathy. Brain *127*, 723-734.

Golenhofen, N., Arbeiter, A., Koob, R., and Drenckhahn, D. (2002). Ischemia-induced association of the stress protein alpha B-crystallin with I-band portion of cardiac titin. J Mol Cell Cardiol *34*, 309-319.

Golenhofen, N., Htun, P., Ness, W., Koob, R., Schaper, W., and Drenckhahn, D. (1999). Binding of the stress protein alpha B-crystallin to cardiac myofibrils correlates with the degree of myocardial damage during ischemia/reperfusion in vivo. J Mol Cell Cardiol *31*, 569-580.

Golenhofen, N., Perng, M.D., Quinlan, R.A., and Drenckhahn, D. (2004). Comparison of the small heat shock proteins alphaB-crystallin, MKBP, HSP25, HSP20, and cvHSP in heart and skeletal muscle. Histochem Cell Biol *122*, 415-425.

Goudeau, B., Dagvadorj, A., Rodrigues-Lima, F., Nedellec, P., Casteras-Simon, M., Perret, E., Langlois, S., Goldfarb, L., and Vicart, P. (2001). Structural and functional analysis of a new desmin variant causing desmin-related myopathy. Hum Mutat *18*, 388-396.

Goudeau, B., Rodrigues-Lima, F., Fischer, D., Casteras-Simon, M., Sambuughin, N., de Visser, M., Laforet, P., Ferrer, X., Chapon, F., Sjoberg, G., *et al.* (2006). Variable pathogenic potentials of mutations located in the desmin alphα-helical domain. Hum Mutat *27*, 906-913.

Goulielmos, G., Gounari, F., Remington, S., Muller, S., Haner, M., Aebi, U., and Georgatos, S.D. (1996). Filensin and phakinin form a novel type of beaded intermediate filaments and coassemble de novo in cultured cells. J Cell Biol *132*, 643-655.

Granzier, H.L., and Labeit, S. (2004). The giant protein titin: a major player in myocardial mechanics, signaling, and disease. Circ Res *94*, 284-295.

Gupta, R., and Srivastava, O.P. (2004). Effect of deamidation of asparagine 146 on functional and structural properties of human lens alphaB-crystallin. Invest Ophthalmol Vis Sci *45*, 206-214.

Hagemann, T.L., Boelens, W.C., Wawrousek, E.F., and Messing, A. (2009). Suppression of GFAP toxicity by alphaB-crystallin in mouse models of Alexander disease. Hum Mol Genet *18*, 1190-1199.

Haley, D.A., Bova, M.P., Huang, Q.L., McHaourab, H.S., and Stewart, P.L. (2000). Small heat-shock protein structures reveal a continuum from symmetric to variable assemblies. J Mol Biol *298*, 261-272.

Haley, D.A., Horwitz, J., and Stewart, P.L. (1998). The small heat-shock protein, alphaB-crystallin, has a variable quaternary structure. J Mol Biol *277*, 27-35.

Harada, M., Strnad, P., Toivola, D.M., and Omary, M.B. (2008). Autophagy modulates keratin-containing inclusion formation and apoptosis in cell culture in a context-dependent fashion. Exp Cell Res *314*, 1753-1764.

Haslbeck, M., Franzmann, T., Weinfurtner, D., and Buchner, J. (2005a). Some like it hot: the structure and function of small heat-shock proteins. Nat Struct Mol Biol *12*, 842-846.

Haslbeck, M., Ignatiou, A., Saibil, H., Helmich, S., Frenzl, E., Stromer, T., and Buchner, J. (2004). A domain in the N-terminal part of Hsp26 is essential for chaperone function and oligomerization. J Mol Biol *343*, 445-455.

Haslbeck, M., Miess, A., Stromer, T., Walter, S., and Buchner, J. (2005b). Disassembling protein aggregates in the yeast cytosol. The cooperation of Hsp26 with Ssa1 and Hsp104. J Biol Chem *280*, 23861-23868.

Hayes, V.H., Devlin, G.L., and Quinlan, R.A. (2008). Truncation of alphaB-crystallin by the myopathy-causing Q151X mutation significantly destabilizes the protein leading to aggregate formation in transfected cells. J Biol Chem.

Head, M.W., Corbin, E., and Goldman, J.E. (1994). Coordinate and independent regulation of alpha B-crystallin and hsp27 expression in response to physiological stress. J Cell Physiol *159*, 41-50.

Head, M.W., and Goldman, J.E. (2000). Small heat shock proteins, the cytoskeleton, and inclusion body formation. Neuropathol Appl Neurobiol *26*, 304-312.

Herrmann, H., and Aebi, U. (2000). Intermediate filaments and their associates: multi-talented structural elements specifying cytoarchitecture and cytodynamics. Curr Opin Cell Biol *12*, 79-90.

Herrmann, H., and Aebi, U. (2004). Intermediate filaments: molecular structure, assembly mechanism, and integration into functionally distinct intracellular Scaffolds. Annu Rev Biochem *73*, 749-789.

Herrmann, H., Haner, M., Brettel, M., Ku, N.O., and Aebi, U. (1999). Characterization of distinct early assembly units of different intermediate filament proteins. J Mol Biol *286*, 1403-1420.

Herrmann, H., Haner, M., Brettel, M., Muller, S.A., Goldie, K.N., Fedtke, B., Lustig, A., Franke, W.W., and Aebi, U. (1996). Structure and assembly properties of the intermediate filament protein vimentin: the role of its head, rod and tail domains. J Mol Biol *264*, 933-953.

Herrmann, H., Hofmann, I., and Franke, W.W. (1992). Identification of a nonapeptide motif in the vimentin head domain involved in intermediate filament assembly. J Mol Biol *223*, 637-650.

Herrmann, H., Strelkov, S.V., Burkhard, P., and Aebi, U. (2009). Intermediate filaments: primary determinants of cell architecture and plasticity. J Clin Invest *119*, 1772-1783.

Herrmann, H., Strelkov, S.V., Feja, B., Rogers, K.R., Brettel, M., Lustig, A., Haner, M., Parry, D.A., Steinert, P.M., Burkhard, P., *et al.* (2000). The intermediate filament protein consensus motif of helix 2B: its atomic structure and contribution to assembly. J Mol Biol *298*, 817-832.

Hijikata, T., Murakami, T., Imamura, M., Fujimaki, N., and Ishikawa, H. (1999). Plectin is a linker of intermediate filaments to Z-discs in skeletal muscle fibers. J Cell Sci *112 (Pt 6)*, 867-876.

Hilario, E., Martin, F.J., Bertolini, M.C., and Fan, L. (2011). Crystal Structures of Xanthomonas Small Heat Shock Protein Provide a Structural Basis for an Active Molecular Chaperone Oligomer. J Mol Biol. 2011 Apr 22;408(1):74-86.

Hoffman, E.P. (2003). Desminopathies: good stuff lost, garbage gained, or the trashman misdirected? Muscle Nerve *27*, 643-645.

Horwich, A.L., Fenton, W.A., Chapman, E., and Farr, G.W. (2007). Two families of chaperonin: physiology and mechanism. Annu Rev Cell Dev Biol *23*, 115-145.

Horwitz, J. (1992). Alpha-crystallin can function as a molecular chaperone. Proc Natl Acad Sci U S A *89*, 10449-10453.

Horwitz, J. (2003). Alpha-crystallin. Exp Eye Res *76*, 145-153.

Horwitz, J. (2008). Alpha crystallin: The quest for a homogeneous quaternary structure. Exp Eye Res.

Horwitz, J., Huang, Q., and Ding, L. (2004). The native oligomeric organization of alpha-crystallin, is it necessary for its chaperone function? Exp Eye Res *79*, 817-821.

Houck SA*, Landsbury A*, Clark JI, Quinlan RA. (2011). Multiple sites in αB-crystallin modulate interactions with desmin filaments assembled *in vitro*. PLoS ONE *6(11)*. (*Joint first author)

Inada, H., Togashi, H., Nakamura, Y., Kaibuchi, K., Nagata, K., and Inagaki, M. (1999). Balance between activities of Rho kinase and type 1 protein phosphatase modulates turnover of phosphorylation and dynamics of desmin/vimentin filaments. J Biol Chem *274*, 34932-34939.

Inagaki, N., Hayashi, T., Arimura, T., Koga, Y., Takahashi, M., Shibata, H., Teraoka, K., Chikamori, T., Yamashina, A., and Kimura, A. (2006). Alpha B-crystallin mutation in dilated cardiomyopathy. Biochem Biophys Res Commun *342*, 379-386.

Ireland, M.E., Klettner, C., and Nunlee, W. (1993). Cyclic AMP-mediated phosphorylation and insolubilization of a 49-kDa cytoskeletal marker protein of lens fiber terminal differentiation. Exp Eye Res *56*, 453-461.

Ireland, M.E., Wallace, P., Sandilands, A., Poosch, M., Kasper, M., Graw, J., Liu, A., Maisel, H., Prescott, A.R., Hutcheson, A.M., *et al.* (2000). Up-regulation of novel intermediate filament proteins in primary fiber cells: an indicator of all vertebrate lens fiber differentiation? The Anatomical record *258*, 25-33.

Irobi, J., Van Impe, K., Seeman, P., Jordanova, A., Dierick, I., Verpoorten, N., Michalik, A., De Vriendt, E., Jacobs, A., Van Gerwen, V., *et al.* (2004). Hot-spot residue in small heat-shock protein 22 causes distal motor neuropathy. Nat Genet *36*, 597-601.

Ito, H., Kamei, K., Iwamoto, I., Inaguma, Y., Garcia-Mata, R., Sztul, E., and Kato, K. (2002). Inhibition of proteasomes induces accumulation, phosphorylation, and recruitment of HSP27 and alphaB-crystallin to aggresomes. J Biochem *131*, 593-603.

Ito, H., Kamei, K., Iwamoto, I., Inaguma, Y., Nohara, D., and Kato, K. (2001). Phosphorylation-induced change of the oligomerization state of alpha B-crystallin. J Biol Chem *276*, 5346-5352.

Ito, H., Kamei, K., Iwamoto, I., Inaguma, Y., Tsuzuki, M., Kishikawa, M., Shimada, A., Hosokawa, M., and Kato, K. (2003). Hsp27 suppresses the formation of inclusion bodies induced by expression of R120G alpha B-crystallin, a cause of desmin-related myopathy. Cell Mol Life Sci *60*, 1217-1223.

Iwaki, T., Iwaki, A., Liem, R.K., and Goldman, J.E. (1991). Expression of alpha B-crystallin in the developing rat kidney. Kidney Int *40*, 52-56.

Iwaki, T., Iwaki, A., Tateishi, J., and Goldman, J.E. (1994). Sense and antisense modification of glial alpha B-crystallin production results in alterations of stress fiber formation and thermoresistance. J Cell Biol *125*, 1385-1393.

Iwaki, T., Iwaki, A., Tateishi, J., Sakaki, Y., and Goldman, J.E. (1993). Alpha B-crystallin and 27-kd heat shock protein are regulated by stress conditions in the central nervous system and accumulate in Rosenthal fibers. Am J Pathol *143*, 487-495.

Iwaki, T., Kume-Iwaki, A., and Goldman, J.E. (1990). Cellular distribution of alpha B-crystallin in non-lenticular tissues. J Histochem Cytochem *38*, 31-39.

Iwaki, T., Kume-Iwaki, A., Liem, R.K., and Goldman, J.E. (1989). Alpha B-crystallin is expressed in non-lenticular tissues and accumulates in Alexander's disease brain. Cell *57*, 71-78.

Jakobs, P.M., Hess, J.F., FitzGerald, P.G., Kramer, P., Weleber, R.G., and Litt, M. (2000). Autosomal-dominant congenital cataract associated with a deletion mutation in the human beaded filament protein gene BFSP2. Am J Hum Genet *66*, 1432-1436.

Janmey, P.A., Winer, J.P., Murray, M.E., and Wen, Q. (2009). The hard life of soft cells. Cell Motil Cytoskeleton *66*, 597-605.

Jaya, N., Garcia, V., and Vierling, E. (2009). Substrate binding site flexibility of the small heat shock protein molecular chaperones. Proc Natl Acad Sci U S A. 2009 Sep 15;106(37):15604-9.

Jehle, S., Rajagopal, P., Bardiaux, B., Markovic, S., Kuhne, R., Stout, J.R., Higman, V.A., Klevit, R.E., van Rossum, B.J., and Oschkinat, H. (2010). Solid-state NMR and SAXS studies provide a structural basis for the activation of alphaB-crystallin oligomers. Nat Struct Mol Biol *17*, 1037-1042.

Jehle, S., Vollmar, B.S., Bardiaux, B., Dove, K.K., Rajagopal, P., Gonen, T., Oschkinat, H., and Klevit, R.E. (2011). N-terminal domain of {alpha}B-crystallin provides a conformational switch for multimerization and structural heterogeneity. Proc Natl Acad Sci U S A;108(16):6409-14

Jiao, W., Qian, M., Li, P., Zhao, L., and Chang, Z. (2005). The essential role of the flexible termini in the temperature-responsiveness of the oligomeric state and chaperone-like activity for the polydisperse small heat shock protein IbpB from Escherichia coli. J Mol Biol *347*, 871-884.

Kamei, A., Hamaguchi, T., Matsuura, N., and Masuda, K. (2001). Does post-translational modification influence chaperone-like activity of alpha-crystallin? I. Study on phosphorylation. Biol Pharm Bull *24*, 96-99.

Kaminska, A., Strelkov, S.V., Goudeau, B., Olive, M., Dagvadorj, A., Fidzianska, A., Simon-Casteras, M., Shatunov, A., Dalakas, M.C., Ferrer, I., *et al.* (2004). Small deletions disturb desmin architecture leading to breakdown of muscle cells and development of skeletal or cardioskeletal myopathy. Hum Genet *114*, 306-313.

Kamradt, M.C., Lu, M., Werner, M.E., Kwan, T., Chen, F., Strohecker, A., Oshita, S., Wilkinson, J.C., Yu, C., Oliver, P.G., *et al.* (2005). The small heat shock protein alpha B-crystallin is a novel inhibitor of TRAIL-induced apoptosis that suppresses the activation of caspase-3. J Biol Chem *280*, 11059-11066.

Kantorow, M., and Piatigorsky, J. (1998). Phosphorylations of alpha A- and alpha B-crystallin. Int J Biol Macromol *22*, 307-314.

Kappe, G., Aquilina, J.A., Wunderink, L., Kamps, B., Robinson, C.V., Garate, T., Boelens, W.C., and de Jong, W.W. (2004). Tsp36, a tapeworm small heat-shock protein with a duplicated alpha-crystallin domain, forms dimers and tetramers with good chaperone-like activity. Proteins *57*, 109-117.

Kappe, G., Franck, E., Verschuure, P., Boelens, W.C., Leunissen, J.A., and de Jong, W.W. (2003). The human genome encodes 10 alpha-crystallin-related small heat shock proteins: HspB1-10. Cell Stress Chaperones *8*, 53-61.

Kasakov, A.S., Bukach, O.V., Seit-Nebi, A.S., Marston, S.B., and Gusev, N.B. (2007). Effect of mutations in the beta5-beta7 loop on the structure and properties of human small heat shock protein HSP22 (HspB8, H11). FEBS J *274*, 5628-5642.

Kasper, M., and Viebahn, C. (1992). Cytokeratin expression and early lens development. Anatomy and embryology *186*, 285-290.

Kato, K., Goto, S., Hasegawa, K., Shinohara, H., and Inaguma, Y. (1993). Responses to heat shock of alpha B crystallin and HSP28 in U373 MG human glioma cells. Biochim Biophys Acta *1175*, 257-262.

Kato, K., Ito, H., Inaguma, Y., Okamoto, K., and Saga, S. (1996). Synthesis and accumulation of alphaB crystallin in C6 glioma cells is induced by agents that promote the disassembly of microtubules. J Biol Chem *271*, 26989-26994.

Kato, K., Shinohara, H., Goto, S., Inaguma, Y., Morishita, R., and Asano, T. (1992). Copurification of small heat shock protein with alpha B crystallin from human skeletal muscle. J Biol Chem *267*, 7718-7725.

Kato, K., Shinohara, H., Kurobe, N., Inaguma, Y., Shimizu, K., and Ohshima, K. (1991). Tissue distribution and developmental profiles of immunoreactive alpha B crystallin in the rat determined with a sensitive immunoassay system. Biochim Biophys Acta *1074*, 201-208.

Kaufmann, E., Weber, K., and Geisler, N. (1985). Intermediate filament forming ability of desmin derivatives lacking either the amino-terminal 67 or the carboxy-terminal 27 residues. J Mol Biol *185*, 733-742.

Kelly, S.P., Thornton, J., Edwards, R., Sahu, A., and Harrison, R. (2005). Smoking and cataract: review of causal association. J Cataract Refract Surg *31*, 2395-2404.

Kim, K.K., Kim, R., and Kim, S.H. (1998). Crystal structure of a small heat-shock protein. Nature *394*, 595-599.

Kim, R., Lai, L., Lee, H.H., Cheong, G.W., Kim, K.K., Wu, Z., Yokota, H., Marqusee, S., and Kim, S.H. (2003). On the mechanism of chaperone activity of the small heat-shock protein of Methanococcus jannaschii. Proc Natl Acad Sci U S A *100*, 8151-8155.

Kim, S., and Coulombe, P.A. (2007). Intermediate filament scaffolds fulfill mechanical, organizational, and signaling functions in the cytoplasm. Genes & development *21*, 1581-1597.

Kirmse, R., Portet, S., Mucke, N., Aebi, U., Herrmann, H., and Langowski, J. (2007). A quantitative kinetic model for the in vitro assembly of intermediate filaments from tetrameric vimentin. J Biol Chem *282*, 18563-18572.

Koretz, J.F., Doss, E.W., and LaButti, J.N. (1998). Environmental factors influencing the chaperone-like activity of alpha-crystallin. Int J Biol Macromol *22*, 283-294.

Kostareva, A., Gudkova, A., Sjoberg, G., Kiselev, I., Moiseeva, O., Karelkina, E., Goldfarb, L., Schlyakhto, E., and Sejersen, T. (2006). Desmin mutations in a St. Petersburg cohort of cardiomyopathies. Acta Myol *25*, 109-115.

Koteiche, H.A., Chiu, S., Majdoch, R.L., Stewart, P.L., and McHaourab, H.S. (2005). Atomic models by cryo-EM and site-directed spin labeling: application to the N-terminal region of Hsp16.5. Structure *13*, 1165-1171.

Koteiche, H.A., and McHaourab, H.S. (2002). The determinants of the oligomeric structure in Hsp16.5 are encoded in the alpha-crystallin domain. FEBS Lett *519*, 16-22.

Koyama, Y., and Goldman, J.E. (1999). Formation of GFAP cytoplasmic inclusions in astrocytes and their disaggregation by alphaB-crystallin. Am J Pathol *154*, 1563-1572.

Kreplak, L., Herrmann, H., and Aebi, U. (2008a). Tensile properties of single desmin intermediate filaments. Biophys J *94*, 2790-2799.

Kreplak, L., Richter, K., Aebi, U., and Herrmann, H. (2008b). Electron microscopy of intermediate filaments: teaming up with atomic force and confocal laser scanning microscopy. Methods Cell Biol *88*, 273-297.

Krissinel, E., and Henrick, K. (2004). Secondary-structure matching (SSM), a new tool for fast protein structure alignment in three dimensions. Acta Crystallogr D Biol Crystallogr *60*, 2256-2268.

Ku, N.O., and Omary, M.B. (2000). Keratins turn over by ubiquitination in a phosphorylation-modulated fashion. J Cell Biol *149*, 547-552.

Kumar, L.V., Ramakrishna, T., and Rao, C.M. (1999). Structural and functional consequences of the mutation of a conserved arginine residue in alphaA and alphaB crystallins. J Biol Chem *274*, 24137-24141.

Kumarapeli, A.R., and Wang, X. (2004). Genetic modification of the heart: chaperones and the cytoskeleton. J Mol Cell Cardiol *37*, 1097-1109.

Kundu, M., Sen, P.C., and Das, K.P. (2007). Structure, stability, and chaperone function of alphaA-crystallin: role of N-terminal region. Biopolymers *86*, 177-192.

Kyhse-Andersen, J. (1984). Electroblotting of multiple gels: a simple apparatus without buffer tank for rapid transfer of proteins from polyacrylamide to nitrocellulose. J Biochem Biophys Methods *10*, 203-209.

Laemmli, U.K. (1970). Cleavage of structural proteins during the assembly of the head of bacteriophage T4. Nature *227*, 680-685.

Laganowsky, A., Benesch, J.L., Landau, M., Ding, L., Sawaya, M.R., Cascio, D., Huang, Q., Robinson, C.V., Horwitz, J., and Eisenberg, D. (2010). Crystal structures of truncated alphaA and alphaB crystallins reveal structural mechanisms of polydispersity important for eye lens function. Protein Sci *19*, 1031-1043.

Laganowsky, A., and Eisenberg, D. (2010). Non-3D domain swapped crystal structure of truncated zebrafish alphaA crystallin. Protein Sci.

Laskowska, E., Matuszewska, E., and Kuczynska-Wisnik, D. (2010). Small Heat Shock Proteins and Protein-Misfolding Diseases. Curr Pharm Biotechnol.

Latham, J.C., Stein, R.A., Bornhop, D.J., and McHaourab, H.S. (2009). Free-Solution Label-Free Detection of alpha-Crystallin Chaperone Interactions by Back-Scattering Interferometry. Anal Chem.

Launay, N., Goudeau, B., Kato, K., Vicart, P., and Lilienbaum, A. (2006). Cell signaling pathways to alphaB-crystallin following stresses of the cytoskeleton. Exp Cell Res *312*, 3570-3584.

Lazarides, E. (1980). Intermediate filaments as mechanical integrators of cellular space. Nature *283*, 249-256.

Lee, G.J., Roseman, A.M., Saibil, H.R., and Vierling, E. (1997). A small heat shock protein stably binds heat-denatured model substrates and can maintain a substrate in a folding-competent state. EMBO J *16*, 659-671.

Lee, G.J., and Vierling, E. (2000). A small heat shock protein cooperates with heat shock protein 70 systems to reactivate a heat-denatured protein. Plant Physiol *122*, 189-198.

Lentze, N., and Narberhaus, F. (2004). Detection of oligomerisation and substrate recognition sites of small heat shock proteins by peptide arrays. Biochem Biophys Res Commun *325*, 401-407.

Levin, J., Bulst, S., Thirion, C., Schmidt, F., Botzel, K., Krause, S., Pertl, C., Kretzschmar, H., Walter, M.C., Giese, A., *et al.* (2010). Divergent molecular effects of desmin mutations on protein assembly in myofibrillar myopathy. J Neuropathol Exp Neurol *69*, 415-424.

Li, D., Tapscoft, T., Gonzalez, O., Burch, P.E., Quinones, M.A., Zoghbi, W.A., Hill, R., Bachinski, L.L., Mann, D.L., and Roberts, R. (1999). Desmin mutation responsible for idiopathic dilated cardiomyopathy. Circulation *100*, 461-464.

Li, R., Johnson, A.B., Salomons, G., Goldman, J.E., Naidu, S., Quinlan, R., Cree, B., Ruyle, S.Z., Banwell, B., D'Hooghe, M., *et al.* (2005). Glial fibrillary acidic protein mutations in infantile, juvenile, and adult forms of Alexander disease. Ann Neurol *57*, 310-326.

Li, Z., Colucci-Guyon, E., Pincon-Raymond, M., Mericskay, M., Pournin, S., Paulin, D., and Babinet, C. (1996). Cardiovascular lesions and skeletal myopathy in mice lacking desmin. Dev Biol *175*, 362-366.

Li, Z., Mericskay, M., Agbulut, O., Butler-Browne, G., Carlsson, L., Thornell, L.E., Babinet, C., and Paulin, D. (1997). Desmin is essential for the tensile strength and integrity of myofibrils but not for myogenic commitment, differentiation, and fusion of skeletal muscle. J Cell Biol *139*, 129-144.

Liberek, K., Lewandowska, A., and Zietkiewicz, S. (2008). Chaperones in control of protein disaggregation. EMBO J *27*, 328-335.

Lin, Y.C., Broedersz, C.P., Rowat, A.C., Wedig, T., Herrmann, H., Mackintosh, F.C., and Weitz, D.A. (2010). Divalent cations crosslink vimentin intermediate filament tail domains to regulate network mechanics. J Mol Biol *399*, 637-644.

Lindsey Rose, K.M., Gourdie, R.G., Prescott, A.R., Quinlan, R.A., Crouch, R.K., and Schey, K.L. (2006). The C terminus of lens aquaporin 0 interacts with the cytoskeletal proteins filensin and CP49. Invest Ophthalmol Vis Sci *47*, 1562-1570.

Liu, J., Chen, Q., Huang, W., Horak, K.M., Zheng, H., Mestril, R., and Wang, X. (2006a). Impairment of the ubiquitin-proteasome system in desminopathy mouse hearts. FASEB J *20*, 362-364.

Liu, J., Tang, M., Mestril, R., and Wang, X. (2006b). Aberrant protein aggregation is essential for a mutant desmin to impair the proteolytic function of the ubiquitin-proteasome system in cardiomyocytes. J Mol Cell Cardiol *40*, 451-454.

Liu, L., Ghosh, J.G., Clark, J.I., and Jiang, S. (2006c). Studies of alphaB crystallin subunit dynamics by surface plasmon resonance. Anal Biochem *350*, 186-195.

Liu, M., Ke, T., Wang, Z., Yang, Q., Chang, W., Jiang, F., Tang, Z., Li, H., Ren, X., Wang, X., *et al.* (2006d). Identification of a CRYAB mutation associated with autosomal dominant posterior polar cataract in a Chinese family. Invest Ophthalmol Vis Sci *47*, 3461-3466.

Liu, Y., Zhang, X., Luo, L., Wu, M., Zeng, R., Cheng, G., Hu, B., Liu, B., Liang, J.J., and Shang, F. (2006e). A novel alphaB-crystallin mutation associated with autosomal dominant congenital lamellar cataract. Invest Ophthalmol Vis Sci *47*, 1069-1075.

Lowe, J., McDermott, H., Pike, I., Spendlove, I., Landon, M., and Mayer, R.J. (1992). alpha B crystallin expression in non-lenticular tissues and selective presence in ubiquitinated inclusion bodies in human disease. J Pathol *166*, 61-68.

Ma, X., Li, F.F., Wang, S.Z., Gao, C., Zhang, M., and Zhu, S.Q. (2008). A new mutation in BFSP2 (G1091A) causes autosomal dominant congenital lamellar cataracts. Mol Vis *14*, 1906-1911.

Maddala, R., Skiba, N.P., Lalane, R., 3rd, Sherman, D.L., Brophy, P.J., and Rao, P.V. (2011). Periaxin is required for hexagonal geometry and membrane organization of mature lens fibers. Dev Biol *357*, 179-190.

Magin, T.M., Hatzfeld, M., and Franke, W.W. (1987). Analysis of cytokeratin domains by cloning and expression of intact and deleted polypeptides in Escherichia coli. EMBO J *6*, 2607-2615.

Maisel, H., and Perry, M.M. (1972). Electron microscope observations on some structural proteins of the chick lens. Experimental eye research *14*, 7-12.

Maloyan, A., Sanbe, A., Osinska, H., Westfall, M., Robinson, D., Imahashi, K., Murphy, E., and Robbins, J. (2005). Mitochondrial dysfunction and apoptosis underlie the pathogenic process in alpha-B-crystallin desmin-related cardiomyopathy. Circulation *112*, 3451-3461.

Marcantonio, J.M. (1992). Susceptibility of the bovine lens 115kDa beaded filament protein to degradation by calcium and calpain. Curr Eye Res *11*, 103-108.

Marini, I., Bucchioni, L., Voltarelli, M., Del Corso, A., and Mura, U. (1995). Alpha-crystallin-like molecular chaperone against the thermal denaturation of lens aldose reductase: the effect of divalent metal ions. Biochem Biophys Res Commun *212*, 413-420.

Marini, I., Moschini, R., Del Corso, A., and Mura, U. (2005). Alpha-crystallin: an ATP-independent complete molecular chaperone toward sorbitol dehydrogenase. Cell Mol Life Sci *62*, 599-605.

Masaki, S., and Quinlan, R.A. (1997). Gene structure and sequence comparisons of the eye lens specific protein, filensin, from rat and mouse: implications for protein classification and assembly. Gene *201*, 11-20.

Masaki, S., and Watanabe, T. (1992). cDNA sequence analysis of CP94: rat lens fiber cell beaded-filament structural protein shows homology to cytokeratins. Biochemical and biophysical research communications *186*, 190-198.

Mayer, M.P., and Bukau, B. (2005). Hsp70 chaperones: cellular functions and molecular mechanism. Cell Mol Life Sci *62*, 670-684.

McCormick, M.B., Kouklis, P., Syder, A., and Fuchs, E. (1993). The roles of the rod end and the tail in vimentin IF assembly and IF network formation. J Cell Biol *122*, 395-407.

McHaourab, H.S., Dodson, E.K., and Koteiche, H.A. (2002). Mechanism of chaperone function in small heat shock proteins. Two-mode binding of the excited states of T4 lysozyme mutants by alphaA-crystallin. J Biol Chem *277*, 40557-40566.

McHaourab, H.S., Godar, J.A., and Stewart, P.L. (2009). Structure and mechanism of protein stability sensors: chaperone activity of small heat shock proteins. Biochemistry *48*, 3828-3837.

McLachlan, R.W., and Yap, A.S. (2007). Not so simple: the complexity of phosphotyrosine signaling at cadherin adhesive contacts. J Mol Med *85*, 545-554.

McLendon, P.M., and Robbins, J. (2011). Desmin-related cardiomyopathy: an unfolding story. Am J Physiol Heart Circ Physiol *301*, H1220-1228.

Meehan, S., Knowles, T.P., Baldwin, A.J., Smith, J.F., Squires, A.M., Clements, P., Treweek, T.M., Ecroyd, H., Tartaglia, G.G., Vendruscolo, M., *et al.* (2007). Characterisation of amyloid fibril formation by small heat-shock chaperone proteins human alphaA-, alphaB- and R120G alphaB-crystallins. J Mol Biol *372*, 470-484.

Mehlen, P., Preville, X., Chareyron, P., Briolay, J., Klemenz, R., and Arrigo, A.P. (1995). Constitutive expression of human hsp27, Drosophila hsp27, or human alpha B-crystallin confers resistance to TNF- and oxidative stress-induced cytotoxicity in stably transfected murine L929 fibroblasts. J Immunol *154*, 363-374.

Melkani, G.C., Cammarato, A., and Bernstein, S.I. (2006). alphaB-crystallin maintains skeletal muscle myosin enzymatic activity and prevents its aggregation under heat-shock stress. J Mol Biol *358*, 635-645.

Merdes, A., Gounari, F., and Georgatos, S.D. (1993). The 47-kD lens-specific protein phakinin is a tailless intermediate filament protein and an assembly partner of filensin. J Cell Biol *123*, 1507-1516.

Messing, A., Head, M.W., Galles, K., Galbreath, E.J., Goldman, J.E., and Brenner, M. (1998). Fatal encephalopathy with astrocyte inclusions in GFAP transgenic mice. Am J Pathol *152*, 391-398.

Michael, R., van Marle, J., Vrensen, G.F., and van den Berg, T.J. (2003). Changes in the refractive index of lens fibre membranes during maturation--impact on lens transparency. Experimental eye research *77*, 93-99.

Milner, D.J., Weitzer, G., Tran, D., Bradley, A., and Capetanaki, Y. (1996). Disruption of muscle architecture and myocardial degeneration in mice lacking desmin. J Cell Biol *134*, 1255-1270.

Mogk, A., Deuerling, E., Vorderwulbecke, S., Vierling, E., and Bukau, B. (2003). Small heat shock proteins, ClpB and the DnaK system form a functional triade in reversing protein aggregation. Mol Microbiol *50*, 585-595.

Mogk, A., Haslberger, T., Tessarz, P., and Bukau, B. (2008). Common and specific mechanisms of AAA+ proteins involved in protein quality control. Biochem Soc Trans *36*, 120-125.

Mokry, J., and Nemecek, S. (1998). Immunohistochemical detection of intermediate filament nestin. Acta medica *41*, 73-80.

Moroni, M., and Garland, D. (2001). In vitro dephosphorylation of alpha-crystallin is dependent on the state of oligomerization. Biochim Biophys Acta *1546*, 282-290.

Muchowski, P.J., Hays, L.G., Yates, J.R., 3rd, and Clark, J.I. (1999a). ATP and the core "alpha-Crystallin" domain of the small heat-shock protein alphaB-crystallin. J Biol Chem *274*, 30190-30195.

Muchowski, P.J., Valdez, M.M., and Clark, J.I. (1999b). AlphaB-crystallin selectively targets intermediate filament proteins during thermal stress. Invest Ophthalmol Vis Sci *40*, 951-958.

Muchowski, P.J., Wu, G.J., Liang, J.J., Adman, E.T., and Clark, J.I. (1999c). Site-directed mutations within the core "alpha-crystallin" domain of the small heat-shock protein, human alphaB-crystallin, decrease molecular chaperone functions. J Mol Biol *289*, 397-411.

Mucke, N., Wedig, T., Burer, A., Marekov, L.N., Steinert, P.M., Langowski, J., Aebi, U., and Herrmann, H. (2004). Molecular and biophysical characterization of assembly-starter units of human vimentin. J Mol Biol *340*, 97-114.

Munoz-Marmol, A.M., Strasser, G., Isamat, M., Coulombe, P.A., Yang, Y., Roca, X., Vela, E., Mate, J.L., Coll, J., Fernandez-Figueras, M.T., *et al.* (1998). A dysfunctional desmin mutation in a patient with severe generalized myopathy. Proc Natl Acad Sci U S A *95*, 11312-11317.

Muntoni, F., Bonne, G., Goldfarb, L.G., Mercuri, E., Piercy, R.J., Burke, M., Yaou, R.B., Richard, P., Recan, D., Shatunov, A., *et al.* (2006). Disease severity in dominant Emery Dreifuss is increased by mutations in both emerin and desmin proteins. Brain *129*, 1260-1268.

Narberhaus, F. (2002). Alpha-crystallin-type heat shock proteins: socializing minichaperones in the context of a multichaperone network. Microbiol Mol Biol Rev *66*, 64-93; table of contents.

Nicholl, I.D., and Quinlan, R.A. (1994). Chaperone activity of alpha-crystallins modulates intermediate filament assembly. EMBO J *13*, 945-953.

Nielsen, A.L., and Jorgensen, A.L. (2003). Structural and functional characterization of the zebrafish gene for glial fibrillary acidic protein, GFAP. Gene *310*, 123-132.

Niesen, F.H., Berglund, H., and Vedadi, M. (2007). The use of differential scanning fluorimetry to detect ligand interactions that promote protein stability. Nat Protoc *2*, 2212-2221.

Nitahara-Kasahara, Y., Fukasawa, M., Shinkai-Ouchi, F., Sato, S., Suzuki, T., Murakami, K., Wakita, T., Hanada, K., Miyamura, T., and Nishijima, M. (2009). Cellular vimentin content regulates the protein level of hepatitis C virus core protein and the hepatitis C virus production in cultured cells. Virology *383*, 319-327.

Nozais, M., Bechet, J.J., and Houadjeto, M. (1992). Inactivation, subunit dissociation, aggregation, and unfolding of myosin subfragment 1 during guanidine denaturation. Biochemistry *31*, 1210-1215.

Ohto-Fujita, E., Fujita, Y., and Atomi, Y. (2007). Analysis of the alphaB-crystallin domain responsible for inhibiting tubulin aggregation. Cell Stress Chaperones *12*, 163-171.

Oka, M., Kudo, H., Sugama, N., Asami, Y., and Takehana, M. (2008). The function of filensin and phakinin in lens transparency. Mol Vis *14*, 815-822.

Olive, M., Armstrong, J., Miralles, F., Pou, A., Fardeau, M., Gonzalez, L., Martinez, F., Fischer, D., Martinez Matos, J.A., Shatunov, A., *et al.* (2007). Phenotypic patterns of desminopathy associated with three novel mutations in the desmin gene. Neuromuscul Disord *17*, 443-450.

Olive, M., Goldfarb, L., Moreno, D., Laforet, E., Dagvadorj, A., Sambuughin, N., Martinez-Matos, J.A., Martinez, F., Alio, J., Farrero, E., *et al.* (2004). Desmin-related myopathy: clinical, electrophysiological, radiological, neuropathological and genetic studies. J Neurol Sci *219*, 125-137.

Palmisano, D.V., Groth-Vasselli, B., Farnsworth, P.N., and Reddy, M.C. (1995). Interaction of ATP and lens alpha crystallin characterized by equilibrium binding studies and intrinsic tryptophan fluorescence spectroscopy. Biochim Biophys Acta *1246*, 91-97.

Park, K.Y., Dalakas, M.C., Goebel, H.H., Ferrans, V.J., Semino-Mora, C., Litvak, S., Takeda, K., and Goldfarb, L.G. (2000a). Desmin splice variants causing cardiac and skeletal myopathy. J Med Genet *37*, 851-857.

Park, K.Y., Dalakas, M.C., Semino-Mora, C., Lee, H.S., Litvak, S., Takeda, K., Ferrans, V.J., and Goldfarb, L.G. (2000b). Sporadic cardiac and skeletal myopathy caused by a de novo desmin mutation. Clin Genet *57*, 423-429.

Parry, D.A. (2005). Microdissection of the sequence and structure of intermediate filament chains. Adv Protein Chem *70*, 113-142.

Parry, D.A., and Steinert, P.M. (1999). Intermediate filaments: molecular architecture, assembly, dynamics and polymorphism. Q Rev Biophys *32*, 99-187.

Parry, D.A., Strelkov, S.V., Burkhard, P., Aebi, U., and Herrmann, H. (2007). Towards a molecular description of intermediate filament structure and assembly. Exp Cell Res *313*, 2204-2216.

Pasta, S.Y., Raman, B., Ramakrishna, T., and Rao Ch, M. (2002). Role of the C-terminal extensions of alpha-crystallins. Swapping the C-terminal extension of alpha-crystallin to alphaB-crystallin results in enhanced chaperone activity. J Biol Chem *277*, 45821-45828.

Pasta, S.Y., Raman, B., Ramakrishna, T., and Rao Ch, M. (2003). Role of the conserved SRLFDQFFG region of alpha-crystallin, a small heat shock protein. Effect on oligomeric size, subunit exchange, and chaperone-like activity. J Biol Chem *278*, 51159-51166.

Pasta, S.Y., Raman, B., Ramakrishna, T., and Rao Ch, M. (2004). The IXI/V motif in the C-terminal extension of alpha-crystallins: alternative interactions and oligomeric assemblies. Mol Vis *10*, 655-662.

Peitzsch, R.M., and McLaughlin, S. (1993). Binding of acylated peptides and fatty acids to phospholipid vesicles: pertinence to myristoylated proteins. Biochemistry *32*, 10436-10443.

Perng, M.D., Cairns, L., van den, I.P., Prescott, A., Hutcheson, A.M., and Quinlan, R.A. (1999a). Intermediate filament interactions can be altered by HSP27 and alphaB-crystallin. J Cell Sci *112 (Pt 13)*, 2099-2112.

Perng, M.D., Muchowski, P.J., van Den, I.P., Wu, G.J., Hutcheson, A.M., Clark, J.I., and Quinlan, R.A. (1999b). The cardiomyopathy and lens cataract mutation in alphaB-crystallin alters its protein structure, chaperone activity, and interaction with intermediate filaments in vitro. J Biol Chem *274*, 33235-33243.

Perng, M.D., Wen, S.F., van den, I.P., Prescott, A.R., and Quinlan, R.A. (2004). Desmin aggregate formation by R120G alphaB-crystallin is caused by altered filament interactions and is dependent upon network status in cells. Mol Biol Cell *15*, 2335-2346.

Perng, M.D., Zhang, Q., and Quinlan, R.A. (2007). Insights into the beaded filament of the eye lens. Exp Cell Res *313*, 2180-2188.

Peschek, J., Braun, N., Franzmann, T.M., Georgalis, Y., Haslbeck, M., Weinkauf, S., and Buchner, J. (2009). The eye lens chaperone {alpha}-crystallin forms defined globular assemblies. Proc Natl Acad Sci U S A.

Pica, E.C., Kathirvel, P., Pramono, Z.A., Lai, P.S., and Yee, W.C. (2008). Characterization of a novel S13F desmin mutation associated with desmin myopathy and heart block in a Chinese family. Neuromuscul Disord *18*, 178-182.

Plater, M.L., Goode, D., and Crabbe, M.J. (1996). Effects of site-directed mutations on the chaperone-like activity of alphaB-crystallin. J Biol Chem *271*, 28558-28566.

Postlethwait, J., Amores, A., Cresko, W., Singer, A., and Yan, Y.L. (2004). Subfunction partitioning, the teleost radiation and the annotation of the human genome. Trends Genet *20*, 481-490.

Pruszczyk, P., Kostera-Pruszczyk, A., Shatunov, A., Goudeau, B., Draminska, A., Takeda, K., Sambuughin, N., Vicart, P., Strelkov, S.V., Goldfarb, L.G., *et al.* (2007). Restrictive cardiomyopathy with atrioventricular conduction block resulting from a desmin mutation. Int J Cardiol *117*, 244-253.

Qu B*, Landsbury A*, Schönthaler HB, Dahm R, Liu Y, Clark JI, Prescott AR, Quinlan RA. (2012). Evolution of the vertebrate beaded filament protein, Bfsp2; comparing the in vitro assembly properties of a "tailed" zebrafish Bfsp2 to its "tailless" human orthologue. Experimental Eye Research *94*, 192-202. (*Joint first author)

Quinlan, R. (2002). Cytoskeletal competence requires protein chaperones. Prog Mol Subcell Biol *28*, 219-233.

Quinlan, R.A., Brenner, M., Goldman, J.E., and Messing, A. (2007). GFAP and its role in Alexander disease. Exp Cell Res *313*, 2077-2087.

Quinlan, R.A., Carte, J.M., Sandilands, A., and Prescott, A.R. (1996). The beaded filament of the eye lens: an unexpected key to intermediate filament structure and function. Trends Cell Biol *6*, 123-126.

Quinlan, R.A., Carter, J.M., Hutcheson, A.M., and Campbell, D.G. (1992). The 53kDa polypeptide component of the bovine fibre cell cytoskeleton is derived from the 115kDa beaded filament protein: evidence for a fibre cell specific intermediate filament protein. Curr Eye Res *11*, 909-921.

Rajan, S., Chandrashekar, R., Aziz, A., and Abraham, E.C. (2006). Role of arginine-163 and the 163REEK166 motif in the oligomerization of truncated alphaA-crystallins. Biochemistry *45*, 15684-15691.

Rajaraman, K., Raman, B., Ramakrishna, T., and Rao, C.M. (2001). Interaction of human recombinant alphaA- and alphaB-crystallins with early and late unfolding intermediates of citrate synthase on its thermal denaturation. FEBS Lett *497*, 118-123.

Rajasekaran, N.S., Connell, P., Christians, E.S., Yan, L.J., Taylor, R.P., Orosz, A., Zhang, X.Q., Stevenson, T.J., Peshock, R.M., Leopold, J.A., *et al.* (2007). Human alpha B-crystallin mutation causes oxido-reductive stress and protein aggregation cardiomyopathy in mice. Cell *130*, 427-439.

Raju, M., Santhoshkumar, P., and Sharma, K.K. (2011). Cataract-causing alphaAG98R-crystallin mutant dissociates into monomers having chaperone activity. Mol Vis *17*, 7-15.

Ralton, J.E., Lu, X., Hutcheson, A.M., and Quinlan, R.A. (1994). Identification of two N-terminal non-alpha-helical domain motifs important in the assembly of glial fibrillary acidic protein. J Cell Sci *107 (Pt 7)*, 1935-1948.

Ramachandran, R.D., Perumalsamy, V., and Hejtmancik, J.F. (2007). Autosomal recessive juvenile onset cataract associated with mutation in BFSP1. Hum Genet *121*, 475-482.

Ramaekers, F.C., Osborn, M., Schimid, E., Weber, K., Bloemendal, H., and Franke, W.W. (1980). Identification of the cytoskeletal proteins in lens-forming cells, a special epitheloid cell type. Experimental cell research *127*, 309-327.

Raman, B., and Rao, C.M. (1994). Chaperone-like activity and quaternary structure of alpha-crystallin. J Biol Chem *269*, 27264-27268.

Raman, B., and Rao, C.M. (1997). Chaperone-like activity and temperature-induced structural changes of alpha-crystallin. J Biol Chem *272*, 23559-23564.

Ramsay, G.D., and Eftink, M.R. (1994). Analysis of multidimensional spectroscopic data to monitor unfolding of proteins. Methods Enzymol *240*, 615-645.

Rao, P.V., Horwitz, J., and Zigler, J.S., Jr. (1993). Alpha-crystallin, a molecular chaperone, forms a stable complex with carbonic anhydrase upon heat denaturation. Biochem Biophys Res Commun *190*, 786-793.

Reddy, M.C., Palmisano, D.V., Groth-Vasselli, B., and Farnsworth, P.N. (1992). 31P NMR studies of the ATP/alpha-crystallin complex: functional implications. Biochem Biophys Res Commun *189*, 1578-1584.

Reilich, P., Schoser, B., Schramm, N., Krause, S., Schessl, J., Kress, W., Muller-Hocker, J., Walter, M.C., and Lochmuller, H. (2010). The p.G154S mutation of the alpha-B crystallin gene (CRYAB) causes late-onset distal myopathy. Neuromuscul Disord.

Sacconi, S., Feasson, L., Antoine, J.C., Pecheux, C., Bernard, R., Cobo, A.M., Casarin, A., Salviati, L., Desnuelle, C., and Urtizberea, A. (2011). A novel CRYAB mutation resulting in multisystemic disease. Neuromuscul Disord.

Safieh, L.A., Khan, A.O., and Alkuraya, F.S. (2009). Identification of a novel CRYAB mutation associated with autosomal recessive juvenile cataract in a Saudi family. Mol Vis *15*, 980-984.

Saha, S., and Das, K.P. (2004). Relationship between chaperone activity and oligomeric size of recombinant human alphaA- and alphaB-crystallin: a tryptic digestion study. Proteins *57*, 610-617.

Saji, H., Iizuka, R., Yoshida, T., Abe, T., Kidokoro, S., Ishii, N., and Yohda, M. (2008). Role of the IXI/V motif in oligomer assembly and function of StHsp14.0, a small heat shock protein from the acidothermophilic archaeon, Sulfolobus tokodaii strain 7. Proteins *71*, 771-782.

Salinthone, S., Tyagi, M., and Gerthoffer, W.T. (2008). Small heat shock proteins in smooth muscle. Pharmacol Ther.

Sandilands, A., Prescott, A.R., Carter, J.M., Hutcheson, A.M., Quinlan, R.A., Richards, J., and FitzGerald, P.G. (1995a). Vimentin and CP49/filensin form distinct networks in the lens which are independently modulated during lens fibre cell differentiation. J Cell Sci *108 (Pt 4)*, 1397-1406.

Sandilands, A., Prescott, A.R., Hutcheson, A.M., Quinlan, R.A., Casselman, J.T., and FitzGerald, P.G. (1995b). Filensin is proteolytically processed during lens fiber cell differentiation by multiple independent pathways. Eur J Cell Biol *67*, 238-253.

Sandilands, A., Prescott, A.R., Wegener, A., Zoltoski, R.K., Hutcheson, A.M., Masaki, S., Kuszak, J.R., and Quinlan, R.A. (2003). Knockout of the intermediate filament protein CP49 destabilises the lens fibre cell cytoskeleton and decreases lens optical quality, but does not induce cataract. Exp Eye Res *76*, 385-391.

Sandilands, A., Wang, X., Hutcheson, A.M., James, J., Prescott, A.R., Wegener, A., Pekny, M., Gong, X., and Quinlan, R.A. (2004). Bfsp2 mutation found in mouse 129 strains causes the loss of CP49' and induces vimentin-dependent changes in the lens fibre cell cytoskeleton. Exp Eye Res *78*, 875-889.

Sathish, H.A., Stein, R.A., Yang, G., and McHaourab, H.S. (2003). Mechanism of chaperone function in small heat-shock proteins. Fluorescence studies of the conformations of T4 lysozyme bound to alphaB-crystallin. J Biol Chem *278*, 44214-44221.

Sawada, K., Agata, J., Eguchi, G., Quinlan, R., and Maisel, H. (1995). The predicted structure of chick lens CP49 and a variant thereof, CP49ins, the first vertebrate cytoplasmic intermediate filament protein with a lamin-like insertion in helix 1B. Current eye research *14*, 545-553.

Schlesinger, M.J. (1990). Heat shock proteins. J Biol Chem *265*, 12111-12114.

Schroder, R., Furst, D.O., Klasen, C., Reimann, J., Herrmann, H., and van der Ven, P.F. (2000). Association of plectin with Z-discs is a prerequisite for the formation of the intermyofibrillar desmin cytoskeleton. Lab Invest *80*, 455-464.

Schroder, R., Goudeau, B., Simon, M.C., Fischer, D., Eggermann, T., Clemen, C.S., Li, Z., Reimann, J., Xue, Z., Rudnik-Schoneborn, S., *et al.* (2003). On noxious desmin: functional effects of a novel heterozygous desmin insertion mutation on the extrasarcomeric desmin cytoskeleton and mitochondria. Hum Mol Genet *12*, 657-669.

Schroder, R., and Schoser, B. (2009). Myofibrillar myopathies: a clinical and myopathological guide. Brain Pathol *19*, 483-492.

Schroder, R., Vrabie, A., and Goebel, H.H. (2007). Primary desminopathies. J Cell Mol Med *11*, 416-426.

Selcen, D. (2011). Myofibrillar myopathies. Neuromuscul Disord. 2011 Mar;21(3):161-71.

Selcen, D., and Engel, A.G. (2003). Myofibrillar myopathy caused by novel dominant negative alpha B-crystallin mutations. Ann Neurol *54*, 804-810.

Selcen, D., Ohno, K., and Engel, A.G. (2004). Myofibrillar myopathy: clinical, morphological and genetic studies in 63 patients. Brain *127*, 439-451.

Sharma, K.K., Kaur, H., and Kester, K. (1997). Functional elements in molecular chaperone alpha-crystallin: identification of binding sites in alpha B-crystallin. Biochem Biophys Res Commun *239*, 217-222.

Sharma, K.K., Kumar, G.S., Murphy, A.S., and Kester, K. (1998). Identification of 1,1'-bi(4-anilino)naphthalene-5,5'-disulfonic acid binding sequences in alpha-crystallin. J Biol Chem *273*, 15474-15478.

Sharma, K.K., Kumar, R.S., Kumar, G.S., and Quinn, P.T. (2000). Synthesis and characterization of a peptide identified as a functional element in alphaA-crystallin. J Biol Chem *275*, 3767-3771.

Sharma, S. (2011). Characterization of Desmin Disease Mutants and their Association with alphaB-Crystallin in Desminopathy. University of Heidelberg PhD Thesis *http://www.ub.uni-heidelberg.de/archiv/11561*.

Sharma, S., Mucke, N., Katus, H.A., Herrmann, H., and Bar, H. (2009). Disease mutations in the "head" domain of the extra-sarcomeric protein desmin distinctly alter its assembly and network-forming properties. J Mol Med *87*, 1207-1219.

Shashidharamurthy, R., Koteiche, H.A., Dong, J., and McHaourab, H.S. (2005). Mechanism of chaperone function in small heat shock proteins: dissociation of the HSP27 oligomer is required for recognition and binding of destabilized T4 lysozyme. J Biol Chem *280*, 5281-5289.

Sigalov, A.B., Kim, W.M., Saline, M., and Stern, L.J. (2008). The intrinsically disordered cytoplasmic domain of the T cell receptor zeta chain binds to the nef protein of simian immunodeficiency virus without a disorder-to-order transition. Biochemistry *47*, 12942-12944.

Simon, S., and Arrigo, A.P. (2011). Small stress proteins and human diseases. Nova Biomedical *ISBN 978-1-61668-198-2*.

Singh, B.N., Rao, K.S., Ramakrishna, T., Rangaraj, N., and Rao Ch, M. (2007). Association of alphaB-crystallin, a small heat shock protein, with actin: role in modulating actin filament dynamics in vivo. J Mol Biol *366*, 756-767.

Sjoberg, G., Saavedra-Matiz, C.A., Rosen, D.R., Wijsman, E.M., Borg, K., Horowitz, S.H., and Sejersen, T. (1999). A missense mutation in the desmin rod domain is associated with autosomal dominant distal myopathy, and exerts a dominant negative effect on filament formation. Hum Mol Genet *8*, 2191-2198.

Sobott, F., Benesch, J.L., Vierling, E., and Robinson, C.V. (2002). Subunit exchange of multimeric protein complexes. Real-time monitoring of subunit exchange between small heat shock proteins by using electrospray mass spectrometry. J Biol Chem *277*, 38921-38929.

Song, S., Hanson, M.J., Liu, B.F., Chylack, L.T., and Liang, J.J. (2008). Protein-protein interactions between lens vimentin and alphaB-crystallin using FRET acceptor photobleaching. Mol Vis *14*, 1282-1287.

Song, S., Landsbury, A., Dahm, R., Liu, Y., Zhang, Q., and Quinlan, R.A. (2009). Functions of the intermediate filament cytoskeleton in the eye lens. J Clin Invest *119*, 1837-1848.

Spinozzi, F., Mariani, P., Rustichelli, F., Amenitsch, H., Bennardini, F., Mura, G.M., Coi, A., and Ganadu, M.L. (2006). Temperature dependence of chaperone-like activity and oligomeric state of alphaB-crystallin. Biochim Biophys Acta *1764*, 677-687.

Sreelakshmi, Y., Santhoshkumar, P., Bhattacharyya, J., and Sharma, K.K. (2004). AlphaA-crystallin interacting regions in the small heat shock protein, alphaB-crystallin. Biochemistry *43*, 15785-15795.

Sreelakshmi, Y., and Sharma, K.K. (2005). Recognition sequence 2 (residues 60-71) plays a role in oligomerization and exchange dynamics of alphaB-crystallin. Biochemistry *44*, 12245-12252.

Sreelakshmi, Y., and Sharma, K.K. (2006). The interaction between alphaA- and alphaB-crystallin is sequence-specific. Mol Vis *12*, 581-587.

Srinivas, V., Raman, B., Rao, K.S., Ramakrishna, T., and Rao Ch, M. (2005). Arginine hydrochloride enhances the dynamics of subunit assembly and the chaperone-like activity of alpha-crystallin. Mol Vis *11*, 249-255.

Stasiak, P.C., and Lane, E.B. (1987). Sequence of cDNA coding for human keratin 19. Nucleic Acids Res *15*, 10058.

Stengel, F., Baldwin, A.J., Painter, A.J., Jaya, N., Basha, E., Kay, L.E., Vierling, E., Robinson, C.V., and Benesch, J.L. (2010). Quaternary dynamics and plasticity underlie small heat shock protein chaperone function. Proc Natl Acad Sci U S A *107*, 2007-2012.

Straub, B.K., Boda, J., Kuhn, C., Schnoelzer, M., Korf, U., Kempf, T., Spring, H., Hatzfeld, M., and Franke, W.W. (2003). A novel cell-cell junction system: the cortex adhaerens mosaic of lens fiber cells. J Cell Sci *116*, 4985-4995.

Strelkov, S.V., Herrmann, H., Geisler, N., Lustig, A., Ivaninskii, S., Zimbelmann, R., Burkhard, P., and Aebi, U. (2001). Divide-and-conquer crystallographic approach towards an atomic structure of intermediate filaments. J Mol Biol *306*, 773-781.

Stromer, T., Ehrnsperger, M., Gaestel, M., and Buchner, J. (2003). Analysis of the interaction of small heat shock proteins with unfolding proteins. J Biol Chem *278*, 18015-18021.

Stromer, T., Fischer, E., Richter, K., Haslbeck, M., and Buchner, J. (2004). Analysis of the regulation of the molecular chaperone Hsp26 by temperature-induced dissociation: the N-terminal domail is important for oligomer assembly and the binding of unfolding proteins. J Biol Chem *279*, 11222-11228.

Sugawara, M., Kato, K., Komatsu, M., Wada, C., Kawamura, K., Shindo, P.S., Yoshioka, P.N., Tanaka, K., Watanabe, S., and Toyoshima, I. (2000). A novel de novo mutation in the desmin gene causes desmin myopathy with toxic aggregates. Neurology *55*, 986-990.

Sun, Y., and MacRae, T.H. (2005). Small heat shock proteins: molecular structure and chaperone function. Cell Mol Life Sci *62*, 2460-2476.

Szeverenyi, I., Cassidy, A.J., Chung, C.W., Lee, B.T., Common, J.E., Ogg, S.C., Chen, H., Sim, S.Y., Goh, W.L., Ng, K.W., *et al.* (2008). The Human Intermediate Filament Database: comprehensive information on a gene family involved in many human diseases. Hum Mutat *29*, 351-360.

Takeda, K., Hayashi, T., Abe, T., Hirano, Y., Hanazono, Y., Yohda, M., and Miki, K. (2011). Dimer structure and conformational variability in the N-terminal region of an archaeal small heat shock protein, StHsp14.0. J Struct Biol *174*, 92-99.

Tang, B., Liu, X., Zhao, G., Luo, W., Xia, K., Pan, Q., Cai, F., Hu, Z., Zhang, C., Chen, B., *et al.* (2005a). Mutation analysis of the small heat shock protein 27 gene in chinese patients with Charcot-Marie-Tooth disease. Arch Neurol *62*, 1201-1207.

Tang, B.S., Zhao, G.H., Luo, W., Xia, K., Cai, F., Pan, Q., Zhang, R.X., Zhang, F.F., Liu, X.M., Chen, B., *et al.* (2005b). Small heat-shock protein 22 mutated in autosomal dominant Charcot-Marie-Tooth disease type 2L. Hum Genet *116*, 222-224.

Tang, G., Xu, Z., and Goldman, J.E. (2006). Synergistic effects of the SAPK/JNK and the proteasome pathway on glial fibrillary acidic protein (GFAP) accumulation in Alexander disease. J Biol Chem *281*, 38634-38643.

Tang, G., Yue, Z., Talloczy, Z., and Goldman, J.E. (2008). Adaptive autophagy in Alexander disease-affected astrocytes. Autophagy *4*, 701-703.

Tannous, P., Zhu, H., Johnstone, J.L., Shelton, J.M., Rajasekaran, N.S., Benjamin, I.J., Nguyen, L., Gerard, R.D., Levine, B., Rothermel, B.A., *et al.* (2008). Autophagy is an adaptive response in desmin-related cardiomyopathy. Proc Natl Acad Sci U S A *105*, 9745-9750.

Tawk, M., Titeux, M., Fallet, C., Li, Z., Daumas-Duport, C., Cavalcante, L.A., Paulin, D., and Moura-Neto, V. (2003). Synemin expression in developing normal and pathological human retina and lens. Experimental neurology *183*, 499-507.

Taylor, M.R., Slavov, D., Ku, L., Di Lenarda, A., Sinagra, G., Carniel, E., Haubold, K., Boucek, M.M., Ferguson, D., Graw, S.L., *et al.* (2007). Prevalence of desmin mutations in dilated cardiomyopathy. Circulation *115*, 1244-1251.

Thampi, P., and Abraham, E.C. (2003). Influence of the C-terminal residues on oligomerization of alpha A-crystallin. Biochemistry *42*, 11857-11863.

Thedieck, C., Kalbacher, H., Kratzer, U., Lammers, R., Stevanovic, S., and Klein, G. (2008). alpha B-crystallin is a cytoplasmic interaction partner of the kidney-specific cadherin-16. J Mol Biol *378*, 145-153.

Theriault, J.R., Lambert, H., Chavez-Zobel, A.T., Charest, G., Lavigne, P., and Landry, J. (2004). Essential role of the NH2-terminal WD/EPF motif in the phosphorylation-activated protective function of mammalian Hsp27. J Biol Chem *279*, 23463-23471.

Tompa, P., and Csermely, P. (2004). The role of structural disorder in the function of RNA and protein chaperones. FASEB J *18*, 1169-1175.

Traub, P., and Vorgias, C.E. (1983). Involvement of the N-terminal polypeptide of vimentin in the formation of intermediate filaments. J Cell Sci *63*, 43-67.

Treweek, T.M., Ecroyd, H., Williams, D.M., Meehan, S., Carver, J.A., and Walker, M.J. (2007). Site-Directed Mutations in the C-Terminal Extension of Human alphaB-Crystallin Affect Chaperone Function and Block Amyloid Fibril Formation. PLoS ONE *2*, e1046.

Treweek, T.M., Rekas, A., Lindner, R.A., Walker, M.J., Aquilina, J.A., Robinson, C.V., Horwitz, J., Perng, M.D., Quinlan, R.A., and Carver, J.A. (2005). R120G alphaB-crystallin promotes the unfolding of reduced alpha-lactalbumin and is inherently unstable. FEBS J *272*, 711-724.

Tskhovrebova, L., and Trinick, J. (2003). Titin: properties and family relationships. Nat Rev Mol Cell Biol *4*, 679-689.

Tsoka, S., Simon, D., and Ouzounis, C.A. (2004). Automated metabolic reconstruction for Methanococcus jannaschii. Archaea *1*, 223-229.

Utsumi, T., Sakurai, N., Nakano, K., and Ishisaka, R. (2003). C-terminal 15 kDa fragment of cytoskeletal actin is posttranslationally N-myristoylated upon caspase-mediated cleavage and targeted to mitochondria. FEBS Lett *539*, 37-44.

Valentine, R.C., Shapiro, B.M., and Stadtman, E.R. (1968). Regulation of glutamine synthetase. XII. Electron microscopy of the enzyme from Escherichia coli. Biochemistry *7*, 2143-2152.

Van Montfort, R., Slingsby, C., and Vierling, E. (2001a). Structure and function of the small heat shock protein/alpha-crystallin family of molecular chaperones. Adv Protein Chem *59*, 105-156.

Van Montfort, R.L., Basha, E., Friedrich, K.L., Slingsby, C., and Vierling, E. (2001b). Crystal structure and assembly of a eukaryotic small heat shock protein. Nat Struct Biol *8*, 1025-1030.

Van Spaendonck-Zwarts, K., van Hessem, L., Jongbloed, J.D., de Walle, H.E., Capetanaki, Y., van der Kooi, A.J., van Langen, I.M., van den Berg, M.P., and van Tintelen, J.P. (2010). Desmin-related myopathy: a review and meta-analysis. Clin Genet.

Vicart, P., Caron, A., Guicheney, P., Li, Z., Prevost, M.C., Faure, A., Chateau, D., Chapon, F., Tome, F., Dupret, J.M., *et al.* (1998). A missense mutation in the alphaB-crystallin chaperone gene causes a desmin-related myopathy. Nat Genet *20*, 92-95.

Vogel, V., and Sheetz, M.P. (2009). Cell fate regulation by coupling mechanical cycles to biochemical signaling pathways. Curr Opin Cell Biol *21*, 38-46.

Vrabie, A., Goldfarb, L.G., Shatunov, A., Nagele, A., Fritz, P., Kaczmarek, I., and Goebel, H.H. (2005). The enlarging spectrum of desminopathies: new morphological findings, eastward geographic spread, novel exon 3 desmin mutation. Acta Neuropathol *109*, 411-417.

Wallace, P., Signer, E., Paton, I.R., Burt, D., and Quinlan, R. (1998). The chicken CP49 gene contains an extra exon compared to the human CP49 gene which identifies an important step in the evolution of the eye lens intermediate filament proteins. Gene *211*, 19-27.

Walter, M.C., Reilich, P., Huebner, A., Fischer, D., Schroder, R., Vorgerd, M., Kress, W., Born, C., Schoser, B.G., Krause, K.H., *et al.* (2007). Scapuloperoneal syndrome type Kaeser and a wide phenotypic spectrum of adult-onset, dominant myopathies are associated with the desmin mutation R350P. Brain *130*, 1485-1496.

Wang, X., Klevitsky, R., Huang, W., Glasford, J., Li, F., and Robbins, J. (2003). AlphaB-crystallin modulates protein aggregation of abnormal desmin. Circ Res *93*, 998-1005.

Wang, Z., Obidike, J.E., and Schey, K.L. (2009). Posttranslational Modifications of Bovine Lens Beaded Filament Proteins Filensin and CP49. Invest Ophthalmol Vis Sci.

Wendeler, M.W., Praus, M., Jung, R., Hecking, M., Metzig, C., and Gessner, R. (2004). Ksp-cadherin is a functional cell-cell adhesion molecule related to LI-cadherin. Exp Cell Res *294*, 345-355.

Wickert, U., Mucke, N., Wedig, T., Muller, S.A., Aebi, U., and Herrmann, H. (2005). Characterization of the in vitro co-assembly process of the intermediate filament proteins vimentin and desmin: mixed polymers at all stages of assembly. Eur J Cell Biol *84*, 379-391.

Wieske, M., Benndorf, R., Behlke, J., Dolling, R., Grelle, G., Bielka, H., and Lutsch, G. (2001). Defined sequence segments of the small heat shock proteins HSP25 and alphaB-crystallin inhibit actin polymerization. Eur J Biochem *268*, 2083-2090.

Wintrode, P.L., Friedrich, K.L., Vierling, E., Smith, J.B., and Smith, D.L. (2003). Solution structure and dynamics of a heat shock protein assembly probed by hydrogen exchange and mass spectrometry. Biochemistry *42*, 10667-10673.

Wisniewski, T., and Goldman, J.E. (1998). Alpha B-crystallin is associated with intermediate filaments in astrocytoma cells. Neurochem Res *23*, 385-392.

Yang, J., Bian, W., Gao, X., Chen, L., and Jing, N. (2000). Nestin expression during mouse eye and lens development. Mechanisms of development *94*, 287-291.

Yoneda, K., Furukawa, T., Zheng, Y.J., Momoi, T., Izawa, I., Inagaki, M., Manabe, M., and Inagaki, N. (2004). An autocrine/paracrine loop linking keratin 14 aggregates to tumor necrosis factor alpha-mediated cytotoxicity in a keratinocyte model of epidermolysis bullosa simplex. J Biol Chem *279*, 7296-7303.

Yoon, K.H., and FitzGerald, P.G. (2009). Periplakin interactions with lens intermediate and beaded filaments. Invest Ophthalmol Vis Sci *50*, 1283-1289.

Yoshioka, M., Tanaka, H., Shono, N., Snyder, E.E., Shindo, M., and St-Amand, J. (2003). Serial analysis of gene expression in the skeletal muscle of endurance athletes compared to sedentary men. FASEB J *17*, 1812-1819.

Young, J.C., Agashe, V.R., Siegers, K., and Hartl, F.U. (2004). Pathways of chaperone-mediated protein folding in the cytosol. Nat Rev Mol Cell Biol *5*, 781-791.

Yun, S.J., Hahm, D.H., and Lee, E.H. (2002). Immobilization stress induces the expression of alphaB-crystallin in rat hippocampus: implications of glial activation in stress-mediated hippocampal degeneration. Neuroscience letters *324*, 45-48.

Zha, J., Weiler, S., Oh, K.J., Wei, M.C., and Korsmeyer, S.J. (2000). Posttranslational N-myristoylation of BID as a molecular switch for targeting mitochondria and apoptosis. Science *290*, 1761-1765.

Zhang, Q., Guo, X., Xiao, X., Yi, J., Jia, X., and Hejtmancik, J.F. (2004). Clinical description and genome wide linkage study of Y-sutural cataract and myopia in a Chinese family. Mol Vis *10*, 890-900.

Zhu, Y., Boglomovas, J., Labeit, S., and Granzier, H. (2009). Single molecule force spectroscopy of cardiac titin's N2B element-effects of the molecular chaperone alpha B-crystallin with disease causing mutations. J Biol Chem.